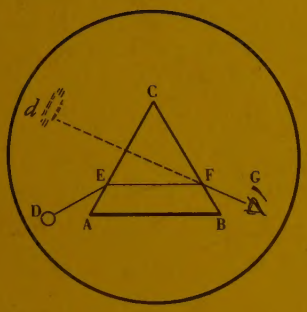

UNIVERSITY OF ILLINOIS
LIBRARY
NOV 27 1961
CHICAGO

optics and spectroscopy

volume xi
number 1
july 1961

OPTICAL SOCIETY OF AMERICA

USSR ACADEMY OF SCIENCES

RUSSIAN EDITORIAL STAFF FOR
OPTIKA I SPEKTROSKOPIYA sponsored by
USSR ACADEMY OF SCIENCES

Editor: S. E. FRISH

Assistant Editor: P. P. FEOFILOV
Corresponding Secretary: L. S. SAZONOV

Associate Editors:

M. V. VOLKENSTEIN	V. P. LINNIK	N. N. SOBOLEV
M. M. GUREVICH	S. L. MANDEL'SHTAM	A. N. TERENIN
M. A. EL'IASHEVICH	I. V. OBREIMOV	A. I. TUDOROVSKII
A. A. LEBEDEV	V. K. PROKOF'EV	V. M. CHULANOVSKII

Translated from *OPTIKA I SPEKTROSKOPIYA* on the initiative of THE OPTICAL SOCIETY OF AMERICA, INC. with a grant-in-aid from THE NATIONAL SCIENCE FOUNDATION. *Optics and Spectroscopy* is a cover-to-cover translation of *Optika i Spektroskopiya* and no attempt is made to edit the material other than to correct obvious misprints. The views are those of the original authors and do not represent the Optical Society of America.

TRANSLATION EDITORIAL STAFF

Scientific Editors

CYRUS FELDMAN, *Oak Ridge National Laboratory*

CARL W. GARLAND, *Massachusetts Institute of Technology*

MATHEW G. GIBBONS, *Oakland, California*

Administrative Editor: PATRICIA R. WAKELING, *OSA*

Published monthly by the Optical Society of America, Inc. Executive office: 1155 Sixteenth Street, N.W., Washington, D.C. Subscriptions for one year to members of the Society: Associates $13.00; Regular members and Fellows $17.00. Subscriptions for non-members of the Society: One year U. S. and Possessions, $25.00; Foreign $28.00. Back numbers: $3.00 per copy. Subscriptions, changes of address and undeliverable copies should be referred to the Executive offices in Washington, D.C. The office of publication is 2500 South State Street, Ann Arbor, Michigan. Second class postage paid at Ann Arbor, Michigan.

Printed in the U.S.A. by Edwards Brothers, Inc., Ann Arbor, Michigan.

THE MEASUREMENT OF THE ABSOLUTE VALUES OF OSCILLATOR STRENGTHS IN ATOMIC SPECTRA
I. Sodium

Yu. I. Ostrovskii and N. P. Penkin (pp. 3-11)

Received 20 July 1960

A method of determining the absolute values of f-numbers is given. It is based on the simultaneous measurements of absorption and dispersion. A setup is described for photoelectrically recording the equivalent width of an absorption line. Formula are derived for calculating the wings of a line. The oscillator strength of the yellow doublet of sodium was found to be $f_D = 1.15 \pm 0.03$.

RODUCTION

In 1958, we proposed a new method for measuring absolute values of oscillator strengths.[1] In ref. 1, it hown that by simultaneously measuring the equivalent th A_λ of a line and the distance Δ between the hooks he same line, it is possible to determine the damping stant γ from the formula

$$\gamma = \frac{c}{\pi k(\lambda)\lambda_{ik}}\left(\frac{A_\lambda}{\Delta}\right)^2, \qquad (1)$$

re c is the velocity of light, λ_{ik} is the wavelength of line, and $k(\lambda)$ is the constant of the hook method, as rmined by the thickness and the index of refraction of plate which is introduced into the interferometer to n the hooks.

The value of γ is determined by the lifetime of the er and lower levels corresponding to the spectral , and also by the coefficient of collision damping $\gamma_{coll.}$:

$$\gamma = \frac{1}{\tau_i} + \frac{1}{\tau_k} + \gamma_{coll.}. \qquad (2)$$

In a transition to the normal or metastable state $\to\infty$) when line-broadening collisions are absent oll. $= 0$), we have

$$\gamma = \frac{1}{\tau_i} = \sum_k A_{ik}. \qquad (3)$$

e A_{ik} is the Einstein coefficient of spontaneous ission.

When only one transition to a lower state k is posle from a given upper level i, then (1) and (3), along h the well-known relationship between the oscillator ength f and the probability of transition A_{ik}, give[2]

$$f_{ki} = \frac{g_i}{g_k}\frac{mc^2\lambda_{ik}}{32\pi^3e^2k(\lambda)}\left(\frac{A_\lambda}{\Delta}\right)^2. \qquad (4)$$

If the sum in formula (3) is composed of several ms, then in order to calculate the absolute value of it is necessary to know the relative f-numbers of all nsitions from the given upper level i to lower levels.

Thus, by simultaneously measuring the total abrption and the hooks of a line, it is possible to obtain absolute value of the oscillator strength. It must be ed that in deriving formula (1), we did not make any sumptions about the temperature and density distribun of the vapor along the absorption tube. Therefore, heterogeneity of the vapor column does not affect the sults of the measurements. However, it is necessary t the following conditions be satisfied:

1. The Nfl value must be large enough to satisfy formula (1), which is valid only when the line profile is determined by a single damping collision. In this case

$$Nfl\gamma = \frac{mc^3}{e^2\lambda^2}A_\lambda^2. \qquad (5)$$

This condition determines the lower limit of the optical thickness of the layer (Nfl). These values are essential for performing these measurements. According to van der Held (see ref. 2), formula (5) is satisfied when $A_\lambda/\Delta\lambda_D \geq 10$. For smaller A_λ the basic premises of the method are violated. In this range of optical thicknesses, both damping and Doppler broadening occur, so that A_λ decreases with decreasing Nfl much more slowly than formula (5) requires. We thus obtain high f values, which increase rapidly as the optical thickness of the layer decreases (Fig. 4).

2. The concentration N of the investigated atoms and the pressure of residual gases must be fairly low in order to make the term $\gamma_{coll.}$ in formula (2) negligible. The Lorentz broadening of a line is easily eliminated by evacuating the tube to a pressure of a few microns. The Holtsmark broadening determines the upper limit of Nfl values (for a given l) at which the method gives a correct value of f. After this limit is reached, it is possible to increase the optical thickness of the vapor column only by increasing the length of the tube. The effect of Holtsmark broadening, as follows from formula (2), is to increase the measured values of f (Fig. 4).

Thus, the lower limit of applicability of the method is determined by the value of Nfl, which depends on the oven temperature and the atomic weight of the element under investigation. The upper limit of applicability of the method can be moved in the direction of large Nfl values by increasing the length of the tube. In ref. 1 it is shown that a 50-60 cm tube is sufficient for the application of the method to the resonance lines of alkaline earth atoms over a wide range of optical thicknesses. We also measured the f-numbers of the resonance lines of MgI, CaI, SrI, and BaI.

METHOD FOR MEASURING THE EQUIVALENT WIDTH OF A LINE

We measured A_λ (see ref. 1) by photographic photometry. These measurements are very time-consuming, because they require point-by-point planimetry of the profile of a line. Apart from this, it is scarcely possi-

ble to measure A_λ by this method with an accuracy better than 5%, which leads to an error of 10% in the value of f. In the present investigation we therefore changed to a photoelectric method of recording the equivalent width of a line.

In principle, the following methods of photoelectric recording of A_λ are possible:

1. Scanning the spectrum and recording the absorption line profile, then measuring the profile. The disadvantages of this method are: (a) the time-consuming reduction of recordings which do not permit the application of this method to a large number of measurements: (b) the necessity of using narrow monochromator slits to provide sufficient resolution of the profile of the line. This reduces the light output of the system, thereby leading to an unfavorable signal-to-noise ratio.

2. The main features of the second method, which is free from the above disadvantages, are evident from the following. The equivalent width of a line can be defined in the following manner:

$$A_\lambda = \int_{\lambda_0-\frac{\Delta\lambda}{2}}^{\lambda_0+\frac{\Delta\lambda}{2}} \frac{I_{\lambda 0} - I_\lambda}{I_{\lambda 0}}\, d\lambda, \qquad (6)$$

where $\Delta\lambda$ is a fairly large interval of wavelengths taken symmetrically with respect to the center of the line; $I_{\lambda 0}$ is the intensity of radiation of wavelength λ_0 entering the absorption tube; I_λ is the intensity of the same radiation leaving the tube.

Assuming the intensity of the background $I_{\lambda 0}$ to be constant within the limits of integration, we obtain

$$A_\lambda = \Delta\lambda \left[\frac{I_{\lambda 0}\Delta\lambda - \int_{\lambda_0-\frac{\Delta\lambda}{2}}^{\lambda_0+\frac{\Delta\lambda}{2}} I_\lambda d\lambda}{I_{\lambda 0}\Delta\lambda} \right] = \Delta\lambda \frac{I_1 - I_2}{I_1}. \qquad (7)$$

When a beam covering the spectral range $\Delta\lambda$ leaves the monochromator and strikes the photoelectric detector, and the absorbing vapor column is absent, we register a photocurrent which is equal* to $I_1 = I_{\lambda 0}\Delta\lambda$. Introducing a column of absorbing vapors into the path of the light beam, we obtain a photocurrent equal to

$$I_2 = \int_{\lambda_0-\frac{\Delta\lambda}{2}}^{\lambda_0+\frac{\Delta\lambda}{2}} I_\lambda d\lambda.$$

From these two readings, it is possible to obtain A_λ directly. Moreover, since the exit slit of the monochromator must be very wide, an apparatus based on this principle appears to have much more optical speed than the setup based on the first principle. For this reason, we have chosen the second method, which we will hereinafter call the "wide slit" method. An apparatus for measuring A_λ was constructed in accordance with the above principles.

*Except for a constant factor which is determined by the parameters of the recording system.

CALCULATION OF THE LINE WINGS

Since the difference of two photocurrents enters into expression (7) for measuring A_λ, it is necessary that this difference be fairly large. Otherwise, the relative erro of measurement of this difference will greatly exceed t relative error of the individual readings, and the accuracy of the measurement of A_λ will decrease appreciab This accuracy can be increased by narrowing the exit s of the monochromator, for at any given A_λ, the differen of the readings is inversely proportional to $\Delta\lambda$. But the wings of the absorption line will not be included in the calculations, and this will introduce a certain systemat error in the measurements. In this paragraph, the prob lem of calculating this error is discussed. Since the wings of a line must be considered in any method of recording A_λ, this discussion is applicable not only to the "wide slit" method, but to all other methods of measuring A_λ as well.

(a) General Relationships. For large Nfl values, th profile of an absorption line is determined by the follow ing value of the coefficient of absorption:[2]

$$k(\omega) = \frac{k_0 a N f \Delta\omega_D^2}{2\sqrt{\pi}\,\omega^2}.$$

k_0 is the absorption coefficient for one oscillator, $a = \gamma/\Delta\omega_D$, ω is the cyclical frequency measured from the center of the line, and $\Delta\omega_D$ is the Doppler half-wid of the line.

Then, according to (6),

$$A_\lambda = \frac{\lambda^2}{2\pi c} \int \left[1 - e^{-\frac{k_0 a N f l \Delta\omega_D^2}{2\sqrt{\pi}\,\omega^2}} \right] d\omega.$$

Integration of this expression leads to the formula (see ref. 2)

$$A_\lambda = \frac{\lambda^2 \Delta\omega_D}{\pi c} \sqrt{\frac{\sqrt{\pi}}{2} k_0 a N f l}.$$

Considering this, we can write the profile of the line determined from Eq. (8) in the form

$$I_\omega = I_{\omega 0} e^{-\frac{A_\omega^2}{4\pi\omega^2}},$$

where

$$A_\omega = \frac{2\pi c}{\lambda^2} A_\lambda.$$

Although the measured equivalent width of a line should not depend on the instrumental profile of the recording instrument, the corrections for the influence o the wings will depend on instrumental distortion. In ac cordance with this, we must distinguish among three methods of recording:

1. Photographic photometry of lines, using a narrow slit microphotometer. In this case, the instrument profile is a rectangle $2\Delta\omega$ wide ($\Delta\omega$ is the spectral ha width of the entrance slit of the spectrograph).* From normalization conditions, the height of the rectangle is $\frac{1}{2}\Delta\omega$.

*The spectrograph is assumed to have a high resolving power. The width of the slit is several times larger th the normal.

2. The method of photoelectric recording and sca ning. The monochromator's slits are of equal width. T instrumental profile is a triangle $4\Delta\omega$ wide and $\frac{1}{2}\Delta\omega$ high.

3. The "wide slit" method. The instrumental pro

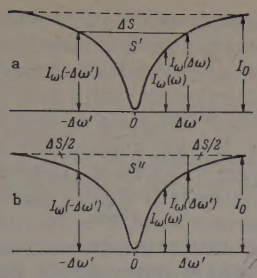

Fig. 1. Diagram for the calculation of wing corrections.

is the same as in the photographic method.

In order to obtain the equivalent widths of lines ng the first two methods in the photometry interval ω', Δω' (Fig. 1,a), the area S' is recorded and then ided by $I_\omega(\Delta\omega')$, since the intensity becomes equal to continuous background at Δω', and instead of the true ue

$$A_\omega = \frac{S}{I_0} \tag{13}$$

record

$$A'_\omega = \frac{S'}{I_\omega(\Delta\omega')}. \tag{14}$$

When recording by the "wide slit" method (Fig. 1,b), errors in the determination of the background inten- y do not enter the calculation, and consequently, the corded area S'' corresponds to the measured equivalent idth

$$A''_\omega = \frac{S''}{I_0}. \tag{15}$$

(b) Photographic Recording As seen from (13), (14), d Fig. 1,a, the relative error in measuring A_ω is

$$\frac{A_\omega - A'_\omega}{A_\omega} = 1 - \frac{I_0}{I_\omega(\Delta\omega')}\left(1 - \frac{\Delta S}{S}\right). \tag{16}$$

assuming $I_0 = 1$

$$\frac{A_\omega - A'_\omega}{A_\omega} = 1 - \frac{1}{I_\omega(\Delta\omega')}\left(1 - \frac{\Delta S}{A\omega}\right). \tag{17}$$

The profile of the absorption line as distorted by e spectrograph is found by integrating the following pression:

$$I_\omega(\omega) = \frac{1}{2\Delta\omega}\int_{-\Delta\omega}^{\Delta\omega} e^{-\frac{A_\omega^2}{4\pi(\omega+\omega')^2}}\, d\omega'. \tag{18}$$

Expanding the integrand as a series and taking only e first two terms, we have

$$I_\omega(\omega) = 1 - \frac{A_\omega^2}{4\pi}\left(\frac{1}{\omega^2 - \Delta\omega^2}\right). \tag{19}$$

The value of ΔS can be found from the expression ig. 1,a)

$$\Delta S = 2\int_{\Delta\omega'}^{\infty} [1 - I_\omega(\omega)]\, d\omega + 2\Delta\omega'[1 - I_\omega(\Delta\omega')]. \tag{20}$$

Substituting $I_\omega(\omega)$ and $I_\omega(\Delta\omega')$ from (19), we obtain

$$\Delta S = \frac{A_\omega^2}{\pi\Delta\omega'}\left[1 + \frac{2}{3}\left(\frac{\Delta\omega}{\Delta\omega'}\right)^2 + \frac{3}{5}\left(\frac{\Delta\omega}{\Delta\omega'}\right)^4\right]. \tag{21}$$

Taking ΔS and $I_\omega(\Delta\omega')$ from (21) and (19) and substituting into (17), we obtain

$$\frac{A_\omega - A'_\omega}{A_\omega} = \frac{1}{\pi k}\left[1 + \frac{2}{3}l^2 + \frac{3}{5}l^4 - \frac{1}{4k}(1 + l^2) + \frac{1}{4\pi k^2}\right], \tag{22}$$

where $k = \Delta\omega'/A_\omega$ and $l = \Delta\omega/\Delta\omega'$.

It must be noted that the series expansion terms which we neglected at various stages in the derivation of formula (22) do not contribute appreciably to the magnitude of $(A_\omega - A'_\omega)/A_\omega$. For example, for $k \geq 1.5$ and $l \leq 1/3$ (which is always easy to achieve) formula (22) permits the calculation of $(A_\omega - A'_\omega)/A_\omega$ with an accuracy better than 2%, which leads to an error of about 0.5% in the value of A_ω, corrected for wings.

(c) Photoelectric Recording and Scanning. Since in this case, the derivation is very similar to the one given above, we will only write the final results:

$$\frac{A_\omega - A'_\omega}{A_\omega} = \frac{1}{\pi k}\left[1 + \frac{4}{3}l^2 + \frac{16}{5}l^4 + \frac{64}{7}l^6 - \frac{1}{4k}(1 + 2l^2) + \frac{1}{4\pi k^2}\right]. \tag{23}$$

(d) The "Wide Slit" Method. As seen from (15) and Fig. 1,b, and assuming that $I_0 = 1$, we obtain

$$\frac{A_\omega - A''_\omega}{A_\omega} = \frac{1}{\Delta\omega A_\omega}\int_{-\Delta\omega}^{\Delta\omega}\left[\int_{\Delta\omega'}^{\infty}\left(1 - e^{-\frac{A_\omega^2}{4\pi(\omega+\omega')^2}}\right)d\omega\right]d\omega'. \tag{24}$$

Integrating and neglecting the higher order terms in the expansion, we obtain

$$\frac{A_\omega - A''_\omega}{A_\omega} = \frac{1}{2\pi k}\left[1 - \frac{1}{24\pi k^2} + \frac{1}{3}l^2 + \frac{1}{5}l^4\right]. \tag{25}$$

We note that the neglected terms in this case introduce a substantially smaller contribution to $(A_\omega - A''_\omega)/A_\omega$ than for formulas (22) and (23). Under conditions similar to the previous ($k \geq 1.5$, $l \leq 1/3$), formula (25) permits the calculation of A_ω from the measured value A''_ω with an accuracy better than 0.2%.

Thus, formulas (22), (23), and (25) permit a very accurate calculation of the wings while using various methods of recording the equivalent widths of lines. For approximate evaluations (with an accuracy of up to several percent), the values in brackets in formulas (22), (23), and (25) can be equated to one.

The necessity of considering the wings when measuring the equivalent width of a line has already been noted by Minnaert.[3] Unfortunately, his calculations from photographic recordings (without correcting for instrumental distortion) contain an error, which in the final calculations leads to the absence of the second term in Eq. (20). Therefore, Minnaert's final results are not useful even for approximate evaluations.

EQUIPMENT

The layout of the optical equipment is given in Fig. 2. The light from the continuous spectrum source S (a projection lamp fed by a battery) passed through lens L_1 and fell on the semitransparent mirror A of the Rozhdestvenskii interferometer as a parallel beam. A cell containing sodium vapor was placed in the path of one of the interfering beams (CB). The other beam (AD)

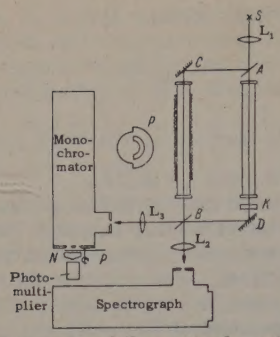

Fig. 2. Diagram of the optical equipment.

passed through an evacuated tube of the same length, sealed in the same way as the cell, namely, with plane-parallel quartz windows. To form the hooks, a plane-parallel plate (K) was inserted across this beam. The interference pattern formed by beams (DBL_2) and (CBL_2) was focused on the slit of the spectrograph by an achromatic lens (L_2).

A spectrograph with a plane diffraction grating and a concave mirror (1200 lines per mm, total 10^5 lines, F = 2000 mm) was used for photographing the hooks.

The other pair of interfering beams (DBL_3) and (CBL_3) fell on the slit of the monochromator which recorded the magnitude of A_λ.

The interferometer's semitransparent mirrors (A and B) had a reflection coefficient of about 85% and transmitted about 3% of the incident light at an angle of 45°. This insured almost complete extinction of the beam ($ADBL_3$) whose influence on the measurement of A_λ is equivalent to that of scattered light. The intensity of this beam was less than 0.15% of the intensity of the beam ($ACBL_3$). It is very essential to mention a great gain in the intensity of the useful beam ($ACBL_3$), which was 3 to 4 times greater than the intensity of the corresponding beam in an "ideal" interferometer having reflection and transmission coefficients of 45%. This was achieved at the cost of a tenfold loss of light in the interference pattern, but it did not cause any difficulties. Since the intensities of the beams (DBL_2) and (CBL_2) were equal, the contrast of the interference fringes remained at its maximum.

The abovedescribed arrangement permitted us to measure the absorption and the dispersion simultaneously, and not alternately (as was done in a previous work[1]). This made it unnecessary to stabilize conditions in the absorbing vapor column.

The monochromator is very similar to the above-described spectrograph. A set of double slits was placed at its exit. The slits were arranged 10 mm apart along the spectrum. The set contained 10 pairs of slits having widths from 1.5 to 0.1 mm. Depending on the magnitude of the absorption, one pair of slits was moved so as to obtain $1.5 \leq k \leq 5$. When this condition is fulfilled, the accuracy of the measurements and the calculation of the wing correction, as stated above, are satisfactory.

The region of the spectrum containing the absorption line passed through one of the slits onto the photocathode, and reading I_2 was recorded [see formula (7)]. The region of the continuous spectrum situated 10 mm from the absorption line passed through the other slit, and the value I_1 was recorded. The light was passed through the slits alternately for 7 sec by means of a disk P rotated by a Warren motor. A quartz biprism N directed the beams onto the same spot of the photocathode of the FEU-19. The signal from the photomultiplier was amplified by a dc balancing amplifier using two 6ZhIP tubes, in accordance with the circuit given in ref. 4. The drift of the amplifier does not exceed 0.1μa/hr, which is about one five-hundredth of full scale on an EPP-09 recorder (τ = 1 sec, 10 mv, R = 200 ohms). The amplifier appears to be linear between 0 and 75μa. Therefore, it can be assumed that the nonlinearity did not exceed 0.2%. The current amplification was about 10^3. The time constant was 0.5 sec. No fluctuation of the dark current was detected at the operating voltage (900 volts) of the photoelectric multiplier. The signal-to-noise ratio was greater than 500.

When the signal was recorded in the absence of the absorbing vapor column, the pen of the recorder traced a step-curve due to the unevenness in the width of the slits, and also to the selectivity of the light source and the photoelectric multiplier FEU (Fig. 3,a). This intensity ratio (α) was carefully measured for each pair of slits and was considered in subsequent calculations. When the oven was heated and the absorption line formed one of the beams became weaker and the other remained unchanged (Fig. 3,b).

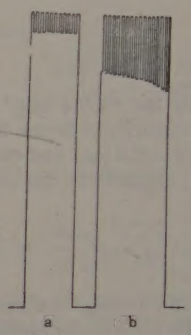

Fig. 3. Recording: a—when the absorbing vapor is absent; b—when the oven is heated and the absorption lines appear.

PROCESSING OF THE RESULTS; ERROR OF MEASUREMENT

The value of A_λ was calculated from the formula

$$A_\lambda = \Delta\lambda \left(1 - \frac{I_2}{I_1}\alpha\right), \qquad (26$$

where α is the accurately measured value of I_1/I_2 when the absorption vapor column is absent. The corrections for wings were introduced by Eq. (25) which was solved for A_λ.*

*Using Eq. (12), it is easy to find a similar expression for A_λ.

An IZA-2 comparator was used for measuring the hooks of absorption lines. The calculations were corrected for the effects of dispersion near neighboring lines on the position of the hooks.[5]

The value of f was calculated from formula (4).

The error in the determination of f depends on the following measuring errors: (1) the error in measuring the distance between hooks; (2) the error in measuring the tracings; (3) the inaccuracy in determining the exit slit width $\Delta\lambda$; (4) the error in calculating the wings; (5) the presence of scattered light in the monochromator

the influence of the beam ADBL$_3$ (Fig. 2) and the grating sts; (6) the nonlinearity of the recording system.

Let us investigate these errors individually.

1. The error in measuring distances between hooks ally does not exceed 1%. Only in the case of very weak persion can this error be greater, but this region of ical thicknesses generally does not satisfy the conditions required by the method.

2. The error in the measurement of the tracings can ount to 0.5 mm. This is about 0.2% of the usual value he reading, which is 200-250 mm.

3. As was indicated above, the accuracy in the calation of the wings using formula (25) at the optimum width, corresponding to k = 1.5-5, is better than 0.2%.

4. The width of the exit slit of the monochromator s measured with a microscope to an accuracy of one cron. For the slits generally used, this is less than %.

5. Glass filters were used to reduce the amount of ttered light in the instrument. For the yellow doublet sodium, an OS-13 filter was placed in front of the slit the monochromator. This filter cut off all of the short welength region of the spectrum up to 5700 A. In the ger wavelength region of the spectrum, the sensitivity the photocathode rapidly decreases and no filter was cessary. The amount of scattered light was measured the 2500 A region. Without the filter, the signal ounted to less than 1/500 of the signal in the 5890 A gion. When the filter was put in, the signal disappeared the 2500 A region.

The grating ghosts, which in general greatly influe- e A_λ measurements, were negligibly small for our cially selected grating. They were about 0.05% as in- se as the line, and the error which they introduced into measurement of A_λ was therefore of the same order.

The other interfering beam was discussed above. Its luence does not exceed 0.2%.

6. There is apparently no doubt about the linearity the photomultiplier for photocurrents which do not eed 0.1μa.[6] The remaining parts of the apparatus are ear to within 0.2%.

The errors enumerated in 1 and 2 appear at random. cording to the above statements, the random error of individual measurement should not exceed 5-6%. When arge number of measurements (100-200) is made, the luence of these errors is small.

Errors 5 and 6 are systematic. Their total effect on measurement of f does not exceed 0.5-0.6%.

Errors 3 and 4 are mixed in nature. They appear stematic for a small group of measurements performed h the same slit and at neighboring values of A_λ. For ge variations of A_λ, they appear at random.

According to the statements in this paragraph, it can concluded that the systematic errors in the measurent of f do not exceed 0.7-1%. The random error of an dividual measurement does not exceed 5-6%.

EASUREMENT OF THE ABSOLUTE VALUE OF THE OSCILLATOR STRENGTH OF THE YELLOW DOUBLET OF SODIUM

The sodium vapor column was obtained from sodium tal placed in a quartz tube, which was then evacuated a mercury diffusion pump. The tube was heated by a King oven 65 cm long. The hooks and the absorption were measured for the short wavelength component of the doublet. The hooks were photographed in the second order (dispersion was about 1.7 A/mm) with an exposure of 40 sec. During this time, five readings were recorded, two of the line and three of the background. About 200 exposures were obtained. The results are shown in Fig. 4. The abscissae represent values of Nfl and the ordinates give measured values of f. As seen from Fig. 4, the conditions for which the method is valid encompass only a small interval of optical thicknesses. The 74 points between Nfl = 3.5×10^{14} and Nfl = 8.6×10^{14}, give

$$f_{5890} = 0.764(\pm 0.3\%).$$

The root mean square error is given in parentheses. However, correcting for the possible systematic errors discussed above, the value can be calculated to be

$$f_{5890} = 0.76 \pm 0.02.$$

Since the ratio[7,8] $f_{5890}/f_{5896} = 1.98 \pm 0.01$, for the entire doublet we have

$$f_D = 1.15 \pm 0.03.$$

Our program for further measurements consists of the determination of the absolute values of the oscillator strengths for the resonance lines of the alkali metals (Li, K, Rb, Cs), and also the improvement of the accuracy of the f-numbers obtained in ref. 1 for the resonance lines of the alkaline earth atoms (Mg, Ca, Sr, Ba).

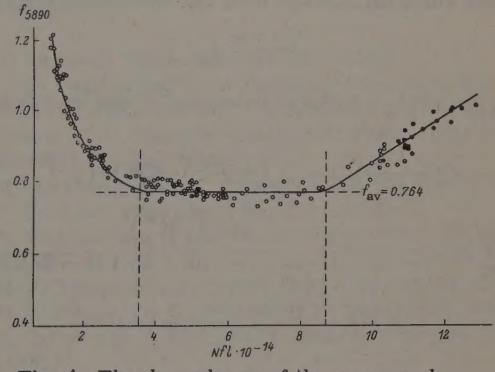

Fig. 4. The dependence of the measured f-numbers on the optical thickness.

REFERENCES

1. Yu. I. Ostrovskii, N. P. Penkin, and L. N. Shabanova, Doklady Akad. Nauk SSSR 120, 66 (1958), Soviet-Phys.-Doklady 3, 538 (1958).
2. A. Unsöld, "Physics of Stellar Atmospheres." Izd. Inostrannoi Lit., Moscow, 1949.
3. M. Minnaert, Z. Astrophys. 10, 40 (1935).
4. V. I. Moroz, Astron. Zhur. 33, 717 (1956).
5. D. S. Rozhdestvenskii, "Simple Relations in the Spectra of Alkali Metals." SPb., 1915; "Works on the Anomalous Dispersion." Izd. Akad. Nauk SSSR, Moscow-Leningrad, 1952.
6. N. O. Chechik, S. M. Fainshtein, and T. M. Lifshits, "Electron Multipliers." Moscow, 1954.
7. D. S. Rozhdestvenskii, Zhur. Russ. Fiz.-Khim. Obshchestva 7, 1 (1912).
8. G. S. Kvater, Vestnik Leningrad. Gosudarst. Univ. No. 2, 135 (1947).

THE EFFECT OF VIBRATION ON HYPERFINE STRUCTURE CONSTANTS

A. G. Makhanek (pp. 12-15)

Received 7 June 1960

A simple equation has been derived for calculating $\langle[(r - r_e)/r_e]^n\rangle_v$, which is the basis of the calculation of the effect of vibrations on hyperfine structure constants. Calculations have been carried out for diatomic molecules described by a Morse potential. Several numerical results are given.

When microwave spectroscopy is applied to high precision molecular studies, allowance must be made for the effect of vibrations and centrifugal stretching of the molecules on the constants of the electrical and magnetic interactions of the nucleus with the electron shells. This is necessary both for the interpretation of the experimental results and for a better understanding of the properties of the electron shells of the molecules and the nature of the chemical bond.

Allowing for the effect of vibration and centrifugal perturbations enables us to find the appropriate corrections in nuclear spin-spin magnetic interaction, in spin-rotational magnetic interaction, in calculating the magnetic shielding of the nucleus, etc. As Ramsey[1] has shown, calculating the effect of vibrations on the hyperfine structure constants for a diatomic molecule reduces to evaluating the following average over the vibrational states:

$$\left\langle\left(\frac{r-r_e}{r_e}\right)^n\right\rangle_v. \qquad (1)$$

In the case of a Morse potential,[2] it can be shown that:

$$\left\langle\left(\frac{r-r_e}{r_e}\right)^n\right\rangle_v = \int_{-\infty}^{+\infty}\left(\frac{r-r_e}{r_e}\right)^n \Psi_v^2 dr = \left(\frac{1}{r_e}\right)^n \times \sum_{i=0}^{v}\sum_{j=0}^{v} N_v^2 \frac{(-1)^{i+j}\binom{v}{i}\binom{v}{j}}{(k-2v)\ldots(k-2v+i-1)(k-2v)\ldots(k-2v+j-1)} \times\left[\frac{1}{2a}\ln k + \frac{d}{dv}\right]^n \Gamma(k-2v+i+j-1), \qquad (2)$$

where

$$\Psi_v(z) = N_v e^{-\frac{z}{2}} z^{\frac{1}{2}(k-2v-1)} F_v(z),$$

$$N_v^2 = \frac{(k-v-1)(k-v-2)\ldots(k-2v)}{v!\,\Gamma(k-2v-1)}\, a,$$

$$F_v = \sum_{i=0}^{v} \frac{(-1)^i\binom{v}{i} z^i}{(k-2v)(k-2v+1)\ldots(k-2v+i-1)},$$

$$z = k e^{-a(r-r_e)},$$

$$\frac{1}{k} = \left(\frac{B_e}{\omega_e}\right)(ar_e)^2.$$

However, the complexity of Eq. (2) makes it unsuitable for practical computation.

Starting from the following expression, the calculation of $\langle[(r - r_e)/r_e]^n\rangle_v$ can be considerably simplified:

$$\int_{-\infty}^{+\infty}\left(\frac{r-r_e}{r_e}\right)^n \Psi_v^2(r)\,dr = \int_0^{\infty}\frac{1}{za}\left[-\frac{1}{ar_e}\times\ln\left(\frac{z}{k}\right)\right]^n \Psi_v^2\,dz. \qquad (3)$$

Expanding $\log(z/k)$ in a series about the point $z/k = 1$ (that is, $r = r_e$) we obtain:

$$\ln\left(\frac{z}{k}\right) = \frac{z-k}{k} - \frac{1}{2}\left(\frac{z-k}{k}\right)^2 + \frac{1}{3}\left(\frac{z-k}{k}\right)^3 - \frac{1}{4}\left(\frac{z-k}{k}\right)^4 + \frac{1}{5}\left(\frac{z-k}{k}\right)^5 - \frac{1}{6}\left(\frac{z-k}{k}\right)^6 + \ldots \qquad (4)$$

If we now raise the series in Eq. (4) to the n-th degree and integrate, then with accuracy up to terms containing $1/k^3$, $\langle[(r - r_e)/r_e]^n\rangle_v$ may be expressed in the simple form:

$$\left\langle\left(\frac{r-r_e}{r_e}\right)^n\right\rangle_v = \left(\frac{1}{ar_e}\right)^n\left[\frac{av+\alpha_1}{k} + \frac{\beta v(v+1)+\beta_1}{k^2} + \frac{\gamma v(v+1)(v+2)+\gamma_1 v(v+1)(2v+1)+\gamma_2 v(v-1)(2v-1)+\gamma_3}{k^3}\right] \qquad (5)$$

where α, α_1, β, β_1, γ, γ_1, γ_2, and γ_3 are numerical constants independent of the nature of the molecule or of the vibrational quantum number (see the Table).* The quantity $1/k$ for different molecules is a number of the order of 0.01 to 0.001, and it is therefore obvious that Eq. (5) gives considerable accuracy for the low vibrational levels at which the hyperfine structure is usually measured. However, the above averaging can be applied to high vibrational levels also, since series (4) converges in the interval $0 < z/k \leq 2$ or $0 < e^{-a(r-r_e)} \leq 2$, that is, over the entire region bounded by the potential curve where the wave function is not essentially zero. The accuracy obtained from Eq. (5) depends greatly on the error in the value of the anharmonicity parameter (ar_e).

*In the case $v = 0$, Eq. (5) reduces to that given in ref. 1. Calculating the nondiagonal terms by a similar method, we obtain equations which easily reduce to those obtained in refs. 5, 7, and 8.

n	α	α_1	β	β_1	γ	γ_1	γ_2	γ_3
1	3	3/2	7/2	13/12	11/6	1	1/2	1
2	2	1	23/2	15/4	323/36	89/18	13/6	65/12
3	0	0	15	11/2	193/8	151/12	29/6	131/8
4	0	0	6	3	239/6	50/3	6	61/2
5	0	0	0	0	75/2	25/3	10/3	65/2
6	0	0	0	0	15	0	0	15

For example, calculating $\langle 1/r^2\rangle_v$ with an anharmonicity constant $ar_v = 1.5$, for the hydrogen molecule we obtain*:

*Calculating these quantities using only the first term of Eq. (5), containing $1/k$, gives the values:

$$\left\langle\frac{1}{r^2}\right\rangle_{v=2} = \frac{1}{r_e^2}(1 - 0.1038),$$

$$\left\langle\frac{1}{r^2}\right\rangle_{v=4} = \frac{1}{r_e^2}(1 - 0.1868), \qquad \left\langle\frac{1}{r^2}\right\rangle_{v=} = \frac{1}{r^2}(1 - 0.2698).$$

$$\left\langle \frac{1}{r^2} \right\rangle_{v=2} = \left(\frac{1}{r_e^2} \right)(1 - 0.1090),$$

$$\left\langle \frac{1}{r^2} \right\rangle_{v=4} = \left(\frac{1}{r_e^2} \right)(1 - 0.2096),$$

$$\left(\frac{1}{r^2} \right)_{v=6} = \left(\frac{1}{r_e^2} \right)(1 - 0.3179).$$

The experimental values of these quantities are[3]:

$$\left\langle \frac{1}{r^2} \right\rangle_{v=2} = \frac{1}{r_e^2}(1 - 0.1205),$$

$$\left\langle \frac{1}{r^2} \right\rangle_{v=4} = \frac{1}{r_e^2}(1 - 0.2134),$$

$$\left\langle \frac{1}{r^2} \right\rangle_{v=6} = \frac{1}{r_e^2}(1 - 0.3033).$$

The large relative error for v = 2 (~ 10%) and the nsiderably lower error for v = 4 (1.9%) are explained the fact that the anharmonicity constant $ar_v = 1.5$, de-mined from the dissociation energy of the molecule, ntains a larger error for the second vibrational level. these cases the anharmonicity constant should be cor-cted by comparing the expansion of the Morse poten-l with Dunham's potential,[4] which leads to the expres-on $ar_e \simeq 1 + (\alpha_e \omega_e / 6B_e^2)$. Calculating $\langle 1/r^2 \rangle_{v=2}$ from . (5) with a corrected anharmonicity constant for the molecule, we obtain:

$$\left\langle \frac{1}{r^2} \right\rangle_{v=2} = \frac{1}{r_e^2}(1 - 0.027799).$$

The experimental value of $\langle 1/r^2 \rangle_{v=2}$ is:[5]

$$\left\langle \frac{1}{r^2} \right\rangle_{v=2} = \frac{1}{r_e^2}(1 - 0.027708).$$

Equation (5) shows in particular that the hyperfine ructure constants should show a fairly accurately linear pendence on v for vibrational levels that are not too gh; this is usually found experimentally. For example, in treating the variation of the nuclear quadrupole in-raction constants (eqQ) with the vibrations of the dia-mic molecules, we assume that the field gradient q at e location of the nucleus of one of the atoms is a func-tion of the interatomic distance of the form:

$$q(r) = q_0 + q_1\xi + q_2\xi^2 + \ldots, \qquad (6)$$

where $\xi = (r - r_e)/r_e$, then averaging q(r) with accuracy up to terms containing 1/k we obtain:

$$\langle q \rangle_v = q_0 + \left[3q_1 \left(\frac{B_e}{\omega_e} \right) ar_e + 2q_2 \left(\frac{B_e}{\omega_e} \right) \right] \left(v + \frac{1}{2} \right). \qquad (7)$$

If we replace ar_e in Eq. (7) by $1 + (\alpha_e \omega_e / 6B_e^2)$, the variation of the nuclear quadrupole interaction constant of the atom with the vibrational number v is expressed as follows:

$$\langle eqQ \rangle_v = eQq_0 + eQ \left[3q_1 \left(\frac{B_e}{\omega_e} \right) \left(1 + \frac{\alpha_e \omega_e}{6B_e^2} \right) + 2q_2 \left(\frac{B_e}{\omega_e} \right) \right] \left(v + \frac{1}{2} \right). \qquad (8)$$

Equation (8) is identical with the equation obtained in ref. 6 by averaging Eq. (6) using the potential:

$$V(r) = a_0\xi^2 + a_1\xi^3 + a_2\xi^4.$$

The linear relation (8) found in ref. 6 explains the asymmetrical line shape for the quadrupole interaction in several molecules, for example, $TlCl^{35}$, $TlCl^{37}$, $Na^{23}F$, etc.

The author thanks M. A. El'yashevich for his interest in this work and for his valuable advice.

REFERENCES

1. N. Ramsey, Phys. Rev. **87**, 1075 (1952).
2. L. D. Landau and E. M. Lifshits, "Quantum Mechanics: Nonrelativistic Theory." Gosudarst. Izd. Tekh.-Teoret. Lit., Moscow-Leningrad, 1948. Addison Wesley, Reading, Mass., 1958.
3. G. Herzberg, Can. J. Research. **28**, 144 (1950).
4. J. Dunham, Phys. Rev. **41**, 713 (1932).
5. R. Herman and K. Shuler, J. Chem. Phys. **22**, 481 (1954).
6. H. J. Zeiger and D. Bolef, Phys. Rev. **85**, 789 (1952).
7. H. S. Heaps and G. Herzberg, Z. Physik **133**, 48 (1952).
8. L. Infeld and T. Hull, Revs. Modern Phys. **23**, 21 (1951).

HAVE YOU SENT IN YOUR SUBSCRIPTION FOR NEXT YEAR? – SEE ORDER CARD IN THIS ISSUE.

Filler Material – Not in Russian original.

QUANTUM EFFECTS IN A DOUBLE POTENTIAL WELL AND SPECTROSCOPY OF THE HYDROGEN BOND

E. A. Pshenichnov and N. D. Sokolov (pp. 16-23)

Received 22 July 1960

The quantum effects in a double potential well are investigated by a quasi-classical method applied in the region near the top of the potential barrier. The model examined enables one to interpret certain regularities in the spectra of the hydrogen bond.

INTRODUCTION

The possibility of the existence of two minima in the potential energy curve of the hydrogen bond has already been discussed more than once in the literature.[1-6] This concept has been introduced for the purpose of elucidating the cause of the appearance of two absorption maxima in the vibrational spectra of the hydrogen bond. The splitting of the vibrational energy levels of the proton brought about by the presence of two potential wells separated by a low barrier explains this peculiarity of the spectra in a natural way. Calculation of the energy levels in such a double potential well presents great mathematical difficulties in the general case, even for a one-dimensional model. A symmetrical double well is relatively more amenable to calculation.[7,8] The calculation of an unsymmetrical well, however, is considerably more interesting. Blinc and Hadži[2] carried out some computations for this case, representing the wave function of the proton as a linear combination of the wave functions of two harmonic oscillators, each of which corresponded to its respective potential well.

In the present work, a quasi-classical method, applied in the region near the top of the potential barrier, is proposed for the solution of the problem. On the assumption that the potential curve has a parabolic shape in this region, the energy levels of the system can be determined with the help of this method. It has recently been applied to the analysis of quantum effects near the top of the barrier in the case of two symmetric wells, and to certain other problems.[9] The limitations of the results of such calculations are set by the approximate character of both the method itself and the specific form of the potential curve which is chosen as an example in the numerical calculations.

The analysis of the experimental data on the infrared spectra of the hydrogen bond carried out by Barrow and his collaborators[6] shows that in many cases, for example, for sufficiently strong bases BR′, the minimum of the second potential well, which corresponds to the state with the proton near atom B: A—H...B → A⁻...H⁺B, lies above the minimum of the first well by a quantity Q which is less than 2500 $cm^{-1} \simeq 7$ kcal/mole (Fig. 1). This follows from the circumstance that, for sufficiently strong bases (pyridine, triethylamine, etc.), even the first excited energy level of the O—D bond, which lies ~2500 cm^{-1} away from the ground level, is split into two by virtue of "interaction" with the second well.[6] The height of the barrier must be small, since the splitting of the first excited level amounts to 800 cm^{-1} in the case of O—H and 300 cm^{-1} in the case of O—D.

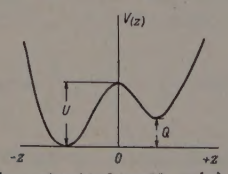

Fig. 1. Double potential well, V(z).

SOLUTION OF THE QUASI-CLASSICAL PROBLEM

Let us denote the mass of the proton by μ and its wave function by ψ. Then the Schrödinger equation for our problem has the form

$$-\frac{\hbar^2}{2\mu}\frac{d^2\psi}{dz^2} + V(z)\psi = E\psi, \tag{1}$$

where $-\infty < z < +\infty$. The origin is taken at the top of the potential barrier, and we suppose that near it

$$V(z) = U\left[1 - \left(\frac{z}{a}\right)^2\right], \tag{2}$$

where U is the barrier height, counted from the deeper minimum of the potential curve (Fig. 1). We introduce the dimensionless quantities

$$\rho = \rho_0 \frac{U - E}{U}, \quad \rho_0 = \frac{1}{\hbar}\frac{a}{2}\sqrt{2\mu U}, \tag{3}$$

$$x = z\left(4\frac{2\mu}{\hbar^2}\frac{U}{a^2}\right)^{1/4}. \tag{4}$$

In these symbols, Eq. (1) takes the form

$$\frac{d^2\psi}{dx^2} + [v(x) - \rho]\psi = 0, \tag{5}$$

while

$$v(x) = \frac{1}{4}x^2 \tag{6}$$

near x = 0. The wave equation with a parabolic barrier has an exact solution.[10] The linearly independent solutions, which are real along the real axis, have the asymptotic form

$$\psi_1(x) \underset{x\to+\infty}{=} \left(\frac{2}{x}\right)^{1/2} e^{\frac{\pi\rho}{2}} [(1 + e^{-2\pi\rho})^{1/2} + 1]^{1/2} \sin[g(x)] \left\{1 + O\left(\frac{1}{x}\right)\right\}, \tag{7a}$$

$$\psi_2(x) \underset{x\to+\infty}{=} \left(\frac{2}{x}\right)^{1/2} e^{\frac{\pi\rho}{2}} [(1 + e^{-2\pi\rho})^{1/2} - 1]^{1/2} \cos[g(x)] \left\{1 + O\left(\frac{1}{x}\right)\right\}, \tag{7b}$$

where

$$g(x) = \frac{1}{4}x^2 - \rho \ln x + \frac{\pi}{4} + \frac{1}{2}\gamma,$$

and

$$\gamma = \arg\Gamma\left(\frac{1}{2} + i\rho\right),$$

ile $\psi_2(-x) = \psi_1(x)$.

From the asymptote of the exact solution for a poten- l having the form of a parabolic barrier, we find the ase of the quasi-classical function outside the barrier, the right and the left of it. This function (and its rivative), far from the points of inflection, follows the asi-classical functions whose phases $(\pi/4)$ may be nd in the usual way[11,12] from the asymptote of the so- ion for a linear potential near the points of inflection and x_4 (Fig. 2). (It is assumed that the potential curve ar the points of inflection x_1 and x_4 may be broken wn into power series beginning with a linear term.)

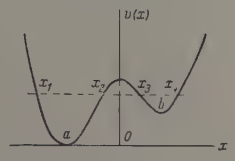

Fig. 2. Double potential well, v(x). x is a dimensionless variable; x_1, x_2, x_3, and x_4 are points of inflection.

e agreement with the quasi-classical functions leads the following equation for the eigenvalues:

$$\tan[\alpha] \cdot \tan[\beta] = \sigma, \tag{8}$$

ere

$$\alpha = \left(n + \frac{1}{2}\right)\pi - \int_{x_1}^{x_2} p\,dx - \frac{1}{2}\left(\gamma - \rho \ln\left|\frac{\rho}{e}\right|\right),$$

$$\beta = \left(k + \frac{1}{2}\right)\pi - \int_{x_3}^{x_4} p\,dx - \frac{1}{2}\left(\gamma - \rho \ln\left|\frac{\rho}{e}\right|\right),$$

$$\sigma = \frac{(1 + e^{-2\pi\rho})^{1/2} - 1}{(1 + e^{-2\pi\rho})^{1/2} + 1},$$

and $k = 0, 1, 2\ldots$; x_1, x_2, x_3, and x_4 are the points of flection, and $p = \sqrt{v(x) - \rho}$. Equation (8) may be trans- med into the form

$$\int_{x_2}^{x_3} p\,dx = \left(n + \frac{1}{2}\right)\pi - \arctan\left\{\sigma \cdot \tan\left[\int_{x_3}^{x_4} p\,dx + \frac{1}{2}\left(\gamma - \rho \ln\left|\frac{\rho}{e}\right|\right)\right]\right\} - \frac{1}{2}\left(\gamma - \rho \ln\left|\frac{\rho}{e}\right|\right). \tag{9}$$

In the symbols abopted by us, $\rho > 0$ corresponds to ergies below the maximum and $\rho < 0$ to energies above e maximum of the barrier. In the particular case of a mmetric potential well, we obtain from (8)

$$\int_{x_1}^{x_2} p\,dx = \left(n + \frac{1}{2}\right)\pi \pm \frac{1}{2}\arctan e^{-\pi\rho} - \frac{1}{2}\left(\gamma - \rho \ln\left|\frac{\rho}{e}\right|\right). \tag{10}$$

We note that, for energy levels lying considerably ove the top of the barrier ($\sigma \to 1$) and considerably be- w it ($\sigma \to 0$), Eq. (9) goes over into the corresponding rdinary quasi-classical expressions for the case of a arabolic barrier (for $|\rho| \gg 1$, $\gamma \to \rho \ln|\rho/e|$).[9]

The ratio of the amplitudes of the wave function cor- esponding to a given ρ in the left (a) and right (b) po- ential wells (to the same approximation has the form

$$\frac{A(b)}{A(a)} = [\sigma^{-1}\sin^2\alpha + \sigma\cos^2\alpha]^{1/2} \tag{11}$$

or

$$\frac{A(a)}{A(b)} = [\sigma^{-1}\sin^2\beta + \sigma\cos^2\beta]^{1/2}. \tag{12}$$

CALCULATION OF THE ENERGY LEVELS FOR THE SIMPLEST MODEL

In order to follow qualitatively the behavior of the energy levels near the top of the barrier as a function of its height (U) and width and of the relative position of the minima (Q) of the two potential wells, we have chosen the following simplest model (Fig. 3):

$$\left.\begin{aligned} V(z) &= \tfrac{1}{2}\mu\omega_a^2(z + a)^2; && -\infty < z \leqslant -a \\ V(z) &= U\left[1 - \left(\frac{z}{a}\right)^2\right]; && -a \leqslant z \leqslant b \\ V(z) &= \tfrac{1}{2}\mu\omega_b^2(z - b)^2 + Q; && b \leqslant z < +\infty \\ & \left[Q \equiv U\left[1 - \left(\frac{b}{a}\right)^2\right]\right]. \end{aligned}\right\} \tag{13}$$

In place of the original independent parameters a, b, and U, we introduce the following dimensionless quantities:

$$s = \frac{b}{a}, \qquad U_0^a = \frac{U}{\hbar\omega_a}, \qquad \rho_0 = \frac{1}{\hbar}\frac{a}{2}\sqrt{2\mu U}. \tag{14}$$

[cf. (3)]. We also introduce the symbols: $E_0 = E/\hbar\omega_a$, $Q_0 = Q/\hbar\omega_a$, $U_0^b = U_0^a - Q_0$. The calculation will be carried out on the assumption that $\omega_a = \omega_b$. In order to follow the change in the relative position of the energy levels as a function of the parameters ρ_0, U_0^a, and s, we shall vary the latter in such a way that the equality $\rho_0 = U_0^a$ is satisfied; i.e., so that a coming-together of the minima of the potential curve (diminution of a) is accompanied by a simultaneous reduction in the height of the potential barrier, U. Hereafter, for brevity, we shall speak simply of the approach of the minima.

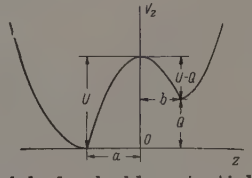

Fig. 3. Model of a double potential well [formula (13)].

$$V(0) = U,\ Q \equiv U\left[1 - \left(\frac{b}{a}\right)^2\right].$$

The energy values $E_{0,n}(\rho_0, U_0^a, s)$ obtained by means of a numerical solution of Eqs. (9) and (10) are graphically represented in Figs. 4-6. The values of ρ_0 are laid off along the horizontal axis and the energy values $E_{0,n}$ along the vertical axis [the reading is made from the deeper minimum (a)]. The values of the parameter $U_0^a = \rho_0$ are also laid off along the vertical axis. Then the points of the energy curves which, on our graphs, lie below (above) the line $U_0^a = \rho_0$ correspond to those values of the parameter ρ_0 for which the calculated $E_{0,n}$'s lie below (above) the top of the barrier. The point of intersection of the straight line with the curves corresponds to the case

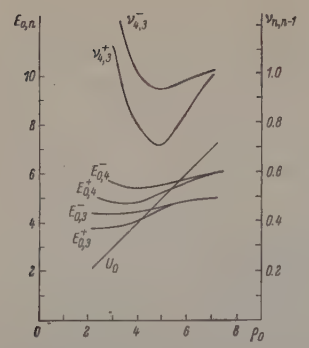

Fig. 4. Dependence of the energy levels ($E_{0,n}$) and the distances between them ($\nu_{n,n-1}$) on $\rho_0(=U_0^a)$ in the case of a symmetric double well. The straight line corresponds to $U_0^a = \rho_0$.

$E_{0,n} = U_0^a$. The curves of the dependence of $\nu_{n,n-1} = E_{0,n} - E_{0,n-1}$ on ρ_0 are also shown on the graphs.

Figure 4 refers to the symmetric double potential well ($s = 1$, $Q_0 = 0$). In this case, as is well known, the energy levels corresponding to each of the wells are split ($E_{0,n}^{\mp}$). Approach of the minima (diminution of ρ_0) leads to an increase in the splitting and a lowering of the levels. In that region of variation of the parameter ρ_0 where the corresponding levels $E_{0,n}^{\mp}$ lie above the top of the barrier and where the quantum effects of reflection over the barrier are small, further approach of the minima leads to elevation of the energy levels. On reduction of n, the splitting of the levels and the beginning of the elevation of $E_{0,n}$ take place at steadily smaller distances between the minima. The "frequencies" $\nu_{n,n-1}^{+} = E_{0,n}^{+} - E_{0,n-1}^{+}$ and $\nu_{n,n-1}^{-} = E_{0,n}^{-} - E_{0,n-1}^{-}$ take on their minimum values near the top of the barrier, when the upper level is above the top and the lower one is beneath it. These results are in qualitative agreement with the calculations of Morse et al.[13]

Lowering of the levels as the minima approach each other, with a subsequent increase when $E_{0,n}$ becomes markedly larger than U_0^a, is also observed in the general case of an unsymmetric potential. The behavior of certain levels, selected from those for which the deeper potential well (a) is the "parent"—i.e., these levels are in well a even on infinite separation of the minima—is shown in Fig. 5 for $s^2 = 0.9$ and $s^2 = 0.5$. Here is shown also the variation in the "frequencies" $\nu_{n,n-1}$, for which, as in Fig. 4, a minimum is observed near the top of the barrier. (The numbering of the levels is conventional: $n = 0$ corresponds to the first level lying above the shallower minimum (b), i.e., $E_{0,0} > Q_0$.)

Some of the $E_{0,n}$ curves for two cases are presented in Fig. 6: in Fig. 6a are shown the energy curves computed on the assumption that $U_0^b = \text{const}$.; Fig 6b corresponds to the case $Q_0 = \text{const}$. In the computations, three parameters were varied simultaneously: ρ_0, U_0^a, and s. Primed numbers refer to levels for which potential well b is the "parent." As follows from the figure, the penetrability of the barrier leads to the appearance of additional levels in each potential well, although it stands to reason that the total number of levels remains unchanged. Analysis of the solutions of Eq. (9) shows that, in the case of imperfect resonance, i.e., when a level $(E_{0,n})_{\text{isol.}}$ in the isolated well a does not coincide with the nearest level $(E'_{0,n})_{\text{isol.}}$ of the isolated well b, the shift of the levels in the double well with respect to their unperturbed positions quickly decreases as the difference $\Delta E_{0,n} = |(E_{0,n})_{\text{isol.}} - (E'_{0,n})_{\text{isol.}}|$ increases. Analogously, as $\Delta E_{0,n}$ increases, the ratio of the amplitudes of the wave functions $|A(b)/A(a)|$ for the levels $E_{0,n}$ diminishes rapidly (for $E'_{0,n}$, correspondingly, $|A(a)/A(b)|$).

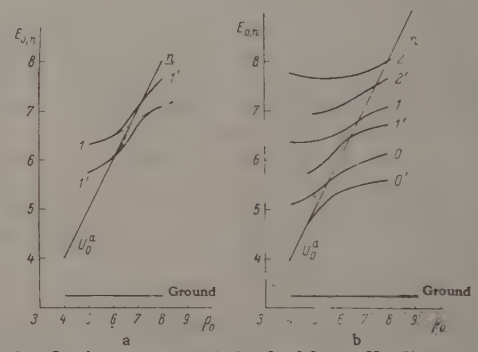

Fig. 6. An unsymmetric double well. $E_{0,n}$ (ρ_0, U_0^a, s). a—$U_0^b = \text{const}$.; b—$Q_0 = \text{const}$.

The course of the variation of $|A(a)/A(b)|$ for the primed levels is depicted in Fig. 7 (which corresponds to Fig. 6). It can be seen from the figure that $|A(a)/A(b)|$ increases as the minima approach each other, which is explained by the increase in penetrability of the barrier. The amplitude ratio $|A(a)/A(b)|$ reaches a maximum, namely unity, at the point of resonance. It can also be seen from Figs. 6 and 7 that the quantum effects of reflection over the barrier play a substantial role, since in the absence of resonance $|A(a)/A(b)|$ tends to unity only for values of $E'_{0,n}$ which are markedly larger than U_0^a

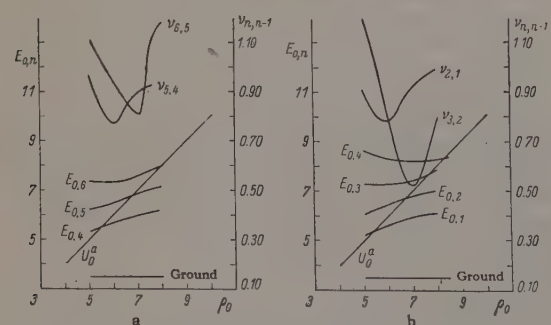

Fig 5. Dependence of $E_{0,n}$ and $\nu_{n,n-1}$ on $\rho_0(=U_0^a)$ in the case of an unsymmetric double well; s = const. a—$s^2 = 0.9$; b—$s^2 = 0.5$.

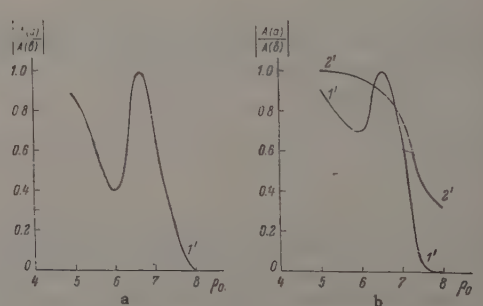

Fig. 7. Dependence of the amplitude ratio $|A(a)/A(b)|$ of a wave function which corresponds to a level for which well b is the "parent." a—$U_0^b = \text{const}$.; b—$Q_0 = \text{const}$.

CUSSION OF THE RESULTS AS APPLIED TO THE HYDROGEN BOND

As was noted above, there is a quantity of spectro-pic data leading to the hypothesis that, in sufficiently ong hydrogen bridges A—H...B, the potential energy he proton has two minima, the second one (next to B) ng above the first (A—H) as a rule. Let us examine certain of these data may be interpreted from the nt of view of our model.

1. As ρ_0 decreases (Figs. 5 and 6), provided that ρ_0 not too small, the energy levels are lowered. In hydro- bonds, the proton in the ground state is in the deeper ential well (a). Let us suppose that the ground level of well lies lower than the bottom of the second well (b) that the position of this level does not change with a nge in ρ_0 (actually, it does change, by virtue of the nge in the shape of the potential curve, but to a smaller ree than for the higher levels, and we neglect this ect for now). The ground level is represented arbi- rily (without scale) in Figs. 5 and 6 by the straight e "Ground." Evidently the distance between the ground el of well a and the lowest level of well b (the level in Fig. 6b) is the heat effect q of the proton transfer action $AH...B \rightarrow A^-...H^+B$, a diminution in q corre- nding, for a given molecule A—H, to an increase in basicity of molecule B. Then the above-mentioned ering of the excited levels with a diminution in ρ_0 ., with a diminution in the length of the hydrogen bond) ll imply, on the one hand, a reduction in the frequency the vibrations corresponding to transitions of the sys- m from the ground level to these excited ones and, on other hand, a reduction in the heat effect q. Thus it lows from the calculations that, with an increase in the sicity of B, the A—H vibration frequency diminishes. is is a generally known fact, which, however, has usu- y been interpreted within the framework of ideas con- rning the presence of a single potential well.[14]

2. It follows from Fig. 6 that the frequencies corre- nding to transitions from the ground level to primed cited levels (frequencies appearing in consequence of penetrability of the barrier) also diminish as ρ_0 minishes (up to some fixed value of ρ_0). Analogously point 1, this may be interpreted as the result of a engthening of the hydrogen bond as the basicity of olecule B increases. Just such an effect has been ex- rimentally observed for certain alcohols (A—H) in lvents (B) of different basicity.[6] (It must be noted that g. 6a (U_0^b = const.) and Fig. 6b (Q_0 = const.) correspond limiting cases of the variation in the potential curve. real systems with a hydrogen bond, simultaneous var- tion in U_0^b and Q_0 takes place; i.e., an intermediate se.)

3. It may be expected that, the greater the quantity A(a)/A(b)| for a given level, the greater will be the robability of a transition to it from the ground level of ell a. On this basis one may suppose that the increase |A(a)/A(b)| (as ρ_0 diminishes) represented in Fig. 7 r the primed levels implies an increase in the inten- ty of transitions to these levels as the basicity of mole- ule B increases. Such an effect has been observed by arrow[6] both for the fundamental frequency and for the vertones.

4. In the series of bases with which Barrow worked,[6] e additional frequency ν' which originates as a result f splitting (with increasing intensity on going to stronger bases B), corresponding in Fig. 6 to the frequency of a transition to a primed level, is less than the unprimed one (ν). Furthermore, $\Delta\nu = \nu - \nu'$ diminishes[6] on going to stronger bases. In the table, the values of $\Delta\nu$ for the O—H group of ethyl alcohol, observed in the first overtone,[6] are presented as an example. This corresponds, in our model, to the case where U_0 falls off more rapidly than Q_0 as ρ_0 diminishes. Actually, holding U_0^b = const. (Fig. 6) gives a more rapid fall in the primed level than in the unprimed one as ρ_0 diminishes, while it appears, in contradiction to the experimental data, that, in the region of variation of ρ_0 which is of interest to us, $\nu' > \nu$. In the other limiting case, when Q_0 is constant (Fig. 6b), one obtains a sign and trend of $\Delta\nu$ for each overtone in its own region of the variation of ρ_0 which agree qualitatively with experiment (curves 1 and 1′, 0 and 0′, Fig. 6b). On the other hand, it is well known from chemical data that, in a series of bases, the change in activation energy is approximately proportional to the change in heat of reaction (Polanyi's rule[15]):

Values of $\Delta\nu = \nu - \nu'$ for the O—H Group of Ethyl Alcohol in Mixtures with Various Bases (First Overtone)

Base	$\Delta\nu$ (cm^{-1})
Toluene	541
Mesitylene	531
Acetone	517
Diethyl ether	436
Dimethylformamide	386

$$\Delta\mathcal{E} = k\Delta q \quad \text{for } k < 1. \tag{15}$$

In order to explain this fact, one should take into account that the experimentally determined activation energy $\mathcal{E}$ does not coincide with the classical barrier height U, but is equal to the distance between the ground level and the lowest of the levels located above the barrier in the region where the quantum effects of reflection over the barrier are comparatively small. The variation in the position of the latter level in the indicated region is less than the variation in q, since the region of lowering of the higher levels ends at greater ρ_0 values than that for the low ones (see, for example, Figs. 5 and 6b, upper levels). In this case, evidently, Polanyi's rule[15] will be fulfilled, and at the same time it may turn out that the relationship $\Delta U = k'\Delta Q$ with $k' < 1$ is not fulfilled (in our case, it turns out that $k' > 1$). All this is apparently valid if U is not too small.

Another possible mechanism for the processes of proton transfer from molecule A to B consists of a tunneling transition accompanying excitation of the proton to a level located below the top of the barrier. But this can play a part only if the resonance condition is sufficiently well fulfilled, which apparently is seldom the case. The deviations from Polanyi's rule which are sometimes observed may be explained by the presence of such a mechanism.

Thus the model of a double potential well which we have examined enables us to interpret certain spectroscopic regularities of the hydrogen bond.

REFERENCES:

1. A. I. Stekhanov, Doklady Akad. Nauk SSSR 106, 433 (1956).

2. R. Blinc and D. Hadŝi, J. Chem. Phys. 27, 991 (1957); Molecular Phys. 1, 391 (1958).
3. C. G. Cannon, Spectrochim. Acta 10, 341 (1958).
4. E. R. Lippincott and R. S. Schroeder, J. Chem. Phys. 23, 1131 (1955).
5. P. C. McKinnery and G. M. Barrow, J. Chem. Phys. 31, 294 (1959).
6. C. L. Bell and G. M. Barrow, J. Chem. Phys. 31, 300 (1959); C. L. Bell and G. M. Barrow, J. Chem. Phys. 31, 1158 (1959).
7. M. A. Kovner and V. A. Chuenkov, Izvest. Akad. Nauk SSSR, Ser. Fiz. 14, 435 (1950); M. A. Kovner and V. N. Kapshtal', Izvest. Akad. Nauk SSSR, Ser. Fiz. 17, 561 (1953).
8. V. I. Gol'danskii, Doklady Akad. Nauk SSSR 127, 1037 (1959).
9. K. W. Ford, D. L. Hill, M. Wakana, and J. A. Wheeler, Ann. Phys. (NY) 7, 239 (1959).
10. H. Bateman, "Higher Transcendental Functions," Vol. II, Chap. VIII. New York, Toronto, London, 1953.
11. L. D. Landau and E. M. Lifshits, "Quantum Mechanics; Nonrelativistic Theory." Gosudarst. Tekh. Teoret. Izd., Moscow-Leningrad, 1948. Addison Wesley, Reading, Mass., 1958.
12. Ta You-Wu, Phys. Rev. 44, 727 (1933).
13. P. Morse and E C. Stueckelberg, Helv. Phys. Acta 4, 337 (1931).
14. N. D. Sokolov, Uspekhi Fiz. Nauk 57, 205 (1955).
15. R. P. Bell, "Acid-Base Catalysis." Oxford Univ. Press, 1941.

THE THEORY OF LINE INTENSITIES IN THE SPECTRUM OF SCATTERED LIGHT
I. The Quantum Model (Condon Approximation)

L. L. Krushinskii and P. P. Shorygin (pp. 24-34)

Received 26 July 1960

Using harmonic oscillator wave functions in the Condon approximation, the contributions of the vibrational structure of an excited electronic level to the elements of the polarizability of a different order are calculated. An analysis of the distribution of these contributions as a function of the parameters characterizing the location and form of the potential curves of the ground and excited states is given. The relationship between the intensities of the fundamental frequency and overtones in Raman spectra is examined.

INTRODUCTION

It was shown in ref. 1 that in the region of an absorption band, the approximate agreement of the classical and quantum theories of Raman line intensities is obtained only for the very short lifetime of the excited electronic-vibrational states (i.e., ~1000 cm^{-1} for particularly large damping constants). The established limits of applicability of the classical model necessitate a more detailed examination of the quantum theory of Raman line intensities. We will use the model proposed in ref. 2.

Quantum theory relates Raman line intensities to the respective elements of the polarizability matrix determined by the Kramers-Heisenberg relations[3,4]

$$(a_{\sigma\rho})^{v_1'' v_2''} = \frac{1}{hc} \sum_e {\sum_{v'}}' \left[\frac{(M_\sigma)^{ev'}_{0v_1''} (M_\rho)^{ev'}_{0v_2''}}{\nu^{ev'}_{0v_1''} - \nu + i\gamma_{ev'}} + \frac{(M_\sigma)^{ev'}_{0v_2''} (M_\rho)^{ev'}_{0v_1''}}{\nu^{ev'}_{0v_2''} + \nu + i\gamma_{ev'}} \right]. \quad (1)$$

Here $a_{\sigma\rho}$ is a component of the polarizability tensor; $\sigma, \rho = x, y, z$ are cartesian coordinates; 0 and e are the numbers of the electronic excited levels; v_1'' and v_2'' are the vibrational quantum numbers in the ground electronic state; v' is the number of the vibrational sublevel of the excited electronic state; $(M_\sigma)^{ev'}_{0v_1''}$, $(M_\rho)E^{ev'}_{0v_2''}$ and others are the probability amplitudes; $\nu^{ev'}_{0v_1''}$, $\nu^{ev'}_{0v_2''}$ are the frequencies of the corresponding vibrational transitions; $\gamma_{ev'}$ is a damping constant determining the width of the level (e, v'); ν is the frequency of the exciting light.

Formula (1) is valid for any ν. However, systematic calculations using it have so far been carried out for only the simplest molecules. In practice, it is used in conjunction with a number of simplifications: First of all, we limit ourselves to the diagonal components of the tensor $(a_{\sigma\rho})^{v_1'' v_2''}$; secondly, we make use of the adiabatic approximation,[5] permitting an independent examination of the motion of the electrons and the nuclear vibrations in the molecule; thirdly, we make use of the Condon approximation[6] in which the matrix element of the dipole moment transition, calculated with the help of one-electron wave functions, does not depend on the nuclear vibrational coordinates; fourthly, we limit outselves to consideration of one excited electronic level.*

*It is easy to see that the third simplification is the most essential. It considerably narrows the region of applicability of the theory. Deviations from the Condon approximation will be considered in the second part of this paper.

Diagonalization of the tensor $a_{\sigma\rho}$, considered in the first condition, can be achieved only for the nonresonance case (real $a_{\sigma\rho}$). In the resonance region, the tensor $a_{\sigma\rho}$ contains an antisymmetric part with purely imaginary nondiagonal components. However, generalization of the results obtained in the case $\sigma \neq \rho$ does not present any difficulty in the Condon approximation.

The fourth condition is not of major importance.

The complete wave function $\Psi_{e,v}(\xi, r)$ for a diatomic molecule can be represented in the form of a product of the electronic (ψ_e) and vibrational $(u_v^{(e)})$ functions:

$$\Psi_{e,v}(\xi, r) = \psi_e(\xi | r)\, u_v^{(e)}(r),$$

where ξ is the totality of the electronic coordinates and r is the internuclear distance. Then

$$(M_\sigma)_{0v_1''}^{ev'} = \int_{-\infty}^{\infty} u_{v'}^{(e)}(r)\, M_{0e}^{(\sigma)}(r)\, u_{v_1''}^{(0)}(r)\, dr = \langle v' \mid M_{0e}^{(\sigma)}(r) \mid v_1'' \rangle,$$

ere

$$M_{0e}^{(\sigma)}(r) = \int_{-\infty}^{\infty} \psi_e(\xi|r)\, M^{(\sigma)}(\xi, r)\, \psi_0(\xi|r)\, d\xi \qquad (2)$$

he matrix element of the dipole moment of the elec- nic transition for stationary nuclei (separated by the tance **r**). Analogously

$$(M_\sigma)_{0v_2''}^{ev'} = \langle v' \mid M_{0e}^{(\sigma)}(r) \mid v_2'' \rangle.$$

he Condon approximation

$$M_{0e}(r) = \text{const} \qquad (3)$$

e index σ is omitted for brevity). As a result of se assumptions, formula (1) is transformed into the m

$$a^{v_1'' v_2''} = \frac{1}{hc}\,(M_{0e})^2 \sum_{v'} F(\nu;\, v')(v',\, v_1'')(v',\, v_2''), \qquad (4)$$

ere

$$F(\nu;\, v') = \frac{2\nu_{0v_1''}^{ev'} - \nu_k + 2i\gamma_{ev'}}{(\nu_{0v_1''}^{ev'})^2 - \nu^2 - (\gamma_{ev'})^2 + 2i\nu_{0v_1''}^{ev'} - \nu_k\,(\nu_{0v_1''}^{ev'} - \nu + i\nu_k\gamma_{ev'})} \qquad (5)$$

the frequency factor and $hc\nu_k$ is the magnitude of the akes energy loss. For the overlap integral of the vibra- nal wave functions, we use the symbol

$$(v',\, v'') = \langle v' \mid 1 \mid v'' \rangle.$$

Without restricting the generality of the treatment, e can take $v_1'' = 0$, $v_2'' \equiv v'' = 0,1,2,\ldots$. We will call the antity

$$A_{ev'}^{0v''} = F(\nu;\, v)(v',\, 0)(v',\, v'') \qquad (6)$$

e contribution of the vibrational sublevel v′ of the ectronic excited level under consideration to the ele- nt of the polarizability matrix determining the Raman e intensity of order v″ (v″ = 0,1,2).

Thus a central place in the quantum model is occu- d by the calculation of the contributions of the vibra- nal sublevels to the corresponding elements of the larizability matrix.

STRIBUTION OF THE CONTRIBUTIONS OF THE VIBRATIONAL SUBLEVELS (HARMONIC VIBRATIONS, WITH $\omega_0' = \omega_0''$)

The calculation of the sublevel contributions (6) is lated to the calculation of the overlap integrals (v′, v″). itially, we will limit ourselves to an examination of brational wave functions of a harmonic oscillator.

Overlap integrals can be calculated most easily nen the potential curves of the ground and excited elec- onic states have the same form ($\omega_0' = \omega_0'' \approx \omega_0$) but are splaced relative to one another by the distance $\Delta = r_0'' - r_0'$ (ω_0', ω_0'' are the frequencies of the nuclear vibra- ons, r_0', r_0'' the equilibrium internuclear distances in the xcited and ground electronic states).

The calculation is based on the integral*

$$(v',\, v'') = \int_0^{\infty} u_{v'}^{(e)}(r)\, u_{v''}^{(0)}(r)\, dr \simeq \int_{-\infty}^{\infty} u_{v'}^{(e)}(r)\, u_{v''}^{(0)}(r)\, dr, \qquad (2)$$

where $u_v(r) = N_v \exp(-1/2\ \alpha(r - r_0)^2) H_v(\sqrt{\alpha}(r - r_0))$ is a Hermite function and $N_v = (\sqrt{\alpha}/2^v v!\pi)^{1/2}$ is a normalizing factor, $H_v(\sqrt{\alpha}(r - r_0))$ is a Hermite polynomial, and $\alpha = (4\pi^2 c\mu\omega_0)/h$ (μ is the reduced mass of the molecule).

The analytical methods for calculating (v′, v″) when $\alpha' = \alpha'' = \alpha$ have been examined by Ruamps[7] and Wagner.[8] The method used in the present study is similar to that described by Ruamps.

We will describe the wave functions in terms of a new coordinate x, whose origin has been shifted to the point $\bar{r} = 1/2(r_0' + r_0'')$; we define

$$X = \sqrt{\alpha}\, x; \qquad K = \sqrt{\alpha}\, \frac{\Delta}{2},$$

then

$$(v'\ v'') = \left(\frac{1}{2^{v'+v''} v'!\, v''!\, \pi}\right)^{1/2} \exp(-K^2) \cdot \int_{-\infty}^{\infty} \exp(-X^2)\, H_{v'}(X - K) \times H_{v''}(X + K)\, dX. \qquad (7)$$

The factors $H_{v'}(X - K)$ and $H_{v''}(X + K)$ appearing in the expression under the integral of Eq. (7) can be ex- panded as a power series in K:

$$H_{v'}(X - K) = \sum_i (-1)^i \frac{2^i}{i!} \frac{v'!}{(v' - i)!} H_{v'-i}(X)\, K^i,$$

$$H_{v''}(X + K) = \sum_k \frac{2^k}{k!} \frac{v''!}{(v'' - k)!} H_{v''-k}(X)\, K^k.$$

Taking account of the known relationship

$$\int_{-\infty}^{\infty} \exp(-X^2)\, H_m(X)\, H_n(X)\, dX = \begin{cases} 0, & \text{if } m \neq n \\ 2^n n!\sqrt{\pi}, & \text{if } m = n \end{cases}$$

(cf., for example, ref. 9), it is easy to show that

$$(2^{v'+v''})^{-1/2} \int_{-\infty}^{\infty} \exp(-X^2)\, H_{v'}(X - K)\, H_{v''}(X + K)\, dX = (-1)^{v'-v''} v''!\, (\sqrt{2}\ K)^{v'-v''} \times \sum_{k=0}^{\infty} (-1)^k \frac{1}{k!\,(v'' - k)!} \frac{v'!}{(v' - v'' + k)!} (2K^2)^k. \qquad (8)$$

The infinite sum in formula (8) can be replaced by a Laguerre polynomial determined by the following equality[9]

$$L_{n+\beta}^{\beta}(z) = \sum_{k=0}^{n} (-1)^k \frac{1}{k!\,(n - k)!} \frac{(\beta + n)!}{(\beta + k)!} z^k.$$

Setting $\beta = v' - v''$, $n = v''$, and noting that if $k > n$, then $(n - k)! = \infty$, we obtain

$$(v',\, v'') = (-1)^{v'-v''} \left(\frac{v''!}{v'!}\right)^{1/2} \exp\left(-\frac{\alpha\Delta^2}{4}\right) \left(\sqrt{\frac{\alpha}{2}}\,\Delta\right)^{v'-v''} L_{v'}^{v'-v''}\left(\frac{\alpha\Delta^2}{2}\right) \quad \text{for } v' \geqslant v'' \qquad (9a)$$

and, analogously,

$$(v',\, v'') = \left(\frac{v'!}{v''!}\right)^{1/2} \exp\left(-\frac{\alpha\Delta^2}{4}\right) \left(\sqrt{\frac{\alpha}{2}}\,\Delta\right)^{v''-v'} L_{v''}^{v''-v'}\left(\frac{\alpha\Delta^2}{2}\right) \quad \text{for } v' \leqslant v'' \qquad (9b)$$

If we examine the polarizability matrix elements de- termining the intensity of the Rayleigh component (a^{00})

*Changing the lower limit of integration from 0 to $-\infty$ oes not introduce a large error, since the exponential nction under the integral decreases rapidly for large alues of $|r|$.

the fundamental frequency (a^{01}), and the overtone (a^{02}) in Raman spectra, then we must calculate the integrals (v′, 0), (v′, 1) and (v′, 2). The results of these calculations are*

*The prime on v′ is omitted from here on.

$$(v,0)=(-1)^v\left(\frac{1}{v!}\right)^{1/2}\exp\left(-\frac{\alpha\Delta^2}{4}\right)\left(\sqrt{\frac{\alpha}{2}}\,\Delta\right)^v; \qquad (10a)$$

$$(v,1)=(-1)^v\left(\frac{1}{v!}\right)^{1/2}\exp\left(-\frac{\alpha\Delta^2}{4}\right)\left(\sqrt{\frac{\alpha}{2}}\,\Delta\right)^{v-1}\left(\frac{\alpha\Delta^2}{2}-v\right); \qquad (10b)$$

$$(v,2)=\frac{\sqrt{2}}{2}(-1)^v\left(\frac{1}{v!}\right)^{1/2}\exp\left(-\frac{\alpha\Delta^2}{4}\right)\left(\sqrt{\frac{\alpha}{2}}\,\Delta\right)^{v-2}$$
$$\times\left[\left(\frac{\alpha\Delta^2}{2}\right)^2-2v\,\frac{\alpha\Delta}{2}+v(v-1)\right](v=0,1,2,\ldots). \qquad (10c)$$

The overlap integrals obtained from formulas (10) possess particularly important property—they form an orthonormal system*:

*This result is true for any choice of functions $u_v(r)$, the only restriction being that they form a complete orthonormal system.

$$\sum_{v=0}^{\infty}(v,m)(v,n)=\begin{cases}1, & \text{if } m=n\\ 0, & \text{if } m\neq n.\end{cases} \qquad (11)$$

Formulas (10) show that under the conditions of the Condon approximation, and for identical forms of the potential curves of the ground and excited states, a necessary condition for the appearance of Raman lines (fundamental and overtones) is that the equilibrium internuclear distances r_0'' and r_0' be different ($\Delta \neq 0$).* On the other hand, scattering may occur without a frequency shift for $\Delta = 0$ as a result of the contribution $A_0^{00} = F(\nu; 0)$; the contributions of all of the remaining sublevels $v \neq 0$ are identically equal to zero.

*A similar result occurs in the semiclassical theory.[10]

We note that A_v^{00} and A_v^{02} are symmetric functions and A_v^{01} antisymmetric functions of Δ (the sign of Δ determines the direction of shift of the potential curve as a result of electronic excitation).

The contribution of the vibrational sublevel v to the matrix element a^{00} (determining the Rayleigh line intensity) is equal to

$$A_v^{00}=F_0(\nu;v)\,B_v^{00}=F_0(\nu;v)\,[(v,0)]^2, \qquad (12)$$

where $F_0(\nu; v)$ is obtained from formula (5) with $\nu_k = 0$ and

$$B_v^{00}=\frac{1}{v!}\exp\left(-\frac{\alpha\Delta^2}{2}\right)\left(\frac{\alpha\Delta^2}{2}\right)^v. \qquad (13)$$

Initially, we limit ourselves to an examination of the distribution of the quantity B_v^{00}. It is evident that for $\Delta \neq 0$, all $B_v^{00} > 0$, and $\sum_v B_v^{00} = 1$ (in agreement with ref. 11). To find the number of the sublevel making the largest contribution to a^{00}, we replace the discrete variable v in (13) by the continuous variable s. Standard operations lead to the following equation for determining the maximum of the function B_v^{00}:

$$\Psi(s)=\ln\frac{\alpha\Delta^2}{2}, \qquad (14)$$

where $\Psi(s)$ is the logarithmic derivative of the Euler Γ-function. It is evident that Eq. (14) has a unique solution $s = s^*$. The sublevel with the number $v^* = E(s^*)$† thus makes the largest contribution to a^{00}. A graphical solution of Eq. (14) is presented in the Figure.

†The symbol E(s) denotes the whole number which lies closest to s.

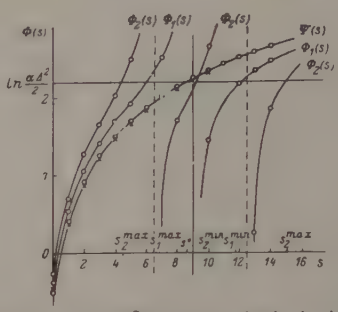

A graphical solution of Eqs. (14), (15), (18), and (21). Curve $\Psi(s)$ is taken from ref. 11; curves $\Phi_1(s)$ and $\Phi_2(s)$ are plotted for the case $\alpha = 445 \times 10\ cm^{-2}$, $\Delta = 0.2 \times 10^{-8}$ cm; the crosses denote points determined by the left-hand part of equality (15) with a = 0.025, b = 0.5.

If we use as an approximate representation of the Ψ-function (see ref. 11)

$$\Psi(s)\simeq\ln s+\frac{1}{2s},$$

then, for values of Δ which are not very small, we obtain a rather trivial expression for the number of the Franck-Condon sublevel: $v^* = E(\alpha\Delta^2/2)$.

The equation for determining the sublevel making the greatest contribution to a^{00}, taking account of the frequency factor, has the following form

$$\Psi(s)-\frac{F_0'(s)}{F_0(s)}=\ln\frac{\alpha\Delta^2}{2}. \qquad (15)$$

Here the frequency factor is rearranged in the form

$$F_0(s)=\frac{2}{\nu_e}\,\frac{1+as}{(1+as)^2-b^2}$$

(symbols: ν_e is the frequency of the $0 \rightarrow 0$ transition in absorption; $\omega_0/\nu_e = a$ and $\nu/\nu_e = b$; typical values are $a \sim 0.02$-0.03 and $b \sim 0.7$-0.1; $\gamma_{ev} = 0$). Numerical estimates using the indicated values of a and b show that $|F_0'(s)/F_0(s)| \ll \Psi(s)$ for any s (in the Figure, the corresponding points, taking account of the frequency factor, are denoted by crosses; a = 0.025, b = 0.5).

Thus under the conditions of nonresonance excitation of the spectra, taking account of the frequency factor does not actually change the nature of the distribution of the contributions. In resonance excitation, on the other hand, the distribution of the contributions will be fundamentally determined by the distribution of the frequency factors. These results also apply to other cases (A_v^{01}, A_v^{02} and others).

The distribution of the contributions of the vibrational sublevels to the matrix element a^{01} (determining the intensity of the Raman fundamental) follows from the formula

$$A_v^{01}=F_1(\nu;v)\,B_v^{01}=F_1(\nu;v)\,(v,0)(v,1), \qquad (16)$$

where $F_1(\nu; v)$ is obtained from (5) if $\nu_k = \omega_0''$, and

$$B_v^{01} = \frac{1}{v!}\exp\left(-\frac{\alpha\Delta^2}{2}\right)\left(\sqrt{\frac{\alpha}{2}}\,\Delta\right)^{2v-1}\left(\frac{\alpha\Delta^2}{2}-v\right). \quad (17)$$

Analysis of formulas (16) and (17) show that the anck-Condon sublevel $v^* = E(\alpha\Delta^2/2)$ makes a zero (or gligible) contribution to a^{01}. The sublevels making the reme contributions are determined from the equation

$$\Phi_1(s) \equiv \Psi(s) + \frac{1}{\frac{\alpha\Delta^2}{2} - s} = \ln\frac{\alpha\Delta^2}{2}. \quad (18)$$

Equation (18) is solved most expediently by graphical thods. It is easy to show, however, that it has two nts. In this case the function $\Phi_1(s)$ has two branches ich asymptotically approach the straight line $s = \alpha\Delta^2/2$ the left and right (cf. the Figure). For $s \leq \alpha\Delta^2/2$, (s) > Ψ(s), and for $s \geq \alpha\Delta^2/2$, $\Phi_1(s) < \Psi(s)$. Accordly, $s_1 < v^* < s_2$ (s_1 and s_2 are roots of Eq. (18)). We te that for large Δ, the sublevels $v_1 = E(s_1)$ and $v_2 = s_2$) are located approximately symmetrically with reect to v^* (their position is determined by the formula $_2 = \frac{1}{2}(2x^2 \pm 2x + 1)$, $x = \sqrt{\alpha/2}\Delta$).*

corresponds approximately to the half-width limits the vibrational structure of the absorption band.

The group of sublevels, one of which lies higher and other lower than the Franck-Condon sublevel v^*, ake contributions of opposite signs. It is important to te that, according to formula (11), $\sum_v B_v^{01} = 0$. Neverless, because of differences in the $F_1(\nu, v)$ factors, $A_v^{01} \neq 0$; thus in the Condon approximation, the phenomn of Raman scattering is caused by differences in the quency factors of the separate sublevels.

The nature of the distribution of the contributions of sublevels to a^{02} is somewhat more complicated. In is case

$$A_v^{02} = F_2(\nu; v)\,B_v^{02} = F_2(\nu; v)\,(v, 0)\,(v, 2), \quad (19)$$

order to calculate $F_2(\nu; v)$, one must put $\nu_k = 2\omega_0''$ in rmula (5).

$$B_v^{02} = \frac{\sqrt{2}}{2}\,\frac{1}{v!}\exp\left(-\frac{\alpha\Delta^2}{2}\right)\left(\frac{\alpha\Delta^2}{2}\right)^{v-1} \times\left[\left(\frac{\alpha\Delta^2}{2}\right)^2 - 2v\,\frac{\alpha\Delta^2}{2} + v(v-1)\right]. \quad (20)$$

It is evident that for nonresonance excitation, the blevels determining the extreme values of B_v^{01} make ractically no contribution to a^{02}. Their number $v^{**} = s^{**}$) can be found from the formula $s^{**} = \frac{1}{2}(2x^2 + 1 \pm x^2 + 1)$ (where $x = \sqrt{\alpha/2\Delta}$). For $x^2 > 1$, the sublevels re distributed symmetrically with reference to v^* and re farther from it, the larger the value of Δ. The exema (two maxima and one minimum) in the distribution B_v^{02} can be found from the equation

$$\Phi_2(s) \equiv \Psi(s) + \frac{(2x^2+1) - 2s}{s^2 - (2x^2+1)\,s + x^4} = \ln x^2. \quad (21)$$

is easy to see that $B_v^{02} > 0$ for $v < v_1^{**}$ and $v > v_2^{**}$, $^{02}_{v} < 0$ for $v_1^{**} < v < v_2^{**}$. Equation (11) gives $\sum_v B_v^{02} = 0$.

he appearance of an overtone, just as for the fundaental, is related in the Condon approximation to differnces in the frequencies of the separate sublevels, reulting in a destruction of the over-all mutual compensaon of the various contributions to A_v^{02}. It is obvious that e indicated differences in the frequency factors are rticularly large close to an absorption band. In this region of exciting frequencies, one can often neglect deviations from the Condon approximation.

Far from a resonance region, the fundamental in the Raman spectrum of the totality of the vibrational sublevels of an electronic excitation level can be replaced approximately by two effective sublevels which respectively sum up the roles of the upper and lower (with relation to v^*) groups of sublevels, and make contributions of opposite signs whose magnitudes are of the order

$$a^{01} = \frac{1}{hc}\,(M_{0e})^2\left(A_{e_1}^{01} + A_{e_2}^{01}\right),$$

where v_1 and v_2 are the numbers of the sublevels giving the extreme contributions. In this case

$$(v_1 - v_2)\,q^{01} = \Delta \quad (22)$$

(q^{01} is the zero point vibrational amplitude in the ground electronic state).

Analogously, under the same conditions one can construct a system of three effective sublevels for an overtone.

For resonance excitation, if the damping constants are not too large, one should observe a pronounced predominance of the contributions of one or two sublevels, along with a significant increase of the overtones, i.e., an approximation to the distribution of intensities characteristic of resonance fluorescence.

DISTRIBUTION OF THE CONTRIBUTIONS OF THE VIBRATIONAL SUBLEVELS (HARMONIC VIBRATIONS, THE GENERAL CASE)

The results obtained in the preceding section can also be generalized to the case in which the form of the potential curve in the ground and excited electronic states is different ($\omega_0' \neq \omega_0''$).

The most general expression for (v', v'') (in the harmonic oscillator approximation) has been given by Ansbacher.[12] Even in special cases it is very cumbersome. We will write out several of the simplest formulas (for small v) and compare them with the analogous relationships for the case $\omega_0' = \omega_0''$. These formulas can easily be found by the method of Manneback.[13]

We will first introduce some results for the integrals (v, 0). It is not hard to show that

$$(0, 0) = \frac{2(\alpha'\alpha'')^{1/2}}{\alpha' + \alpha''}\exp\left(-\frac{\bar{\alpha}\Delta^2}{4}\right), \quad (23a)$$

where $\bar{\alpha} = (2\alpha'\alpha'')/(\alpha' + \alpha'')$ is a parameter characterizing the average form of the potential curves. At the same time it follows from Eq. (10a) that*

*Hereinafter, the index 0 in (v', v'') denotes that $\omega_0' = \omega_0''$; $\alpha^{(1)} = 4\pi^2 c\mu\omega_0^{(1)}/h$.

$$(0, 0)_0 = \exp\left(-\frac{\alpha\Delta^2}{4}\right). \quad (23b)$$

It is obvious that both these expressions coincide for $\alpha' = \alpha''$. Furthermore,

$$(1, 0) = -\frac{2(\alpha'\alpha'')^{1/2}}{\alpha' + \alpha''}\left(\frac{2\alpha''}{\alpha' + \alpha''}\right)^{1/2}\exp\left(-\frac{\bar{\alpha}\Delta^2}{4}\right)\sqrt{\frac{\bar{\alpha}}{2}}\,\Delta \quad (24a)$$

and

$$(1, 0)_0 = -\exp\left(-\frac{\alpha\Delta^2}{4}\right)\sqrt{\frac{\alpha}{2}}\,\Delta; \quad (24b)$$

$$(2,\ 0)=\frac{\sqrt{2}}{2}\,\frac{2\,(\alpha'\alpha'')^{1/2}}{\alpha'+\alpha''}\exp\left(-\frac{\bar{\alpha}\Delta^2}{4}\right)\times\left[\frac{2\alpha''}{\alpha'+\alpha''}\left(\sqrt{\frac{\bar{\alpha}}{2}}\,\Delta\right)^2-\frac{\alpha''-\alpha'}{\alpha''+\alpha'}\right] \tag{25a}$$

and

$$(2,\ 0)_0=\frac{\sqrt{2}}{2}\exp\left(-\frac{\alpha\Delta^2}{4}\right)\left(\sqrt{\frac{\alpha}{2}}\,\Delta\right)^2. \tag{25b}$$

The overlap integrals for higher values of v can be found from the recursion formula

$$(v'+1,\ v'')=-\left(\frac{v'}{v'+1}\right)^{1/2}\frac{\alpha''-\alpha'}{\alpha''+\alpha'}(v'-1,\ v'')+\left(\frac{v''}{v'+1}\right)^{1/2}\frac{2\,(\alpha'\alpha'')^{1/2}}{\alpha'+\alpha''}(v',\ v''-1)-\left(\frac{1}{v'+1}\right)^{1/2}\sqrt{2}\,\frac{\alpha''}{\alpha'+\alpha''}\sqrt{\alpha'}\,\Delta(v',\ v''). \tag{26}$$

We will also introduce a few of the first formulas for the integrals (v, 1):

$$(0,\ 1)=\frac{2\,(\alpha'\alpha'')^{1/2}}{\alpha'+\alpha''}\left(\frac{2\alpha'}{\alpha'+\alpha''}\right)^{1/2}\exp\left(-\frac{\bar{\alpha}\Delta^2}{4}\right)\sqrt{\frac{\bar{\alpha}}{2}}\,\Delta \tag{27a}$$

and

$$(0,\ 1)_0=\exp\left(-\frac{\alpha\Delta^2}{4}\right)\sqrt{\frac{\alpha}{2}}\,\Delta; \tag{27b}$$

$$(1,\ 1)=-\left(\frac{2\,(\alpha'\alpha'')^{1/2}}{\alpha'+\alpha''}\right)^2\exp\left(-\frac{\bar{\alpha}\Delta^2}{4}\right)\left(\frac{\bar{\alpha}\Delta^2}{2}-1\right), \tag{28a}$$

while

$$(1,\ 1)_0=-\exp\left(-\frac{\alpha\Delta^2}{4}\right)\left(\frac{\alpha\Delta^2}{2}-1\right). \tag{28b}$$

Finally,

$$(2,\ 1)=\frac{\sqrt{2}}{2}\,\frac{2\,(\alpha'\alpha'')^{1/2}}{\alpha'+\alpha''}\exp\left(-\frac{\bar{\alpha}\Delta^2}{4}\right)\sqrt{\frac{\bar{\alpha}}{2}}\,\Delta\times\left(\frac{2\alpha''}{\alpha'+\alpha''}\sqrt{\frac{2\alpha'}{\alpha'+\alpha''}}\,\frac{\bar{\alpha}\Delta^2}{2}-2\,\frac{2\,(\alpha'\alpha'')^{1/2}}{\alpha'+\alpha''}\sqrt{\frac{2\alpha''}{\alpha'+\alpha''}}-\sqrt{\frac{2\alpha'}{\alpha'+\alpha''}}\cdot\frac{\alpha''-\alpha'}{\alpha''+\alpha'}\right) \tag{29a}$$

and

$$(2,\ 1)_0=\frac{\sqrt{2}}{2}\exp\left(-\frac{\alpha\Delta^2}{4}\right)\sqrt{\frac{\alpha}{2}}\,\Delta\left(\frac{\alpha\Delta^2}{2}-2\right). \tag{29b}$$

The values of (v, 1) for $v > 2$ can be found from the recursion formula (26).

The differing forms of the potential curves ($\alpha' \neq \alpha''$) appear in formulas (23) to (29) in the form of the following factors: (1) the "scale" factor $2(\alpha'\alpha'')^{1/2}/(\alpha'+\alpha'')$, equal to the ratio of the geometric and arithmetic means of α' and α'' (common to all of the overlap integrals); (2) a series of factors and terms containing only α' and α'' (and numerical coefficients which become more complicated with increasing v and revert respectively to 1 and 0 for $\alpha' = \alpha''$; (3) the replacement of α by $\bar{\alpha}$ in those factors which are common to formulas (10) and (23a)-(29a).

It is important to note that the nature of the dependence of the magnitude of the contributions on Δ remains as before. In particular, the conclusions on the symmetry of the functions $B_v^{0v''}(v'' = 0, 1, 2)$ remain the same. Some peculiarities do occur for the case $\Delta = 0$. As before, $a^{01} = 0$ for $\Delta = 0$, but $a^{00} \neq 0$; however, this is not only due to the sublevel v = 0 but also to the other (even) sublevels whose contributions are also different from zero due to the fact that $\alpha' \neq \alpha''$ [cf., for example, formula (24a)]. Of course, if the difference between α' and α'' is not large, the sublevels do not introduce large corrections. One change in the conclusions is the fact that the first overtone can appear in the Raman spectrum even when $\Delta = 0$. In this case, for $\Delta = 0$ all of the $B_v^{02} = (v, 0)(v, 2) \neq 0$, if v is an even number [from formula (23) and one similar to it it is seen that for $v > 0$ this arises due to terms of the type $(\alpha'' - \alpha')/(\alpha'' + \alpha')$]. In particular

$$\left.\begin{aligned}&(0,\ 0)=\frac{2\,(\alpha'\alpha'')^{1/2}}{\alpha'+\alpha''};\\&(1,\ 0)=0;\\&(2,\ 0)=-\frac{\sqrt{2}}{2}\,\frac{2\,(\alpha'\alpha'')^{1/2}}{\alpha'+\alpha''}\,\frac{\alpha''-\alpha'}{\alpha''+\alpha'};\\&(0,\ 2)=\frac{\sqrt{2}}{2}\,\frac{2\,(\alpha'\alpha'')^{1/2}}{\alpha'+\alpha''}\,\frac{\alpha''-\alpha'}{\alpha''+\alpha'}\ \text{etc.}\end{aligned}\right\}\ (\Delta=0) \tag{30}$$

The conclusions on the character of the distribution of the sublevel contributions (on the number of sublevels making negligible contributions, the number of extrema, the signs of the contributions, etc.) remain the same (at least in qualitative form). The analytical dependences here are complex, and we will limit ourselves to these remarks. We emphasize here that, as before in the Condon approximation, the difference of the quantities a^{01} and a^{02} from zero is caused by differences of the frequency factors of the separate sublevels, leading to noncompensation of the sublevel contributions A_v^{01}, A_v^{02}. All of the conclusions can be illustrated by numerical calculations for a specific diatomic molecule.

The NO molecule was chosen for the calculation. Three of its states—the grand state X and two excited states A and B—possess fairly typical, but essentially different parameters. Thus in the X state, $r_0'' = 1.146$ A, $\omega_0'' = 1904$ cm^{-1}; in the A-state $r_0' = 1.06$ A, $\omega_0' = 2374$ cm^{-1}, $\nu_e = 44{,}199$ cm^{-1}; in the B-state $r_0' = 1.41$ A, $\omega_0' = 1037$ cm^{-1}; $\nu_e = 45{,}486$ cm^{-1}.* The overlap integrals are

*These parameters are taken essentially from ref. 14, with recent corrections from ref. 15.

Table 1. Contributions of the Vibrational Sublevels of Excited Electronic Level A of the NO Molecule to the Polarizability Matrix Elements (Harmonic Oscillator Approximation)

v	$F_0(v;\ v)\cdot 10^4$	α^{00}: $[(v,0)]^2$	α^{00}: $F_0(v;v)\cdot[(v,0)]^2\cdot 10^4$	α^{01}: $(v,0)(v,1)$	α^{01}: $F_1(v;v)(v,0)(v,1)\cdot 10^4$	α^{02}: $(v,0)(v,2)$	α^{02}: $F_2(v;v)\cdot(v,0)(v,2)\times$
0	0.6193	0.1761	0.1091	−0.2441	−0.1525	+0.2255	+0.1422
1	0.5670	0.2713	0.1538	−0.1587	−0.0908	−0.0785	−0.0453
2	0.5236	0.2398	0.1256	+0.0262	+0.0138	−0.1926	−0.1021
3	0.4870	0.1581	0.0770	0.1161	0.0571	−0.1001	−0.0497
4	0.4556	0.0861	0.0392	0.1126	0.0518	+0.0034	+0.0016
5	0.4284	0.0408	0.0175	0.0751	0.0325	0.0450	0.0196
6	0.4053	0.0173	0.0070	0.0407	0.0166	0.0432	0.0175
7	0.3834	0.0068	0.0026	0.0191	0.0074	0.0280	0.0107
8	0.3645	0.0025	0.0009	0.0081	0.0030	0.0148	0.0054
9	0.3476	0.0008	0.0003	0.0031	0.0011	0.0068	0.0024
10	0.3322	0.0003	0.0001	0.0011	0.0004	0.0028	0.0009
11	0.3183	0.0001	0.0000	0.0004	0.0001	0.0011	0.0003
12	0.3056	0.0000	—	0.0001	0.0000	0.0004	0.0001
13	—	—	—	—	—	0.0001	0.0000

$$\sum_v[(v,0)]^2=1.0000,\quad \sum_v(v,0)(v,1)=0.0000,\quad \sum_v(v,0)(v,2)=0.0000$$

$$\sum_v F_0(v;v)[(v,0)]^2=0.5331\cdot 10^{-4},\quad \sum_v F_1(v;v)(v,0)(v,1)=-0.0595\cdot 10^{-4},$$

$$\sum_v F_2(v;v)(v,0)(v,2)=0.0036\cdot 10^{-4}.$$

Table 2. Contributions of the Vibrational Sublevels of Excited Electronic Level B of the NO Molecule to the Polarizability Matrix Elements (Harmonic Oscillator Approximation)

	a^{00}		a^{01}		a^{02}	
$F_0(\nu; v) \cdot 10^4$	$[(v, 0)]^2$	$F_0(\nu - \omega)[(v, 0)]^2 \cdot 10^4$	$(v, 0)(v, 1)$	$F_1(\nu, \omega)(v, 0)(v, 1) \cdot 10^4$	$(v, 0)(v, 2)$	$F_2(\nu; \omega)(v, 0)(v, 2)$
0.5896	0.0000	0.0000	+0.0001	+0.0001	+0.0002	+0.0001
0.5880	0.0005	0.0003	0.0013	0.0007	0.0023	0.0013
0.5480	0.0033	0.0018	0.0070	0.0039	0.0109	0.0061
0.5295	0.0131	0.0070	0.0240	0.0128	0.0316	0.0170
0.5124	0.0369	0.0189	0.0561	0.0290	0.0589	0.0306
0.4964	0.0782	0.0388	0.0935	0.0467	0.0688	0.0347
0.4816	0.1298	0.0625	0.1097	0.0532	+0.0343	+0.0168
0.4676	0.1722	0.0805	0.0804	0.0379	−0.0385	−0.0183
0.4546	0.1849	0.0840	+0.0098	+0.0045	−0.1020	−0.0471
0.4423	0.1613	0.0713	−0.0656	−0.0292	−0.1084	−0.0486
0.4307	0.1141	0.0492	−0.1062	−0.0461	−0.0580	−0.0254
0.4198	0.0648	0.0272	−0.1001	−0.0423	+0.0044	+0.0019
0.4094	0.0287	0.0118	−0.0663	−0.0273	0.0373	0.0155
0.3996	0.0095	0.0038	−0.0316	−0.0127	0.0352	0.0143
0.3904	0.0021	0.0008	−0.0104	−0.0041	0.0184	0.0073
0.3815	0.0002	0.0001	−0.0019	−0.0007	0.0052	0.0020
0.3731	0.0000	0.0000	−0.0000	−0.0000	0.0001	0.0000

$$\sum_v [(v, 0)]^2 = 0.9999, \quad \sum_v (v, 0)(v, 1) = 0.0000, \quad \sum_v (v, 0)(v, 2) = 0.0001,$$

$$\sum_v F_0(\nu; v)[(v, 0)]^2 = 0.4581 \cdot 10^{-4}, \quad \sum_v F_1(\nu; v)(v, 0)(v, 1) = 0.0263 \cdot 10^{-4},$$

$$\sum_v F_2(\nu; v)(v, 0)(v, 2) = 0.0080 \cdot 10^{-4}.$$

lculated by the method of Manneback.[13] The frequency the exciting light is taken as $\nu = 22{,}938\ \text{cm}^{-1}$. The sults of the calculation are presented in Tables 1 and

or economy of space, only the $F_0(\nu; v)$ are given in tables; both $F_1(\nu; v)$ and $F_2(\nu; v)$ are used in the propriate places.

If we limit outselves to an examination of the contributions of the excited level A, then

$$\left(\frac{a^{00}}{a^{01}}\right)^2 = 80; \quad \left(\frac{a^{01}}{a^{02}}\right)^2 = 273.$$

If we limit ourselves to the examination of the B level, then

$$\left(\frac{a^{00}}{a^{01}}\right)^2 = 303; \quad \left(\frac{a^{01}}{a^{02}}\right)^2 = 11.$$

Thus, even at a distance of the order of 20,000-25,000 cm^{-1} from the resonance region, the ratio of the intensities of the fundamental and overtone lines is quite sensitive to the value of Δ: It increases rapidly increasing Δ (if the values of the other parameters are comparable).

REFERENCES

1. P. P. Shorygin and L. L. Krushinskii, Doklady Akad. Nauk SSSR **133**, 337 (1960), Soviet Phys.-Doklady **5**, 790 (1961).
2. P. P. Shorygin, Zhur. Fiz. Khim. **25**, 341 (1951).
3. H. Kramers, and W. Heisenberg, Z. Physik **31**, 681 (1925).
4. V. Weisskopf, Ann. Physik **9**, 23 (1931).
5. M. Born and J. R. Oppenheimer, Ann. Physik **84**, 457 (1927).
6. E. U. Condon, Phys. Rev. **32**, 858 (1928).
7. J. Ruamps, Compt. rend. acad. sci. **243**, 2034 (1957).
8. M. Wagner, Z. Naturforsch. **14a**, 81 (1959).
9. E. U. Condon and P. Morse, "Quantum Mechanics." New York, 1929.
10. P. P. Shorygin, Zhur. Fiz. Khim. **21**, 1125 (1947).
11. E. Jahnke and F. Emde, "Tables of Functions." Fizmatgiz, Moscow, 1959.
12. F. Ansbacher, Z. Naturforsch. **14a**, 889 (1959).
13. C. Manneback, Physica **17**, 1001 (1951).
14. H. Sponer, "Molekülspektren," Bd. I. Berlin, 1935.
15. B. Kivel, H. Mayer and H. Bethe, Ann. Phys. (NY) **2**, 57 (1957).

CALCULATION OF THE ELECTRO-OPTICAL PARAMETERS AND INTEGRATED INFRARED BAND INTENSITIES OF THE ACETYLENE AND HYDROCYANIC ACID MOLECULES AND THEIR DEUTERIUM SUBSTITUTION PRODUCTS

L. M. Sverdlov (pp. 35-40)

Received 27 June 1960

A calculation of the electro-optical parameters and the integrated intensities has been carried out in the first approximation of the valence-optical scheme for acetylene and its deuterium substitution products C_2HD and C_2D_2, and for hydrocyanic acid and DCN. The magnitude of the dipole moment of CH bonds is determined by two factors—the valence state of the carbon atom (fundamental factor) and the influence of the other atoms attached to the carbon (subsidiary factor).

1. For the elucidation of the polar properties of CH bonds of various types, it is of interest, together with methane,[1] ethane,[2] and ethylene,[3] to examine also the acetylene and hydrocyanic acid molecules, in which there is sp-hybridization of the wave functions of the carbon atom.

Various authors,[4-7] having measured the integrated infrared band intensities of the deuterioacetylenes, have at the same time calculated the electro-optical parameters of C_2H_2, C_2HD, and C_2D_2 in the zeroth approximation of the valence-optical scheme; however, in none of these works was the calculation of the intensities of all the molecules listed carried out with a single set of electro-optical parameters. The calculation of the electro-optical parameters of HCN and DCN has been carried out in ref. 8. However, the authors made use of an insufficiently accurate set of force constants, since at that time only the frequencies were available for their determination.

In the present work, the calculation of the electro-optical parameters of C_2H_2, HCN, and their deuterium substitution products is carried out in the first approximation of the valence-optical scheme. In calculating the electro-optical parameters of acetylene, we used the experimental data of Eggers[6] for the C_2HD molecule and the intensities of the ν_3 stretching vibrations of the C_2H_2 and C_2D_2 molecules, and the data of Wingfield[7] for the intensities of the deformation vibrations of these molecules, since his data are more exact than Eggers's results. In the case of HCN and DCN, the intensities measured in the work of Hyde and Hornig[8] were used.

2. To carry out the calculations, let us introduce the internal vibrational coordinates: q_1(C—H), q_2, q_c(CC), δ_1(CCH), δ_2-C_2H_2; q_1(C—H), q_2(CN), γ-HCN, and the angular valence-optical coordinates β_{ni}, φ_1, ψ_1. The C_2H_2 molecule belongs to the symmetry group $D_{\infty h}$, the C_2HD and HCN molecules to $C_{\infty v}$. Vibrations of the following symmetry types exist.

$$C_2H_2:\ \Gamma = 2\Sigma g^+ + \Sigma u^+ + \Pi g + \Pi u;$$

$$C_2HD:\ \Gamma = 3\Sigma^+ + 2\Pi;\quad HCN:\ \Gamma = 2\Sigma^+ + \Pi.$$

We introduce symmetry coordinates and express them in terms of the normal coordinates Q_i.

The C_2H_2 molecule:

$$q^{\Sigma u^+} = \frac{1}{\sqrt{2}}(q_1 - q_2) = C^{\Sigma u^+}_{q^3} Q_3;\quad \delta^{\Pi u I} = \frac{1}{\sqrt{2}}(\delta_1 + \delta_2) = D^{\Pi u I}_{\delta 5} Q_{5a}. \quad (1)$$

The C_2HD molecule:

$$\left.\begin{aligned} q^{\Sigma^+}_{1H} &= \sum_{i=1}^{3} C^{\Sigma^+}_{Hi} Q_i;\quad q^{\Sigma^+}_{2d} = \sum_{i=1}^{3} C^{\Sigma^+}_{di} Q_i;\quad q^{\Sigma^+}_{i} = \sum_{i=1}^{3} C^{\Sigma^+}_{ci} Q_i; \\ \delta^{\Pi I}_{1H} &= \sum_{i=4}^{5} D^{\Pi I}_{iH} Q_i;\quad \delta^{\Pi I}_{2d} = \sum_{i=4}^{5} D^{\Pi I}_{id} Q_i. \end{aligned}\right\} \quad (2)$$

The HCN molecule:

$$\left.\begin{aligned} q^{\Sigma^+}_{i} &= \sum C^{\Sigma^+}_{1i} Q_i;\quad q^{\Sigma^+}_{2} = \sum C^{\Sigma^+}_{2i} Q_i;\ (i = 1, 3), \\ \gamma^{\Pi I} &= D^{\Pi I}_{\gamma 2} Q_2;\quad \varphi^{\Pi I}_{1} = E^{\Pi I}_{12} Q_2;\quad \varphi^{\Pi I}_{2} = E^{\Pi I}_{22} Q_2. \end{aligned}\right\} \quad (3)$$

$$D^{\Pi I}_{\gamma 2} = -E^{\Pi I}_{12} - E^{\Pi I}_{22}. \quad (4)$$

We find one more relationship among the coefficients for the symmetry type ΠI from the condition that the components of the angular momentum must equal zero:

$$[m_N r_{CN} + (m_C + m_N) r_{CH}]\, m_N r_{CN} E^{\Pi I}_{22}$$

$$- [m_H r_{CH} + (m_C + m_H) r_{CN}]\, m_H r_{CH} E^{\Pi I}_{12} = 0. \quad (5)$$

Furthermore, we obtain the following expressions for the derivatives of the dipole moment with respect to the normal coordinates, $\partial P/\partial Q_i$, in the first approximation of the valence-optical scheme.

The C_2H_2 molecule:

$$\frac{\partial P_\xi}{\partial Q^{\Sigma g^+}_i} = \frac{\partial P_\eta}{\partial Q^{\Sigma g^+}_i} = \frac{\partial P_\zeta}{\partial Q^{\Sigma g^+}_i} = 0\ (i = 1, 2);\quad \frac{\partial P_i}{\partial Q^{\Pi g}_4} = 0\ (i = \xi, \eta, \zeta); \quad (6)$$

$$\frac{\partial P_\zeta}{\partial Q^{\Sigma u^+}_3} = \sqrt{2}\left(\frac{\partial \mu^{(1)}_{CH}}{\partial q_1} - \frac{\partial \mu^{(2)}_{CH}}{\partial q_1}\right) C^{\Sigma u^+}_{q^3};\quad \frac{\partial P_\xi}{\partial Q^{\Sigma u^+}_3} = \frac{\partial P_\eta}{\partial Q^{\Sigma u^+}_3} = 0; \quad (7)$$

$$\frac{\partial P_\xi}{\partial Q^{\Pi u I}_5} = \sqrt{2}\,\frac{\mu_{CH}}{r_{CH}} D^{\Pi u I}_{\delta 5};\quad \frac{\partial P_\eta}{\partial Q^{\Pi u I}_5} = \frac{\partial P_\zeta}{\partial Q^{\Pi u I}_5} = 0. \quad (8)$$

The C_2HD molecule:

$$\left.\begin{aligned} \frac{\partial P_\zeta}{\partial Q^{\Sigma^+}_i} &= \left(\frac{\partial \mu^{(1)}_{CH}}{\partial q_1} - \frac{\partial \mu^{(2)}_{CH}}{\partial q_1}\right)(C^{\Sigma^+}_{Hi} - C^{\Sigma^+}_{di}), \\ \frac{\partial P_\xi}{\partial Q^{\Sigma^+}_i} &= \frac{\partial P_\eta}{\partial Q^{\Sigma^+}_i} = 0\quad (i = 1, 2, 3); \end{aligned}\right\} \quad (9)$$

$$\frac{\partial P_\xi}{\partial Q^{\Pi I}_i} = \mu_{CH}(D^{\Pi I}_{iH} + D^{\Pi I}_{id});\quad \frac{\partial P_\eta}{\partial Q^{\Pi I}_i} = \frac{\partial P_\zeta}{\partial Q^{\Pi I}_i} = 0\quad (i = 4, 5). \quad (10)$$

The HCN molecule:

$$\left.\begin{aligned}\frac{\partial P_\zeta}{\partial Q_l^{\Sigma+}} &= \left(\frac{\partial \mu_{CH}^{(1)}}{\partial q_1} - \frac{\partial \mu_{CN}^{(2)}}{\partial q_1}\right) C_{1l}^{\Sigma+} - \left(\frac{\partial \mu_{CN}^{(2)}}{\partial q_2} - \frac{\partial \mu_{CH}^{(1)}}{\partial q_2}\right) C_{2l}^{\Sigma+},\\ \frac{\partial P_\xi}{\partial Q_l^{\Sigma+}} &= \frac{\partial P_\eta}{\partial Q_l^{\Sigma+}} = 0 \quad (l = 1, 3);\end{aligned}\right\} \tag{11}$$

$$\frac{\partial P_\xi}{\partial Q_2^{\Pi I}} = -\frac{\mu_{CH}}{r_{CH}} E_{12}^{\Pi I} - \frac{\mu_{CN}}{r_{CN}} E_{22}^{\Pi I}; \quad \frac{\partial P_\eta}{\partial Q_2^{\Pi I}} = \frac{\partial P_\zeta}{\partial Q_2^{\Pi I}} = 0. \tag{12}$$

3. To compute the form coefficients L_{kl}, the mechanical problem was solved. The force constants of acetylene were computed with the help of the zero-order frequencies for C_2H_2 and C_2D_2 which are presented in Jansen's work:[9]

$$\left.\begin{aligned}&K_q(C{-}H) = 10.8594;\ h_{qq} = 0.0332;\ K_\varepsilon(C{\equiv}C) = 27.6149;\\ &H_{qq\varepsilon} = -0.1182;\ K_\delta = 0.3936;\ l_{\delta\delta} = 0.1453 (\text{units } 10^6\ \text{cm}^{-1}).\end{aligned}\right\} \tag{13}$$

The force constants for HCN were taken from ref. 1, in which the zero-order frequencies for the HCN and DCN molecules were determined:

$$\left.\begin{aligned}&K_1(C{-}H) = 10.6847;\ K_2(CN) = 31.5566;\ H = -0.2474;\\ &K_\gamma = 0.3886 (\text{units } 10^6\ \text{cm}^{-1}).\end{aligned}\right\} \tag{14}$$

The following geometrical parameters were used:

$r(C{-}H) = 1.061$ Å; $r(C{\equiv}C) = 1.2067$ Å [11] (C_2H_2);

$r(C{-}H) = 1.064$ Å; $r(CN) = 1.156$ Å [12] (HCN).

The secular equations were solved according to Wayants's iteration method.[13] The normalized form coefficients are presented in Table 1.

Table 1. The Coefficients L_{kl} for the Molecules C_2H_2, C_2HD, C_2D_2, HCN, and DCN (units, 10^{12} gm$^{-1/2}$)

C_2HD

Coordinates	Q_1	Q_2	Q_3	Coordinates	Q_5	Q_6
$q_H^{\Sigma+}$	0.7953	−0.0963	0.0713	$\delta_H^{\Pi I}$	0.8467	−0.3109
$q_d^{\Sigma+}$	0.0482	0.552	0.2084	$\delta_d^{\Pi I}$	0.0665	0.7146
$q_N^{\Sigma+}$	−0.106	−0.1732	0.2429	—	—	—

$C_2H_2: C_{q_3}^{\Sigma u+} = D_{\delta 5}^{\Pi u} = 0.8048$; $C_2D_2: C_{q_3}^{\Sigma u+} = D_{\delta 5}^{\Pi u} = 0.5909$

HCN

Coordinates	Q_1	Q_2	Coordinates	Q_3
$q_H^{\Sigma+}$	.7961	0.1186	$\varphi_1^{\Pi I}$	−0.7668
$q_N^{\Sigma+}$	−0.1057	0.2864	$\varphi_2^{\Pi I}$	−0.1383

DCN

Coordinates	Q_3	Q_1	Coordinates	Q_2
$q_d^{\Sigma+}$	0.5299	0.2615	$\varphi_1^{\Pi I}$	−0.548
$q_N^{\Sigma+}$	−0.2059	0.2254	$\varphi_2^{\Pi I}$	−0.1735

As a result of the calculation, we obtain the following average values for the electro-optical parameters of acetylene, C_2HD, and C_2D_2:

$$\left(\frac{\partial \mu_{CH}^{(1)}}{\partial q_1} - \frac{\partial \mu_{CH}^{(2)}}{\partial q_1}\right) = 0.8265 \frac{D}{\text{Å}}, \tag{15}$$

$$\frac{\mu_{CH}}{r_{CH}} = -0.889 \frac{D}{\text{Å}}; \quad \mu_{CH} = -0.9433 \frac{D}{\text{Å}}. \tag{16}$$

In the case of HCN and DCN, we have for the type Σ^+:

$$\frac{\partial \mu_{CH}^{(1)}}{\partial q_1} - \frac{\partial \mu_{CN}^{(2)}}{\partial q_1} = 1.0818 \frac{D}{\text{Å}}; \quad \frac{\partial \mu_{CN}^{(2)}}{\partial q_2} - \frac{\partial \mu_{CH}^{(1)}}{\partial q_2} = -0.3347 \frac{D}{\text{Å}} \tag{17}$$

(the value found by $\partial \mu_{CN}/\partial q$ is smaller than in ref. 8 by nearly a factor of two).

To determine the dipole moments of the C—H and CN bonds, it is necessary to use two relationships separately for each of the molecules HCN and DCN—expression (12) for $\partial P/\partial Q_2^{II}$ and the expression for the dipole moment of the molecule,

$$P_{HCN} = -\mu_{CH} + \mu_{CN} \tag{18}$$

(the dipole moment equals 3D).[12]

As a result of averaging, we have:

$$\left.\begin{aligned}&\mu_{CH} = -1.1534D;\ \mu_{CN} = 1.8466D,\\ &\frac{\mu_{CH}}{r_{CH}} = -1.0841 \frac{D}{\text{Å}};\ \frac{\mu_{CN}}{r_{CN}} = 1.5974 \frac{D}{\text{Å}}.\end{aligned}\right\} \tag{19}$$

It can be seen from Eqs. (18) and (19) that the C—H and CN dipoles are oriented in the same direction. If we assume that the negative end of the CN dipole is on the nitrogen atom, since nitrogen is considerably more electronegative than carbon, then the positive end of the CH dipole must be on the hydrogen atom. This conclusion agrees with the greater electronegativity of carbon as compared to hydrogen. Thus the absolute sign of the dipole moment of the CH bond has been determined in the case of HCN.

In Tables 2 and 3 are presented the values of the quantities $\partial P/\partial Q_1$ and of the integrated intensities I_1 for the molecules C_2H_2, C_2HD, C_2D_2, HCN, and DCN, as computed with the help of the parameters (15), (16), (17), and (19). For most of the bands, the discrepancy between the calculated and observed intensities does not exceed 10-12%. The error in the measurement of the intensities amounts to roughly the same quantity.

The maximum discrepancy is observed for the very weak bands $\nu_2(C{\equiv}C)$ of the C_2HD molecule (43%) and $\nu_1(C{-}H)$ of the HCN molecule (49%). This pronounced deviation is to be explained entirely by experimental error, which, for example, equals ~50% for the $\nu_2(C{\equiv}C)$ band.

4. Comparison of the dipole moments of the C—H bonds in the molecules which we have examined (CH_4, C_2H_6, C_2H_4, C_2H_2, HCN, CH_3Cl, CH_3Br, CH_3I) shows that

Table 2. Infrared Band Intensities I_1 (units, cm^{-1}/cm · atm) and the Quantities $\partial P/\partial Q_1$ (esu/gm$^{1/2}$) for the Molecules C_2H_2, C_2HD, and C_2D_2

Symmetry	Observed frequency ν (cm^{-1})	Zero-order frequency ω(cm^{-1})	$\frac{\partial P}{\partial Q_l}$	Calc.	Expt.	I_l calc.	I_l expt.	Error (%)
			C_2HD					
Σ^+	3334.8	3464	$\frac{\partial P}{\partial Q_1}$	61.75	± 58.8	119.22	109.08	9.3%
Σ^+	1851.2	1885	$\frac{\partial P}{\partial Q_2}$	−11.32	± 9.4	4.01	2.8	43.3%
Σ^+	2584	2657	$\frac{\partial P}{\partial Q_3}$	−53.58	± 51.4	89.76	83.4	7.6%
Π	518.8	538	$\frac{\partial P}{\partial Q_4}$	−35.88	± 37.1	80.54	87.06	7.5%
Π	683	706	$\frac{\partial P}{\partial Q_5}$	−81.18	± 76.7	412.17	372.28	10.7%
			C_2H_2					
Σu^+	3287	3409.2	$\frac{\partial P}{\partial Q_3}$	94.07	± 98.8	276.69	308.6	10.3%
Πu	729.1	759.5	$\frac{\partial P}{\partial Q_5}$	−101.18	±107.6	640.21	723.9	11.6%
			C_2D_2					
Σu^+	2427	2507	$\frac{\partial P}{\partial Q_3}$	69.07	± 65.6	149.16	136.1	9.6%
Πu	539.1	560.2	$\frac{\partial P}{\partial Q_5}$	−74.29	± 74.5	345.13	346.9	0.5%

Table 3. Infrared Band Intensities I_i (units, $cm^{-1}/cm \cdot atm$) and the Quantities $\partial P/\partial Q_i$ ($esu/gm^{1/2}$) for the Molecules HCN and DCN

Symmetry	Observed frequency ν (cm^{-1})	Zero-order frequency ω (cm^{-1})	$\frac{\partial P}{\partial Q_i}$	Calc.	Expt.	I_i calc.	I_i expt.	Error (%)
HCN								
Σ^+	2089	2125	$\frac{\partial P}{\partial Q_1}$	3.24	± 4.5	0.32	0.64	49%
Π	712	727	$\frac{\partial P}{\partial Q_2}$	−59.12	±57	220.68	204	8.2%
Σ^+	3312	3446	$\frac{\partial P}{\partial Q_3}$	89.65	±88	251.33	241	4.3%
DCN								
Σ^+	1921	1953	$\frac{\partial P}{\partial Q_1}$	20.74	±20	13.46	12	12.2%
Π	569	580	$\frac{\partial P}{\partial Q_2}$	−29.30	±31	54.22	61	11.1%
Σ^+	2629	2700	$\frac{\partial P}{\partial Q_3}$	64.22	±66	128.94	136	5.2%

the magnitude of the dipole moment is determined by two factors: the valence state of the carbon atom and the influence of the other atoms attached to the carbon.

In methane[1] and ethane,[2] there is sp^3-type hybridization of the carbon wave functions. The dipole moments of the CH bonds of these molecules have values which lie close together, 0.34 D and 0.3 D respectively (however, the difference of 12% nevertheless indicates real changes in the distribution of the electron cloud of the CH bonds when one hydrogen atom in methane is replaced by a CH_3 group).

With a change in the valence state of the carbon atom—transition from sp^3-type hybridization of the wave functions to sp^2 and sp—a considerable increase in the dipole moment of the C—H bond takes place: 0.69 D in ethylene[3] and 0.94 D in acetylene. In HCN, the carbon atom finds itself in the same valence state as in C_2H_2, and correspondingly the dipole moment of the CH bond in HCN has a large value like that in acetylene (however, in consequence of the change in the nature of the group bonded to the carbon atom, the dipole moment of the CH bond in HCN is 22% greater than in C_2H_2).

In the methyl halides (CH_3Cl, CH_3Br, CH_3I), the carbon atom is in the sp^3 valence state, as in methane. As a result of the influence of the halogen atom, the dipole moment of the CH bond (~0.48 D)[14] is increased by ~43%.

From these examples it can be seen that the valence state of the carbon atom is the fundamental factor determining the magnitude of the dipole moment of the CH bond. A change in the surroundings has a less powerful effect.

As for the direction of the C—H dipole, it is the same in all the cases examined—the negative end is on the carbon atom and the positive end on the hydrogen atom.

REFERENCES

1. L. M. Sverdlov, Opt. i Spektr. **10**, 33 (1961), Optics and Spectroscopy **10**, 17 (1961).
2. L. M. Sverdlov, Opt. i Spektr. **7**, 21 (1959), Optics and Spectroscopy **7**, 11 (1959).
3. L. M. Sverdlov, Opt. i Spektr. **4**, 697 (1958); **8**, 594 (1960), Optics and Spectroscopy **8**, 316 (1960).
4. H. Callomon, D. McKean, and H. Thompson, Proc. Roy. Soc. **A208**, 341 (1951).
5. R. Kelly, A. Rollefson, and B. Shurin, J. Chem. Phys. **19**, 1595 (1951).
6. D. Eggers, J. Hisatsune, and I. S. van Alten, J. Phys. Chem. **59**, 1124 (1955).
7. E. Wingfield and J. Straley, J. Chem. Phys. **23**, 731 (1955).
8. G. Hyde and D. Hornig, J. Chem. Phys. **20**, 647 (1952).
9. A. V. Iogansen, Proc. Tenth All-Union Conf. on Specscopy, L'vov, 1957, Vol. 1, p. 93.
10. A. Douglas and D. Sharma, J. Chem. Phys. **21**, 448 (1953).
11. M. M. Sushchinskii, Uspekhi Fiz. Nauk **65**, 441 (1958).
12. W. Gordy, V. Smith, and R. Trambarulo, "Microwave Spectroscopy." Gosudarst. Izd. Tekh. i Teoret. Lit., Moscow, 1955. Wiley, New York, 1953.
13. L. S. Mayants, Trudy Fiz. Inst., Akad. Nauk SSSR **5**, 63 (1959).
14. L. M. Sverdlov, Opt. i Spektr. **6**, 729 (1959), Optics and Spectroscopy **6**, 477 (1959).

THE INFRARED SPECTRUM OF LITHIUM VAPOR

K. P. Vasilevskii and V. I. Baikov (pp. 41-45)

Received 1 August 1960

The infrared spectrum of lithium fluoride vapor in the 2000-250 cm^{-1} region was measured. The following constants for the molecule Li^7F^{19} were obtained from an analysis of the spectra: $\omega_e = 897 \pm 5$ cm^{-1}, $\alpha_e = 0.016 \pm 0.002$ cm^{-1}, $\omega_e x_e = 7.3 \pm 0.5$ cm^{-1}, $r_e = 1.56 \pm 0.05$ A, $B_e = 1.36 \pm 0.09$ cm^{-1}.

Up till the present time data on the infrared spectra the vapors of alkali metal fluorides was absent from e literature. The available experimental results on the bration frequencies of alkali metal halides, obtained om analysis of ultraviolet absorption spectra[1] and elec- on resonance in molecular beams,[2-5] differ widely mong each other and do not agree adequately with the sults of theoretical calculations.[6-8] The most reliable eck of the available data would be the measurement of e infrared vibration spectra of the vapors of the corre- onding molecules.

Recently Klemperer and Rice[9,10] obtained the infra- d spectra of the vapors of a number of alkali metal lides (excluding the fluorides). These authors pointed t that in some cases there was a substantial discrep- cy between their values for the vibration frequencies d the ones obtained earlier from the electronic band ectra.[1,11]

In the present investigation the infrared spectrum lithium fluoride vapor was measured and certain con- ants of the molecule Li^7F^{19} were calculated.

The spectra were measured with a spectrometer rking in the 5000-250 cm^{-1} region using a high-tem- rature vacuum cell. A modified monochromator of the andard instrument IKS-11 was used in the spectrometer. mobile Littrow-Wadsworth dispersing system was bstituted for the immobile prism mount, and a CsI ism with an apex angle of 16° and standard NaCl and Br prisms were used in the investigation. The radia- on beam was modulated at 9 cps and registered with the lp of an optical-acoustic detector.[12] The spectra were corded by means of an electronic potentiometer EPP-09. attered radiation below 700 cm^{-1} was eliminated by ing a frosted mirror.

Figure 1 shows a schematic diagram of the high-tem- rature vacuum cell. It consists of the oven 1, the mix- g chamber 2, dry chamber 3, and the loading chamber A graphite tube 5, 70 mm in diameter and 650 mm long rved as the heating element in the oven. Mirrors

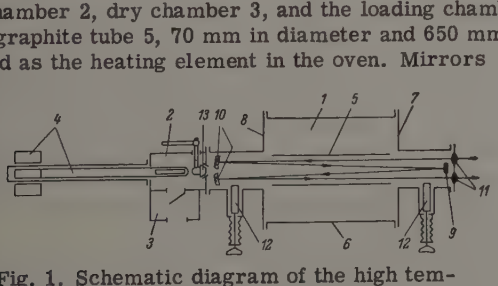

Fig. 1. Schematic diagram of the high temperature vacuum cell. 1—oven; 2—mixing chamber; 3—dry chamber; 4—loading chamber; 5—heater; 6—oven wall; 7,8—plane oven lids; 9,10—spherical mirrors (R = 1250 mm); 11—crystalline windows; 12—shields; 13—valve.

placed inside the cell formed a multiple-reflection system whose total length was 1250 mm.

The substance could be introduced into the cell at any oven temperature. Once prepared, it was kept either in the dry chamber 3 or directly in the mixing chamber 2. The cell will be described in greater detail in a forthcoming publication.

Before an experiment the cell was filled with pure argon. The pressure of argon was chosen such that at the given temperature it would approach atmospheric pressure. Lithium fluoride of natural isotopic composition was used. The absorption and emission of radiation by lithium fluoride vapor was investigated predominantly at temperatures in the neighborhood of 1500°C. The vapor pressure of LiF is 220 mm of mercury[14] at this temperature. However the actual partial pressure of LiF in the cell was somewhat lower because of the presence of a temperature gradient along the cell axis. It should be noted that during experiments the lithium fluoride vapor would condense on the walls and the windows forming a solid film deposit.

We obtained the absorption and emission spectra of the cell containing lithium fluoride at temperatures in the range 1300-1500°C and over the region 2000-250 cm^{-1}. No bands were observed in the 2000-1000 cm^{-1} region. In the 1000-750 cm^{-1} region an intense band occurs with a sharp boundary at 975 cm^{-1} together with several additional maxima. Figure 2 shows a trace of this band obtained with a NaCl prism. The background level due to the empty cell at 1500°C is indicated by the dotted line. Two bands at 520 and 315 cm^{-1} were observed in the 700-250 cm^{-1} region. Figure 3 shows the emission spectrum of the cell filled with lithium fluoride at 1300°C over the 1500-250 cm^{-1} region using a CsI prism.* The

*Because of the poor dispersion of the CsI prism the 900 cm^{-1} band is not well resolved.

ordinate gives the ratio of the emission intensities of the filled cell (minus the background) to the background. The intensity and shape of the bands in the emission spectra change with formation of the deposit on the cell windows.

The absorption spectrum of the cell with deposit on its windows corresponds to the absorption spectrum of a deposit of lithium fluoride on a polyethylene film placed

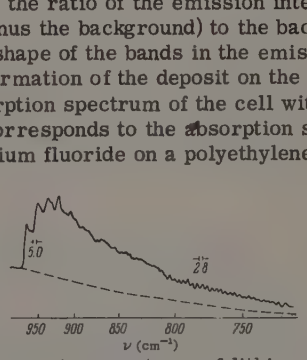

Fig. 2. Emission spectrum of lithium fluoride vapor (T = 1500°C, NaCl prism).

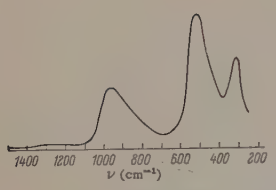

Fig. 3

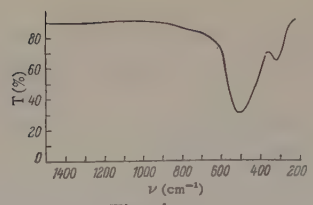

Fig. 4

Fig. 3. Emission spectrum of the cell filled with lithium fluoride (T = 1300°C, CsI prism).
Fig. 4. Absorption spectrum of the lithium fluoride deposit (CsI prism).

near a window, and consists of two overlapping bands at 510 and 315 cm^{-1} (Fig. 4). The correspondence between the emission (absorption) spectrum of the heated cell filled with lithium fluoride in the 700-250 cm^{-1} region and the absorption spectrum of the deposit allows us to suppose that the bands at 520 and 315 cm^{-1} are determined by the emission (absorption) of lithium fluoride occurring in the condensed state.

It should be noted that our results on the absorption spectra of lithium fluoride deposits differ from the published results on the absorption spectra of thin films of LiF.[15,16] While there is good agreement insofar as the absorption regions are concerned, the intensity distribution of the bands is opposite: the 510 cm^{-1} band is strong and the 315 cm^{-1} is weak.

The structure of the short wavelength band permits its assignment to the free diatomic molecules where the vibration-rotation interaction constant and the anharmonicity are positive. The fact that this band appears when lithium fluoride is introduced in the cell and disappears after its evaporation supports the assignment.

Since the vibration frequencies of the alkali metal halides are relatively low, a temperature of about 1500°C is sufficient to increase appreciably the population of the first few vibrational levels. Transitions between these levels would lead to a spectrum consisting of a series of overlapping bands. The sharp long wavelength boundary at 975 cm^{-1} is the edge of the R branch of the 1—0 band. The subsequent maxima represent the edges of the R branches of the 2—1, 3—2, and 4—3 bands. The structure observed in the spectra at frequencies lower than 820 cm^{-1} represents the rotational structure of the P branch of the most intense 1—0 band.

In order to calculate the constant B_e of lithium fluoride we chose the value $r_e = (1.53 \pm 0.06) \times 10^{-8}$ cm calculated by Rittner[6] and close to the value 1.527×10^{-8} cm obtained by Honig et al.[17] Then we have for Li^7F^{19},

$$B_e = \frac{h}{8\pi^2 c\mu r_e^2} = (1.406 \pm 0.08)\ \text{см}^{-1}.$$

It is seen from the spectrum (Fig. 2) that the average distance between the edges of the 1—0 and 2—1 bands ($\nu_k^{1-0} - \nu_k^{2-1}$) is 16.7 ± 1 cm^{-1}. Assuming that $\omega_e y_e = 0$ and $D_v = D_e$ ($\beta = 0$), we have

$$\nu_k^{1-0} - \nu_k^{2-1} = 16.7 = 2\omega_e x_e + 2\alpha_e (J_k + 1), \qquad (1)$$

where J_k is the rotational quantum number corresponding to the edge of the R branch of the 1—0 band (it is assumed that $J_k^{1-0} = J_k^{2-1}$).

Starting with the expression for the line frequency in a vibrational-rotational band we find that rotation of the R branch and formation of the edge occurs for a value of J_k satisfying the following condition (assuming $D_v = D_e$):

$$12D_e (J_k + 1)^2 + 2\alpha_e (J_k + 1) - 2(B_e - \alpha_e) = 0, \qquad (2)$$

where the centrifugal force constant D_b is determined by the relation[11]:

$$D_e = \frac{4B_e^3}{\omega_e^2}. \qquad (3)$$

To evaluate the variation in α_e we can use the following approximate relation[9]:

$$\omega_e \alpha_e = 6\left(\sqrt{\omega_e x_e B_e^3} - B_e^2\right). \qquad (4)$$

The distance between the edge and the beginning of the band is determined by the equation

$$\nu_k^{1-0} - \omega_e + 2\omega_e x_e = 2(B_e - \alpha_e)(J_k + 1) - \alpha_e (J_k + 1)^2 - 4D_e (J_k + 1)^3, \qquad (5)$$

where $\omega_e - 2\omega_e x_e = \nu_0^{1-0}$ is the frequency corresponding to the beginning of the 1—0 band.

Using Eqs. (1)-(5) we find the following values for the constants, assuming $B_e = 1.406 \pm 0.08$ cm^{-1}*:

*The precision of the constants depends mainly on the precision of the assumed value of r_e and the degree to which Eq. (4) holds true.

$\omega_e = 896 \pm 5$ см$^{-1}$; $\alpha_e = 0.0169$ см$^{-1}$;
$\omega_e x_e = 7.3 \pm 0.5$ см$^{-1}$; $J_k = 63$;
$D_e = 13.8 \cdot 10^{-6}$ см$^{-1}$.

The value of the constant B_e can also be evaluated from the distance between the resolved rotational lines of the P branch. From the spectrum we find that the average distance between two lines J and J + 1 in the 780 cm^{-1} region is 3.6 ± 0.2 cm^{-1}. It is easy to show that

$$\nu_J - \nu_{J+1} = 3.6 = 2B_e + \alpha_e (2J - 1) + 4D_e [J^3 - (J + 1)^3]. \qquad (6)$$

The values of J corresponding to $\nu_J = 780$ cm^{-1} are obtained from the equation for the frequencies of the lines in the P branch

$$\nu_J = 780 = \omega_e - 2\omega_e x_e - 2(B_e - \alpha_e) J - \alpha_e J^2 + 4D_e J^3. \qquad (7)$$

Solution of Eqs. (6) and (7) together with Eqs. (1)-(5) yields the values for the constants given in the Table. The precision of the latter is determined by the precision of the value assumed, $\Delta\nu = 3.6 \pm 0.2$ cm^{-1}.

B_e (cm^{-1})	r_e (A)	ω_e (cm^{-1})	$\omega_e x_e$ (cm^{-1})	α_e (cm^{-1})	$D_e \times 10^6$ (cm^{-1})
1.36±0.09	1.56±0.05	897 ± 5	7.3 ± 0.5	0.016	12.6

The value for ω_e obtained for the molecule Li^7F^{19} in the present investigation differs considerably from the calculated values of Berkowitz[7] (655 cm^{-1}) and Rittner[6] (773 cm^{-1}) as well as from the experimental results of Braunstein and Trischka[2] (646 ± 32). Our data is in good agreement with the ω_e value calculated from the value $\omega_e = 1039$ cm^{-1} obtained by Benson and van der Hoff[8] for the molecule Li^6F^{19}. According to the isotopic rule the ratio of the frequencies $\omega_e(Li^6F)/\omega_e(Li^7F)$ equals 1.06. However, in reality the ratio is 1.17 ± 0.02* as found experimentally by Braunstein and Trischka.[2] In this case we obtain for Li^7F^{19}, $\omega_e = 889 \pm 15$ cm^{-1}.

*The authors of ref. 2 point out that the reason for deviation from the isotopic rule is not clear.

In a number of investigations it is pointed out that

Under certain conditions, a considerable number of dimer molecules are present in the vapors of the alkali metal halides.[18-21] Starting with the ionic molecular model, Berkowitz[7] calculated the following values for the infrared-active frequencies of $(LiF)_2$: $\nu_{B_{2u}} = 441$ and $\nu_{3u} = 448\ cm^{-1}$. However the calculation was based on the assumption that the vibration frequency of monomeric LiF was 655 cm^{-1}. This value is quite different from our value $\omega_e = 897\ cm^{-1}$. Taking Berkowitz's ratio of dimer frequencies to monomer frequency, the new values for the dimer frequencies are 615 and 605 cm^{-1}. However, it is hard to draw any conclusions from the results obtained in the present investigation concerning the presence of dimer bands, particularly since they fall in the short wavelength region where there is a sharp change in the absorption due to condensed lithium fluoride.

In conclusion the authors would like to express their gratitude to B. S. Neporent for his constant interest in this investigation.

REFERENCES

1. R. F. Barrow and A. D. Caunt, Proc. Roy. Soc. **A219**, 120 (1953).
2. R. Braunstein and J. W. Trischka, Phys. Rev. **98**, 1092 (1955).
3. V. Hughes and L. Grabner, Phys. Rev. **79**, 314 (1950).
4. L. Grabner and V. Hughes, Phys. Rev. **79**, 819 (1950).
5. J. W. Trischka, Phys. Rev. **74**, 718 (1948).
6. E. S. Rittner, J. Chem. Phys. **19**, 1030 (1951).
7. J. Berkowitz, J. Chem. Phys. **29**, 1386 (1958).
8. G. C. Benson and B. M. E. van der Hoff, J. Chem. Phys. **22**, 469 (1954).
9. W. Klemperer and S. A. Rice, J. Chem. Phys. **26**, 618 (1957).
10. S. A. Rice and W. Klemperer, J. Chem. Phys. **27**, 573 (1957).
11. G. Herzberg, "Molecular Spectra and Molecular Structure. I. Spectra of Diatomic Molecules." Izd. Inostrannaya Lit., Moscow, 1949. 2nd ed., Van Nostrand, Princeton, New Jersey, 1950.
12. N. A. Pankratov, Optiko-Mekh. Prom. No. 1, 37 (1960).
13. J. U. White, J. Opt. Soc. Am. **32**, 285 (1942).
14. O. Ruff, G. Schmidt, and S. Mugdan, Z. anorg. allgem. Chem. **123**, 83 (1922).
15. R. B. Barnes, Z. Physik **75**, 723 (1932).
16. D. J. Montgomery and R. H. Misho, Nature **183**, 103, 654 (1959).
17. A. Honig, M. Mandel, M. L. Stitch, and C. H. Townes, Phys. Rev. **96**, 629 (1954).
18. S. A. Ochs, R. E. Cotes, and A. P. Kusch, J. Chem. Phys. **21**, 459 (1953).
19. P. Kusch, J. Chem. Phys. **21**, 1442 (1953).
20. J. Berkowitz and W. A. Chupka, J. Chem. Phys. **29**, 653 (1953).
21. L. Friedman, J. Chem. Phys. **23**, 477 (1955).

MOLECULAR VIBRATIONS OF SULFUR COMPOUNDS: SF_5Cl

K. Venkatesvarlu and K. Sathianandan* (pp. 46-50)
*Physics Faculty, Annamalainagar University, Annamalainagar, South India.

Received 11 February 1961

The force constants of the octahedral molecule SF_5Cl have been evaluated using Wilson's F–G matrix method. The force constant for the S–F valence vibration along the S–F–Cl axis is found to be slightly higher than that of the valence vibration S–F for a bond lying in the perpendicular plane. Thermodynamic properties were also calculated for the ideal gaseous state at one atmosphere pressure on the basis of a rigid-rotor harmonic-oscillator approximation.

INTRODUCTION

The vibrational spectrum of SF_5Cl has been described by Cross et al.[1]; their assignment of frequencies was based on a C_{4v} symmetry. The SF_5Cl was prepared by substituting a chlorine atom for a fluorine atom in SF_6. The monosubstituted octahedral molecule has not yet been examined in normal coordinates. From symmetry considerations it follows that this molecule has vibrations $4A_1 + 2B_1 + 1B_2 + 4E$ which are all Raman-active; only the A_1 and E vibrations are infrared-active. The general potential function of the valence force field[2] was used to calculate the force constants by the F–G matrix method.

SYMMETRY COORDINATES

The changes in the distances between the bonds D, d_1, d_2, d_3, d_4, d_5 and in the angles between the bonds α_{15}, α_{25}, α_{35}, α_{45}, β_{16}, β_{26}, β_{36}, β_{46}, β_{12}, ν_{23}, ν_{34}, and ν_{41} (see Figure), were used as internal coordinates in constructing the symmetry coordinates. Eighteen symmetry coordinates were determined, of which three were found to be superfluous.

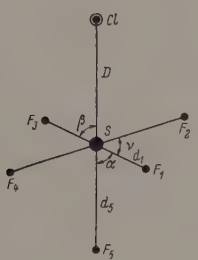

Type A_1:

$$R_1 = \Delta D,$$

$$R_2 = \Delta d_5,$$

$$R_3 = \frac{\Delta d_1 + \Delta d_2 + \Delta d_3 + \Delta d_4}{2},$$

$$R_4 = \frac{\Delta\alpha_{15} + \Delta\alpha_{25} + \Delta\alpha_{35} + \Delta\alpha_{45} - \Delta\beta_{16} - \Delta\beta_{26} - \Delta\beta_{36} - \Delta\beta_{46}}{\sqrt{8}},$$

$$R_{01} = \frac{\Delta\alpha_{15} + \Delta\alpha_{25} + \Delta\alpha_{35} + \Delta\alpha_{45} + \Delta\beta_{16} + \Delta\beta_{26} + \Delta\beta_{36} + \Delta\beta_{46}}{\sqrt{8}} \equiv 0,$$

$$R_{02} = \frac{\Delta\nu_{12} + \Delta\nu_{23} + \Delta\nu_{34} + \Delta\nu_{41}}{2} \equiv 0.$$

Type B_1:

$$R_5 = \frac{\Delta d_1 - \Delta d_2 + \Delta d_3 - \Delta d_4}{2},$$

$$R_6 = \frac{\Delta\alpha_{15} - \Delta\alpha_{25} + \Delta\alpha_{35} - \Delta\alpha_{45} - \Delta\beta_{16} + \Delta\beta_{26} - \Delta\beta_{36} + \Delta\beta_{46}}{\sqrt{8}}$$

$$R_{03} = \frac{\Delta\alpha_{15} - \Delta\alpha_{25} + \Delta\alpha_{35} - \Delta\alpha_{45} + \Delta\beta_{16} - \Delta\beta_{26} + \Delta\beta_{36} - \Delta\beta_{46}}{\sqrt{8}} \equiv 0.$$

Type B_2:

$$R_7 = \frac{\Delta\nu_{12} - \Delta\nu_{23} + \Delta\nu_{34} - \Delta\nu_{41}}{2}.$$

Type E:

$$R_{8a} = \frac{\Delta d_1 - \Delta d_3}{\sqrt{2}},$$

$$R_{8b} = \frac{\Delta d_2 - \Delta d_4}{\sqrt{2}},$$

$$R_{9a} = \frac{\Delta\alpha_{15} - \Delta\alpha_{35}}{\sqrt{2}},$$

$$R_{9b} = \frac{\Delta\alpha_{25} - \Delta\alpha_{45}}{\sqrt{2}},$$

$$R_{10a} = \frac{\Delta\nu_{12} - \Delta\nu_{34}}{\sqrt{2}},$$

$$R_{10b} = \frac{\Delta\nu_{23} - \Delta\nu_{41}}{\sqrt{2}},$$

$$R_{11a} = \frac{\Delta\beta_{16} - \Delta\beta_{36}}{\sqrt{2}},$$

$$R_{11b} = \frac{\Delta\beta_{26} - \Delta\beta_{46}}{\sqrt{2}}.$$

THE F-MATRIX

The general potential function which we used, included the force constants f_D, f_d, f_{d_5}, f_α, f_β, f_ν, f_{Dd}, f_{dd}, f_{dd_5}, $f_{\nu\nu}$, $f_{\alpha\beta}$, $f_{D\beta}$, and $f_{d_5\alpha}$, where f_D, f_d, and f_{d_5} belong to valence vibrations, f_α, f_β, and f_ν belong to the deformation vibrations, and rest being interaction force constants. Below are given the elements of the potential energy matrix obtained from the potential function and the U and U′ matrices constructed from the coefficients of the internal coordinates used in the symmetry coordinates:

Type A_1:

$$\begin{vmatrix} F_{11} & F_{12} & F_{13} & F_{14} \\ F_{21} & F_{22} & F_{23} & F_{24} \\ F_{31} & F_{32} & F_{33} & F_{34} \\ F_{41} & F_{42} & F_{43} & F_{44} \end{vmatrix} = \begin{vmatrix} f_D & 0 & 2f_{Dd} & -\sqrt{2Dd}\, f_{D\beta} \\ 0 & f_{d_5} & 2f_{dd_5} & \sqrt{2dd_5} f_{d_5\alpha} \\ 2f_{Dd} & 2f_{dd_5} & f_d + 2f_{dd} & 0 \\ -\sqrt{2}\, Dd f_{D\beta} & 2dd_5 f_{d_5\alpha} & 0 & \frac{1}{2}(dd_5 f + Dd f_\beta) - d^2 f_{\alpha\beta} \end{vmatrix}$$

Type B_1:

$$\begin{vmatrix} F_{55} & F_{56} \\ F_{65} & F_{66} \end{vmatrix} = \begin{vmatrix} f_d - 2f_{dd} & 0 \\ & \frac{1}{2}(dd_5 f_\alpha + D d f_\beta) - d^2 f_{\alpha\beta} \end{vmatrix}$$

Type B_2:

$$|F_{77}| = |d^2(f_\gamma - 2f_{\gamma\gamma})|$$

Type E:

$$\begin{vmatrix} F_{88} & F_{89} & F_{8\,10} & F_{8\,11} \\ F_{98} & F_{99} & F_{9\,10} & F_{9\,11} \\ F_{10\,8} & F_{10\,9} & F_{10\,10} & F_{10\,11} \\ F_{11\,8} & F_{11\,9} & F_{11\,10} & F_{11\,11} \end{vmatrix} = \begin{vmatrix} f_d & 0 & 0 & 0 \\ 0 & d d_5 f_\alpha & 0 & d^2 f_{\alpha\beta} \\ 0 & 0 & d^2 f_\gamma & 0 \\ & d^2 f_{\alpha\beta} & 0 & D d f_\beta \end{vmatrix}$$

THE G-MATRIX

Below are given the elements corresponding to different types of vibrations of the kinetic energy matrix calculated according to Wilson's method.[2]

Type A_1:

$$\begin{vmatrix} G_{11} & G_{12} & G_{13} & G_{14} \\ G_{21} & G_{22} & G_{23} & G_{24} \\ G_{31} & G_{32} & G_{33} & G_{34} \\ G_{41} & G_{42} & G_{43} & G_{44} \end{vmatrix} = \begin{vmatrix} \mu_{Cl} + \mu_S & -\mu_S & 0 & \frac{\sqrt{8}\,\mu_S}{d} \\ & \mu_F + \mu_S & 0 & \frac{-\sqrt{8}\,\mu_S}{d} \\ & & \mu_F & 0 \\ & & & \frac{2\mu_F + 8\mu_S}{d^2} \end{vmatrix}$$

Type B_1:

$$\begin{vmatrix} G_{55} & G_{56} \\ G_{65} & G_{66} \end{vmatrix} = \begin{vmatrix} \mu_F & 0 \\ & \frac{2\mu_F}{d^2} \end{vmatrix}$$

Type B_2:

$$|G_{77}| = \left| \frac{4\mu_F}{d^2} \right|$$

Type E:

$$\begin{vmatrix} G_{88} & G_{89} & G_{8\,10} & G_{8\,11} \\ G_{98} & G_{99} & G_{9\,10} & G_{9\,11} \\ G_{10\,8} & G_{10\,9} & G_{10\,10} & G_{10\,11} \\ G_{11\,8} & G_{11\,9} & G_{11\,10} & G_{11\,11} \end{vmatrix} =$$

$$= \begin{vmatrix} \mu_F + 2\mu_S & \frac{-2\mu_S}{d} & \frac{-2\mu_S}{d} & -\frac{2\mu_S}{D} \\ & \frac{3\mu_F + 2\mu_S}{d^2} & \frac{2\mu_S}{d^2} & \frac{2\mu_S}{Dd} - \frac{\mu_F}{d^2} \\ & & \frac{2\mu_F + 4\mu_S}{d^2} & \frac{2\mu_S}{Dd} \\ & & & \frac{\mu_F}{d^2} + \frac{2(\mu_{Cl} + \mu_S)}{D^2} \end{vmatrix},$$

where μ_F, μ_{Cl}, and μ_S are the reduced masses of fluorine, chlorine, and sulfur respectively.

RESULTS

The secular equations obtained from the F- and G-matrices were solved by the method of successive approximations. The results are given in Table 1, which also gives the observed frequencies, the molecular parameters,[3,4] and the principal moments of inertia.

Table 1. Potential Constants (10^5 dynes/cm^{-1}) of the Molecule SF_5Cl

Molecular parameters	Principal moments of inertia	Type	Frequency (cm^{-1})	Force constants	Numerical value
S—F_1 = S—F_5 = = 1.56 Å	$I_{xx} = 184.95$ $I_{yy} = I_{zz} =$ $= 207.54$ . . . Å^2	A_1	834	f_D	3.210
			703	f_d	4.682
			599	f_{dd}	5.072
S—Cl = 2.00 Å $\alpha = \beta = 90°$			404	f_α	0.493
		B_1	624	f_β	0.926
			396	f_γ	0.450
		B_2	504	f_{Dd}	0.170
		E	916	$f_{D\beta}$	0.336
			579	f_{dd_5}	0.080
			442	$f_{d_{\alpha\alpha}}$	0.406
			270	f_{dd}	0.160
				$f_{\alpha\beta}$	—0.039
				$f_{\gamma\gamma}$	—0.131

The force constant for the S—F valence vibration along the S—F—Cl axis is found to be slightly higher than that of the valence vibration S—F for a bond lying in the perpendicular plane.

THERMODYNAMIC PROPERTIES[5,6]

Using the molecular parameters and the observed vibrational frequencies the following molar thermodynamic properties were calculated for different temperatures: enthalpy, free energy, entropy, and heat capacity. The results are given in Table 2. The calculations were based on the rigid-rotator harmonic-oscillator approximation for an ideal gas at atmospheric pressure.

Table 2. Ideal Gas Calculations of Enthalpy, Free Energy, Entropy, and Heat Capacity of SF_5Cl at Atmospheric Pressure (in cal.deg^{-1} mole^{-1})

T (in °K)	$(H-E_0^0)/T$	$-(F-E^0)/T$	S^0	C_p
200	11.278	56.122	67.400	18.334
273.16	13.883	60.015	73.898	23.339
300	14.807	61.362	76.169	24.974
400	17.929	66.078	84.007	29.145
500	20.431	70.336	90.767	31.676
600	22.438	74.233	96.671	33.281
700	24.087	77.846	101.933	34.360
800	25.407	81.119	106.526	35.087
900	26.516	84.193	110.709	35.613
1000	27.453	87.045	114.498	36.001
1100	28.235	89.704	117.939	36.287
1200	28.945	92.337	121.282	36.519
1300	29.515	94.513	124.028	36.696
1400	30.030	96.719	126.749	36.836
1500	30.495	98.849	129.344	36.952

REFERENCES

1. L. H. Cross, H. L. Roberts, P. Goggin, and L. A. Woodward, Trans. Faraday Soc. 56, 945 (1960).
2. E. V. Wilson, Jr., J. Chem. Phys. 7, 1947 (1939).
3. Interatomic Distances. Chem. Soc., Special Publication No. 11, 1958.
4. R. A. Crawford, F. B. Dudley, and K. Hedberg, J. Am. Chem. Soc., 81, 5287 (1959).
5. K. S. Pitzer, "Quantum Chemistry," p. 457. Prentice Hall, Englewood Cliffs, New Jersey, 1954.
6. E. A. Braude and F. C. Nachod, "Determination of Organic Structures by Physical Methods," pp. 225, 525. Academic Press, New York, 1955.

MOLECULAR VIBRATIONS OF SULFUR COMPOUNDS: SF_4

K. Venkatesvarlu and K. Pillai* (pp. 51-54)
*Physics Faculty, Annamalainagar University, Annamalainagar, South India.

Received 11 February 1961

An orthonormalized set of symmetry coordinates satisfying transformation conditions has been constructed for the SF_4 molecule belonging to the point group C_{2v}. Using these symmetry coordinates the elements of potential and kinetic energy matrices have been obtained and from the observed Raman and infrared frequencies the force constants pertaining to the molecule have been calculated.

INTRODUCTION

The Wilson F–G matrix method[1] has been used in the calculation of the force constants of the SF_4 molecule. The Raman and infrared spectra of this molecule have been investigated by Dodd et al.[2] who came to the conclusion that this molecule belongs to the point group C_{2v}. Such a structure must have the vibrations $4A_1 + 1A_2 + 2B_2 + 2B_1$. According to the selections rules, all these vibrations should be Raman-active while only the type A_2 vibrations should be infrared-inactive. Dodd et al. have classified the observed frequencies in the following manner:

Type A_1 . . . 889, 235, 557, 715 cm^{-1}
Type A_2 . . . 645 or 401 cm^{-1}
Type B_1 . . . 532, 867 cm^{-1}
Type B_2 . . . 663, 728 cm^{-1}.

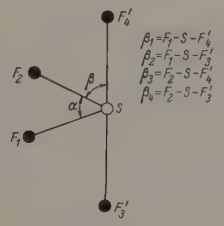

SYMMETRY COORDINATES

Since there exist nine different frequencies, nine internal coordinates were selected to construct the symmetry coordinates. These internal coordinates were the variations in the distances between the bonds d(S=F) and D(S–F′) and the variations in the angles between the bonds β(F–S–F′) and α(F–S–F) (see Figure). On the basis of these internal coordinates the following orthonormalized set of symmetry coordinates were constructed:

For type A_1:

$$R_1 = \frac{\Delta d_1 + \Delta d_2}{\sqrt{2}},$$

$$R_2 = \frac{\Delta D_1 + \Delta D_2}{\sqrt{2}},$$

$$R_3 = \Delta\alpha,$$

$$R_4 = \frac{\Delta\beta_1 + \Delta\beta_2 + \Delta\beta_3 + \Delta\beta_4}{2}.$$

For type A_2:

$$R_5 = \frac{\Delta\beta_1 - \Delta\beta_2 - \Delta\beta_3 + \Delta\beta_4}{2}.$$

For type B_1:

$$R_6 = \frac{\Delta d_1 - \Delta d_2}{\sqrt{2}},$$

$$R_7 = \frac{\Delta\beta_1 - \Delta\beta_2 + \Delta\beta_3 - \Delta\beta_4}{2}.$$

For type B_2:

$$R_8 = \frac{\Delta D_1 - \Delta D_2}{\sqrt{2}},$$

$$R_9 = \frac{\Delta\beta_1 + \Delta\beta_2 - \Delta\beta_3 - \Delta\beta_4}{2}.$$

THE F-MATRIX

The following force constants enter the general potential function used in our calculations: f_d, f_D, f_α, f_β, f_{DD}, f_{dd}, f_{Dd}, $f_{d\alpha}$, $f_{d\beta}$, $f_{D\beta}$, and $f_{\beta\beta}$. Using this potential function and the U- and U′-matrices constructed from the internal coordinates, the following F-matrix elements were obtained:

For type A_1:

$$\begin{vmatrix} F_{11} & F_{12} & F_{13} & F_{14} \\ F_{21} & F_{22} & F_{23} & F_{24} \\ F_{31} & F_{32} & F_{33} & F_{34} \\ F_{41} & F_{42} & F_{43} & F_{44} \end{vmatrix} = \begin{vmatrix} f_d + f_{dd} & 2f_{Dd} & \sqrt{2}\,df_{d\alpha} & \sqrt{2}\,df_{d\beta} \\ & f_D + f_{DD} & 0 & \sqrt{2}\,Df_{D\beta} \\ & & d^2f_\alpha & 0 \\ & & & d^2f_\beta + D^2f_{\beta\beta} + d^2f_{\beta\beta} \end{vmatrix}$$

For type A_2:

$$|F_{55}| = |d^2f_\beta - D^2f_{\beta\beta} - d^2f_{\beta\beta}|$$

For type B_1:

$$\begin{vmatrix} F_{66} & F_{67} \\ F_{76} & F_{77} \end{vmatrix} = \begin{vmatrix} f_\alpha - f_{\alpha\alpha} & 2df_{d\alpha} \\ & d^2f_\beta - d^2f_{\beta\beta} - D^2f_{\beta\beta} \end{vmatrix}$$

For type B_2:

$$\begin{vmatrix} F_{88} & F_{89} \\ F_{98} & F_{99} \end{vmatrix} = \begin{vmatrix} f_d - f_{dd} & 2Df_{D\beta} \\ & d^2f_\beta - d^2f_{\beta\beta} - D^2f_{\beta\beta} \end{vmatrix}$$

THE G-MATRIX

Below are given the elements of the G-matrix for the kinetic energy of the molecule calculated according to Wilson's method.

For type A_1:

$$G_{11} = \mu_F + \mu_S(1 + \cos\alpha),$$

$$G_{22} = \mu_F,$$

$$=\frac{\mu_F+2\mu_S(1+\cos\alpha)}{d^2}.$$

$$=-\frac{2\mu_F\cos^2\beta}{d^2\sin^2\beta}+\frac{\mu_F}{2d^2\sin\beta}\{2(1-\cos\alpha))$$

$$+8\cos\beta\left(\frac{1}{d}-\frac{\cos\beta}{D}\right)\left(\frac{1}{D}-\frac{\cos\beta}{d}\right).$$

$$=2\mu_S\cos\beta,$$

$$=\frac{-\sqrt{2}\mu_S\sin\alpha}{d}.$$

$$=\frac{-\mu_S}{\sqrt{2}\sin\beta}\left[2\left(\frac{1}{D}-\frac{\cos\beta}{d}\right)(1+\cos\alpha)\right.$$

$$\left.+\left(\frac{1}{d}-\frac{\cos\beta}{D}\right)4\cos\beta\right],$$

$$=\frac{-4\mu_S}{\sqrt{2}\sin\beta}\left[\frac{1}{D}-\frac{\cos\beta}{d}\right]\cos\beta,$$

$$=\frac{-4\mu_S}{\sqrt{2}\sin\beta}\left(\frac{1}{D}-\frac{\cos\beta}{d}\right)\cos\beta,$$

$$=\frac{\mu_S(1-\cos\alpha)}{d\sin\alpha\sin\beta}\left[2(1+\cos\alpha)\left(\frac{1}{D}-\frac{\cos\beta}{d}\right)+\left(\frac{1}{d}-\frac{\cos\beta}{D}\right)4\cos\beta\right].$$

For type A_2:

$$=\frac{2\mu_F}{d^2\sin^2\beta}+\frac{\mu_S(1-\cos\alpha)}{D^2\sin^2\beta}.$$

For type B_1:

$$=\mu_F+\mu_S(1-\cos\alpha),$$

$$=\frac{2\mu_F\cos^2\beta}{d^2\sin^2\beta}+\frac{\mu_F(1-\cos\alpha)}{D^2\sin^2\beta}+\frac{2\mu_S(1-\cos\alpha)\left(\frac{1}{D}-\frac{\cos\beta}{d}\right)^2}{\sin^2\beta},$$

$$=-\sqrt{2}\frac{\mu_S(1-\cos\alpha)}{\sin\beta}\left(\frac{1}{D}-\frac{\cos\beta}{d}\right).$$

For type B_2:

$$=\mu_F+2\mu_S,$$

$$=\frac{2\mu_F}{d^2\sin^2\beta}+\frac{2\mu_F(1-4\cos^2\beta)}{4D^2\sin\beta}+4\mu_S\left(\frac{1}{d}-\frac{\cos\beta}{D}\right)^2,$$

$$=\frac{2\sqrt{2}\mu_S}{\sin\beta}\left(\frac{1}{d}-\frac{\cos\beta}{D}\right)^2.$$

RESULTS

The secular equations for each type of vibration were derived from the F- and G-matrices given above, and solved for the force constants using the known values of the vibration frequencies. The S—F distance used was 1.58 A the same as in the SF_6 molecule.[3] The calculated force constants are given in the Table.

Force Constants of the Molecule SF_4 (10^5 dynes/cm^{-1})

Numerical values	Constants
f_d	5.346
f_D	2.077
f_α	1.571
f_β	1.303
$f_{d\alpha}$	0.873
$f_{d\beta}$	0.177
$f_{D\beta}$	0.725
f_{Dd}	0.432
f_{dd}	1.131

The results of our calculations showed that the force constant for the valence S—F vibration for the fluorine atoms in the equatorial positions is considerably greater than for the fluorine atoms at the apex of the pyramidal structure. Assuming the value 401 cm^{-1} for the A_2 frequency with Dodd et al., the calculated value of f_β is found to be very small. Substituting it in the secular equations for B_1 and B_2 and solving them it was found that no real roots could be obtained. However if the value of 645 cm^{-1} is used, then satisfactory values for f_D and $(f_d - f_{dd})$ were obtained. The force constants in the equations for type A_1 frequencies were selected in the same way; the A_1 frequencies calculated were 606, 235, 557, and 697 cm^{-1}; the observed frequencies were 889, 235, 557, and 715 cm^{-1} respectively. In the case of frequencies of types A_2, B_1, and B_2 the calculated and observed frequencies agreed closely with each other.

REFERENCES

1. E. B. Wilson, Jr., J. Chem. Phys. 7, 1047 (1939); Ibid. 9, 76 (1941).
2. R. E Dodd, L. A. Woodward, and H. L. Roberts, Trans. Faraday Soc. 52, 1052 (1956).
3. L. O. Brockway and L. Pauling, Proc. Natl. Acad. Sci. (US) 19, 68 (1933).

INFRARED ABSORPTION SPECTRUM AND SYMMETRY OF THE HEXAETHYLDISILOXANE MOLECULE

G. G. Kirei and M. P. Lisitsa (pp. 55-60)

Received 22 July 1960

Optical density curves for liquid hexaethyldisiloxane have been obtained in the frequency region $\nu = 500\text{-}3050\ cm^{-1}$. An assignment of the observed absorption bands is given, and considerations on the symmetry group of the molecule are stated.

INTRODUCTION

The role of silicon-organic compounds in technology is generally known. Many of them are starting materials for the production of plastics, low-temperature oils and greases, and heat- and moisture-resistant insulators. Accordingly, the interest of chemists and physicists in silicon-organic compounds is continually increasing. Within the broad range of investigations, a particular place is occupied by x-ray and spectroscopic methods, which enable one to establish the structural peculiarities of the molecules and to make definite conclusions concerning their symmetry. Certain information of this sort about the hexaethyldisiloxane molecule has already been obtained in the past. Thus, for example, Skryshevskii with his collaborators has not only determined the SiOSi angle ($130° \pm 5°$) with the help of x-ray data, but has also established the fundamental geometric parameters of the skeleton of the molecule.[1] For other siloxanes, the determination of the angle referred to has been carried out by various methods. The electron diffraction method[2] has given the value $130° \pm 10°$ for it. In ref. 3, the dielectric constant of hexamethyldisiloxane was measured, and the dipole moment and SiOSi angle were computed. In this case, it came out equal to $160° \pm 15°$. However, analogous measurements undertaken in ref. 4 gave the value $130° \pm 10°$. The value 150° has been obtained from spectroscopic data.[5] Thus all the methods lead to the same result—the SiOSi angle is different from 180° and apparently equals 130°, its value in different linear siloxanes probably being one and the same.

On the basis of the literature data, it is difficult to form a definite conclusion about the symmetry group of the hexaethyldisiloxane molecule, the spectrum of which has not been sufficiently thoroughly studied. Thus in ref. 6 there is information only on the absorption bands located in the region $\nu = 680\text{-}1250\ cm^{-1}$. The frequency interpretation offered by these authors is far from complete. The short wavelength portion of the spectrum ($\nu = 1000\text{-}4200\ cm^{-1}$) of a carbon tetrachloride solution has been studied by Kreshkov et al.[7] Of the absorption bands discovered by them, assignments were given for only three. The results of the latter works are presented in Table 1. The Raman spectrum has given considerably more information on the fundamental vibration frequencies of liquid hexaethyldisiloxane.

Like many other silicon-organic compounds, hexaethyldisiloxane is characterized by a broad existence region for the liquid phase, −70 to +233°C, and thus represents a suitable material for the investigation of the temperature dependence of the intensities of intra-molecular vibrations. The present work sets up the goal not only of obtaining sufficiently complete information on the frequencies and relative intensities of the absorption bands of the pure substance to enable us to fill the existing gap, but also of furnishing a basis for experiments relating to the study of the temperature dependences, a rational treatment of the results of which is impossible without a preliminary establishment of the form of the vibrations; i.e., without a correct interpretation of the observed maxima.

Table 1. Frequencies of the Maxima of the Absorption Bands of Hexaethyldisiloxane According to the Literature Data

Simon and McMahon[6] (liquid)		Kreshkov et al.[7] (CCl_4 solution)	
Frequency	Assignment	Frequency	Assignment
688	C-Si skeletal vibration	–	–
735	–	–	–
972	–	–	–
1008	–	–	–
1015	–	1020	–
–	–	1053	Si–O vibration
1075	Si–O vibration	1075	–
–	–	1111	–
1241	CH_3 symmetric vibration	1250	–
–	–	1439	CH_3 deformation vibration
–	–	1695	–
–	–	1887	CH_3 stretching vibration
–	–	2941	–
–	–	4167	–

RESULTS OF THE MEASUREMENTS AND DISCUSSION OF THEM

The spectrum in the frequency region $\nu = 500\text{-}3050\ cm^{-1}$ was obtained with an IKS-6 infrared spectrophotometer. Since the thicknesses of the cells used were determined by the average thickness of the aluminum gasket—i.e., with a large uncertainty—the absorption coefficient was not calculated. The curve of the optical density distribution is presented in the Figure. In the regions not shown here ($\nu = 1500\text{-}2600\ cm^{-1}$ and $\nu > 3100\ cm^{-1}$), no intense bands were found. The frequency assignment is given in Table 2, where the frequencies of the lines in the Raman spectrum* are also presented along with the absorption spectra.

*The authors are grateful to I. I. Kondilenko and V. F. Kulik for communicating the data on the Raman spectrum of hexaethyldisiloxane.

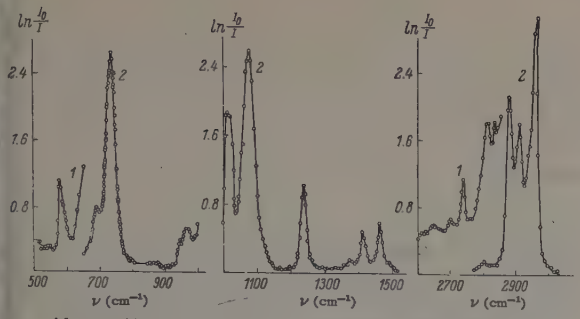

Absorption spectrum of hexaethyldisiloxane. Curve 1—0.05 mm cell; curve 2—0.01 mm cell.

As follows from the Figure and Table 2, regardless of the complexity of the $(C_2H_5)_3SiOSi(C_2H_5)_3$ molecule, the latter is characterized by a relatively simple spectrum of fundamental vibrations. However, this is associated not so much with the symmetry of the molecule, which cannot be high, as with the presence of six ethyl groups, which ensure a high degree of accidental degeneracy. The latter circumstance makes it difficult to use the group representations to establish an unequivocal correspondence between the observed maxima and the vibration type. Therefore, in the assignment of the frequencies, it is more convenient to make use of the specificity of vibrations and of the previously-obtained data on the spectra of organic and silicon-organic compounds which have analogous atom groups and a similar structure of the molecules or of their separate parts.

Table 2. Frequency Assignment of the Intramolecular Vibrations of Hexaethyldisiloxane

Assignment	Frequencies (cm^{-1}) absorption spectrum	Frequencies (cm^{-1}) raman spectrum[6]	Assignment	Frequencies (cm^{-1}) absorption spectrum	Frequencies (cm^{-1}) raman spectrum[6]
OSi	—	171	δ_s CH_2, CH_3	1240	—
iOSi	—	502		1375	—
iOSi	580	—	δ_{as} CH_2, CH_3	1412	1410
SiC_3	—	614		1456	1455
SiC_3	690	—	1240+1375	2614	—
CH_2, CH_3	—	725	1240+1412	2646	—
CH_2, CH_3	743	—	1240+1456	2694	—
	946	—	2×1375	2732	2727
—C	964	—	2×1412	2804	—
	970	970	1375+1456	2832	2840
	1004	1004	ν_s CH_2	—	2867
P	1017	—		2881	—
C—C	1030	—	ν_{as} CH_3	—	2897
SiOSi	1082	—		2912	—
	—	1230	ν_{as} CH_2	2940	2932
			ν_{as} CH_3	2960	2955

(a) Stretching Vibrations of the C—H Bond. On the basis of an analysis of the numerous experimental results referring to hydrocarbons, it is not difficult to come to the conclusion that the stretching vibrations of C—H bonds are distinguished by quite a high specificity with respect to frequency. Closely placed absorption bands correspond to saturated hydrocarbons, specifically to the CH, CH_2, and CH_3 groups. An analogous picture is observed in the case of silicon-organic compounds as well. This circumstance substantially simplifies the interpretation of the frequencies of the fundamental vibrations of hexaethyldisiloxane.

Two bands are usually associated with the stretching vibrations of the C—H bonds of methyl groups. One of them corresponds to the antisymmetric vibration and lies, for aliphatic hydrocarbons, at $\nu = 2962$ cm^{-1}. The second is observed at somewhat greater wavelengths ($\nu = 2872$ cm^{-1}) and pertains to the symmetric vibration. The bands of the same vibrations of such silicon-organic compounds as the methylsilanes and methylsiloxanes are located in the ranges $\nu = 2950$-2973 cm^{-1} and $\nu = 2890$-2910 cm^{-1} respectively. For the above-mentioned hydrocarbons, the vibration frequencies of the C—H bonds of methylene groups are lowered to $\nu = 2926$ cm^{-1} (antisymmetric vibration) and to 2853 cm^{-1} (symmetric vibration). In the part of the hexaethyldisiloxane spectrum being considered, four absorption bands are observed with maxima at $\nu = 2881$, 2912, 2940 (appears clearly only at low temperatures), and 2960 cm^{-1}, and the same number of lines in the Raman spectrum, but with somewhat different frequency values (Table 2). According to the above remarks, it is appropriate to assign the bands with maxima at $\nu = 2960$ and 2912 cm^{-1} respectively to the antisymmetric and symmetric vibrations of the bonds in the CH_3 groups, and the bands at $\nu = 2940$ and 2881 cm^{-1} to the analogous vibrations of the same bonds in the CH_2 groups. The proposed assignment is confirmed by the absence of the frequencies $\nu = 2881$ and 2940 cm^{-1} from the spectra of silicon-organic compounds whose molecules have no methylene groups. On the other hand, the hexaethyldisiloxane frequencies $\nu = 2912$ and 2960 cm^{-1} coincide with the C—H vibration frequencies of the methyl groups of other silicon-organic compounds.

(b) Deformation Vibration of C—H Bonds. The bands corresponding to the antisymmetric vibrations of the C—H bonds of the methyl groups of normal paraffins lie at $\nu = 1460$ cm^{-1}. For the symmetric vibrations, the frequency is lowered to $\nu = 1380$ cm^{-1}. In the methylsilanes and methylsiloxanes, the bands of the analogous vibrations are located in the ranges $\nu = 1440$-1462 cm^{-1} and $\nu = 1247$-1312 cm^{-1} respectively. In the case of hexaethyldisiloxane, the frequencies of the deformation vibrations of the CH_2 and CH_3 groups are near each other, and the bands belonging to them are correspondingly difficult to separate. It is therefore expedient to consider them together. From a comparison of the spectrum of hexaethyldisiloxane with the spectra of simpler silicon-organic compounds, the following assignment proves to be the most plausible: in the infrared spectrum, the bands with the maxima at $\nu = 1456$ and 1412 cm^{-1} correspond to the antisymmetric deformation vibration, and those at $\nu = 1240$-1375 cm^{-1} to the symmetric one; in the Raman spectrum, $\nu = 1410$ and 1455 cm^{-1} for the antisymmetric vibrations and $\nu = 1230$ cm^{-1} for the symmetric ones. No less than two different vibrations apparently correspond to the band $\nu = 1456$ cm^{-1}: the deformation vibration of the C—H bonds of the methyl groups and the "scissors" vibration of the methylene groups (the frequency of the latter in hydrocarbon spectra is $\nu = 1467$ cm^{-1}).

The assignment of the frequencies of the rocking vibrations ρ_s and ρ_{as} of the CH_2 and CH_3 groups has been completed on the basis of a comparison with the frequencies of the analogous vibrations of related compounds.

(c) Vibrations of the Molecular Skeleton. An interpretation of the absorption bands associated with the vibrations of the skeleton has previously been carried out for certain siloxanes.[5,8-11] In the spectra of the methylsiloxanes which are nearest in structure, bands located in the interval $\nu = 1030$-1083 cm^{-1} correspond to the antisymmetric stretching vibration of the Si—O—Si bridge. The intense band $\nu = 1082$ cm^{-1} of hexaethyldisiloxane is

to be associated with the same vibration, since no other intense bands are to be found in the indicated portion of the spectrum. In the Raman spectrum, the vibration under consideration must also be allowed, but it is not observed.

For various methylsiloxanes, the symmetric stretching vibration of the same bridge gives absorption bands in the frequency interval $\nu = 519\text{-}579\ cm^{-1}$. The infrared spectrum of hexaethyldisiloxane has a single band which can be assigned to the indicated interval. Its maximum is located at $\nu = 580\ cm^{-1}$. A band located in the longest-wavelength part of the fundamental vibration spectrum corresponds to the deformation vibration of the Si—O—Si bridge. In the Raman spectrum, such a band is found at $\nu = 171\ cm^{-1}$. For lack of the appropriate apparatus, we could not verify its presence in the infrared spectrum.

The assignment of the vibration frequencies of the Si—C bonds is completed in an analogous way; i.e., by means of a comparison of the hexaethyldisiloxane spectrum with the partially interpreted spectra of the methylsilanes and methylsiloxanes. For these compounds, the frequencies of the antisymmetric and symmetric vibrations of the Si—C bonds of the SiC_3 tetrahedral groups fall into the intervals $\nu = 685\text{-}712\ cm^{-1}$ and $\nu = 614\text{-}660\ cm^{-1}$ respectively. A band with a maximum at $\nu = 690\ cm^{-1}$ (infrared spectrum) and a line in the Raman spectrum with a frequency of $\nu = 614\ cm^{-1}$ at the maximum correspond to these intervals. Thus the first of these lines must belong to the antisymmetric vibration of the atom groups under consideration, and the second to the symmetric one.

The bands belonging to the vibrations of the C—C bonds in the ethyl groups are interpreted with less certainty. It is well known[12] that, for the n-paraffins, vibration of the carbon skeleton gives bands located in the interval $\nu = 850\text{-}1150\ cm^{-1}$. Making use of the specificity criterion, one may suppose that the medium-intensity bands at $\nu = 946$, 964 (appears at a temperature of −65° C), and $970\ cm^{-1}$ belong to just this type of vibration. Since vibrations of C—C bonds usually manifest themselves in the form of absorption bands of relatively low intensity, the intense bands at $\nu = 1004$ and $1017\ cm^{-1}$ may not belong to them, although their frequencies fully correspond to the above-mentioned interval. It is entirely permissible to assign the weak band at $\nu = 1030\ cm^{-1}$ (stands out more prominently from the background at a temperature of −65° C) to an antisymmetric vibration of C—C bonds.

In the region $\nu = 2614\text{-}2840\ cm^{-1}$, several bands of far lower intensity (cell thickness 50 μ) are observed. It does not appear possible to ascribe them to fundamental vibrations, although the intensities of these bands (at least of the short-wavelength group) markedly exceed those usually encountered in spectroscopic practice for overtones and combination frequencies. In our view, the interpretation set forth in Table 2 is most suitable. It may be considered as correct if we admit that the overtones $\nu = 2804$ and $2732\ cm^{-1}$ and the combination frequency $2832\ cm^{-1}$ enter into Fermi resonance with the corresponding fundamental vibrations of the CH_2 and CH_3 groups, the bands of which are located in the interval $\nu = 2850\text{-}3000\ cm^{-1}$.

(d) Symmetry of the Molecule. Comparison of the infrared spectrum with the Raman spectrum (Table 2) shows that the overwhelming majority of the fundamental bands appearing in the absorption spectrum are not found in the Raman spectrum, and vice versa. This circumstance can indicate the operation of the law of mutual exclusion, testifying to the presence of a center of symmetry in the molecule of the substance under investigation. However, such a conclusion is disproved by the following definitely established facts: first, the SiOSi angle does not equal 180°; second, the two vibrational spectra have, after all, some coincident fundamental vibrations. This means that the symmetry of the molecule is relatively low. The choice may be restricted to the point groups C_1, C_s, and C_{2v}. The first two correspond to the case where all vibrations are allowed in both the infrared and the Raman spectrum. As Table 2 shows, this is not realized in fact. According to the selection rules which hold for the group C_{2v}, vibrations of symmetry A_2 are forbidden in the infrared spectrum of the hexaethyldisiloxane molecule, while vibrations of any type are allowed in the Raman spectrum; i.e., the latter must be richer (overtones and combinations of the fundamental frequencies are not taken into consideration). However, Table 2 leads to the diametrically opposite conclusion. This inconsistency is a serious obstacle to the assignment of the molecule under study to group C_{2v}. Nevertheless, it is just this group which corresponds best to experiment. Actually, on the basis of the x-ray data,[1] it is easy to come to the conclusion that the skeletal part of the molecule, consisting of two silicon atoms, one oxygen atom, and twelve carbon atoms, possesses C_{2v} symmetry. It is difficult to admit that the hydrogen atoms of the ethyl groups can destroy this symmetry. Then the absence of a number of frequencies in the Raman spectrum is to be explained by the low intensity of the corresponding lines, since the majority of them pertain to antisymmetric vibrations, the intensities of which, as a rule, are not large. It may well be that, with an increase in the exposure, there will be a possibility not only of fixing the absence of a line, but also of revealing new details of the spectrum.

REFERENCES

1. A. F. Skryshevskii, V. P. Klochkov, and Yu. V. Pasechnik, Proc. IV Ukrainian Conf. on Phys. Chem., p. 49. Izd. Khar'kovsk. Univ., 1960.
2. K. Yamasaki, A. Kotera, M. Yokoi, and I. Ueda, J. Chem. Phys. 18, 1414 (1950).
3. R. O. Sauer and D. J. Mead, J. Am. Chem. Soc. 68, 1794 (1946).
4. H. Freiser, M. V. Eagle, and J. Speier, J. Am. Chem. Soc. 75, 2824 (1953).
5. H. Kreigsmann, Z. Electrochem. 61, 1088 (1957).
6. J. Šimon and H. O. McMahon, J. Chem. Phys. 20, 905 (1952).
7. A. P. Kreshkov, Yu. Ya. Mikhailenko, and G. F. Yakimovich, Zhur. Fiz. Khim. 28, 537 (1954).
8. H. Kreigsmann, Z. anorg. allgem, Chem. 299, 78 (1959).
9. R. E. Richard and A. W. Thompson, J. Chem. Soc. (London), No. 1, 124 (1958).
10. A. N. Lazarev, M. G. Voronkov, and T. F. Tenisheva, Opt. i Spektr. 5, 365 (1958).
11. V. A. Zeitler and Ch. A. Brown, J. Phys. Chem. 61, 1174 (1957).
12. "Application of Spectroscopy to Chemistry," W. West ed. Izd. Inostrannoya Lit., Moscow, 1959.

TRANSMISSION OF ORGANIC SOLVENTS IN THE FAR INFRARED REGION OF THE SPECTRUM

A. E. Stanevich and N. G. Yaroslavskii (pp. 61-66)

Received 1 August 1960

The transmission of liquid carbon tetrachloride, chloroform, benzene, and dioxane at room temperature and of crystalline quartz and polyethylene at −175°, +20°, and +110°C were investigated in the wavelength region 20-2000 μ.

INTRODUCTION

One of the areas for possible investigation by means of far infrared spectroscopy is the study of intermolecular interactions in condensed phases. Investigation of the low-frequency vibration spectra of molecular complexes formed as the result of weak intermolecular interactions, in particular, of hydrogen (and also lithium) bonding, is of substantial interest not only from the standpoint of molecular structure but also from that of obtaining additional information concerning the spectroscopic manifestations of intermolecular interactions.

In investigating intermolecular interaction occurring in liquid systems, the concentration- and temperature-dependence of the positions and intensities of the corresponding absorption bands are usually studied, in inert solvents such as carbon tetrachloride, carbon disulfide, benzene, chloroform, dioxane, etc. The transmission of these solvents in the short wavelength region of the infrared spectrum (up to 20 μ) is well known. In the far infrared region, where the appearance of absorption bands is to be expected, the transmission of these solvents has not been sufficiently investigated.

This report presents the results of an investigation, performed with the instrumentation described earlier,[1-4] of the transmission in the 20-2000 μ region of a number of liquid solvents—carbon tetrachloride, chloroform, benzene, and dioxane—and also of solid polyethylene and crystalline quartz. The latter materials were used as cell windows and as protective windows in the spectrometer. The spectra of polyethylene and quartz were obtained at room temperature and at −175°C.

EXPERIMENTAL RESULTS

1. Carbon tetrachloride. Figure 1 gives the transmission curves of a 0.5 mm thickness of carbon tetrachloride in the 20-50 μ and 50-2000 μ regions. These in addition to all the other curves presented here are each the result of the difference between two spectra—one recorded by the instrument with the empty cell in position and the other with the cell filled with the solvent. The curves were calculated point by point as shown in the figures. For the 20-50 μ region the cell windows were of the crystal KRS-5 while for the 50-2000 μ region they were cut out of crystalline quartz perpendicular to the optical axis. The cells had to be vacuum-tight since they were placed inside the vacuum chamber of the spectrometer.

As can be seen from Fig. 1, absorption bands in the spectrum of carbon tetrachloride can be observed only in the short wavelength region of the spectrum, namely, in the 20-80 μ region. In the 80-2000 μ region 0.5 and 1.0 mm thicknesses of CCl_4 do not exhibit selective absorption and the transmission of a 0.5 mm layer is around 80%.

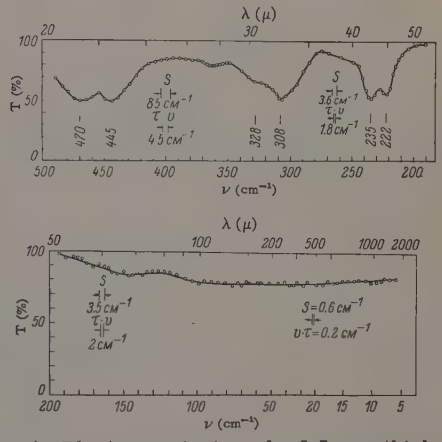

Fig. 1. The transmission of a 0.5 mm thickness of liquid carbon tetrachloride in the 20-50 μ region (top) and 50-2000 μ region (bottom) at room temperature. S is the spectral slit-width of the monochromator; $\tau \cdot v$ is the product of the time constant of the radiation detector τ (in sec) and the rate of recording of the spectrum v (in cm^{-1}/sec).

The bands in the 20-80 μ region belong to the vibrational spectrum of CCl_4 and occur at 470, 445, 328, 308, 235, 222, and 140 cm^{-1}. These frequencies agree satisfactorily with the results of a Raman spectral investigation[5] and also with the results of an infrared spectral investigation of liquid CCl_4 in the region up to 100 μ where bands were observed at 477.5 ($\nu_1 + \nu_4 - \nu_4$), 448.4 ($\nu_3 - \nu_4$), 327.8, 309.9 (ν_4), 218 (ν_2) and 144 cm^{-1} ($\nu_1 - \nu_4$).[6]

2. Chloroform. Four absorption bands at 490, 390, 363, and 260 cm^{-1} were observed in the spectrum of a 0.5 mm thickness of liquid chloroform in the 20-50 μ re-

Present investigation	Results of ref. 7		Results of ref. 8	Results of ref. 9	Assignment according to refs. 5, 8
	Exptl.	Calc.			
260	—	262	260	—	$\nu_6(E)$
—	—	302	303	—	$\nu_2 - \nu_3(A_1)$
363	—	365.9	364	370	$\nu_3(A_1)$
390	—	406	—	392	$\nu_2 - \nu_6(E)$
490	498	499	488	488	$\nu_5 - \nu_6(A_1 + A_2 + E)$

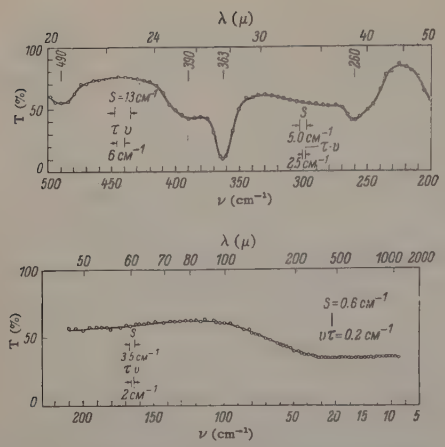

Fig. 2. Transmission of a 0.5 mm thickness of liquid chloroform in the 20-50 μ region (top) and 45-1500 μ region (bottom) at room temperature.

gion (Fig. 2, top). The table gives the assignment of these bands and the frequencies found by other investigators.

In the long wavelength 50-1500 μ region, liquid chloroform 0.5 mm thick does not exhibit selective absorption. Its transmission remains fairly constant at 55-60% over the interval 50-100 μ, decreases monotonically over the 100-300 μ region to 35-40%, and remains constant at that value to 1500 μ (Figure 2, bottom).

3. Benzene and dioxane. A 0.5 mm thickness of liquid benzene has a transmission of 80% in the 20-50 μ region and its spectrum exhibits two absorption bands at 398 and 300 cm^{-1} (Fig. 3, top). The first and strongest of these bands corresponds to the vibration $\nu_{20} = 404$ cm^{-1} observed in the Raman spectrum of liquid benzene.[5] The weak band at 300 cm^{-1} is apparently one of the difference vibrations of benzene, active only in the infrared. The transmission of liquid benzene is 70-75% in the region 50-110 μ, decreases to 60% at about 200 μ, and then increases again reaching 80% at 1000 μ, due to the presence of a broad absorption band possessing a maximum at 50-60 cm^{-1} (Fig. 3, bottom).

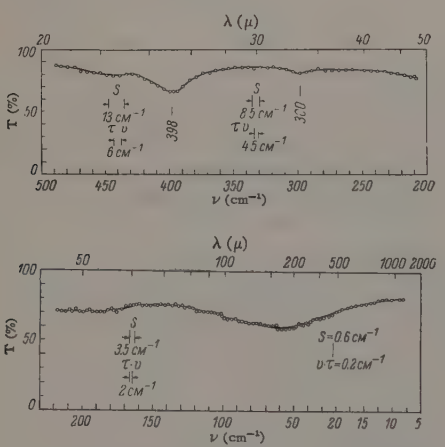

Fig. 3. Transmission of a 0.5 mm thickness of liquid benzene in the 20-50 μ region (top) and 45-1500 μ region (bottom) at room temperature.

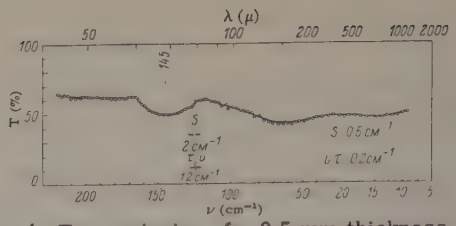

Fig. 4. Transmission of a 0.5 mm thickness of liquid dioxane in the 45-1500 μ region at room temperature.

The transmission of 0.5 mm of liquid dioxane is 60% in the interval 45-60 μ and about 50% in the 300-1000 μ region (Fig. 4). The spectrum has a distinct band at 145 cm^{-1} and a weak broad band having a maximum at 60-70 cm^{-1}. The assignment of this band and of the weak band of benzene at 50-60 cm^{-1} is difficult because of the present scarcity of information concerning low-frequency spectra. It can be supposed that these broad bands are either difference vibrations or are due to intermolecular vibrations.

It must be noted that for a more detailed examination of weak low-frequency absorption bands, the thickness of the substances must be increased to several millimeters, similar to what was done in the investigations of the spectra of liquid benzene and chloroform.[6-10] Nevertheless the results obtained show that all the substances investigated, in particular carbon tetrachloride and benzene, are sufficiently transparent in the far infrared to be used as solvents.

4. Polyethylene and crystalline quartz. It is known that polyethylene and crystalline quartz, together with paraffin, teflon, and polystyrene, are transparent in the far infrared.[2] Polyethylene and crystalline quartz have been studied previously several times at room temperature,[11-13] but their transmission in the far infrared at low temperatures has not been investigated, although this knowledge is important since these substances are used as materials for cell windows in spectral investigations of various substances at low temperatures.

According to results obtained in our investigation, the transmission of a polyethylene plate 1.8 mm thick is about constant at 70% in the 45-1000 μ region. Cooling the plate down to −175° C does not affect its transmission within the experimental error (3-5%).

As distinct from polyethylene, the transmission of crystalline quartz cut perpendicular to the optical axis, is strongly temperature-dependent. Comparison of the curves in Fig. 5 representing the transmission in the 45-400 μ region, of a crystalline quartz plate 5 mm thick, at +20° C (curve 1) and at −175° C (curve 2), shows that the transmission of crystalline quartz over the whole

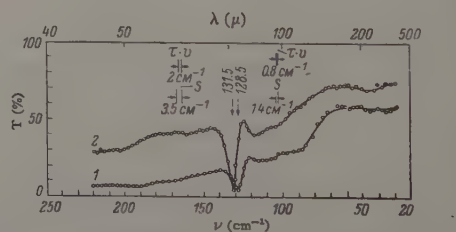

Fig. 5. Transmission of 5 mm of crystalline quartz in the 45-300 μ region at +20° C (curve 1) and −175° C (curve 2).

00-25 cm^{-1} range increases with a decrease in temperure. This increase in transmission is greater in the ort wavelength part of the region than in its long wavength part (if, for example, at 45 μ the transmission inreases 4 times, then at 200 μ it increases by only 1/4 lative to its transmission at room temperature).

Apart from this, we detected a decrease in the width d a shift in the band maximum at 128.5 cm^{-1} to the ort wavelength part of the spectrum on decreasing the mperature of the quartz to −175° C. At this temperare the band maximum shifts by 3 cm^{-1} to 131.5 cm^{-1}, e latter value being in good agreement with the result ref. 14, where it was shown that the Raman lines at 8, 207, and 466 cm^{-1} of crystalline quartz are shifted 131.5, 218.5, and 468 cm^{-1}, respectively, at liquid air mperature.

Apparently, the frequency at 207 cm^{-1} which is quite ense in the Raman spectrum is infrared-inactive and ppears only as a weak band with a maximum at 190 cm^{-1}, ifting to 200 cm^{-1} on the cooling of quartz to −175° C. ne bands at 88 and 112 cm^{-1} (curve 1, Fig. 5) are also eak and on cooling become narrower and are shifted to gher frequencies, to 100 and 118 cm^{-1} respectively urve 2).

The general increase in transmission of crystalline artz on cooling can be explained by assuming that a action of the absorption over the range 45-400 μ at om temperature is due to the long wavelength edge of strong absorption band at 21 μ. Decrease in temperare to −175° C leads to a narrowing of this band and to shifting of it to a shorter wavelength part of the specum. As a result, the decrease (with a decrease in mperature) of the absorption due to the "wing" of this nd affects the transmission of quartz in the 45-400 μ gion to a lesser degree than in the 20-45 μ region.

Note added in proof. The increase in the transmison of quartz on cooling, discussed towards the end of e present report, is substantiated by the effect of temrature increase on transmission.

On heating quartz to +110° C its transmission over e region 220-70 cm^{-1} decreases still further and is 40% er the region 220-180 cm^{-1} and 75% over the region around 100 cm^{-1}, of the transmission at +20° C. The band at 128.5 cm^{-1} shifts to 127 cm^{-1} and the weak bands at 88 and 112 cm^{-1} become wider and their maxima shifted to 85 and 110 cm^{-1} respectively. It is possible that the group of bands with maxima at 128.5, 112, and 88 cm^{-1} is related to the presence of hydroxyl groups in crystalline quartz. However this hypothesis requires additional measurements with quartz of varying hydroxyl group content.

REFERENCES

1. N. G. Yaroslavskii, B. A. Zheludov, and A. E. Stanevich, Opt. i Spektr. 1, 507 (1956); Repts. Tenth All-State Conf. on Spectroscopy 1, 399 (1957).
2. N. G. Yaroslavskii, Uspekhi Fiz. Nauk 62, 159 (1957).
3. A. E. Stanevich and N. G. Yaroslavskii, Inzh. Fiz. Zhur. 1, 49 (1958).
4. N. G. Yaroslavskii and A. E. Stanevich, Opt. i Spektr. 7, 626 (1959), Optics and Spectroscopy 7, 380 (1959).
5. G. Herzberg, "Molecular Spectra and Molecular Structure. II. Infrared and Raman Spectra of Polyatomic Molecules," 2nd ed. Van Nostrand, Princeton, New Jersey, 1945. Izd. Inostrannaya Lit., Moscow, 1949.
6. H. Yoshinaga, J. Chem. Phys. 23, 2206 (1955).
7. M. P. Lisitsa and Iu. P. Tsiaschenko, Opt. i Spektr. 6, 604 (1959), Optics and Spectroscopy 6, 396 (1959).
8. P. Barschewitz and M. Parody, J. phys. radium 10, 143 (1939).
9. E. K. Plyler and W. Benedict, J. Research Natl. Bur. Standards 47, 202 (1951).
10. R. B. Barnes, W. S. Benedict, and C. M. Lewis, Phys. Rev. 47, 129 (1935).
11. T. K. McCubbin and W. M. Sinton, J. Opt. Soc. Am. 42, 113 (1952).
12. A. Hadni, Ch. Janot, and E. Décamps, Rev. opt. 38, 463 (1959).
13. E. Décamps and A. Hadni, Compt. Rend. Acad. Sci. 250, 1827 (1960).
14. P. K. Narayanaswamy, Proc. Indian Acad. Sci. A26, 521 (1947).

STUDY OF THE EQUILIBRIA IN NONAQUEOUS SOLUTIONS OF ELECTROLYTES BY MEANS OF ABSORPTION SPECTRA

III. Picric Acid and Sodium Picrate in Dioxane-Water and Benzene-Alcohol Mixtures

N. A. Izmailov and E. L. Gurevich* (pp. 67-73)

*Translation editor's note: Certain symbols in this and article II (June 1961 issue) are different from the symbols given in the translation of article I of this series (January 1961 issue). Both sets of symbols are internally defined and clear but we believe the second set are better.

Received 5 July 1960

The absorption spectra of picric acid and sodium picrate have been studied in dry dioxane and in dioxane-water mixtures, as well as in benzene-ethyl alcohol mixtures. Equilibria have been found between the solvated ions and molecules, the ions and ionic aggregates, and the molecules and ionic aggregates of picric acid, as well as equilibria between the ions and ionic aggregates of sodium picrate. It has been established that the ionic aggregates of picric acid and sodium picrate possess identical absorption spectra. Values have been computed for the dissociation constants $K_{diss.}$ and the conversion constants $K_{conv.}$ of picric acid, as well as for the association constants $K^{-1}_{ass.}$ of sodium picrate in mixtures of different solvents. The results of the investigation of the absorption spectra of picric acid and sodium picrate, as set forth in the present and earlier communications, are discussed.

We have previously studied the absorption spectra of picric acid and sodium picrate in water, methyl, ethyl, and n-butyl alcohols, acetic acid, pyridine, acetone, and acetonitrile.[1] Equilibria between the ions and molecules of picric acid and between the ions and ionic aggregates of sodium picrate were found. The present communication is devoted to a study of the dissociation of picric acid and picrate in media with low values of the dielectric constant. We selected dioxane-water mixtures with small amounts of water (2, 5, and 15% water), and ethyl alcohol-benzene mixtures (1, 16, and 50% alcohol).

All the absorption spectra were obtained using an SF-4 spectrophotometer. The measuring procedure was the same as in our previous articles. We chose concentrations of 5×10^{-5}, 1×10^{-3}, and 8.8×10^{-3} moles/liter and, correspondingly, cells of 1, 0.05, and 0.0057 cm thickness. All substances were carefully purified, and the work was done with freshly prepared solutions.

Let us turn to an examination of the experimental results. The purpose of the present work consisted in the study of the equilibrium between the various equilibrium forms of picric acid and sodium picrate in the above-named solvents. In Fig. 1, we present the spectra of the various limiting equilibrium forms (ionic, molecular, and associated) which may be obtained by the selection of certain definite conditions in solvents with different dissociating powers.

Picric acid and sodium picrate in water at concentrations of 5×10^{-5}, 1×10^{-3}, and 8.8×10^{-3} moles/liter are characterized by a single spectral curve with a maximum in the 355-356 mμ region, which is an ionic spectrum (all the solutions are colored yellow). In dichloroethane, picric acid at all the concentrations indicated also possesses a single spectral curve with a maximum in the 238 mμ region and a small maximum around 340 mμ (this is the spectrum of undissociated picric acid). Picric acid at a concentration of 8.8×10^{-3} moles/liter in dry dioxane has an analogous spectrum (here all the solutions are colorless).

Sodium picrate at concentrations of 5×10^{-5}, 1×10^{-3}, and 8.8×10^{-3} moles/liter in dry dioxane is also characterized by a single spectral curve with two maxima in the 345 and 417-420 mμ regions, which is the spectrum of associated sodium picrate ions (all the solutions are colored yellow).

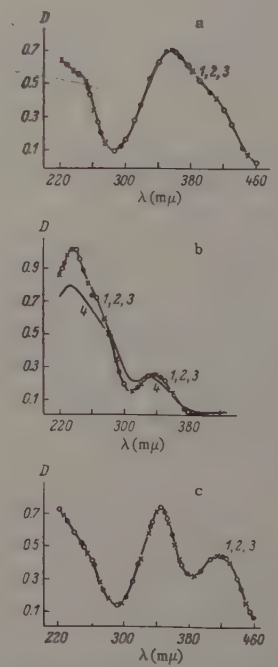

Fig. 1. Absorption spectra of solutions of the limiting equilibrium forms of picric acid and sodium picrate in different solvents. a—Ionic form of HPk and NaPk in water; b—molecular form of HPk in dichloroethane (curves 1, 2, 3) and dioxane (curve 4); c—associated form of NaPk in dioxane. Concentration (moles/liter): curve 1—5×10^{-5}, curve 2—1×10^{-3}, curves 3 and 4—8.8×10^{-3}.

Beer's law is applicable in all the cases presented

picric acid in water and dichloroethane, and sodium picrate in dioxane). This indicates that the equilibrium is shifted toward the limiting equilibrium forms.

The spectra of picric acid and sodium picrate in 95 and 85% dioxane-water mixtures are presented in Fig. 2. In a 95% dioxane-water mixture, picric acid at concentrations of 5×10^{-5}, 1×10^{-3}, and 8.8×10^{-3} moles/liter is characterized by three different spectral curves which intersect at a point. Picric acid at a concentration of $\times 10^{-5}$ moles/liter has a spectrum which is completely identical with the spectrum of sodium picrate in 95% dioxane and is characterized by two maxima in the 350 and 410-415 mμ regions. In other words, picric acid under these conditions is entirely converted into ionic aggregates, the point of intersection indicating an equilibrium between the undissociated molecules and ionic aggregates of picric acid.

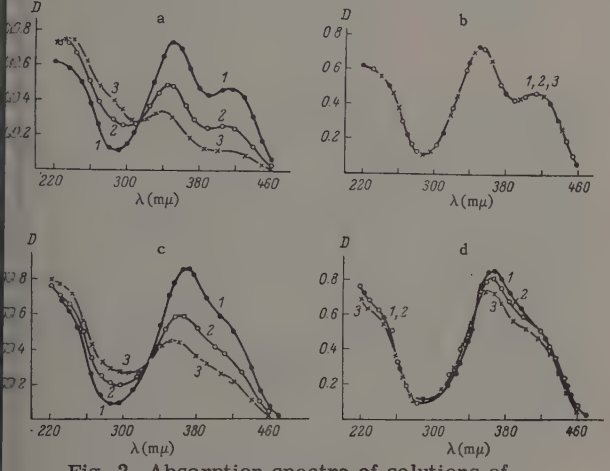

Fig. 2. Absorption spectra of solutions of picric acid (a, c) and sodium picrate (b, d) at various concentrations in dioxane-water mixtures. Composition of the mixture: a, b—95% dioxane + 5% water; c, d—85% dioxane + 15% water. For concentrations (curves 1, 2, 3), see legend to Fig. 1.

In an 85% dioxane-water mixture, picric acid at concentrations of 5×10^{-5}, 1×10^{-3}, and 8.8×10^{-3} moles/liter is also characterized by three different spectral curves which intersect at a point but differ in shape from the spectral curves for the 95% dioxane-water mixture. Picric acid at a concentration of 5×10^{-5} moles/liter has the same spectrum as sodium picrate at the same concentration (with a maximum in the 368 mμ region). This is the ionic spectrum. The ionic spectrum in 85% dioxane is displaced toward longer wavelengths relative to the ionic spectrum in water. In the 85% dioxane-water mixture, an equilibrium is observed between the molecules and ions of picric acid.

Sodium picrate at concentrations of 5×10^{-5}, 1×10^{-3}, and 8.8×10^{-3} moles/liter in an 85% dioxane-water mixture is also characterized by three spectral curves, a shift of the spectra toward the spectra of the ionic aggregates being observed as the concentration increases (the maximum shifts from 368 to 365 mμ for a concentration of 1×10^{-3} moles/liter and to 362 mμ for a concentration of 8.8×10^{-3} moles/liter).

The absorption spectra of picric acid and sodium picrate in alcohol-benzene mixtures are very similar to the analogous spectra for dioxane-water mixtures. The alcohol-benzene mixtures were chosen in such a way that their dielectric permeabilities were approximately equal to those for the dioxane-water mixtures (the dielectric constants of the mixtures were computed on the basis of additivity).

The spectra of picric acid and sodium picrate in the following alcohol-benzene mixtures are presented in Fig. 3: 16% alcohol and 84% benzene (the dielectric constant of this mixture corresponds approximately to the 95% dioxane-water mixture) and a 50% alcohol-benzene mixture (the dielectric permeability of the medium is near the 85% dioxane-water mixture in magnitude).

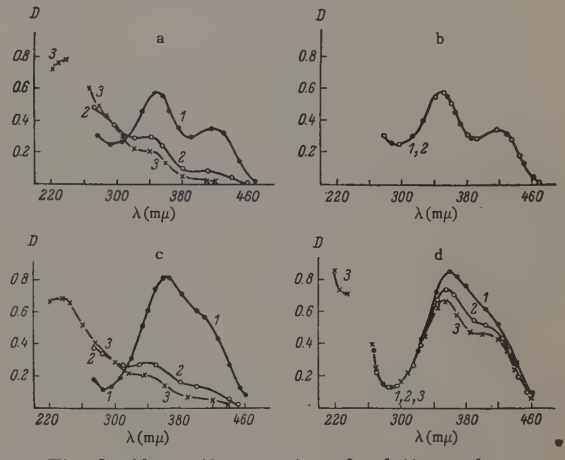

Fig. 3. Absorption spectra of solutions of picric acid (a, c) and sodium picrate (b, d) at various concentrations in benzene-ethyl alcohol mixtures. Composition of the mixture: a, b—84% benzene + 16% alcohol; c, d—50% benzene + 50% alcohol. For concentrations (curves 1, 2, 3), see legend to Fig. 1.

In a mixture consisting of 84% benzene and 16% alcohol (just as in 95% dioxane), an equilibrium is observed between the molecules and ionic aggregates of picric acid; i.e., the character of the spectra indicates the absence of free ions. The spectra of picric acid and sodium picrate at concentrations of 5×10^{-5} moles/liter are completely identical and are characterized by two maxima in the 348-350 and 417-420 mμ regions (spectra of the associated ions), which indicates the complete conversion of picric acid into ionic aggregates.

In a 50% benzene-alcohol mixture, an equilibrium is observed between the molecular and ionic forms of picric acid. The spectra of picric acid and sodium picrate at a concentration of 5×10^{-5} moles/liter coincide both in shape and in intensity (this is an ionic spectrum with a maximum at 360 mμ). The ionic spectrum in ethyl alcohol is characterized by a maximum around 357 mμ, whence it follows that, on addition of 50% of benzene, a small displacement of this spectrum toward longer wavelengths takes place.

The spectra of sodium picrate in a 50% benzene-alcohol mixture are displaced toward the spectrum of the ionic aggregates as the concentration increases (a shift of the maximum from 360 to 355-357 mμ is observed for sodium picrate at concentrations of 1×10^{-3} and 8.8×10^{-3} moles/liter, and a lowering of the intensity of the bands).

As can be seen from Figs. 2 and 3, the spectra of picric acid and sodium picrate in dioxane-water mixtures and in alcohol-benzene mixtures possess a great similarity. However, differences are observed also; thus the spectral curves of picric acid at various concentrations in benzene-alcohol mixtures do not give such a sharp point of intersection as in dioxane-water mixtures. In this connection, we note that benzene at a layer thickness of 1 cm completely absorbs light up to a wavelength of 275 mμ. In thinner layers (for example, at a thickness of 0.0057 cm), it remains optically transparent over the whole wavelength region studied, with the exception of a band from 236 to 265 mμ. Therefore, the spectra of picric acid and sodium picrate in benzene-alcohol mixtures cannot be obtained in their entirety.

In dry dioxane (freezing point 11.78°), picric acid at concentrations of 5×10^{-5}, 1×10^{-3}, and 8.8×10^{-3} moles/liter is characterized by three spectral curves which intersect at a point (Fig. 4). In the spectrum of picric acid at a concentration of 5×10^{-5} moles/liter, a small maximum appears in the 415-420 mμ region. This spectrum recalls the spectrum of the ionic aggregates in shape, whence one may form the hypothesis that, as a solution of picric acid in dry dioxane is diluted, a gradual conversion of undissociated picric acid into the ionic aggregate takes place.

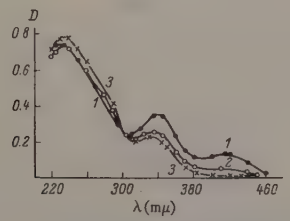

Fig. 4. Absorption spectra of solutions of picric acid in dry dioxane at various concentrations. For concentrations (curves 1, 2, 3), see legend to Fig. 1.

Up to now, we have discussed the equilibria of the various forms of picric acid and sodium picrate in a given solvent. It is interesting to trace how the addition of water to dioxane and of alcohol to benzene influences the spectra of picric acid and sodium picrate. The spectra of sodium picrate in dioxane, dry and with additions of water, are drawn in Fig. 5. It is interesting to note that Beer's law applies for sodium picrate both in dioxane and in mixtures of dioxane with small amounts of water (2 and 5%); i.e., in a given solvent one and the same spectrum, different from the spectrum in another solvent, is obtained at all three concentrations investigated. As water is added to dioxane, a shift of the absorption maximum of the sodium picrate spectrum from 345 mμ in dry dioxane to 350 mμ in 95% dioxane is observed, and also a displacement of the small maximum from 417-420 mμ in dry dioxane to 410 mμ in 95% dioxane, as well as an increase in the intensity of the spectral curves to values characteristic of the ionic spectrum (the spectrum of sodium picrate in 85% dioxane). Since the ionic aggregates are differently solvated in dry dioxane, 98% dioxane, and 95% dioxane, the indicated spectral shifts are apparently associated with a different degree of solvation of the ion pairs. The point of intersection of the spectral curves in the 348 mμ region indicates the presence of an equilibrium between the free ions and ionic aggregates.

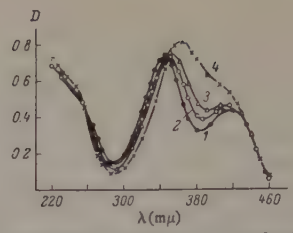

Fig. 5. Absorption spectra of solutions of sodium picrate in dry dioxane (curve 1) and in dioxane-water mixtures (curves 2, 3, 4). Composition of the mixture: curve 2—98% dioxane + 2% water; curve 3—95% dioxane + 5% water; curve 4—85% dioxane + 15% water. Curves 1, 2, 3—ionic aggregates (each spectrum was obtained at concentrations of 5×10^{-5}, 1×10^{-3}, and 8.8×10^{-3} moles/liter); curve 4—ionic form (concentration 5×10^{-5} moles/liter).

In Fig. 6 are presented the spectra of the limiting equilibrium forms of picric acid in dioxane-water and alcohol-benzene mixtures (curves 1-3), and also the spectra of nonlimiting equilibrium forms in the case of dioxane-water mixtures (curves 4-7). The spectra of undissociated picric acid were obtained in water with sulfuric acid added (15 moles/liter) and in benzene with 1% ethyl alcohol added (curves 1). The spectra of the ionic aggregates of picric acid were obtained at a concentration of 5×10^{-5} moles/liter in 95% dioxane and in benzene with 16% alcohol added (curves 2). In 85% dioxane and in a 50% ethyl alcohol-benzene mixture, picric acid at a concentration of 5×10^{-5} moles/liter has a purely ionic spectrum (curves 3).

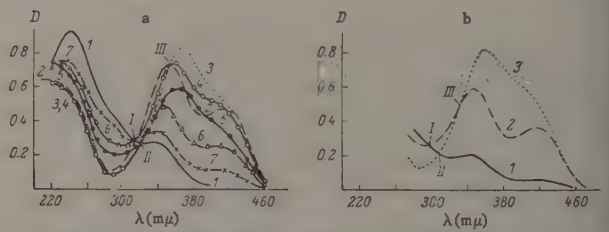

Fig. 6. Absorption spectra of solutions of picric acid in dioxane-water and benzene-ethyl alcohol mixtures. Curves 1—undissociated acid; curves 2—ionic aggregates; curves 3—ions; curve 4—8.8×10^{-3} moles/liter HPk in 85% dioxane; curve 5—1×10^{-3} moles/liter HPk in 85% dioxane; curve 6—1×10^{-3} moles/liter HPk in 95% dioxane; curve 7—8.8×10^{-3} moles/liter HPk in 95% dioxane. I, II, III—intersection points of the curves.

It can be seen from Fig. 6 that the spectral curves 1, 2, and 3 intersect in three points. We have established that the first intersection point (I) indicates the equilibrium between undissociated molecules and ionic aggregates, $HPkM_n \rightleftharpoons MH_s^+Pk_s^-$; the second point (II) indicates that equilibrium between molecules and ions, $HPkM_n \rightleftharpoons MH_s^+ + Pk_s^-$; and the third point (III) indicates the equilibrium between ions and ionic aggregates, $MH_s^+ + Pk_s^- \rightleftharpoons MH_s^+Pk_s^-$ (the index "s" indicates that we are here speaking of equilibria between solvated ions, both free and in ionic aggregates). The three intersection

pints can be seen especially plainly in the case of di-xane-water mixtures when the spectral curves of the nlimiting equilibrium forms are plotted on the graph urves 4-7).

v. Halban and Litmanowitsch[2] have studied the ab-rption spectra of picric acid in dioxane-water mix-tres. They found only one equilibrium—the equilibrium etween picric acid ions and molecules (they took a di-xane-water mixture with a high water content—15.26%). ur investigations have shown that, when 15% of water is dded to dioxane, the equilibrium between the ions and olecules of picric acid is observed, but the ionic aggre-ates are not found.

In the first communication,[1] a general scheme for e dissociation of an electrolyte CA in a solvent M was esented. In the present work it has been shown that, in e dioxane-water mixtures, all the equilibria indicated in e scheme (with the exception of the first equilibrium) e spectrally observable.

In the general form, the constants of these equilibria ay be written down in the following way:

$$K_{diss.} = \frac{a_{C_s^+} \cdot a_{A_s^-}}{a_{CAM_n}};\quad K_{ass.}^{-1} = \frac{a_{C_s^+} \cdot a_{A_s^-}}{a_{C_s^+ A_s^-}};\quad K_{conv.} = \frac{a_{C_s^+ A_s^-}}{a_{CAM_n}}$$

We have computed the values of the dissociating con-ant ($K_{diss.}$) of picric acid at concentrations of 1×10^{-3} nd 8.8×10^{-3} moles/liter in 85% dioxane (1.1×10^{-3} and $.8 \times 10^{-3}$ respectively) and at a concentration of 1×10^{-3} oles/liter in a 50% alcohol-benzene mixture (3.7×10^{-5}). he association constants ($K_{ass.}^{-1}$) of sodium picrate have lso been computed at concentrations of 1×10^{-3} and $.8 \times 10^{-3}$ moles/liter in 85% dioxane (4.1×10^{-3} and $.9 \times 10^{-3}$ respectively), and also in a 50% benzene-alcohol ixture (1.6×10^{-3} and 3.2×10^{-3} respectively). Further-ore, the values of the conversion constant ($K_{conv.}$) of icric acid have been computed at concentrations of $1 \times$ 0^{-3} and 8.8×10^{-3} moles/liter in 95% dioxane (1.06 and .23 respectively) and at a concentration of 1×10^{-3} oles/liter in a mixture consisting of 84% benzene and 6% ethyl alcohol (0.12). In the calculations, we always ssumed that the ions associate into ion pairs.

The variation of the constants with concentration ppears because of the fact that we could not compute e thermodynamic constants of picric acid and sodium icrate in mixtures of dioxane with water or of alcohol ith benzene, nor in acetone or acetonitrile, as we did ot have data on the activity coefficients of picric acid nd sodium picrate in these solvents. We succeeded in omputing the thermodynamic dissociation constants of icric acid only for solutions in water and in methyl, thyl, and n-butyl alcohols. We have compared these alues with the values of the dissociation constants of icric acid obtained by other authors from electrical onductivity and emf data. It turned out that the dis-ociation constants for picric acid in alcohols obtained y us from absorption spectra were several times as arge as those determined from electrical conductivity nd emf. We explain this by the fact that the ion pairs, hich absorb in the same spectral region as the ions, o not take part in current transport, i.e., do not affect he electrical conductivity and emf, and consequently ehave like undissociated molecules in electrometric nvestigations.

Comparison of the optical dissociation constants ith the electrometric ones has shown that ionic associ-tion increases from methyl to n-butyl alcohol; i.e., with a decrease in dielectric constant. In water, the values of the dissociation constants computed from our data and from the emf's coincide. This indicates the absence of ionic association of picric acid in water.

The lowering of the dielectric permeability of water and alcohol on addition of large quantities of dioxane and benzene respectively gives us a possibility of discovering the absorption spectra of the ionic aggregates of picric acid. The spectra of the associated ions of sodium picrate have been found in all solvents investigated by us, and it has been established that the spectra of the associated ions of sodium picrate and of picric acid are completely identical. The absorption spectra of the associated ions of sodium picrate in alcohols, acetone, acetonitrile, dioxane-water mixtures, and benzene-alcohol mixtures display a great similarity. They are characterized (just like the spectra of the associated ions of picric acid) by two maxima in the 350 and 410 mμ regions. From this, consequently, one may draw the conclusion that the picrate ions which enter into ion pairs of such types as $(H_3O^+ \cdot Pk^-)$, $(C_2H_5OH_2^+ \cdot Pk^-)$, $(CH_3COCH_4^+ \cdot Pk^-)$, $(H_2ONa^+ \cdot Pk^-)$, etc., possess completely identical absorption spectra.

v. Halban and his collaborators[2-4] studied the absorption spectra of picrates and picric acid in water and in solvents of low dielectric constant—dioxane, chloroform, dichloroethane, and dioxane-water mixtures. They obtained spectra of undissociated picrates which were identical to the spectra observed by us. For the picrates, the entirely correct assumption was made in refs. 2-4 that the indicated spectra are the spectra of ion pairs. However, for picric acid the spectrum of the ion pairs was not experimentally obtained in refs. 2-4, for which reason the authors made an attempt to determine the position of this spectrum by calculation. In this connection v. Halban and Litmanowitsch themselves point out that the spectrum of the ion pairs can be only approximately computed. Actually, the spectral curve which they computed lies higher than the spectrum of the free ions and, naturally, does not reflect the real picture.

Thus our investigations have shown that, in leveling solvents—in water and alcohols—and also in such differentiating solvents as acetone and acetonitrile, equilibria are observed between the free ions and ionic aggregates, and also between the ions and undissociated molecules. In aprotic solvents, the equilibrium is shifted toward the undissociated state. In an acid solvent—acetic acid—the equilibrium is shifted toward undissociated picric acid, while in a basic solvent—pyridine—the equilibrium is shifted toward free ions and ionic aggregates. In dioxane-water mixtures and benzene-alcohol mixtures, equilibria which depend on the dielectric constant of the mixture are observed between ions and molecules, ions and ionic aggregates, and molecules and ionic aggregates.

REFERENCES

1. N. A. Izmailov and E. L. Gurevich, Opt. i Spektr. 10, 19, 767 (1961), Optics and Spectroscopy 10, 9, 405 (1961).
2. H. v. Halban and M. Litmanowitsch, Helv. Chim. Acta. 26, 771 (1943).
3. H. v. Halban and B. Stigeti, Helv. Chim. Acta. 20, 746 (1937).
4. H. v. Halban and M. Litmanowitsch, Helv. Chim. Acta, 24, 38 (1941).

SPECTRAL INVESTIGATION OF THE AGGREGATION OF DYES IN SOLVENTS OF LOW POLARITY

Kh. L. Arvan and N. E. Zaitseva (pp. 74-77)

Received 29 July 1960

The saltlike organic dyes are in general insoluble in nonpolar solvents, as well as certain solvents of low polarity (benzene, hexane, dioxane, etc.). The dye is usually brought into solution in a nonpolar solvent by first dissolving it in a small quantity of a polar solvent in which it is very soluble and by subsequently introducing it into the nonpolar solvent. The dye falls out in the form of a colloid, but some part of it remains in the true solution.[1] The absorption spectrum of such a solution differs from that of the solution in the polar solvent.

Our experiments have shown that some dyes form considerably concentrated solutions (10^{-3} M) in mixtures in which the nonpolar solvent predominates significantly (up to 90-95 percent by volume).

Figure 1 shows the change in the absorption spectrum of Rhodamine 6G in a mixture of dioxane with methanol as a function of the composition of the mixed solvent. It is seen from this figure that a change in the composition of the solvent results in a shifting of the absorption line, as usually happens when one solvent is replaced by another. At the same time an increase in the percentage of the nonpolar solvent results in the appearance of a short wavelength absorption maximum at the expense of a lowering of the long wavelength absorption.

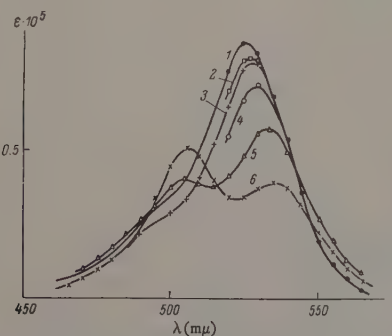

Fig. 1. The effect of the solvent mixture dioxane-methanol on the absorption spectra of Rhodamine 6G ($C = 1.74 \times 10^{-3}$ M). Dioxane composition (in %): curve 1—5; curve 2—10; curve 3—25; curve 4—50; curve 5—75; curve 6—95.

These changes in the ratios of the maxima in the absorption spectra are similar to the changes which take place during the aggregation of the dye, usually observed in the aqueous solutions of the dye with the increase in concentration. In order to understand these changes it was necessary to investigate in detail the dependence of these absorption spectra on the concentration, temperature, the solvent composition and several other conditions.

Figure 2 shows the absorption spectra of Rhodamine 6G for different concentrations of the dye in a solvent of fixed composition—dioxane with 5 percent methanol by

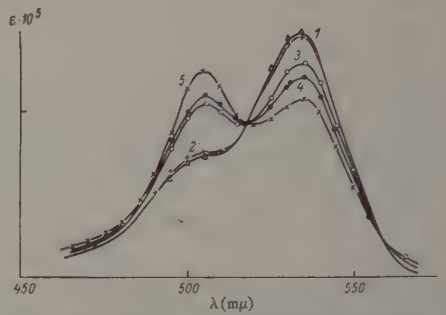

Fig. 2. The effect of concentration on the absorption spectra of Rhodamine 6G in the solvent mixture dioxane-methanol (5 percent methanol). Concentration (in moles/liter): curve $1—9.3 \times 10^{-6}$; curve $2—2.3 \times 10^{-5}$; curve $3—2.3 \times 10^{-4}$; curve $4—3.5 \times 10^{-4}$; curve $5—9.3 \times 10^{-4}$.

volume. It is seen that an increase in the dye concentration intensifies the short wavelength absorption and lowers the long wavelength absorption, i.e., results in the same changes as an increase in concentration of the same dye in aqueous solutions.[2]

An increase in temperature results in a relative decrease of the short wavelength absorption maximum (Fig. 3). A relative increase of the short wavelength maximum is accompanied by significant weakening in the luminescence of the solution.

On the basis of these results, it is natural to conclude, by analogy with the changes taking place in the aqueous solutions, that in the media which we have ex-

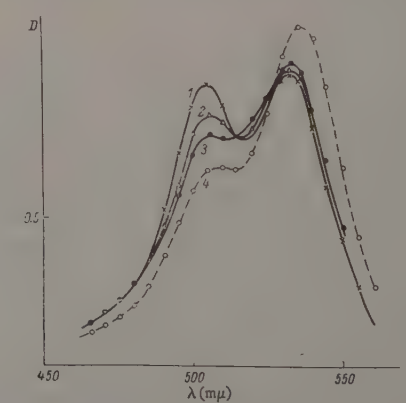

Fig. 3. The effect of temperature and of the addition of pyridine on the absorption spectra of Rhodamine 6G in the solvent mixture of dioxane with 5 percent methanol ($C = 3.5 \times 10^{-4}$). Temperature (in °C): curve 1—20; curve 2—70; curve 3—84; curve 4—20, but with the addition of pyridine.

mined aggregation of the dye is indeed taking place.

In the same way as in aqueous solutions the fraction f the aggregated dye decreases in these media with a ecrease in the dye concentration, an increase in tem- erature, or upon addition of a small amount of pyridine o the solvent (Fig. 3).[3] Besides, a decrease in aggre- ation is also observed when some quantity of another ye is added, analogously to what is observed in aqueous olutions.[4]

As in aqueous solutions the curves of the absorption pectra corresponding to the solutions of different con- entration intersect only at one point, which presents vidence for the existence in these solutions of only two ypes of absorption centers. It is reasonable to suppose hat there are two types of dyes existing in equilibrium, i.e., the unassociated dye—the monomer—and the first tage of aggregation—the dimer.

From the experimentally obtained absorption spec- ra of Rhodamine 6G in the solvent mixture dioxane- ethanol at different concentrations of the dye we made alculations according to the method previously applied o aqueous solutions of Methylene Blue.[5] The absorption pectra of the monomer and of the dimer obtained from hese calculations are shown in Fig. 4. The correspond- ng spectra for this dye in aqueous solutions are also hown in the same figure for the sake of comparison. It s seen that the character of the absorption lines of the onomer and of the dimer is the same in both cases. However, a somewhat greater absorptivity of the dimer n dioxane must be noted. The association constant K of he Rhodamine 6G, calculated according to $K = (1 - \alpha)/\alpha^2 C$, where α is the fraction of the monomers in the solution, C is the molar concentration of the dye) is equal to 2400 nd to 540 for the aqueous solution and dioxane-methyl lcohol mixture, respectively.

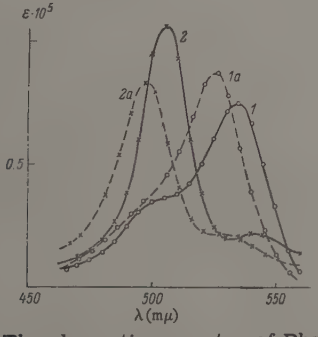

Fig. 4. The absorption spectra of Rhodamine 6G in the mixture of dioxane with 5 percent methanol and in water. Curve 1—monomer in the mixture; curve 1a—monomer in water; curve 2—dimer in the mixture; curve 2a—dimer in water.

The change in the absorption spectra accompanying an increase in dye concentration in similar media was also observed by us for several other dyes (pyronine, pinacyanol iodide, and others).*

*The formation of the aggregated dye in media of low polarity (hexane-alcohol mixture) was previously observed by Lewis.[6] However, the fast precipitation of the dye did not permit him to conduct a spectroscopic investigation.

The state of the dye in different combinations of the solvents is determined by the different ratios of their components. Thus, for example, the precipitation from solutions of Rhodamine 6G at a dye concentration of 1.74×10^{-3} M takes place in a toluene-methanol mixture when methanol is decreased to 14 percent molal concentration, whereas in a dioxane-methanol mixture it takes place at concentrations of alcohol smaller than 1 percent.

The effect of the solvent is probably determined by the nature of the interaction between the molecules of the dye with those of the solvent. The possibility of aggregation is provided by the dissimilarity of the solvents under investigation and the saltlike dyes. This is in agreement with the point of view of Sheppard[7] and Scheibe,[8] who relate the decrease in aggregation of the organic dyes which follows the change from water to organic solvents to the relatively greater similarity between the latter and the dye. It is significant that the dielectric constants of all the media which we have investigated are very small. This is in contradiction with the point of view that the role of the magnitude of dielectric constant is decisive in the process of aggregation.[9]*

*Note added in proof: See also Kh. L. Arvan and N. E. Zaitseva, Opt. i Spektr. 10, 272 (1961), Optics and Spectroscopy 10, 137 (1961).

In conclusion we wish to thank M. V. Savost'yanova for the interest she has expressed in our work.

REFERENCES

1. M. V. Savost'yanova, Izvest. Akad. Nauk SSSR, Ser. Fiz. 17, 747 (1953).
2. V. L. Levshin and E. G. Baranova, Izvest. Akad. Nauk SSSR, Ser. Fiz. 20, 424 (1956).
3. Kh. L. Arvan, Sci. Tech. Conf. on Problems of Synthesis and Applications of the Organic Dyes, p. 127. Leningrad, 1956.
4. Kh. L. Arvan, Doklady Akad. Nauk SSSR 121, 123 (1958).
5. T. P. Kravets, Kh. L. Pes'kina, and Z. V. Zhidkova, Izvest. Akad. Nauk SSSR, Ser. Fiz. 14, 493 (1950).
6. G. Lewis, O. Goldschmidt, P. Magel, and J. Bigeleisen, J. Am. Chem. Soc. 65, 1150 (1943).
7. S. Sheppard and A. Geddes, J. Am. Chem. Soc. 66, 1995 (1944).
8. G. Scheibe, Naturwissenschaften 25, 75 (1937).
9. L. D. Derkacheva, Izvest. Akad. Nauk SSSR, Ser. Fiz. 20, 410 (1956).

STUDY OF ELECTRONIC PHOTOTRANSFER REACTIONS IN THE SOLID PHASE BY EPR

N. N. Bubnov, V. V. Voevodskii, N. V. Fock, and B. N. Shelimov (pp. 78-83)

Received 3 August 1960

Photochemical reactions involving electron transfer in frozen solid solutions of sulfuric and phosphoric acids containing $FeSO_4$ and KI are investigated by means of electron paramagnetic resonance (EPR). The correctness of the hypothesis of free atomic hydrogen formation in electron transfer reactions is demonstrated experimentally. On the basis of EPR spectra of frozen benzene solutions, an inference is made about the separability of the elementary processes of electron and proton transfer.

Recently there has been great interest in studying chemical changes which take place in the solid phase at low temperatures under the effect of light or ionizing radiation. In these investigations the methods of radiofrequency spectroscopy, particularly electron paramagnetic resonance (EPR), have begun to be used extensively, along with ordinary spectroscopic methods. This method has several significant advantages and makes it possible to broaden our concepts of the effect of radiation on matter. It permits one to detect free radicals and atoms in very small concentrations and to identify them by their EPR hyperfine structures.

Reactions taking place in the solid phase at low temperatures have their own specific peculiarities. This is explained by the difference between the condensed and gaseous phases in energy transfer processes, by the "cage effect," and by the change in the thermodynamic characteristics of charged particles under these conditions. For example, reactions which cannot take place in the liquid or gaseous phase can occur in the solid phase. It is well known that benzene does not decompose in the gas or liquid phase under the effect of light with $\lambda > 2000$ A, whereas in the solid phase at 77° K, according to Gibson et al.,[1] the benzene ring is ruptured.

The quantum yields of low temperature reactions evidently differ substantially from quantum yields of liquid and gaseous reactions.[2] It is well known that the ionization potentials of molecules are lowered significantly in the condensed phase;[3] the greater the dielectric constant of the material, the more significant is the decrease. In agreement with this, photoionization reactions, as well as photodissociation reactions, can also occur in the condensed phase. In 1942 Lewis and Lipkin,[4] investigating the absorption spectra of frozen clear solutions of complex organic compounds such as polyphenylhydrazines and polyphenylamines irradiated with ultraviolet light, showed that these compounds not only dissociate into free radicals, but can also undergo photoionization according to the scheme,

$$(Ph)_2N{-}N(Ph)_2 \xrightarrow{h\nu} \begin{cases} (Ph)_2N{-}\ddot{N}(Ph)_2 + e \\ 2(Ph)_2N\cdot \end{cases}.$$

Low temperature technique makes it possible to stabilize the free radicals and atoms. This greatly facilitates the use of both optical spectroscopy and EPR for investigating their formation processes and structure.

In this work EPR was used to investigate certain photochemical reactions which involve electron transfer.

During the last 20 years, a number of papers on electron phototransfer reactions in the liquid phase (e.g. refs. 5-7) have suggested that atomic hydrogen may be formed in water or dilute acids by reactions of the type

$$M + H_2O \xrightarrow{h\nu} M^+ + OH^- + H. \quad (1)$$

M can be a metallic ion of variable valency (for example, V^{2+}, Cr^{2+}, Fe^{2+}, Mn^{2+}, Co^{2+}, etc.) or any one of a number of anions, such as I^-, N_3^-, SH^-, SO_3^{--}, etc.

In each case, the occurrence of such a process was inferred from the analysis of the reaction products, investigation of the kinetic characteristics of the process, initiation of polymerization, and determination of the location of the deuterium atom in the molecule of the polymer when the experiment was performed in heavy water. However, the authors of these papers[7] point out a number of difficulties which limit the use of polymerization as a method of investigating electron phototransfer occurring in the course of the above-mentioned process.

EPR is a direct and convenient method of detecting hydrogen atoms produced in reaction (1), since they have a characteristic spectrum consisting of two lines with a very large hyperfine splitting (approximately 500 oersteds). No other atom or radical possesses such a spectrum.

In order to investigate electron phototransfer reactions by EPR, it is necessary to work under conditions which insure the stabilization of the hydrogen atoms, since under ordinary conditions the high mobility and reactivity of hydrogen atoms make it difficult to obtain them in sufficient concentration for detection by means of the EPR spectrometers available at the present time. In order to stabilize the $\dot{H}$ atoms, we made the measurements in the solid phase at low temperatures.

It follows from the existing literature that in the majority of frozen solids, including ice, hydrogen atoms diffuse easily even at 77° K; it is necessary to work at hydrogen and helium temperatures in order to detect them.[8] In frozen dilute and concentrated solutions of sulfuric, phosphoric, and perchloric acids, however, hydrogen atoms do not recombine at 77° K; this is shown by the data of Livingston et al.[9] Upon irradiating these acids with γ rays, they detected a significant concentration of $\dot{H}$ atoms, which did not decrease with time.

Considering these facts, we performed EPR experiments in frozen aqueous solutions of sulfuric and phosphoric acids which contained $FeSO_4$ and KI.

The concentration of the sulfuric acid ranged from 40 to 96%; phosphoric acid, from 40 to 85%. The $FeSO_4$ and KI were about 0.1 molar. The $FeSO_4$ was purified by precipitating it from aqueous solution with ethyl alcohol.[10] Reagent grade potassium iodide was used without additional purification. The samples were irradiated in

artz ampules 4 mm in diameter placed in a quartz ewar containing liquid nitrogen. The samples were not bjected to vacuum treatment. The irradiation was per-rmed with ultraviolet light from a PRK-7 mercury mp located 3-4 cm from the samples; the irradiation sted one hour. After irradiation, the samples were ansferred immediately into a Dewar (T = 77° K) located the cavity of an EPR spectrometer with high frequency agnetic field modulation.[11]

Upon irradiation of the $FeSO_4$ solutions in sulfuric d phosphoric acids frozen at 77° K, a doublet with a litting of 507 oersteds was detected in the EPR spec-um. This result clearly substantiates the hypothesis at free hydrogen atoms are formed in electron photo-ansfer reactions. An analogous spectrum consisting of o components with the same splitting but lower inten-ty was also observed upon irradiation of frozen solu-ns of KI in H_2SO_4 and H_3PO_4. For a definite check of e conclusion about the nature of the process of elec-on phototransfer reactions, experiments were per-rmed with solutions containing heavy water. In addition the doublet with 507 oersted splitting, the EPR spec-um (Fig. 1) showed a triplet produced by the deuterium oms with a hyperfine splitting ≃77 oersteds, which is good agreement with the theoretical value.

Fig. 1

The quantum yield of this reaction was also deter-ined by measuring the number of hydrogen atoms pro-uced. These experiments showed that the quantum yield mounted to ~0.1 for an $FeSO_4$ concentration of 0.1 ole/liter and a ratio of $H_2O : H_2SO_4 = 2 : 1$ by volume. ur data do not give an accurate value for the quantum ield of this reaction because of the instability of the or-anic free radical diphenylpicrylhydrazyl (DPPH) used s a standard for measuring the hydrogen atom concen-ration.*

*The difficulty of making accurate quantitative measure-ents with the help of DPPH is analyzed in detail in a umber of papers (for example, refs. 17 and 18). The naximum error evidently amounts to 30-50%.

The lowering of ionization potentials noted above ermits one to suppose that, in strongly polar condensed naterials, ultraviolet light can ionize not only complex nolecules of the polyphenylhydrazine and polyphenylamine ypes, but simpler aromatic compounds as well. This is n spite of the fact that in the gaseous phase, because of he appreciable ionization potentials of such molecules 10 ev and more), photoionization reactions practically do ot occur at all.

Actually, in the EPR spectra of benzene solutions concentration about 2×10^{-2} mole/liter in dilute sulfuric nd phosphoric acids) irradiated by ultraviolet light at 7° K, lines characteristic of hydrogen atoms were de-ected, which evidently indicates photoionization. To-ether with the hydrogen atom lines (b in Fig. 2) addi-

Fig. 2

tional lines of rather complicated structure (a in Fig. 2) are detected in the center. Evidently, the EPR spectra of several radicals are superposed in the center. The fact that the four most intense central components, marked by arrows in Fig. 3, differ from the side components in width and saturation level* also indicates this.

*When the intensity of the microwave field is increased to $H_1 \sim 0.2$ oersted, the side components undergo appreciable saturation, but the central components show practically no saturation.

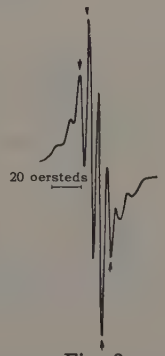

Fig. 3

The intensity distribution of the four central components is 1 : 3 : 3 : 1, which can only be the result of the interaction of an unpaired electron spin with the spins of three equivalent protons. The total hyperfine splitting is about 24 oersteds, which is very close to the splitting in in the $C_6H_6^-$ radical whose EPR spectrum was investigated in our laboratory.[12]

Since it is known[13] that the EPR spectra of positive and negative aromatic radicals are very similar, it is possible to suppose that in our case the $C_6H_6^+$ radical is responsible for this spectrum. However, the number of hyperfine structure components does not correspond to this (in the spectrum of the $C_6H_6^-$ radical, whose charge is uniformly distributed around the benzene ring, the number of hyperfine components is 7, corresponding to the number of protons which interact with the unpaired electron.[12] It is possible to explain this discrepancy by assuming that in our case the charge is localized near one carbon atom in the ring. This in turn can be a consequence of ion pair formation by the reaction

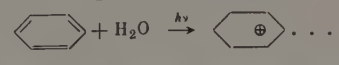

In the $C_6H_6^+$ radical, with its localized charge, the unpaired valence can be found only in the ortho and para positions, thus interacting with only three, not six, protons. This must give four lines in the EPR spectrum with an intensity distribution of 1 : 3 : 3 : 1.

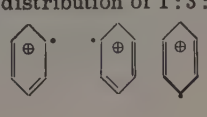

Changes in the EPR spectrum which take place on heating the system and indicate transformation of the radicals can be used as an argument in support of this hypothesis. The EPR spectrum obtained at −100°C is shown in Fig. 4b. The number of components and magnitude of the hyperfine splitting of the side-components is very close to the corresponding quantities in the EPR spectrum of the phenyl radical[14] obtained by bombarding frozen benzene with fast electrons (Fig. 4a). The central part of the spectrum in our case is more complex, which evidently is due to the superposition of the spectra of two or more radicals.

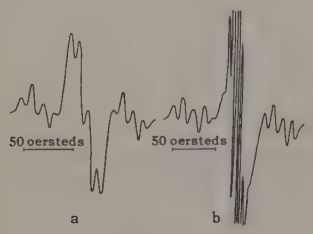

Fig. 4

One can explain the transition from the spectrum of Fig. 3 to the spectrum of Fig. 4b by assuming that during the heating there is a transition of the proton from the $C_6H_6^+$ ion to the ^-OH ion with the formation of a phenyl radical:

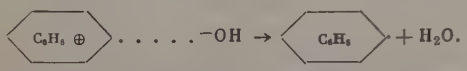

A similar spontaneous splitting off of a proton at low temperatures was observed by Lewis and Lipkin[4] in the positive diphenylamine ion

$$(Ph)_2\overset{+}{N}H \longrightarrow (Ph)_2N\cdot + H^+.$$

If the proposed explanation is correct, then our experiments with benzene can be considered as a new direct experimental demonstration of the separability of the elementary processes of electron and proton transfer.

It is necessary to note that the above-described action of ultraviolet light on benzene molecules in the condensed phase occurs only in polar materials. When benzene is irradiated at 77°K in a nonpolar hydrocarbon, the EPR spectrum is completely different (Fig. 5). This spectrum has the hyperfine splitting characteristic of the hydrocarbon radicals.

Fig. 5

It is also necessary to make note of an interesting characteristic of the EPR spectrum of hydrogen atoms. Figure 6 shows one component of the spectrum of the hydrogen atom produced during irradiation of the systems

$$H_2O—H_2SO_4—FeSO_4 \qquad (a)$$

and

$$H_2O—H_2SO_4—C_6H_6, \qquad (b)$$

with ultraviolet light. At least two weaker lines are observed on each side of the main component. One can attribute these additional lines to the flipping of proton spins in molecules surrounding the hydrogen atom, simultaneously with flipping of the electron spin of the hydrogen atom.[15] The fact that the separation of the supplementary components (5 oersteds), expressed as a frequency, is close to the proton resonance frequency in the magnetic field (H ≃ 3300 oersteds) which we used tends to support this view. We should also note the phenomenon of saturation of the hydrogen atom signal. In our experiments with benzene, the lines from the H atoms saturated strongly, but in the experiments with Fe^{2+} saturation was not observed. This is evidently due to the high concentration of paramagnetic ions with short relaxation times.

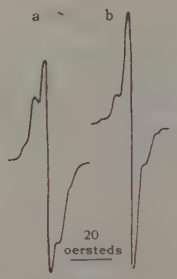

Fig. 6

The question of how far one can transfer an electron during a phototransfer reaction is very important and interesting. According to the authors of papers on electron phototransfer in solutions,[5,6] the hydrogen atom is formed from water molecules in the solvate shell of the ion being ionized. On the other hand, investigation of absorption spectra of certain semiconducting crystals and glasses containing different pairs of ions showed that in these systems one can assume that electrons are transferred distances of the order of 10 atomic diameters.[16] Detailed investigation of the dependence of saturation effects, g-factor, and hyperfine splitting on the conditions and material in which the hydrogen atoms are formed during an electron phototransfer reaction would presumably permit one to answer the question to some extent.

In conclusion, let us emphasize once more that in order to study processes which occur in solids under the effect of radiation, it is necessary to apply various complex spectroscopic methods in order to account for the many diverse processes which take place in the system. For example, in studying the effect of ultraviolet radiation on molecules of aromatic compounds, it is necessary to consider not only the processes of phosphorescence and fluorescence, which have been investigated in detail by physicists, but the processes of photodissociation and photoionization as well.

REFERENCES

1. G. E. Gibson, N. Blake, and M. Kalm, J. Chem. Phys. 21, 1000 (1953).
2. I. L. Mador, J. Chem. Phys. 22, 1617 (1954).
3. E. L. Lyons, J. Chem. Soc., 5001 (1957).
4. G. N. Lewis and D. Lipkin, J. Am. Chem. Soc. 64, 2801 (1942).

N. Uri, Chem. Revs. 50, 375 (1952).
B. Ya. Dain and E. A. Liberzon, Doklady Akad. Nauk SSSR 28, 228 (1940); Acta Physicochim. U.R.S.S. 19, 410 (1944).
F. S. Dainton and D. James, Trans. Faraday Soc. 54, 649 (1957).
M. S. Matheson and B. Smaller, J. Chem. Phys. 28, 1169 (1958). See also Science 128, 623 (1958).
R. Livingston, H. Zeldes, and E. Taylor, Discussions Faraday Soc. 19, 166 (1955).
Yu. V. Karyakin and I. I. Angelov, "Pure Chemical Reagents," p. 147. Goskhimizdat, Moscow, 1955.
A. G. Semenov and N. N. Bubnov, Pribory i Tekh. Ekspt. 1, 92 (1959).
12. V. V. Voevodskii, S. P. Solodovnikov and V. M. Chibrikin, Doklady Akad. Nauk SSSR 129, 1082 (1959).
13. A. Carrington, F. Drawnieks, and M. Symons, J. Chem. Soc., 947 (1959).
14. Yu. N. Molin, V. V. Voevodskii, I. I. Chkheidze, and N. Ya. Buben, Doklady Akad. Nauk SSSR 130, 1291 (1960).
15. G. T. Trammel, H. Zeldes, and R. Livingston, Phys. Rev. 110, 630 (1958).
16. W. A. Weyl, J. Phys. & Colloid Chem. 55, 507 (1951).
17. G. Feher, Bell System Tech. J. 36, 449 (1957).
18. J. Uebersfeld, J. chim. phys. 56, 805 (1959).

EFFECT OF MECHANICAL TREATMENT ON THE ABSORPTION SPECTRUM OF CADMIUM SULPHIDE CRYSTALS AT LOW TEMPERATURE

E. F. Gross, M. Bancie-Grillot, E. Grillot, and B. S. Rasbirin (pp. 84-86)

Received 1 August 1960

The absorption spectra of cadmium sulphide crystals obtained by various methods were studied at the temperature 4.2° K. It was found that mechanical treatment of the samples (grinding and polishing) leads to a considerable change of the appearance of the spectrum at the edge of the fundamental absorption. Discussion and interpretation of the results obtained is given.

In the course of study of the absorption spectra of ngle cadmium sulphide crystals at low temperatures, a mplex fine structure of the edge of the fundamental ab-rption band had been found.[1] At the temperature 4.2° K, consists of a group of broad intensive absorption lines d a group of weak, very narrow lines located on the ng wavelength side of the former. On the basis of cer-in considerations and of a series of experiments, two the writers[2,3] suggested an exciton origin for the first oup of lines. The second group of lines (of longer wave-ngths) was not thought to be connected with the absorp-n in the basic lattice of the crystal. Furthermore, two the writers[4] have found that the method of growing very re single cadmium sulphide crystals greatly affects me of their optical properties.

The first experiments[1] were performed with CdS ystals obtained by the method of Frerichs.[5] One of the esent writers[6] suggested a new method for obtaining rge CdS crystals of considerable thickness (up to 5 mm) y isothermal growing in an atmosphere of H_2S), which ave some properties that are different from those of the rystals grown by the Frerichs' method. We undertook n investigation of the absorption spectra of these crystals low temperature.

It did not appear possible to study the thick crystals irectly, since the structure of the absorption edge can e distinctly observed only in the spectra of fairly thin rystals of CdS, because of the large absorption coeffi-ient. Therefore, in the preliminary experiments small ieces were sawed off or cleaved from the large crys-ls; on grinding and polishing these pieces small thin lates were prepared of a thickness of several tens of nicrons. We succeeded in polishing some of the plates own to a thickness of 20 μ.

The study of the absorption spectra of these crys-ls gave an unexpected result: No traces of a line struc-re were detected in the absorption edge, whereas in the crystals obtained by the Frerichs' method which had the same thickness, the line structure was observed very distinctly. Furthermore, it was noticed that the edge of continuous absorption in the spectra of the investigated crystals which were ground and polished to a 20 μ thickness is very diffuse and is shifted toward the red region of the spectrum for about 20 A (Fig. 1, curve a), in comparison with the crystals of the same thickness prepared by the Frerichs' method. This result can be explained either by some peculiarity in the structure of the crystals obtained by the new method, or by the treatment (grinding and polishing).

The effect of grinding and polishing on the absorption spectrum of crystals could be ascertained very simply. We had at our disposal some relatively thick

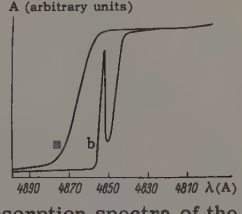

Fig. 1. Absorption spectra of the CdS crystal prepared by the method described in the paper by Grillot[6] (microphotograms). Curve a—ground and polished crystal (thickness d = 20 μ, temperature T = 4.2° K); curve b—crystal prepared by cleaving without grinding and polishing (d = 20-40 μ, T = 4.2° K). The lines of the structure $\lambda\lambda$ = 4889, 4864, 4861, 4857 A, that can be observed in the original photographs, are not noticeable in the above microphotogram because of the low intensity.

(up to 0.3 mm) CdS crystals, obtained by the method of Frerichs, which were kindly given to us by Professor R. Rompe.* After we ascertained that the line structure

*It is a great pleasure to express here our appreciation to Professor R. Rompe (Institut für Strahlungsquellen, Berlin) who kindly sent to us these crystals for our investigations.

at the fundamental absorption edge can be observed in the spectra of these crystals in a thickness of 120 μ (the group of fine lines, Fig. 2, curve a), we ground and polished these crystals on both sides, reducing their thickness from 120 to 80 μ. It was found that after grinding and polishing the structure of the absorption edge cannot be observed any more, and that in its place a diffuse continuous absorption edge appears (Fig. 2, curve b). It is natural to assume that the appearance of the continuous background is connected with the treatment of the surface of the CdS crystal and is caused by the damage of the surface of the crystalline plate in grinding and polishing. In order to test this supposition, we tried to obtain sufficiently thin plates of CdS by cleaving only, from thick crystals obtained by one of the writers,[6] without subsequent grinding and polishing. In this manner we succeeded in preparing samples of cadmium sulphide 20 to 40 μ thick. The investigation of their spectra showed that there was a line structure at the absorption edge of these unground crystals (Fig. 1, curve b), similar to that observed in CdS crystals of the same thickness prepared by the method of Frerichs, although the absorption lines in the spectra of the cleaved crystals were considerably (2-3 times) more diffuse.* This could be caused by small

*The weak long wavelength lines of the structure ($\lambda\lambda$ 4889, 4864, 4861, 4857 A) which can be seen on the original spectrograms, are not noticeable on this microphotogram (Fig. 1, curve b).

nonuniform deformations (see, for instance, ref. 3), which appeared in the present case in growing and cleaving these crystals. There was no enhanced background in the region of the line structure at the absorption edge in the spectra of crystals that were not ground.

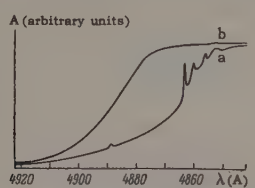

Fig. 2. Absorption spectra of CdS crystals prepared by the Frerichs' method[5] (microphotogram). Curve a—before grinding and polishing (d = 120 μ, T = 4.2° K); curve b—after grinding and polishing (d = 80 μ, T = 4.2° K).

Since we did not succeed in preparing sufficiently thin plates of CdS cy cleaving, we were unable to observe the short wavelength part of the structure, which can be seen only in thin crystals because of the strong absorption. Therefore we tried to observe this structure in the reflection spectrum. It was found that in the reflection spectra of "cleaved" crystals prepared by the new method,[6] the same maxima and minima are observed as in the reflection spectra of crystals grown by the Frerichs' method.

The results of the experiments described above demonstate that the treatment of the surface of CdS crystals (grinding and polishing) produce very large changes in their absorption spectrum. As mentioned before, such an intense continuous background appears at the fundamental absorption edge, after the treatment of the crystalline surface, that the observation of the line structure becomes impossible. Thus, the treatment of the surface results in a strong additional continuous absorption of light.

The question arises as to what changes in the crystal lattice are responsible for this additional absorption. Among possible explanations, we shall point out two. The additional continuous absorption can be connected with the formation on the crystal surface of a cubic modification of CdS through the mechanical action during grinding and polishing. It is indeed possible that during the grinding of the hexagonal CdS, the cubic modification of CdS is formed, as it is in ZnS and the mixed crystals Zn · CdS.[7] Furthermore, the absorption edge of the cubic CdS is apparently somewhat shifted toward the red spectral region, relative to that of the hexagonal CdS. All this makes the aforementioned supposition probable.

Another possible explanation of the action of grinding and polishing of the crystal on its spectrum can be found in the deformations and defect formation in the hexagonal lattice of CdS in such mechanical treatment. It is known[9] that the mechanical treatment of the surfaces of metals and other crystals may result in an "amorphization" of the surface layer, i.e., in the formation on the surface of a layer consisting of extremely small crystals, the layer extending to the depth of several thousand angstroms, depending on the size of the minute crystals. The enormous number of defects in the CdS lattice which are thus formed can produce additional absorption, causing a shift of the absorption edge toward the longer wavelength spectral region. It is also possible that an important part is played here by the formation of a large number of dislocations as a result of a slip of the lattice planes in the mechanical treatment. The strong stresses thus created produce changes of the lattice parameters and, consequently, local changes of the width of the forbidden zone. Distortions of this kind may, on the one hand, shift the edge of the fundamental absorption, and, on the other, produce a considerable decrease of the probability of exciton formation.

REFERENCES

1. E. F. Gross and N. A. Karryev, Doklady Akad. Nauk SSSR **84**, 471 (1952);
E. F. Gross and M. A. Yakobson, Doklady Akad. Nauk SSSR **102**, 485 (1955).
2. E. F. Gross, B. S. Rasbirin, and M. A. Yakobson, Zhur. Tekh. Fiz. **27**, 207 (1957).
3. E. F. Gross, B. S. Rasbirin, and M. A. Yakobson, Zhur. Tekh. Fiz. **27**, 1149 (1957), Soviet Phys.-Tech. Phys. **2**, 1043 (1958).
4. E. Grillot, J. phys. radium **17**, 671 (1956);
E. Grillot and M. Bancie-Grillot, "Festkörperphysik," pp. 226-243. Akad. Verlag, Berlin, 1958;
E. Grillot and M. Bancie-Grillot, Izvest. Akad. Nauk, Ser. Fiz. **22**, 1356 (1958).
5. R. Frerichs, Phys. Rev. **72**, 594 (1957).
6. E. Grillot, Compt. rend. acad. sci. (Paris) **242**, 779 (1956).

V. A. Levshin and I. V. Veits, Zhur. Tekh. Fiz. 20, 411 (1950).
E. Mollwo, Reichsber. Physik 1, 1 (1944);
F. Möglich, Arbeitstag. Festkörperphys. II, 94 (1955).
Z. G. Pinsker, "Electron Diffraction," p. 333. Izd. Inostrannaya Lit., Moscow, 1949;
P. B. Hirsch and I. N. Kellar, Nature 162, 609 (1948);
P. Gei and P. Hirsch, "Properties of Metal Surfaces," p. 112. Izd. Inostrannaya Lit., Moscow, 1954.

MICROSCOPIC STUDIES OF ELECTROLUMINESCENCE IN ZnS-Cu,Al SINGLE CRYSTALS

A. M. Bonch-Bruevich, Ya. E. Kariss, and V. A. Molchanov (pp. 87-92)

Received 14 July 1960

A setup is described for the microscopic study of electroluminescence in single crystals. A synchronous single method with a variable phase shift (sliding phase) was used. It was found possible to investigate the shape, amplitude, etc., of the light pulses emitted by individual crystal regions. Preliminary experiments with ZnS-Cu,Al single crystals indicated the possibility of separating the turn-on and turn-off luminescence; a rule was found to govern the distribution of the ratio of the amplitudes of the turn-on and turn-off luminescence pulses in different parts of the crystal.

The interest in observing the electroluminescence of ingle crystals under a microscope is well-known. It is e, firstly, to the possibility of comparing average characteristics obtained from the observation of electroluminescent capacitors with the luminescence characteristics individual active crystal regions[1-4] and, secondly, to e possibility which it affords of investigating the structure of luminous crystal regions.[1,5] The natural difficulties in performing such experiments stem from the low tensity of the light, which limits the possibility of performing experiments and considerably reduces the accuracy of measurements. In order to circumvent these ifficulties, we used the method of synchronous signal ccumulation with variable phase shift (sliding phase) roposed in 1953[6] and developed in a series of papers.[7-9]

The experimental setup for microscopic studies of ectroluminescence is shown schematically in Fig. 1. he single crystal investigated (which in our experiments d a hexagonal structure with linear dimensions of the der of 60 μ), together with two needle electrodes, was ast into a mixture of melamine-formaldehyde and resyl esins and placed in the focal plane of the microscope bjective, in which it could be smoothly displaced in utually perpendicular directions. Periodic rectangular oltage pulses were applied to the electrodes with a pulse epetition time (T_1) of 10^{-3} sec; the pulse duration (t') nd amplitude (U_m) were variable over a wide range. In ur opinion, this pulse shape makes it possible to obtain ae clearest information on the rules governing the production of light pulses. Such rules can then be validly ompared to the rules for the luminescence of electroluminescent capacitors (also excited, of course, by quare-wave voltage pulses). A diaphragm was placed in ne focal plane of the eyepiece, making it possible to isolate the luminescence of crystal regions about 10 μ in ize. The location of such regions with respect to the lectrodes could be visually adjusted by introducing a pecial deflecting prism into the light beam in the microscope. The signal taken off the load resistor of a photoultiplier placed behind the eyepiece of the microscope as fed to a special gating stage. This stage let the signal pass only during the short time interval t_0 with a f the oscilloscope. The sweep period T_2 is much longer han the repetition period of the signals on the load of the

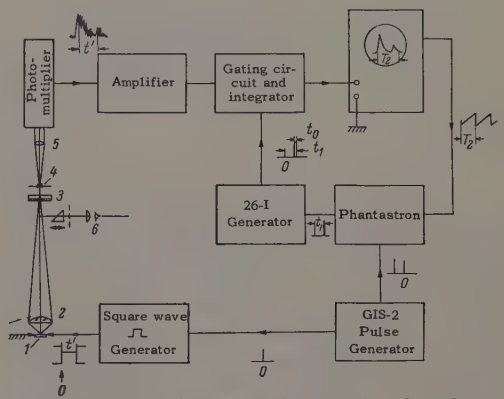

Fig. 1. Block diagram of apparatus for observing the luminescence of single crystals under a microscope. 1—sample; 2—40 × objective; 3—filter; 4—diaphragm; 5,6—15 × oculars.

photomultiplier (in our case 10^4 times). The time constant of the integrating circuit (storage device) which follows the gating stage is selected by using the condition $T_1 \ll \tau_n \ll T_2$. It can easily be seen that there is considerable averaging of noise (the noise level being lowered approximately $\sqrt{\tau_n/T_1}$-fold), as well as a slight distortion of the shape of the signals (which can be demonstrated by varying the value of τ_n for fairly strong signals).

A GIS-2 generator was used to synchronize the gating circuit with the voltage pulse generator; one of the signals produced by the generator triggers a phantastron, and the second, delayed by 10-15 μsec, triggers the square-wave generator. The duration of the pulses put out by the phantastron is controlled by the sawtooth voltage of the oscilloscope (ENO-1) sweep, and the trailing edge of these pulses triggers a type 26-I generator. Pulses received from the output of the latter and delivered to the gating circuit are therefore gradually displaced with respect to the pulses applied to the sample, this displacement being synchronized with the sweep of the oscilloscope. The oscillograms shown in Fig. 2 illustrate the effect obtained by treating the signals in this

Fig. 2. Oscillograms illustrating the decrease in the noise level when synchronous accumulation with variable phase shift is used. a and b: oscillograms of electroluminescence pulses for voltage pulses of different durations t′, taken directly off the load resistor of the multiplier; c and d are the same pulses after passing through the synchronous accumulator.

way. These oscillograms show that this method permits investigation of pulse shapes of the luminescence of separate parts of the crystal, observation of details, measurement of pulse amplitudes, etc.

Preliminary observations of the luminescence of a number of crystals indicated that there exists a general rule for the distribution of the ratios of pulse amplitudes corresponding to the turn-on and turn-off emission in various parts of the crystals. Near the electrode, whose potential is rising, the turn-on pulse exceeds the turn-off pulse; at the other electrode the amplitude ratio of these light pulses is reversed. Light pulses with approximately equal amplitudes are likewise observed in the central part of the crystal (Fig. 3). The presence of total internal reflection in the crystal (together with a drop of

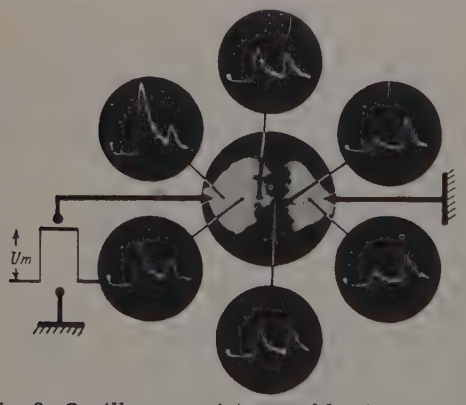

Fig. 3. Oscilloscope pictures of luminescence pulses in various regions of a ZnS-Cu,Al single crystal. In the center is shown a micrograph of the single crystal to which rectangular voltage pulses were applied. The distance between the electrodes was 60 μ.

polymerized resin) made it impossible to state that there are really two light pulses at each electrode. It is equally impossible to affirm that the sources of excitation of electroluminescence are located in all the regions of the luminescence seen on photographs. It is certain, however, that if a luminescence peak develops at the negative electrode, it is much smaller than the peak generated at the positive electrode.

On the basis of an investigation of light pulse amplitudes and of the light sum in the green emission band of the electroluminescent capacitor, the conclusion was drawn in refs. 10 and 1 that luminescence decreases when the direction of the electric field is reversed. Observation of electroluminescence pulses in individual parts of the crystal permits direct observation of the accelerated drop in luminescence at the positive electrode when this electrode becomes the cathode. This acceleration is clearly displayed when the light produced at the start of the voltage pulse does not have time to decay fully by the end of the pulse. This effect is shown in Fig. 4, which represents two superposed oscillograms of light pulses corresponding to 120 μsec and 40 μsec voltage pulses. It can be seen that for a short duration t′ the turning off of the voltage is accompanied by a decrease in the light sum corresponding to one voltage pulse (light loss effect).

Fig. 4. Oscilloscope pictures of light pulses in the green luminescence band for various durations of the voltage pulse. a—120 μsec; b—40 μsec.

The investigation of electroluminescence kinetics in individual regions of a crystal is of considerable interest because of the complexity of the luminescence decay law in an electroluminescent capacitor (polycrystalline sample). Such an investigation can be made with the method described above. Figure 5 shows luminescence decay curves near the electrode after a voltage had been applied to the crystal, the luminescence of the entire crystal, and the decay of luminescence of an electroluminescent capacitor filled with the same electroluminescent phosphor. As can be seen, the decay law remains complex even for the region in which there is practically only the turn-on pulse. This law is very close to the luminescence decay law of the crystal as a whole. The luminescence of an electroluminescent capacitor decays somewhat more slowly. This may be connected with reabsorption or with some nonuniformity in the properties of the crystal batch, from which only those specimens were selected for microscopic observations which had the clearest (hexagonal) configuration.

In many theoretical models, the dependence of the light sum of luminescence (I) on the amplitude of the applied voltage obtained with electroluminescent capacitors is associated with the mechanism of liberation and ac-

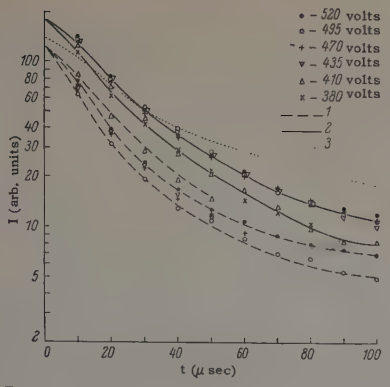

Fig. 5. Luminescence kinetics of a crystal region (curves 1), of the entire crystal (curves 2) and of the electroluminescent capacitor (curve 3).

leration of electrons in the barrier layer and with the ization of luminescence centers by these electrons. otometric measurements made during microscopic obrvation of discrete points in single crystals, and udies of the electroluminescence of large ZnS-Cu crys- s indicate that the formula

$$L = A \exp \frac{B}{\sqrt{U_m}},$$

ich agrees with a corresponding expression for the ctroluminescent capacitor,[12-14] is valid for them too. the other hand, it was found that in electroluminesnt capacitors, the same law is followed by the dendence of light pulse amplitude on voltage; the paraters of this law are not a function of the duration of voltage pulses in the green emission band.[11] Measements of the turn-on pulse amplitude at different ltages, made with the apparatus described, have shown at a law of the form

$$I_m = A' \exp \frac{B'}{\sqrt{U_m}}$$

followed for individual crystal regions (Fig. 6), the lue of the coefficient B′ being practically equal for the

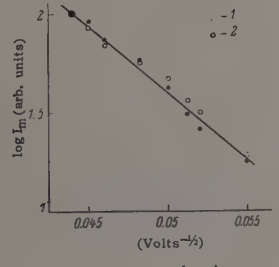

Fig. 6. Dependence $I_m = f(v_m)$ for a crystal region (1) and for an electroluminescent capacitor (2).

electroluminescent capacitor and an individual crystal region (of the order of magnitude of 150 volts$^{1/2}$).

As a result of microscopic studies of the luminescence of ZnS-Cu,Al single crystals, made by synchronous signal accumulation with variable phase shift (sliding phase), it is possible to more or less separate the turn-on and turn-off luminescence. It is thus possible to observe directly the decrease in luminescence caused by a change in the direction of the field—an effect easily correlated with the recombination radiation produced upon the return of electrons to a strongly ionized region.[11] The decrease in light and the excitation of intense luminescence near the positive electrode oppose the idea that only an excitation of luminescence centers, rather than ionization, is taking place.[15] In this connection it is also of interest that the luminescence kinetics of individual crystal regions are found to be nonexponential and do not differ appreciably from the luminescence kinetics of the entire crystal as a whole, or those of the polycrystalline electroluminescent capacitor. This circumstance, as well as the identity of the laws describing luminescence pulse amplitude as a function of the voltage amplitude in individual regions of the crystal and in electroluminescent capacitors, demonstrates that luminescence laws show practically no increase in complexity on going from a single crystal to polycrystalline samples with a dielectric introduced between individual grains of the electroluminescent phosphor.

REFERENCES

1. J. Waymouth and F. Bitter, Phys. Rev. **95**, 941 (1954).
2. G. Diemer, Philips Research Repts. **10**, 194 (1955).
3. K. Buttler and J. Waymouth, Brit. J. Appl. Phys., Suppl. No. 4, 33 (1955).
4. P. Zalm, Philips Research Repts. **11**, 353 (1956).
5. V. E. Oranovskii and B. A. Khmelinin, Opt. i Spektr. **7**, 542 (1959), Optics and Spectroscopy **7**, 336 (1959).
6. D. Steinhaus, H. Crosswhite, and G. Dieke, Spectrochim. Acta **5**, 436 (1953).
7. B. A. Mamyrin, Zhur. Tekh. Fiz. **26**, 652 (1956).
8. C. Hendee and W. Brown, Philips Tech. Rev. **19**, 7, 257 (1957-58).
9. B. A. Ermakov and A. A. Mak, Pribory i Tekh. Ekspt. No. 3, 95 (1959).
10. A. M. Bonch-Bruevich and O. S. Marenkov, Opt. i Spektr. **8**, 855 (1960), Optics and Spectroscopy **8**, 449 (1960).
11. This reference is missing from Russian original text—Translation Ed.
12. J. Waymouth, Phys. Rev. **95**, 941 (1954).
13. P. Zalm, G. Diemer, and H. Klassens, Philips Research Repts. **10**, 205 (1955).
14. G. Alfrey and J. Taylor, Brit. J. Appl. Phys., Suppl. No. 4, 39 (1955).
15. R. Zallen, W. Eriksen, and H. Ahlburg, J. Electrochem. Soc. **107**, 288 (1960).

THE PHASE OF ELECTROLUMINESCENCE LIGHT PULSES AS A FUNCTION OF EXCITATION VOLTAGE PARAMETERS

A. N. Georgobiani and M. V. Fock (pp. 93-97)

Received 25 July 1960

The phase of electroluminescence light pulses was investigated as a function of the amplitude and frequency of the exciting sinusoidal voltage. Experimental results are compared with theoretical data calculated on the assumption that the light pulse is formed as a result of the liberation of trapped electrons by an electric field.[1]

From a comparison of theoretical and experimental data, the depth of the trapping levels was estimated to be $\Delta = 0.64 \pm 0.07$ ev.

INTRODUCTION

In a study[1] of the shape of light pulses excited by trapezoidal voltage pulses, we showed that the main peak of the light pulse is caused by the return of electrons released from trapping levels by the electric field to a region containing a high concentration of ionized luminescence centers.

It was also established that electron liberation is due to collision ionization at low temperatures and to tunneling through a potential barrier (Zener effect) at high temperatures.

The aim of the present investigation is to study the shape of the light pulse as a function of the amplitude and frequency of the exciting sinusoidal voltage. These results can be compared at high temperatures to theoretical curves based on the assumption that electrons are released from trapping levels by tunneling through a potential barrier.

In the low temperature range, where electron liberation by collision ionization is predominant, the comparison of theoretical and experimental relationships between the shape of the light pulse and the parameters of the exciting voltage becomes difficult; because of avalanche processes, the number of electrons released depends essentially on the shape and dimensions of the region of high field strength.

THEORETICAL EXAMINATION OF THE PROCESS AND EXPERIMENTAL RESULTS

The theoretical examination starts with the following assumptions: When an electric potential is applied to an electroluminescent capacitor, a field concentration is created on the cathode side of each crystal. Luminescence centers become ionized and electrons are transported to the anode side of the crystal and trapped in trapping centers. Upon reversal of the electric field the electrons are released. They return to the region where the ionized luminescence centers are concentrated and recombine with them, emitting light quanta. The brightness is determined by the influx of electrons, particularly in the initial stages of emission. As the electric field is increased, the probability of electron liberation also increases, which in turn leads to an increase in the flow of electrons and, consequently, to an increase in brightness. On the other hand, the depletion of traps in the region of an increased value of the electric field limits the increase in brightness at some value of the potential. In other words, the light pulse will have a maximum at some instant t_0. We start counting time when the electric potential applied to the capacitor goes through zero (Fig. 1).

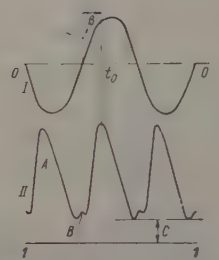

Fig. 1. Oscillograms of the exciting voltage, I, and electroluminescence brightness, II. 0—0, zero potential level; 1—1, zero brightness level; A and B—main and auxiliary peaks of the electroluminescence light pulse, at instant of time t_0 and phase angle β, corresponding to the maximum of the light pulse, counted from the time when the potential applied to the capacitor is zero; C, constant component of luminescence.

This effect is similar to thermoluminescence, the only difference being that in the case of thermoluminescence the probability of release is determined by heat alone, and in the present case by the joint action of heat and an electric field.

An analysis of the light pulse shows that the maximum is reached when less than half of the light sum has been emitted. The probability of electron liberation changes by many orders of magnitude between the reversal of polarity at $t = 0$, and t_0, since this probability is very sensitive to changes in the electric field.

Taking the aforesaid into account, we will disregard the change in the number of ionized luminescence centers between 0 and t_0.

We will therefore assume that the brightness I(t) at the time t is proportional to the loss of electrons from traps, which, in its turn, is equal to the probability of escape by tunneling at this moment W(t), multiplied by the concentration of trapped electrons N(t):

$$I(t) \sim \frac{dN}{dt} = -W(t)\,N(t). \qquad (1)$$

Integrating, we obtain

$$N(t) = N_0 e^{-\int_0^t W(t')\,dt'}, \qquad (2)$$

ere $N_0 = N|_{t=0}$.

Substituting (2) into (1), we obtain

$$I(t) \sim N_0 e^{-\int_0^t W(t')dt' + \ln W(t)}. \quad (3)$$

The brightness maximum coincides in time with the ximum of the exponent in the exponential.

The final condition for the maximum of the light se is

$$W^2(t_0) = W'(t_0). \quad (4)$$

According to theoretical investigations by Keldysh,[2] probability of release of electrons from traps by neling under the joint action of an electric field and rmal vibration of the crystalline lattice is:

$$W = a_0 E \exp\left\{-\frac{\Delta}{kT} + \frac{1}{24}\frac{(e\hbar E)^2}{m(kT)^3}\right\}. \quad (5)$$

ere Δ is the depth of the states from which the elec- ns are released, m and e are the mass and charge of electron, a_0 is a coefficient which is independent of field, k is the Boltzman constant, $\hbar$ is the Planck nstant, E is the electric field strength, and T is the mperature.

Taking into consideration that, according to the nottky model, the field is proportional to the square ot of the applied voltage in a region of concentration the electric field, or:

$$E = d\sqrt{U}, \quad (6)$$

ere d is a proportionality coefficient, and regrouping values which are independent of the field, we can re- ite (5) in the form:

$$W = a\sqrt{U}\exp(bU), \quad (7)$$

ere

$$a = a_0 d e^{-\frac{\Delta}{kT}}; \quad b = \frac{d^2}{24}\frac{(e\hbar)^2}{m(kT)^3}. \quad (8)$$

In our experiments we used a sinusoidal voltage, t is,

$$U(t) = U_0 \sin(\omega t), \quad (9)$$

ere ω is the cyclic frequency of the exciting voltage. bstituting (7), (8), (9) into (4) and introducing the defi- ions

$$\beta = \omega t_0, \quad x = bU_0, \quad C = \frac{\omega}{\sqrt{b}}, \quad (10)$$

obtain a transcendental equation connecting the phase gle β, corresponding to the maximum of light pulse, th x, which is proportional to the amplitude and the equency ω of the exciting sinusoidal voltage.

$$\sqrt{x}\sin^{3/2}\beta e^{x\cdot\sin\beta} = \frac{\omega}{C}\cos\beta\left(\frac{1}{2} + x\cdot\sin\beta\right). \quad (11)$$

Figure 2 shows a family of curves with various val- s of the parameter

$$r = \frac{\omega}{C}, \quad (12)$$

tained by a graphical-analytical solution of Eq. (11). order to achieve a comparison with experimental data d to avoid the influence of the scale multiplier b on e shape of the curves, log x was plotted as ordinate; g U_0 was used for experimental points.

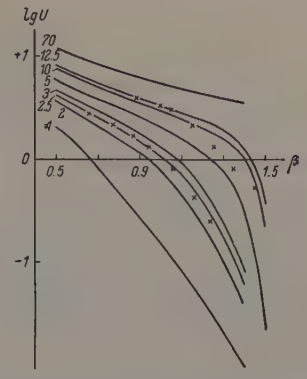

Fig. 2. Relationship between the logarithm of the amplitude of the electric potential applied to the electroluminescent capacitor and the phase angle β, corresponding to the maximum of the light pulse. Solid curves are calculated from Eq. (11) and correspond to different values of the parameter $r = \omega/C$, the crosses are experimental points.

Experimental points were obtained at two frequencies (265 and 1325 cps) differing by a factor of 5. The angles β were measured directly so that in order to compare experimental points with theoretical curves it was necessary to displace the experimental points along the ordinate axis until one set fell on one of the theoretical curves, whereupon the experimental points corresponding to the other frequency had to fall without further displacement on the curve whose parameter r was equal to the first r, multiplied by the ratio of the two frequencies. In Fig. 2, the experimental points corresponding to the frequency 265 cps fall on the curve with the parameter r = 2.5, and the experimental points corresponding to the frequency 1325 cps must therefore fall on the curve with the parameter r = 12.5. This is the case at high voltages, but at low voltages the experimental points fall somewhat under the theoretical curve. The experiment was carried out at 345-355° K.

Some deviation of experimental points from the theoretical curves at low voltages can be explained by assuming that the release of electrons from shallow traps is more pronounced at low voltages than at high voltages.

Let us now estimate the depth of the trapping levels from which the electrons are released to form the main peak of the light pulse at the electrical potentials normally used. According to the definitions (8), (10), and (12)

$$\Delta = kT\ln\frac{a_0 dr}{\omega\sqrt{b}}, \quad (13)$$

and all values entering into the right side of this equation are known to us from the experiment except $a_0 d/\sqrt{b}$. Let us try to evaluate this factor.

The quantity*

$$a_1 = a_0 d\sqrt{U_{cr.}} \approx 10^{12}.$$

has been evaluated in ref. 1.

According to definitions (9), $\sqrt{b} = \sqrt{x/U_0} = \sqrt{x_{cr}/U_{cr}}$, where x_{cr} is the value of x at the point on Fig. 2 corre-

*U_{cr} is defined in ref. 1 as the value of the potential which corresponds to the maximum of the light wave when a linearly increasing electric voltage is applied to the electroluminescent capacitor.

sponding to the critical potential. Thus:

$$\frac{a_0 d}{\sqrt{b}} = \frac{10^{12}}{\sqrt{x_{cr.}}}.$$

In its final form, Eq. (12) will be rewritten as:

$$\Delta = kT \ln \frac{r}{\omega \sqrt{x_{cr.}}} 10^{12}. \qquad (14)$$

Introducing our experimental values T = 350°K, r = 2.5, $\omega = 2\pi \times 265$ cycles, $x_{cr} = 0.14$, into this formula, we obtain the value $\Delta = 0.64$ ev for the depth of the trapping levels. It should be pointed out that the experimental uncertainty only leads to an error in the third decimal. The principal inaccuracy in the calculation of Δ is due to the estimation of the value of $a_1 \approx 10^7 E_{cr}$.*

*E_{cr} is the field strength in the region of a field concentration corresponding to the application of the critical voltage[1] to the electroluminescent capacitor.

We estimate that $E_{cr} \approx 10^5$ volts/cm, because it is smaller than the breakdown value $E_{br} \approx 10^6$ volts/cm. In this case, if a_1 deviates from 10^{12} by an order of magnitude in one direction or the other

$$\Delta = 0.64 \pm 0.07 \text{ ev}.$$

In ref. 1 the value

$$\Delta = 0.71 \pm 0.07 \text{ ev}.$$

was obtained for the depth of the same traps from the temperature dependence of the shape of the light pulse.

Within the limits of accuracy of these different and independent methods, the average depth of traps is therefore

$$\Delta \cong 0.67 \text{ эв}.$$

The methods proposed make it possible to investigate the deep traps in electroluminescent phosphors which cannot be investigated by the thermoluminescence method because of temperature quenching, or by the optical flash method because of small light sum storage in the electroluminor.

CONCLUSION

Both the temperature-dependence of the shape of the light pulse and its dependence on the amplitude and frequency of the exciting voltage are thus in agreement with the mechanism of a forced release of electrons by the electric field. The deepest traps in the electroluminescent crystal ZnS-Cu have a depth of approximately 0.67

REFERENCES

1. A. N. Georgobiani and M. V. Fok, Opt. i Spektr. 9, 775 (1960), Optics and Spectroscopy 9, 407 (1960).
2. L. V. Keldysh, Zhur. Eksptl. i Teoret. Fiz. 34, 962 (1958); Soviet Phys.-JETP 7, 665 (1958).

THE RELATION BETWEEN THE BLUE AND GREEN BANDS IN THE ELECTROLUMINESCENCE OF ZnS:Cu PHOSPHORS

M. V. Fok (pp. 98-104)

Received 10 August 1960

An approximate calculation is performed for the recombination interaction of the centers of blue and green luminescence of the ZnS:Cu phosphor in the presence of an electric field. It is shown that the action of the field greatly complicates the effect being studied.

It is known that the luminescence of the ZnS:Cu phosphors consists of two bands, blue and green. The brightness ratio of these bands depends on both phosphor composition and the conditions of excitation. In particular, under ultraviolet excitation, the brightness of the blue band increases faster than the green one as the intensity of excitation increases. The same is true in electroluminescence if the intensity of excitation is changed by varying the frequency of the applied voltage. If, however, the amplitude is varied rather than the frequency, then the luminescence spectrum remains practically unchanged, aside from a considerable increase in brightness.

No satisfactory explanation of this peculiarity of electroluminescence has been offered up to the present time. The present paper represents an attempt to find at least a rough approximation to such an explanation.

It has been shown[1-3] that the dependence of the ratio of the intensities of the blue and green bands on the intensity of photoexcitation is due to recombination interaction between the centers of blue and green luminescence, i.e., to the exchange of holes between them. The transition of a hole from an ionized center to the valence band requires a definite activation energy, which is greater for the "green" than for the "blue" centers. Therefore, there is an over-all migration of holes from the "blue" to the "green" centers. This migration requires a certain amount of time. If the intensity of photo excitation is low, and the concentration of free electrons is small, such a transition will be able to take place before one of the free electrons approaches the ionized center and recombines with it. On the other hand, if the excitation intensity is high, the recombination of electrons with the ionized "blue" centers is more probable than a transition of holes from the "blue" to the "green" centers. Increased excitation intensity therefore produces a more rapid increase of the brightness of the blue band than of the green one.

The electroluminescence of the ZnS:Cu phosphors is bluer than their photoluminescence. Furthermore, as noted before, the electroluminescent spectrum is independent of the magnitude of the applied voltage. Consequently, we must assume that the mechanism of recombination interaction is to some extent excluded in electroluminescence.

We may imagine that the electroluminescence of dered ZnS:Cu proceeds essentially as follows: Each troluminor crystal subjected to the action of an ac l may be divided into three regions. (See Fig. 1.) At end of the crystal (region 1) there is a concentration ue space charge and the field, a dispersal of electrons, the luminescence centers are ionized. At the other (region 2) there is almost no field at this time, but ead there are many ionized centers which were formed ng the preceding half-cycle. Electrons from the con- rated field region arrive here continuously and re- bine with the ionized luminescence centers. In the fol- ng half-cycle, regions 1 and 2 change places. Finally, ne center of the crystal there is a region 3 where e is no strong electric field and where the concentra- of ionized centers is much lower, since it is main- ed only by the diffusion of holes from the edges of the tal. Apparently, the ac component of electrolumines- e arises at the ends of the crystal and the dc compo- in the center.

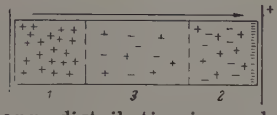

Fig. 1. Charge distribution in an electroluminor crystal during electroluminescence. 1—space charge region, in which the field is concentrated and ionization occurs; 2—region of high concentration of ionized luminescence centers, in which the ac brightness component arises; 3—intermediate region, in which the dc brightness component arises. The arrow indicates the direction of electron motion.

Let us consider the possible reasons for the absence recombination interaction. As stated before, in the e of photoexcitation, the holes liberated from the ized blue luminescence centers may move to the en ones. It is by this process that the blue band is kened and the green one enhanced. Such a transition omes less probable in the presence of a sufficiently ong electric field (i.e., in region 1). This is due to the t that the field causes the holes to drift to the edge of crystal, and they may altogether bypass the lumines- ce centers. Thus in this region the green band may "fed" at the expense of the blue one.

A redistribution of holes may occur in region 2; wever, it also does not proceed in the same manner as the case of photoexcitation. This is because in photo- itation, the number of free electrons capable of re- mbining with the ionized centers is closely connected h the number of ionized centers. This does not occur region 2, since electrons enter it from region 1 and ir number does not depend on the number of ionized nters remaining in region 2. An increased concentra- n of free electrons is therefore always maintained in gion 2. This again decreases the redistribution of les, which in region 3 apparently proceeds almost in same manner as in the case of photoexcitation. This nifests itself, for example, in the fact that the dc com- nent of electroluminescence is much larger in the een band than in the blue band. Region 3 contributes tle to the average brightness of electroluminescence, d therefore will not be considered further.

On the basis of the considerations given above, we have tried to calculate the concentrations of the ionized "green" and "blue" centers as functions of the conditions of excitation. The ratio of these concentrations in region 2 averaged over the half-cycle obviously gives the ratio of the intensities of the corresponding luminescent bands.

To find these concentrations, we must solve systems of kinetic equations separately for regions 1 and 2. The solutions obtained can be related to each other by using the following considerations: The concentration of ionized centers corresponding to the end of the half-cycle in which region 1 is on the left is also the initial concentration for the following half-cycle in which region 2 is at the left. The concentration corresponding to the end of this half-cycle is in turn the initial value for the third half-period, etc.

In region 1, the system of kinetic equations has the form

$$\left.\begin{aligned}\frac{dn'}{dt} &= \delta'_e N_e^+ - w'_e n',\\ \frac{dn''}{dt} &= \delta''_e N_e^+ - w''_e n''.\end{aligned}\right\} \qquad (1)$$

Excitation by an electric field apparently proceeds mainly through ionization of the host lattice, since there are many more of these atoms than luminescence centers. For the sake of simplicity we therefore assumed that a constant concentration N_e^+ of holes is always maintained in region 1. We neglect the recombination of free electrons with ionized centers in this region since the electrons here are very energetic, so that their effective recombination cross section is small. The notation in Eq. (1) is clear from Fig. 2. A single prime refers to "blue" centers and a double prime to the "green" ones. The subscript e indicates that the corresponding quantities refer to the strong field region. (In the absence of a field they can usually assume other values.) The solution of Eqs. (1) has the form

$$\left.\begin{aligned}n' &= n'_\infty - (n'_\infty - n'_0)\, e^{-w'_e t},\\ n'' &= n''_\infty - (n''_\infty - n''_0)\, e^{-w''_e t},\end{aligned}\right\} \qquad (2)$$

where n'_0 and n''_0 are the concentrations of ionized "blue" and "green" centers, respectively, which were present in the region at the beginning of the half-cycle. Also,

$$\left.\begin{aligned}n'_\infty &= \frac{\delta'_e N_e^+}{w'_e},\\ n''_\infty &= \frac{\delta''_e N_e^+}{w''_e}.\end{aligned}\right\} \qquad (3)$$

Note that the value of the ratio

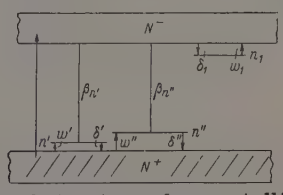

Fig. 2. Band structure of a crystalline phosphor with two kinds of luminescence centers. The arrows indicate the electron transitions; the letters near the arrows denote the corresponding probabilities.

$$\frac{n'_\infty}{n''_\infty} = \frac{\delta'_e w''_e}{\delta''_e w'_e} = c_e \tag{4}$$

is independent of the excitation intensity. For weak photoexcitation the ratio of the concentrations of centers is expressed by the same formula but obviously without the subscript e's.

The kinetic equations for region 2 do include the recombination term

$$\left.\begin{aligned} \frac{dn'}{dt} &= \delta' N^+ - w' n' - \beta n' N^-, \\ \frac{dn''}{dt} &= \delta'' N^+ - w'' n'' - \beta n'' N^-. \end{aligned}\right\} \tag{5}$$

We also assumed here that the hole concentration N^+ is no longer constant, but may be a function of time. It is equal to

$$N^+ = \frac{w' n' + w'' n''}{\delta' + \delta''}. \tag{6}$$

As noted before, the concentration of free electrons in region 2 is independent of the concentration of ionized centers in this region, but is determined by the influx of electrons from region 1. We have assumed that this concentration is constant. In this case the solution of Eqs. (5) has the form

$$\left.\begin{aligned} n' &= \frac{n'_k + n''_k}{c+1} c e^{-(\beta N^-)t} - \frac{n''_k c - n'_k}{c+1} e^{-(B+\beta N^-)t}, \\ n'' &= \frac{n'_k + n''_k}{c+1} e^{-(\beta N^-)t} + \frac{n''_k c - n'_k}{c+1} e^{-(B+\beta N^-)t}. \end{aligned}\right\} \tag{7}$$

where

$$\left.\begin{aligned} B &= \frac{\delta' w'' + \delta'' w'}{\delta' + \delta''}, \\ n'_k &= n'_\infty - (n'_\infty - n'_0) e^{-w'_e t_0}, \\ n''_k &= n''_\infty - (n''_\infty - n''_0) e^{-w''_e t_0}. \end{aligned}\right\} \tag{8}$$

The quantities n'_k and n''_k represent the concentrations of ionized "blue" and "green" centers present in region 1 at the end of the first half of the cycle (t_0 is its duration). The quantity c is determined from a formula analogous to Eq. (4) but without the subscript e's. In Eq. (7), time is measured from the beginning of the second half-cycle. Since the exciting electric pulses may be asymmetrical, t_1, the duration of the second half-cycle, may differ from T_0. When the frequency changes, however, both these quantities vary by the same factor, provided that the shape of the exciting voltage remains unchanged.

At the end of the second half-cycle, the concentrations n' and n'' must again assume the values n'_0 and n''_0 since the beginning of the next period follows immediately. By substituting $t = t_1$ in Eqs. (7) and equating the right-hand sides to n'_0 and n''_0, respectively, we obtain, in addition to Eqs. (8), a system from which we may determine both n_k and n_0. Finally we obtain

$$\left.\begin{aligned} n'_k &= \frac{(1-r')\, n'_\infty [c+1-pr''(1+cq)] + n''_\infty pcr'(1-q)(1-r'')}{c+1-pr'(c+q)-pr''(1+cq)+p^2qr'r''(c+1)}, \\ n''_k &= \frac{(1-r')\, n'_\infty pr''(1-q) + n''_\infty (1-r'')[c+1-pr'(c+q)]}{c+1-pr'(c+q)-pr''(1+cq)+p^2qr'r''(c+1)}, \\ n'_0 &= \frac{n'_\infty (1-r')\, p[c+q-pqr'(c+1)] + n''_\infty (1-r'')\, pc(1-q)}{c+1-pr'(c+q)-pr''(1+cq)+p^2qr'r''(c+1)}, \\ n''_0 &= \frac{n'_\infty (1-r')\, p(1-q) + n''_\infty (1-r'')\, p[1+cq-pqr'(c+1)]}{c+1-pr'(c+q)-pr''(1-cq)+p^2qr'r''(c+1)}, \end{aligned}\right\} \tag{9}$$

where

$$\left.\begin{aligned} p &= e^{-(\beta N^-)t_1}, \\ q &= e^{-Bt_1}, \\ r' &= e^{-w'_e t_0}, \\ r'' &= e^{-w''_e t_0}. \end{aligned}\right\} \tag{10}$$

It is well known that the brightness of luminescence bands is determined by the number of recombinations of free electrons with the corresponding ionized centers occurring per unit time. Thus

$$\left.\begin{aligned} I' &= \beta n' N^-, \\ I'' &= \beta n'' N^-. \end{aligned}\right\} \tag{11}$$

Since we assume that recombinations occur only in the second region, in which the quantity βN^- is assumed to be constant, the average band brightness will be proportional to the average concentration of the corresponding ionized centers,

$$\left.\begin{aligned} I' = \beta n' N^- &\approx \frac{(n'_k + n''_k)\, c(1-p)}{c+1} - \frac{\beta N^-}{B+\beta N^-} \cdot \frac{n''_k c - n'_k}{c+1} (1-pq), \\ I'' = \beta n'' N^- &\approx \frac{(n'_k + n''_k)(1-p)}{c+1} + \frac{\beta N^-}{B+\beta N^-} \cdot \frac{n''_k c - n'_k}{c+1} (1-pq). \end{aligned}\right\} \tag{12}$$

Substituting Eqs. (8) and (9) into Eqs. (12) and dividing $\bar{I}'$ by $\bar{I}''$, we obtain the ratio of the average intensities of the blue and green bands

$$\frac{I'}{I''} = \frac{c(1-p)\, B[c_e(1-r')(1-pqr'') + (1-r'')(1-pqr') + \beta N^-(1-r')] \times [cc_e(1-p)(1-pqr'') + c_e(1-pq)(1-pr'') - cp(1-r'')(1-q)]}{(1-p)\, B[c_e(1-r')(1-pqr'') + (1-r'')(1-pqr')] + \beta N^-(1-r'') \times [(1-p)(1-pqr') + c(1-pq)(1-pr') - c_e p(1-r')(1-q)]} \tag{13}$$

This expression appears rather complicated. We therefore restrict ourselves to the consideration of some special cases.

1. For a sufficiently low excitation intensity, the quantity βN^- can become arbitrarily small. Then

$$\frac{I'}{I''} = c. \tag{14}$$

2. Let the frequency of the exciting voltage have an extremely low value. Then all exponential terms may be neglected as compared to unity and Eq. (13) takes the form

$$\frac{I'}{I''} = \frac{cB(c_e+1) + \beta N^- c_e (c+1)}{B(c_e+1) + \beta N^- (c+1)}. \tag{15}$$

It is easy to see that in this case the ratio of the band intensities lies between c and c_e. Note that in the case of weak photoexcitation this ratio is equal to c. If $c < c_e$, an increase in voltage will displace the spectrum towards the blue; if $c > c_e$, the displacement is towards the green. This displacement can be due either to a change in the value of c_e or to the fact that the concentration of electrons increases with increasing voltage.

3. Another case is apparently realized experimentally. We can estimate the magnitude of B from the data in ref. 1, which is a study of the decay of the blue and green bands after photoexcitation. It turns out to be of the order of 0.2 sec^{-1}. Therefore, for all frequencies

d we may set q equal to one. Then

$$\frac{I'}{I''}=\frac{B\left[c_e(1-r')(1-pr'')+(1-r'')(1-pr')\right]+\beta N^-\frac{c_e}{c}(1-pr'')(1-r')(c+1)}{B\left[c_e(1-r')(1-pr'')+(1-r'')(1-pr')\right]+\beta N^-(1-pr')(1-r'')(c+1)}\,c. \tag{16}$$

As is seen from this formula, at high excitation insities (large value of βN^-) the ratio (16) becomes

$$\frac{I'}{I''}=\frac{(1-r')(1-pr'')}{(1-r'')(1-pr')}\,c_e. \tag{17}$$

is practically independent of the excitation intensity. the same time its value is strongly frequency-depent. At low frequencies it is equal to c_e. As the frency increases, it approaches δ'_e/δ''_e, which is much ger than c_e. Indeed, if at high frequencies we expand expressions inside the parentheses and keep the first vanishing terms, we obtain

$$\frac{I'}{I''}=\frac{\delta'_e}{\delta''_e}\cdot\frac{\beta N^-+w''_e\frac{t_0}{t_1}}{\beta N^-+w'_e\frac{t_0}{t_1}}. \tag{18}$$

ce we have already assumed βN^- to be large, we may sider that the second fraction in this expression will of the order of unity.

Let us try to estimate the values of w'_e and w''_e. For s we must compare the experimental and theoretical ghtness ratio vs. frequency curves. A family of curves mputed from Eq. (17) is shown in Fig. 3. For the theoical curves $\log w't_0$ is plotted as abscissae and $[(\bar{I}'/\bar{I}'')(1/c_e)]$ as ordinates. For the experimental nts we plot $\log\nu$ and $\log(I'/I'')$ as abcissae and ordates, respectively, where ν is the frequency and I' I'' are the band intensities in arbitrary units. The erimental curve drawn in these coordinates can be de to coincide with one of the theoretical ones by ans of a simple displacement. In the drawing, the ex-

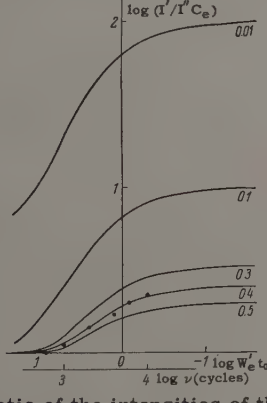

Fig. 3. Ratio of the intensities of the blue and green electroluminescent bands of ZnS:Cu:Al as a function of frequency. Curves—theory; dots—experiment. The numbers near the curves give the values of the ratio w'_e/w''_e.

perimental data are indicated by dots.* It is easily seen that they fall directly on the curve corresponding to the ratio $w'_e/w''_e = 0.4$. We see also from Fig. 3 that the frequency $\nu = 50$ kc corresponds to $w'_e t_0 = 1$. Since t_0 is approximately equal to the duration of the voltage half-cycle, we have $w'_e = 10^5\ \text{sec}^{-1}$ and $w''_e = 4\times10^{-4}\ \text{sec}^{-1}$.

*These results were kindly made available by E. E. Bukke, to whom I express my deep appreciation.

Let us compare these values to the corresponding values without a field, i.e., under photoexcitation. According to Eq. (8) the quantity B falls between w' and w'' and, as indicated, is equal to $0.2\ \text{sec}^{-1}$. At room temperature, the ratio w'/w'' amounts to about 0.01 or less (otherwise we would not observe a nonlinear dependence of the blue band on the intensity of excitation under photoexcitation). Hence, the electric field increases the probability of hole liberation by 5 to 6 orders of magnitude and brings them closer together.

This pronounced effect of the electric field on the probability of liberation of bound charges has been noted previously. Thus it has been shown[4] that in the ZnS:Cu:Al electroluminor the field can empty electron traps exceeding 0.6 ev in depth to a considerable extent in the course of a half-cycle. The hole traps formed by the activator are 0.33 ev deep for the green band[5] and are still shallower for the blue one. Therefore, in this case we may also expect a strong field effect. This effect may also be responsible for the smaller light sum storage by electroluminors excited by a field rather than by light.

The proposed theory for the frequency dependence of the intensity ratio of the blue and green bands does not contradict experiment. However, we must by no means consider this theory to be definitely established. First of all the calculations performed are very approximate and are only exploratory in nature; secondly, the data concerning the magnitudes of w'_e and w''_e have not yet been confirmed by an independent method; thirdly, the comparison with experiment has so far been carried out on one phosphor sample only.

REFERENCES

1. M. V. Fok, Opt. i Spektr. **2**, 475 (1957).
2. L. A. Vinokurov and M. V. Fok, Opt. i Spektr. **4**, 118 (1958).
3. L. A. Vinokurov and M. V. Fok, Inzh.-Fiz. Zhur. **1**, 58 (1958).
4. A. N. Georgobiani and M. V. Fok, Opt. i Spektr. **9**, 775 (1960), Optics and Spectroscopy **9**, 407 (1960).
5. V. V. Antonov-Romanovskii and L. A. Vinokurov, Opt. i Spektr. **1**, 71 (1956).

ON THE LUMINESCENCE OF CHARGED POLYCRYSTALLINE ZnS LAYERS UNDER THE ACTION OF DC ELECTRIC FIELDS

V. M. Fridkin* (pp. 105-111)

*Institute of Crystallography, Academy of Sciences of the USSR, Moscow, USSR. Unfortunately, we cannot quote an author's location in all cases because these are not given in the original Russian journal—Translation Editor.

Received 10 August 1960

Luminescence was detected in zinc sulphide electrets under the action of a dc electric field whose direction was opposite to that of the polarizing field. It was also found that the intensity of this luminescence can be weakened by irradiation of the electret (quenching effect). This effect was used as the basis of a new photographic process.

INTRODUCTION

In ref. 1, we observed the luminescence of charged polycrystalline layers of ZnS:Cu,Cl under the action of a dc field. The experiments were performed with an electroluminescent zinc sulphide activated with copper and chlorine according to a procedure described in ref. 2.

The electroluminor was dispersed in a 1:10 (by weight) solution of polyvinyl butyral in alcohol. The polycrystalline layers were prepared by depositing the emulsion on a conducting glass. The charging of the layers thus obtained was carried out in a flat-plate capacitor in strong electric fields. During the polarization, a discharge occurred in the air between the dielectric and the electrodes, and ions were adsorbed from the discharge at the surface of the dielectric. As was shown by Gross,[3] it is this mechanism which causes the appearance of a homogeneous charge (homocharge) in the electrets.

In ref. 1, the charged layers of ZnS, immediately after polarizing, had a large homochrage which gradually decreased to zero. After repeated application of the field to the charged layer of ZnS, the latter exhibited intense luminescence when the direction of this field was opposite to that used for polarizing the dielectric. The luminescence was not observed when the direction of the repeatedly applied field coincided with the direction of the polarizing field. The layers of ZnS which were not charged likewise did not exhibit any noticeable luminescence under the action of a constant electric field.

It was pointed out in ref. 1 that the strength of the reverse field applied to the charged layer of ZnS which is necessary to obtain a fairly intense luminescence may be much less than that of the polarizing field. The intensity of the luminescence increases as the density of the homocharge on the surface of the layer increases. Our observations indicated that the emission of light might continue for tenths of a second or longer. On repeated application of the reverse field the luminescence does not appear, as a rule, or is considerably weakened. Thus, the total "light sum" is emitted on the first application of the reverse field.

However, when the reversed field is weaker than the polarizing field, then, under certain conditions, the luminescence can be observed repeatedly. We conducted these experiments in the following manner: A layer of ZnS, 3 mm thick was polarized with a potential difference of 6 kv. Then 300 volts were applied to the layer in the opposite direction, causing a noticeable luminescence of the layer (repeated application of this voltage to the layer did not produce any further luminescence). Following this, a voltage of 1 kv was applied, again producing luminescence of the layer. A further increase of the applied voltage was necessary in order to obtain the luminescence again. This was repeated until the total "light sum" stored in the layer was exhausted as a result of repeated application of the electric field of the same polarity, which was opposite to that of the polarizing field. Thus, the luminescence is steplike and may occur many times with a reverse field of increasing intensity.

This luminescence has an interesting feature: its spectral composition is quite different from that of the electroluminescence observed from the same layer. For instance, the luminescence of the ZnS:Cu,Cl layer studied in ref. 1 was green, whereas its electroluminescence was blue. As will be shown later, this difference is also observed in other polycrystalline layers.

As the results of another paper[4] have demonstrated, the hetero- and homocharges of ZnS electrets are relatively stable. Accordingly, emission could still be induced by the field and luminescence could still be observed several tens of hours after polarization. Furthermore, it was shown in ref. 1 that the charged layers of ZnS display a luminescence on heating which is somewhat similar to thermoluminescence.

STUDIES OF SOME LUMINESCENCE FEATURES OF THE CHARGED LAYERS OF ZnS:Cu,Cl

The purpose of the present investigation was to study certain features of the luminescence of ZnS:Cu,Cl layers and to achieve a further elucidation of the mechanism of this phenomenon, particularly in relation to electroluminescence.

A diagram of the measuring capacitor is shown in Fig. 1. A 1.5 mm layer 1 of the material under investigation was placed on an aluminum foil or a plate of conducting glass and attached to the surface of electrode 6. The other electrode was a plate of conducting glass 2, glued to a Teflon insulator 3. Electrode 6 and layer 1 were pressed against upper electrode 2 by means of a spring 7 and could be pulled down with the handle 8 to the stop. The metal case 5 of the capacitor and the insulating bushing 9 were opaque. The luminescence was observed through window 4.

The measuring procedure was as follows: A dc voltage was applied to electrodes 2 (positive) and 6 (netativ) and the sample polarized in darkness for 15 sec. Elec-

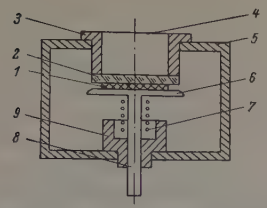

Fig. 1. Diagram of the measuring capacitor. 1—layer under investigation; 2—transparent electrode; 3—Teflon insulator; 4—window; 5—case; 6—electrode; 7—spring; 8—handle of the lower electrode; 9—Teflon bushing.

ies 2 and 6 were then shorted, and the charged layer ntained with the electrodes shorted for a certain iod of time. At the moment of application of the re- sed field to the charged layer (electrode 2 being ative and electrode 6 positive), the intensity of lumi- cence was measured with an FEU-19 photomultiplier ough window 4. The signal from the output of the pho- ultiplier was fed through the cathode follower to the ut of a low-frequency ENO-1 oscillograph, having a gered sweep. The decay curve of the luminescence s photographed directly from the oscillograph screen; s procedure permitted investigation of the kinetics of afterglow. Integration of the curve obtained gave the responding "light sum" in relative units. The charge sity on the surface of the layer was measured by the vated electrode method, which is widely used in work h electrets.[3] Electrodes 2 and 6 were connected for s purpose with the input of an electrostatic voltmeter. er the short between the electrodes was removed, the er electrode was pulled down, together with the arged layer, and the charge Q induced in the electrode ransferred to the capacitance of the voltmeter C charg- it to the potential V. Measuring the potential V gave charge density on the surface of the layer $\sigma = CV/S$, ere S is the area of the charged layer. The measured arge in all cases was a homocharge, which confirms e supposition made in ref. 1 that the observed lumines- nce is due to the presence of a homocharge in the ZnS ers under study.

Figure 2 depicts the results of measuring the "light m" S liberated on application of the reverse field as unction of the density of the homocharge on the sur- ce of the layer σ, for various values of the strength the reverse field E. It is evident from Fig. 2 that the opes of the curves increase as the strength of the re- rse field E increases; i.e., the "light sum" increases more rapidly with increasing charge density σ. Curve 5, which corresponds to a reverse field of 7 kv/cm, is especially interesting. It can be seen from Fig. 2 that this reverse field is so low that the "light sum" no longer depends on the density of the homocharge.

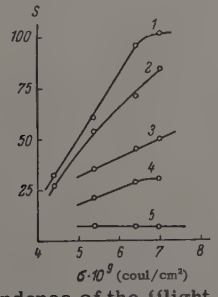

Fig. 2. Dependence of the "light sum" S on the density σ of the homocharge for various values of the reverse field E. E (kv/cm): curve 1—25; curve 2—21; curve 3—17; curve 4—14; curve 5—7.

Figure 3 shows the dependence of the "light sum" S on the strength of the reverse field E for various densities of the homocharge σ. This dependence was obtained from the family of curves given in Fig. 2. Figure 3 shows that the "light sum" increases as the reverse field increases, and the corresponding curves tend to saturate.

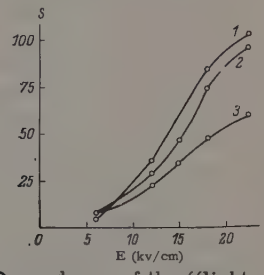

Fig. 3. Dependence of the "light sum" S on the reverse field E for various densities of the homocharge. $\sigma \times 10^9$ (coul/cm²); curve 1—7, curve 2—6.5; curve 3—5.5.

It seemed worthwhile to investigate the connection between the observed luminescence and the possible change of density of the homocharge on the surface of the layer under the action of the reverse field. For this purpose, immediately after the layer was polarized, electric pulses of reverse polarity were applied to electrodes 2 and 6, and simultaneous measurements were made of the decay of luminescence and of the change of charge density on the surface of the layer. The initial charge on the surface of the layer was $\sigma_0 = 7 \times 10^{-9}$ coul/cm² in all cases. The results shown in Table 1 indicate that a reverse field of 7 kv/cm (V = 1 kv) does not produce any noticeable change in the charge; however, the charge decreases at an accelerating rate as the strength of the reverse field increases.

Table 1. Variation of the Charge Density $\Delta\sigma \times 10^9$ (coul/cm²) on the Surface of a ZnS:Cu,Cl Layer Under Action of a Reverse Field of Strength E for the Period τ (Initial Charge Density $\sigma_0 = 7 \times 10^{-9}$ coul/cm²)

E (kv/cm) τ (sec)	7	14	21
0.004	0	3.5	4.5
0.06	0	3.5	4.5
0.1	0	3.5	5
1.2	0	3.5	5

Furthermore, it follows from the results obtained that the change of the charge density $\Delta\sigma$ is almost independent of the pulse duration from 4 msec to several seconds. This, in turn, indicates that it certainly takes no more than 4 msec for the charge to decay under the action of the reverse field. Observation of the decay of luminescence under the action of pulses disclosed that this decay is also independent of the duration of the pulse (for a given strength of the reversed field) over the whole range of decay times given in Table 1. A 4 msec im-

pulse and a constant field of the same strength always cause the same luminescence decay and the same change of density of the homocharge on the surface of the layer. It is possible that the inertia can be detected by using shorter pulses, for which the luminescence decay curve and the corresponding "light sum," as well as the change of the density of the homocharge $\Delta\sigma$, will depend on the duration of the pulse.

It is worth pointing out that, as already mentioned, the luminescence lasts several tenths of a second or more, whereas the shortest exciting pulse lasts no longer than 4 msec. It follows that the role of the reverse electric field consists in excitation of the corresponding electron or hole levels, whereas the subsequent afterglow can occur in the absence of the reverse field, its kinetics being determined by a different mechanism, which is responsible for the recombination and recapture. Figure 4 shows the dependence of the logarithm of the luminescence intensity on the logarithm of time for four values of the strength of the reverse field ($\sigma_0 = 7 \times 10^{-9}$ coul/cm^2). These results demonstrate that the observed afterflow is of the recombination type, and that the corresponding decay of the afterglow follows a linear hyperbolic law

$$I = \frac{1}{a + bt}.$$

The results obtained, not shown in Fig. 4, indicate that the exponent of the hyperbola may vary somewhat with the initial density of the homocharge σ_0.

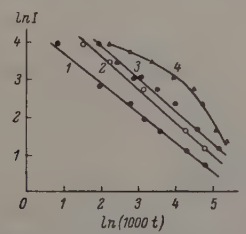

Fig. 4. Dependence of luminescence intensity on time for different strengths of the reverse field E ($\sigma = 7 \times 10^{-9}$ coul/cm^2). Values of E (coul/cm^2): curve 1—7; curve 2—14; curve 3—21; curve 4—25.

We have observed this luminescence in a number of charged polycrystalline zinc sulphide electroluminors. In every case, the spectral composition of the luminescence produced under the influence of the reverse electric field differed from that of the electroluminescence. Table 2 gives data on the spectral composition of electroluminescence, phosphorescence, fluorescence, and luminescence observed in the present investigation of zinc sulphide electroluminors (the synthesis of which was performed by Orlov and described in ref. 2). It can be seen from Table 2 that the luminescence of charged layers under the action of a reverse field is redder than electroluminescence. Furthermore, it is apparent that the effect studied in this paper was not observed in all of the electroluminors reported in ref. 2.

Table 2. Color of Different Types of Luminescence of Electroluminescent Layers

Layer	Electroluminescence	Fluorescence	Phosphorescence	Luminescence of charged layer under action of reverse field
ZnS: Cu, Cl	Blue	Blue-green	None	Green
ZnS: Cu, Pb, Cl	Blue	Green	Green	Green
ZnS: Cu, Mn, Cl	Yellow	Yellow	Yellow	Red-orange
ZnS, ZnSe: Cu, Cl	Yellow	Orange	None	None
ZnS, CdS, ZnSe: Cu, Cl	Red	Red	None	None

It is known from previous work on electroluminescence that the spectral composition of the latter depends on the frequency of the exciting field. It is possible that this fact is connected in some way with the aforementioned difference in the spectral composition of electroluminescence and the luminescence under consideration. We also observed this luminescence in charged single crystals of TlI and TlBr, the electroluminescent properties of which, to our knowledge, have not been studied previously.

Observation with a microscope revealed that this luminescence is emitted at the surface and is localized in narrow layers adjacent to the electrodes. This confirms the supposition that the luminescence is due to a homocharge and to the formation of a strong electrical field in the layers adjacent to the electrodes on application of the reverse field.

INFLUENCE OF RADIATION ON THE LUMINESCENCE OF ZnS:Cu,Cl LAYERS

It was shown in refs. 4 and 5 that the irradiation of ZnS:Cu,Cl layers with ultraviolet light during polarization results in the formation of a photoelectret possessing a relatively stable heterocharge. It is known that the heterocharge of a photoelectret is connected with internal polarization of the dielectric, which in turn is due to the displacement in the dielectric of the free carriers under the action of light and their trapping in fairly deep local levels.[4,5] The irradiation of a ZnS:Cu,Cl photoelectret by ultraviolet light results in its depolarization, which causes the heterocharge to drop to zero.[4,5] All these results were obtained with fairly weak polarizing fields, in which case a homocharge is not produced.

As mentioned before, our polarizing conditions were such that the ZnS:Cu,Cl layers displayed a strong homocharge when polarized in darkness. It was found that under these conditions, irradiation of the layer with ultraviolet light during polarization did not change the measured value of the density of the homocharge; i.e., the density of the heterocharge was much smaller than the density of the homocharge. It was also found that the irradiation of the charged layer did not change the measured value of its homocharge; it was only for very heavy exposures ($Et \geqslant 10^{-2}$ watt-sec/cm^2) that some decrease of the homocharge was observed.

Furthermore, we found that irradiation of the ZnS:Cu,Cl layer with ultraviolet light either during or after polarization greatly reduced the luminescence intensity which appeared in the charged layer on application of a reverse field. In these experiments the layer was polarized in darkness. Electrodes 2 and 6 (Fig. 1) were then shorted and the layer irradiated with a quartz mercury lamp for a certain period of time. After the irradiation was discontinued, the reverse field was applied and the luminescence observed.

It was found that for small exposures ($Et \leqslant 10^{-5}$ watt-sec/cm^2) there is some increase in the luminescence intensity due to the Gudden-Pohl effect.[6] In accordance with this effect, the increase in the luminescence inten-

did not depend on the direction of the applied field, was even observed in a sample which was not charged. h increased exposure ($Et > 10^{-5}$ watt-sec/cm^2) there a sharp decrease in the luminescence intensity. Even gh the Gudden-Pohl effect also occurred in this case, as overshadowed by the observed effect, which can be ed the quenching effect. It is remarkable that the rp decline in luminescence intensity (quenching effect) ot accompanied by any noticeable change in the den- of the homocharge, i.e., the irradiated layers carry- a large homocharge do not exhibit luminescence at same time.

The quenching effect could conveniently be observed reating a latent image on the surface of the charged r. This is analogous to a latent electrophotographic ge.[7] To that end, the layer was polarized in a flat- ce capacitor which produced a homocharge on its sur- e. This layer was then irradiated with ultraviolet light ough a negative of some kind. As a result of this ex- ure, a latent image was formed due to the nonuniform nching. The application of a reversed field to the r produced an intense luminescence of the unirradi- d sections, whereas the irradiated sections did not ibit luminescence. The latent image thus became visi- as a positive. Since the electret state of ZnS:Cu,Cl elatively stable, the latent image could be "developed" eral tens of hours after its formation.

CUSSION OF RESULTS

All of the phenomena which we observed and de- ibed in previous sections depended on prior polari- ion of the ZnS:Cu,Cl layers. It appears to us that they be explained by means of a scheme suggested by F. Vol'kenstein for interpreting the phenomena of lumi- scence.[2] According to this scheme (Fig. 5), when a ld is applied to a crystal, the conductivity band be- nes inclined, so that an electron located in a relatively p level of the activator (I) can go over to the conduc- n band because of the tunnel effect, and recombine h a hole at another level of the activator.

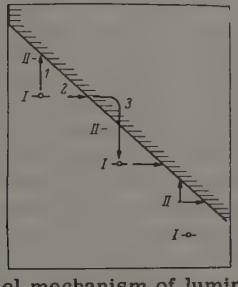

Fig. 5. Tunnel mechanism of luminescence of charged layers under the action of a reverse field.

In a charged layer of ZnS:Cu,Cl there is a nonuni- rm distribution of holes and electrons trapped on some vels (II), the depths of which may vary. The presence an internal field in the layer, caused by a nonuniform stribution of holes and trapped electrons, results in an clined conduction band. When the levels (II) at which e electrons are trapped are deep enough, and the prob- ility of the tunnel effect therefore small, the polariza- n can be preserved in the layer indefinitely (it is as- med here that the probability of thermal transition is gligible).

On the application of a reverse field to the charged layer, the field strength in the dielectric layers adjacent to the electrodes increases sharply, causing a considerable inclination of the conduction band. This increases the probability of a tunnel transition of the electrons localized in the trap levels II into the conduction band, from whence these electrons recombine with the holes at the activator levels I; this is accompanied by luminescence. This scheme explains, in particular, why a considerable luminescence of the layer occurs on application of a reverse field whose strength is much lower than that of the field used for polarizing the layer.

This scheme also explains the aforementioned step-like feature of the luminescence. On repeated application of a reverse field of ever-increasing strength to the charged layer, there is successive excitation of deeper and deeper levels, accompanied by luminescence of the layer. Repeated application of a reverse field of the same strength does not result in the reappearance of luminescence, because all levels which correspond to a given field strength are already excited.

The present results show that the levels can be excited by electric pulses of fairly short duration. As was mentioned before, this does not contradict the experimentally observed long afterglow, since its kinetics are apparently governed by the usual mechanism responsible for phosphorescence. The observed luminescence may be caused by a recombination of charges localized at the excited levels with the luminescence centers, or with the carriers injected into the dielectric from the electrode when the reverse field is applied. This mechanism may explain the observed change in the density of the homocharge on application of a reverse field to the charged layer.

The same scheme also permits explanation of the quenching effect mentioned earlier. Irradiation of the layer during or after polarization produces internal polarization in the layer (heterocharge). Although this heterocharge is much smaller than the homocharge, the internal polarization leads to the formation of a double electric layer caused by the presence of the homo- and heterocharges in the dielectric. The field strength inside this double layer may be sufficient for direct excitation of the shallow II traps. When the reverse field is applied, these levels are therefore already excited, and the corresponding "light sum" decreases.

Since the nature of the luminescence studied in this paper can be explained as a direct excitation of levels by a strong electric field, it can be expected that all dielectrics in which this phenomenon occurs must display electroluminescence. It was shown earlier that the reverse statement is not valid. Nevertheless, it can be expected that a further study of the luminescence of charged dielectrics under the action of electric fields will permit a new approach to the understanding of electroluminescence. It is also interesting in itself.

The writer is grateful to I. N. Orlov for making the samples of electroluminors available and for discussion of some of these results, and also to I. S. Zheludev for his interest in the work and for the support given during its execution.

REFERENCES

1. V. M. Fridkin, Doklady Akad. Nauk SSSR 131, 290 (1960), Soviet Phys.-Doklady 5, 301 (1960).
2. I. N. Orlov, Izvest. Akad. Nauk SSSR, Ser. Fiz. 21, 731 (1957).

3. V. M. Fridkin and I. S. Zheludev, "Photoelectrets and the Electrophotographic Process." Izd. Akad. Nauk SSSR, Moscow, 1960.
4. B. M. Golovin, N. T. Kashukeev, I. N. Orlov, and V. M. Fridkin, Fiz. Tverdodo Tela, 2, 1004 (1960), Soviet Phys.-Solid State 2, 911 (1960).
5. H. Kallman and B. Rosenberg, Phys. Rev. 97, 1596 (1955).
6. B. Gudden and R. Pohl, Z. Physik 2, 192 (1920).
7. V. M. Fridkin, J. Opt. Soc. Am. 50, 545 (1960).

PHOTOELECTRIC METHOD OF RECORDING AN ACHROMATIC INTERFERENCE FRINGE

V. P. Koronkevich, G. A. Lenkova, N. S. Babenko, and A. I. Lokhmatov (pp. 112-117)

Received 23 June 1960

This paper proposes a method of isolating a dark achromatic fringe using the nonlinear volt-ampere characteristics of germanium photodiodes. Interference superposition fringes were recorded photoelectrically.

Several methods of photoelectrically isolating the central achromatic fringe from systems of white light interference fringes have been proposed for automatic measurements with interferometers. Peck[1] has shown that in order to record the achromatic fringe one must use a detector sensitive to a broad region of the spectrum. Cook and Richardson[2] have used photoelectric recording of white light fringes to compare the lengths of Fabry-Perot etalons. They calculated the energy distribution as a function of wavelength corresponding to the experimentally recorded intensity distribution in the interference pattern. They were able to take into account the effect of the dispersion of the phase shift. Kolomitsova and Novikova[3] experimentally tested a method proposed by Linnik for isolation of the achromatic fringe corresponding to the maximum energy and to the maximum rate of increase of energy.

By means of an assortment of filters Trulev (oral communication)* assured uniform sensitivity of the light detector over a sufficiently wide spectral interval, and from the zero-order fringe he obtained a signal 32% different from the signals of the neighboring fringes.

*Note added in proof: Cf. Optiko-Mekh. Prom., No. 11 (1960).

The present article proposes a method for isolation of the achromatic fringe by using germanium photodiodes as detectors.

All experiments were performed on commercial interferometers. A block diagram of the apparatus, previously used for metrological purposes, is shown in Fig. 1. A source of white light 1 is projected by a condenser 2 through the aperture 3 of a collimator 4. After passing through the collimator the parallel rays strike the dividing plate 6 of a Michelson interferometer. Insofar as the lengths of the interferometer arms are not equal the outgoing rays have some difference in path length. The difference determines the intensity of the light and its spectral composition at a given point. Then the light is projected by the lens 7 to the focus of the ocular 8 where there is a diaphragm to cut out part of the fringes. A photoelectric detector 11 is placed at the exit pupil of the system. Motion of the reflecting mirror 9 by means of a motor 10 causes periodic variations in the intensity of the light at the exit of the interferometer. The oscillations of intensity are recorded by a standard photoelectric circuit (a photocompensating amplifier 12 and 13, a recording pen and strip chart 14, 15). For work with superposition fringes the interferometer was combined with a Fabry-Perot etalon 5.

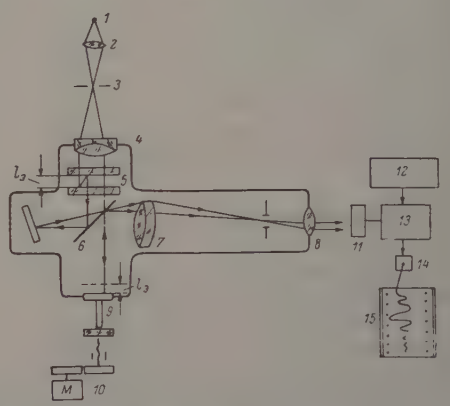

Fig. 1. Block diagram of the apparatus.

The extent to which the photoelectric signal strengt from the achromatic fringe exceeds the signal strength from any of the other fringes is the usual criterion for the degree of isolation of the achromatic fringe from a system of white light interference fringes. Expressed a a percentage of the magnitude of the achromatic fringe signal, this difference serves as a figure of merit for th photoelectric method. The achromatic fringe will be iso lated in the optimum manner if $I(\lambda)v(\lambda)\tau(\lambda) = \text{const}$, whe $I(\lambda)$ is the energy distribution of the source light as a function of wavelength, $v(\lambda)$ is the spectral sensitivity o the detector, and $\tau(\lambda)$ the interferometer transmission as a function of wavelength.

Table 1 gives values of the photoelectric difference which we obtained for various $\tau(\lambda)$ for FEU-19, FEU-2 and photodiode detectors. The value of $\tau(\lambda)$ is changed by putting standard filters following the collimator. Th results pertain to a Michelson interferometer with an u silvered dividing plate.

As the table shows, even a simple choice of filter can attain values of the photoelectric difference C equa to 38% for an FEU-22, i.e., higher than the theoretical value obtained by Kolomiitsova and Novikova[3] for an FEU-22 and an FEU-19 photomultiplier connected in parallel. Figure 2 is a trace of the white light interference fringes for two photodiodes No. 1 and No. 2, while

Table 1

Filter type used	Photoelectric difference (%, FEU-22 detector)	Filter type used	Photoelectric difference (%, FEU-19 detector)	Filter type used	Photoelectric difference (%, photodiode detector)
None	19–20	None	7.0	None	41.0
SZS-11	12.1			None	36.2
OKS-1	0.0	None	8.6	None	38.4
IKS-3	4.7			OS-14	35.0
ZS-2	0.9	None	7.5	OS-14	39.0
SZS-7	38.0	None	10.3	OS-14	36.0
SZS-12	0.4			OS-11	43.0
SS-14	0.6			OS-12	43.7
SZS-17	28.2	SZS-18	7.8	OS-13	31.8
SZS-9	11.0			OZS-12	40.0
SZS-9	6.2	OS-14	0.0	ZhZS-17	0.0
UFS-2	0.4			ZhS-18	41.0
SZS-18	5.3	PS-7	11.7	TS-4	20.0
SS-5	11.0	PS-9	9.4	KS-11	42.5
				IKS-3	27.4
				ZhZS-12	9.2
				OS-5	46.0

g. 3 is the interferogram obtained when an SZS-7 ter is placed in front of the entrance pupil of the de- e. The best results were obtained using germanium otodiodes as detectors. The photoelectric difference n attained values of C = 40–46%.

In most interferometers the reference point for a gth measurements is the dark achromatic fringe, ., the fringe with the smallest photoelectric signal. e can use the nonlinearity of the volt-ampere charac- istic of a photodiode to isolate the dark achromatic inge.

In the absence of a load resistance the voltage drop ross the diode, which is equal to the source voltage, ll remain constant and the current in the circuit will proportional to the light flux incident upon the photo- ode (line 1′ in Fig. 4). When a constant load resistance H is subsequently connected to the photodiode the non- earity of the volt-ampere characteristic causes the ght response characteristic of the circuit to be nonlinear.

Figure 4 shows the construction of the dynamic ght characteristic of a photodiode corresponding to the atic volt-ampere characteristics 1, 2, ... 7, which in rn correspond to constant values of the light flux Φ_1, , ... Φ_7 striking the diode.

When the diode is not illuminated we may consider s resistance to be infinite. In that case the entire volt- ge drop E_a occurs across the diode (i.e., $E_a = E_d$) and e current I_d through the diode equals zero. This cor- esponds to point B in the figure. We may consider the esistance of a very strongly illuminated diode to be ero. Then the current in the circuit is determined only y the load resistance R_H, and $I_d = E_a/R_H$. This corre- ponds to point A in Fig. 4. Let us then draw the load

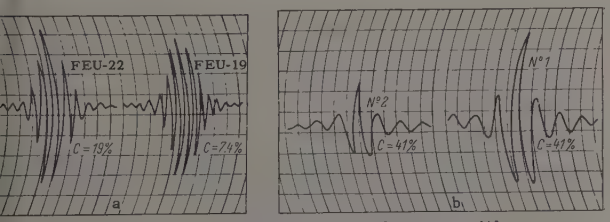

Fig. 2. Traces of interference fringes with different photodetectors. a—photomultipliers; b—photodiodes. (C is the photoelectric difference.)

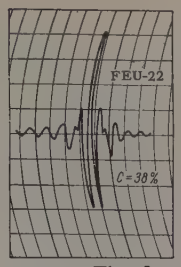

Fig. 3

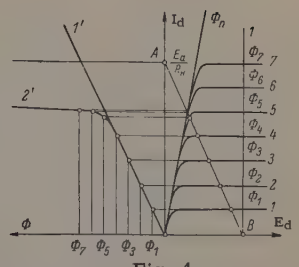

Fig. 4

Fig. 3. Trace of interference fringes with an SZS-7 filter.

Fig. 4. Construction of the dynamic light characteristic. 1′ is the light characteristic of a photodiode with no load resistance; 2′ is the light characteristic of a photodiode when a load resistance is subsequently added to it; R_H is the load resistance; E_a is the supply voltage; I_d is the current in the photodiode circuit; E_d is the voltage drop across the photodiode; Φ is the light flux incident on the diode.

line AB through points A and B. The points of intersection of the load line with the static characteristics 1, 2, ... 7 determine the corresponding points of the dynamic light characteristic $I_d = F(\Phi)$ of the circuit. The dynamic characteristic is shown as curve 2′. From the figure it is obvious that the function is nonlinear.

Figure 5 gives the experimental light characteristic of photodiode No. 1. The current i at the entrance of the recording apparatus is plotted as the ordinate while on the abscissa is plotted the illuminator aperature (which determines the light flux Φ) $\alpha = b/2f$, where b is the width of the entrance aperture of the collimator and f is the collimator focal length.

If the aperture does not exceed $\alpha = 0.0022$ the change in light flux from the interference fringes will not go beyond the sloped portion of the characteristic. In this case the oscillogram of the current will resemble the intensity distribution in the interference pattern. If the aperture is further increased (2 in Fig. 5), the amplitude of vibration of the light flux changes. Now as we move across the fringes, the light flux will fluctuate into the saturation region. The interference pattern at the output will be clipped. The photoelectric difference will be increased. For $\alpha = 0.0075$ even the first order interference fringes fall in the saturation region. The oscillogram of the current (3′ in Fig. 5) will have a single pulse

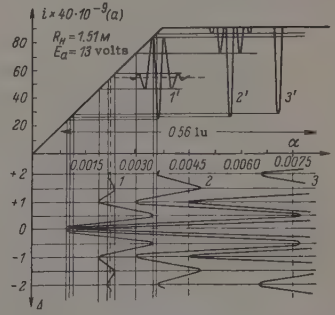

Fig. 5. Light characteristic of photodiode No. 1. Δ is the path difference.

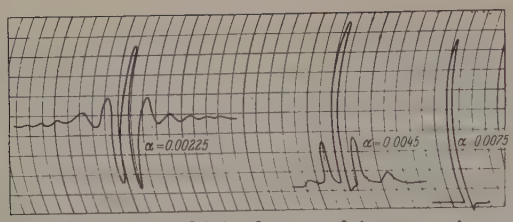

Fig. 6. Traces of interference fringes. α is the aperture of the illuminator.

which corresponds to the dark achromatic fringe, i.e., the photoelectric difference reaches 100%. The fringe traces for apertures 0.002, 0.0045, and 0.0075 are given in Fig. 6. If in the interferometer there is one white achromatic fringe, the fringe trace (Fig. 7) will have two reference marks.

These results can be obtained not only by changing the aperture of the condenser but also by changing the load resistance and the voltage of the power supply or by increasing the intensity of the light source.

Isolation of the achromatic fringe by the proposed method can also be accomplished with a photomultiplier and a load resistance of 200 to 1000 megohms. However, the need for a high voltage power supply (1000 volts) and also the instability of leakage resistances which are of the same order of magnitude as the load resistance are a source of inconvenience when working with high gain amplifiers.*

*Cf. note added in proof at the end of the article.

In present metrological practice interference methods employing superposition fringes are widely used.[5,6] Papers[7] have appeared describing the use of superposition fringes to determine inhomogeneities in gases, liquids, and solids, to measure small angles, and to observe phase objects, etc. For automatic measurement it is desirable to have photoelectric recording of superposition fringes. Photoelectric recording would lead to significant simplification of a number of methods in use and would make possible almost complete automation of the measurement process.

For this purpose a Fabry-Perot etalon (5 in the diagram of Fig. 1) 0.05 mm in length was placed in front of the double beam Michelson interferometer. Inclusion of the Fabry-Perot etalon in the apparatus makes it possible to observe several systems (orders) of white light interference fringes which appear whenever the mirror 9 (Fig. 1) is shifted through an interval exactly equal to the distance between the reflecting surfaces of the etalon.

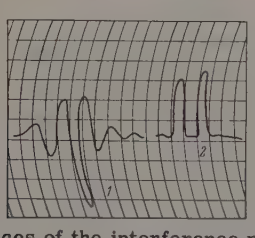

Fig. 7. Traces of the interference pattern with a central white fringe. 1—before isolation of the achromatic fringe; 2—after isolation.

When the order of the superposition fringes is increased, the contrast of the interference pattern decreases, and furthermore, as a consequence of phase shift dispersion, achromatization of adjacent interference fringes is observed. In practice one usually uses only the first five orders for measurement because for higher orders it is difficult to distinguish the achromatic fringe visually.

With photoelectric recording one can ascertain the superposition fringes up to the 7th order. Figure 8 shows traces of the superposition fringes. Table 2 gives values of the photoelectric difference for various orders of superposition fringes. The decrease in photoelectric difference is due to phase shift dispersion. The method we have worked out for the isolation of an achromatic fringe can also be applied to superposition fringes.

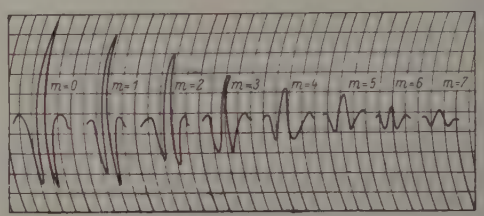

Fig. 8. Traces of superposition fringes. m is the fringe order.

Thus the foregoing work has demonstrated the possibility of a clear 100% isolation of the achromatic fringe from a system of white light interference fringes using germanium photodiodes as detectors.

Table 2

Order of superposition fringes	Photoelectric difference (%)
0	54.8
1	53.2
2	47.2
3	43.8
4	41.2
5	35.6
6	27.0
7	27.0

Note added in proof: A more effective separation of the achromatic fringe can be obtained for small load resistances by using the fact that for large light fluxes the light characteristic of the photomultiplier is nonlinear.

REFERENCES

1. E. Peck, J. Opt. Soc. Am. **45**, 795 (1955).
2. A. H. Cook and H. M. Richardson, Proc. Phys. Soc. **73**, 661 (1959).
3. T. S. Kolomiitsova and I. V. Novikova, Opt. i Spektr. **8**, 363 (1960), Optics and Spectroscopy **8**, 189 (1960).
4. V. P. Koronkevich, V. V. Skidan, and V. A. Afanas'eva, Izmeritel'naya Tekh. No. 5 (1960).
5. M. F. Romanova and A. I. Kartashev, Optiko-Mekh. Prom. Nos. 6, 7 (1939).
6. E. A. Volkova, A. I. Kartashev, and M. F. Romanova, Trudy Vsesoyuz. Nauch.-Issledovatel. Inst. Metrol. 26, 861 (1955).
7. M. Cagnet, Rev. opt. **33**, 1 (1954); Ibid. **33**, 229 (1954).

DURATION OF THE FLASH OF TUBULAR FLASH LAMPS

V. I. Vasiliev, M. S. Levchuk, and I. S. Marchak (pp. 118-122)

Received 21 June 1960

The duration of flashes from tubular flash lamps was investigated as a function of their design (type and pressure of gas, diameter and length of discharge tube) and power supply parameters (operating voltage, capacity of the power supply capacitor, value of ballast resistor). The data obtained make it possible to calculate the duration of flashes from any lamp over a wide range of power supply parameters.

The duration and instantaneous intensity of flashes m a given type of tubular flash lamp can vary over a e range due to changes in the power supply parame-s, particularly in the capacity of the power supply acitor and the operating voltage.[1-4] These character-cs can be varied considerably by using active or re-ive ballast in the discharge circuit, or by supplying lamp with power from an artificial line consisting of etwork of capacitors and inductances.[5-7] Even greater sibilities for changing the duration and instantaneous inous intensity of flashes are revealed when the de-n parameters of the lamp are changed (particularly length and diameter of the discharge tube).

The pertinent information published in the litera-e[1-10] is fragmentary; it refers to individual types of ps, the duration of whose flashes was measured over arrow range of power supply parameters.

The work described here is intended to obtain a gen-l picture of the dependence of the duration of flashes m tubular flash lamps on their design and power sup-parameters.

The duration of flashes was measured in approxi-tely 1000 experimental and production lamps with aight and bent discharge tubes made of glass and artz. The internal diameter of the discharge tubes ged from 0.3 to 12 mm, their length from 10 to 1800 m. The lamps were filled with xenon, krypton, and on at pressures ranging from 20 to 1000 mm Hg. The ctrode design and manufacturing techniques were se used in routine production. Power was supplied to e lamps at potential gradients ranging from 15 to 500 lts/cm, using capacitances ranging from 0.1 to 5000 and with inductances in the discharge circuit ranging m 0.5 to 2000 μh.

The duration of flashes was determined by obtaining oscillograms of the current in the circuit of a vacuum photocell or photomultiplier tube illuminated by flashes from the pulse lamp (a UIF pulse photometer designed by the VNISI, also IO-4 and other oscillographs with appropriate photoelectric attachments). The spectral sensitivity of the photocell was corrected to visual sensitivity by means of an appropriate filter. A great deal of attention was devoted to achieving linearity of the working region of the light flux-current characteristic of the photocell and to eliminating distortion caused by the time constant of the measuring circuit.

The duration of a flash τ was measured as the difference between the abscissae of the points on the luminous intensity I vs. time curve corresponding to 35% of the maximum intensity (Fig. 1).

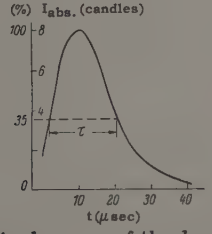

Fig. 1. A typical curve of the luminous intensity of tubular flash lamps plotted against time (with low inductance in the discharge circuit). Design and power supply parameters of the lamp: l = 70 mm, d = 0.5 mm, xenon, L = 1 μh, p = 600 mm Hg, C = 0.25 μf, U = 1.2 kv.

EXPERIMENTAL RESULTS

Oscillograms from different flash lamps having different power supply parameters showed that the corresponding curves had a common shape for all conditions (Fig. 1) for inductances up to approximately 10 μh. By selecting the proper scales for the x- and y-axes in accordance with these conditions, it is possible to obtain almost superposable curves (except for small variations in the steepness of the leading edge and some lack of smoothness of the curve described in ref. 10). In this connection, the values of the ratio K of the luminosity of the flash ($\int_0^\infty I\,dt$) to the product of the amplitude of the luminous intensity I_d and the duration of the flash τ, also the ratio M of the intensity for the time τ to the intensity during the entire flash under the most varied

Table 1. Values of Coefficients K and M for Lamps with Different Internal Diameters d and Interelectrode Distances l, with Different Values of the Operating Voltage U and Power Supply Capacitor C

No.	d (mm)	l (mm)	C (μf)	U (kv)	τ (cm)*	I_d (cm)*	$\int_0^\infty I\,dt$ (cm²)*	K	M (%)
1	4.5	500	152	2.35	6.7	6.7	38	0.9	79
2	4.5	500	152	2	8.5	2.9	20	0.81	90
3	4.5	500	152	1.5	8.1	1.3	10	0.94	75
4	4.5	500	80	2.35	5.4	4	19	0.87	83
5	4.5	500	28	2.35	2.9	2	5	0.86	76
6	4.5	500	7.5	5	1.7	4.8	8	0.89	70
7	4.5	500	7.5	4	1.6	3	4.2	0.83	82
8	4.5	500	7.5	3	1.6	1.3	1.8	0.86	80
9	1.9	500	152	3	7.5	1.8	11	0.82	81
10	1.9	500	80	3	4.1	1.7	6	0.86	83
11	1.9	500	28	3	2.1	1.25	2.1	0.8	86
12	1.9	500	7.5	3	1	0.6	0.5	0.83	90
13	7.5	300	152	2	1.75	4.2	6	0.81	82
14	7.5	300	152	1	2.2	2.7	5.5	0.92	77
15	0.5	70	0.25	1.2	2.15	7.9	17	0.87	81
					Average values . . .			0.86	81
					Average deviation			±0.04	±4

*Note. On oscillogram scale.

conditions have practically the same values. Experimental values of these quantities under different discharge conditions are given in Table 1. The discrepancies in values of K and M under the same conditions (lamps of the same type and the same power supply conditions) did not exceed 3%, and thus were within the limits of accuracy of measurement.

By making use of the values of K obtained, one can calculate the amplitudes of its luminous flux and luminous intensity by the known characteristics of the lamp—its luminous efficiency, the energy, and duration of flashes. Data on the dependence of the flash parameters of tubes, 0.5 mm diam and 70 mm long, on the type and pressure of gas are given in Table 2.

Table 2. Values of the Quantities τ, I_a, and $\int_0^\infty I\,dt$ in Capillary Lamps versus the Type of Gas and Pressure p (C = 0.25 μf, U = 1.2 kv)

No.	Type of Gas	p (mm Hg)	τ (μsec)	I_a (k candles)	$\int_0^\infty I\,dt$ (candle-sec)
1	Argon	600	12.6	2.2	0.025
2	Krypton	600	19.4	5.1	0.08
3	Xenon	600	22.2	8.2	0.15
4	Xenon	300	17.9	12.3	0.15
5	Xenon	100	10.6	12.3	0.1
6	Xenon	50	7	9.8	0.04
7	Xenon	910	22.4	9.7	0.15

The dependence of these parameters on the type of gas and pressure is 1/2-1/3 as great for lamps with diameters of several millimeters. One's attention is attracted to the fact that, in contrast to the duration and total light output of the flash, which first increase monotonously with increasing p and then become constant, the value of the instantaneous luminous intensity reaches a maximum when $p \approx 100$ mm Hg and decreases approximately 30% at higher pressures.

The dependence of τ on the internal diameter of the discharge tube is complicated. When the length of the tube l and the capacitance of the power supply capacitor C is increased, a transition from the relationship $\tau \sim d^{-1/2}$ to the relationship $\tau \sim d^{-2}$ (Fig. 2) is observed. Changing the interelectrode distance l while holding the product $C \cdot l$ constant has almost no effect on τ (if one neglects values of l less than 4 cm). In the latter case, however, one notes a small increase in τ (approximately 10% when l = 2 cm) caused by the fact that the decreases in voltage near the electrodes become comparable with the voltage drop in the body of the tube[11]).

The dependence of τ on the power supply voltage can be expressed for all lamps by the formula:

$$\tau_E = \tau_{E_1} \frac{E}{E_1}^{-0.6},$$

where E and E_1 are two values of the initial potential gradient in the lamp and τ_E and τ_{E_1} are the corresponding values of the duration of the flash (Fig. 3). In this case, the efficiency of the flash increases rapidly with increasing E at small gradient values and reaches saturation at large values of E (in capillary lamps, the "saturation" value of luminous efficiency, which is approximately 35 lumens-sec/joule, is reached when E ~ 400 volts/cm, whereas in wide tubular lamps saturation occurs at E ~ 25 ~ 60 volts/cm).[12]

The dependence of τ and luminous efficiency on C is also complicated. When flash energies are low, the luminous efficiency increases very rapidly with increasing C; when they are high, it ceases to depend on the

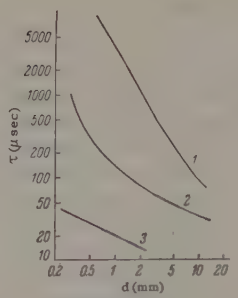

Fig. 2

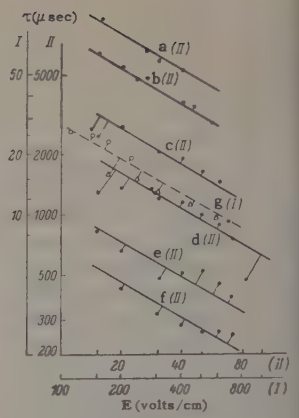

Fig. 3

Fig. 2. Curves of the function $\tau = f(d)$ with different values of the product $C \cdot l$ (xenon, p = 100 mm Hg, E = 100 volts/cm). Value of the product $C \cdot l$ (in μf-cm); curve 1—5000; curve 2—100; curve 3—1.75.

Fig. 3. Linear relationships $\tau = f(E)$ with different values of C for lamps with d = 9 mm (solid lines) and with d = 0.5 mm (dashed lines). Values of C (in μf): a—3050; b—2000; c—1100; d—600; e—300; f—200; g—0.25. Roman numerals I, II indicate corresponding coordinate axes.

capacitance of the power supply (Fig. 4). When a transition is made from low to high values of the product $C \cdot l$ and τ, one observes a change in the nature of the function $\tau = f(C)$; that is, from $\tau \sim \sqrt{C}$ to $\tau \sim C^2$. Thus, the different empirical relationships which define the dependence of τ on C (refer, for example, to ref. 9) and similar formulas for the dependence of τ on E can be applied to only a narrow range of C values.

Figure 5 (left side) shows a family of experimental curves of τ plotted against the product $C \cdot l$ for xenon lamps with internal diameters from 0.3 to 12 mm, with an initial potential gradient of 100 volts/cm. The right side of the same figure shows the shift in the ordinate scale corresponding to changes in the value of the initial potential gradient. Thus, Fig. 5 can be used as a single nomogram for determining the duration of flashes from lamps with different power supply and design parameters (if the ballast resistor in the discharge circuit is sufficiently small). At high τ values (above 1000 μsec) the slopes of the curves and the distance between them are consistent with the idea that the discharge column is an ohmic conductor whose resistance R is determined for given E only by the resistivity of the plasma ρ and the

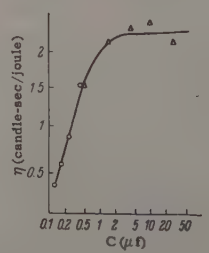

Fig. 4. Luminous efficiency η vs. power supply capacitance for a capillary xenon lamp (d = 0.5 mm, l = 70 mm, U = 1.2 kv).

metric dimensions of the internal channel of the discharge tube, and that the radiation intensity of the discharge is proportional to its electric power. The τ values calculated as the time required for the flash to decay to of its maximum value ($\tau = RC/2$) agree with the experimental data when $\tau \leq 1000$ μsec, if we assume that 1.25×10^{-2} ohm/cm for E = 100 volts/cm.

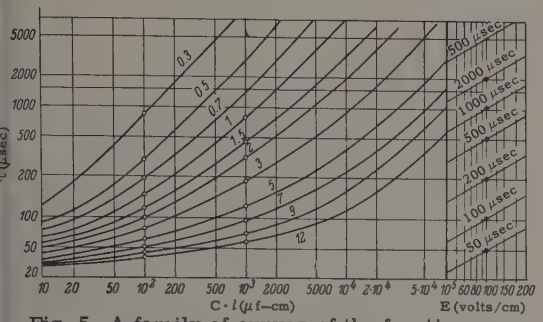

Fig. 5. A family of curves of the function $\tau = f(C \cdot l)$ for lamps with different values (figures near the curves) with an initial potential gradient of 100 volts/cm. To the right—shifts in the ordinate scale with changes in the value of the gradient.

On this basis, one would expect that when the inductance of the discharge circuit is less than $L_{cr} = CR_L^2/4$ the ballast resistance R_0 is negligibly small compared with R (R is the resistance of the discharge column of the lamp), the duration of the flash should not depend on L and R_0. This is confirmed by the fact that, for example, for ISP-70 capillary lamps (d = 0.5 mm, 7 cm, C = 0.25 μf, and U = 1.2 kv) for which $R \cong 40$ ohms and $L_{cr} \cong 100$ μh, the introduction of an inductance of 100 μh into the discharge circuit does not cause any noticeable increase in τ. It takes ~2000 μh to increase the value of τ by a factor of approximately 2.5 (τ increases more slowly than the first power of L due to the inverse effect of L on the resistance of the discharge column). The duration of the flash is affected in a similar manner by a ballast resistor which exceeds the calculated resistance of the lamp.

REFERENCES

1. I. S. Marshak, Svetotekhnika No. 1, 17 (1956).
2. I. S. Marshak, Pribory i Tekh. Ekspt. No. 5, 3 (1957).
3. I. S. Marchak, Uspekhi Nauch. Fot., Akad. Nauk SSSR, Otdel Khim. Nauk **6**, 16 (1959).
4. I. S. Marshak, V. I. Vasiliev, A. I. Mironova, V. P. Ivanov, and R. G. Vdovchenko, Uspekhi Nauch. Fot., Akad. Nauk SSSR, Otdel Khim. Nauk **6**, 43 (1959).
5. I. S. Marshak, Collected Articles on Vacuum Technology, Nos. 22, 27. Gosenergoizdat, Moscow, 1960.
6. W. Griffin, J. Soc. Motion Picture Television Engrs. **66**, 127 (1957).
7. D. P. C. Thackeray, Proc. Third Intern. Congr. on Highspeed Photography, London, p. 21, 1957.
8. H. E. Edgerton, J. Opt. Soc. Am. **36**, 390 (1946).
9. F. E. Carlson and D. A. Pritchard, Illum. Eng. **42**, 235 (1948).
10. H. E. Edgerton, R. Bonazoli, and J. T. Lamb, J. Soc. Motion Picture Television Engrs. **63**, 15 (1954).
11. R. G. Vdovchenko, I. S. Marshak, and S. A. Nikol'skaya, Collected Articles on Vacuum Technology, No. 21, Gosenergoizdat, Moscow, 1959.
12. I. S. Marshak, Svetotekhnika No. 1, 17 (1957).

SHORT COMMUNICATIONS

ON NUCLEAR MAGNETIC RESONANCE IN SOLIDS

B. N. Provotorov (pp. 123-125)

Received 21 May 1960

Bloch[1,2] has obtained the following general equation the density matrix σ of a spin system weakly coupled the lattice:

$$\frac{d\sigma}{dt} + i[E, \sigma] = \Gamma(\sigma - \sigma_0), \qquad (1)$$

ere

$$E = -\frac{\mu}{h} H_0 I_z - \frac{\mu}{h} H_1 (I_x \cos\omega t - I_y \sin\omega t) + \frac{\mu^2}{h} \sum_{i>k} \left(\frac{\mathbf{I}_i \mathbf{I}_k}{r_{ik}^3} \cdot 3 \frac{(\mathbf{I}_i \mathbf{r}_{ik})(\mathbf{I}_k \mathbf{r}_{ik})}{r_{ik}^5} \right)$$

I_y, I_z are the components of the total spin of the system, μ is the magnetic moment of a nucleus located at me lattice point, $\mathbf{I}_i$ is the spin operator of the nucleus cated at the i-th lattice point, $\mathbf{r}_{ik}$ is the vector joining e i-th and k-th lattice points, H_0 is the constant magtic field, H_1 is the amplitude of the rotating magnetic eld, σ_0 is the equilibrium density matrix, and $\Gamma(\sigma - \sigma_0)$ an operator linear in $\sigma - \sigma_0$ which describes the coupg between the spin system and the lattice.

The operator $\Gamma(\sigma - \sigma_0)$ has a very complicated structure. However, it can be simplified by recalling the experimental fact[3] that in most cases, after the field H_1 is switched off, the z-component of the total spin of the system $I_z(t)$ approaches its equilibrium value according to the law

$$\frac{dI_z(t)}{dt} = \frac{I_0 - I_z(t)}{T_1}. \qquad (2)$$

(I_0 is the equilibrium value of the total spin and T_1 is the spin-lattice relaxation time). In view of Eq. (2), we have

$$\Gamma(\sigma - \sigma_0) = \frac{\sigma_0 - \sigma_1}{T_1}.$$

In this way, we obtain the equation

$$\frac{d\sigma}{dt} + i[E, \sigma] = \frac{\sigma_0 - \sigma}{T_1}, \qquad (3)$$

which, as will be shown below, leads to correct results in the case of small and large values of H_1. We can

therefore hope that the complete solution of this equation may produce a true picture of the phenomenon over the entire range of variation in H_1.

Transforming to a rotating system of coordinates

$$\sigma = e^{-i\omega I_z t}\sigma^* e^{i\omega I_z t}$$

and discarding,[4] as usual, the nonsecular parts of the dipole-dipole interaction operator, we obtain

$$\frac{d\sigma^*}{dt} + i\left[\Delta I_z - \frac{\mu H_1}{\hbar} I_x + A,\ \sigma^*\right] = \frac{\sigma_0 - \sigma^*}{T_1}; \quad \Delta = \omega - \omega_0;$$

$$\omega_0 = \frac{\mu H_0}{\hbar}; \quad \frac{\mu H_1}{\hbar} = j, \tag{4}$$

where A is the secular part of the dipole-dipole interaction.

The stationary solution of this equation has the form

$$\sigma^* = \int_0^\infty e^{-\frac{t'}{T_1}} e^{i(\Delta I_z - jI_x + A)t'}\,\sigma_0\, e^{-i(\Delta I_z - jI_x + A)t'}\frac{dt'}{T_1}. \tag{5}$$

Following Bloch,[4] the components of the complex magnetic susceptibility will be derived from the expressions

$$\chi' = \frac{\mu}{H_1}\,\mathrm{Spur}\,(\sigma^* I_x), \tag{6}$$

$$\chi'' = \frac{\mu}{H_1}\,\mathrm{Spur}\,(\sigma^* I_y)$$

$$= \int_0^\infty e^{-\frac{t'}{T_1}}\,\mathrm{Spur}\left(e^{i(\Delta I_z - jI_x + A)t'}\,\sigma_0 e^{-i(\Delta I_z - jI_x + A)t'} I_y\right)\frac{dt'}{T_1}. \tag{7}$$

Expanding the operators under the integral as a power series in H_1 and keeping only the part which is linear in H_1, it is easy to obtain the Van Vleck expression for the shape of the absorption line (see also ref. 4):

$$\chi'' = \frac{h\omega_0}{4kT}\frac{\mu^2}{\hbar}\int_{-\infty}^{+\infty} e^{i(\omega_0 - \omega)t'}\,\mathrm{Spur}\left(a_0 I' e^{iAt'} I^{-1} e^{-iAt'}\right) dt',$$

where

$$I^{\pm 1} = I_x \pm iI_y.$$

If we assume further, as was done in ref. 5, that $I_z(t)$ decreases exponentially in the absence of spin-lattice relaxation ($T_1 = \infty$), i.e., $I_z(t) = I_z(0)\exp[-\alpha H_1^2 g(\omega)t]$, where $g(\omega)$ is the shape function of the absorption line and α is a coefficient depending on the magnitudes of the nuclear spins and magnetic moments, then Eq. (7) gives us

$$\chi'' = \frac{h\alpha g(\omega)\, I_0}{1 + \alpha H_1^2 g(\omega)\, T_1}$$

for the stationary value of χ'', in agreement with ref. 5.

Redfield[6] has shown that this assumption, and along with it the theory of Bloembergen et al.[5] is invalid in the case $H_1 \gg \delta H$ (where δH is the absorption line width). Hence it would be of interest to calculate χ' and χ'' for this case.

If in Eq. (7) we go over to a new system of coordinates whose z-axis coincides with the direction of the effective magnetic field in the rotating coordinate system (see, for example, ref. 4), then

$$\chi'' = \frac{\mu}{H_1}\int_0^\infty e^{-\frac{t'}{T_1}}\,\mathrm{Spur}\left(e^{i\left(-fI_z + \sum_{n=-2}^{+2} a^n e^{in\beta t'}\right)t'} e^{i\theta I_y t'}\right.$$

$$\left.\times\, a_0 e^{-i\theta I_y t'} e^{-i\left(-fI_z + \sum_{n=-2}^{+2} a^n e^{in\beta t'}\right)t'} I_y\right)\frac{dt'}{T_1}, \tag{8}$$

where

$$f = \sqrt{\Delta^2 + j^2}, \quad \sin\theta = \frac{j}{\sqrt{\Delta^2 + j^2}}.$$

If we now discard the rapidly oscillating terms in the exponential factor and use the relations $[I_z, a^0] = 0$ and $h\omega_0 \ll kT$, it is easy to arrive at the expressions:

$$\chi'' = \frac{\frac{\mu^2}{\hbar} I_0}{2\left[(\omega - \omega_0)^2 + \frac{\mu^2 H_1^2}{\hbar^2}\right] T_1},$$

$$\chi' = \frac{\frac{\mu^2}{\hbar}(\omega_0 - \omega)\, I_0}{2\left[(\omega - \omega_0)^2 + \frac{\mu^2}{\hbar^2} H_1^2\right]}.$$

These expressions agree with Redfield's results.[6]

REFERENCES

1. F. Bloch, Phys. Rev. **102**, 104 (1956).
2. F. Bloch, Phys. Rev. **105**, 1206 (1957).
3. E. M. Purcell, Nuovo cimento **6**, 974 (1957).
4. F. Bloch, Phys. Rev. **111**, 841 (1958).
5. N. Bloembergen, E. M. Purcell, and P. V. Pound, Phys. Rev. **73**, 679 (1948).
6. A. G. Redfield, Phys. Rev. **98**, 1797 (1955).

EFFECT OF SPECTROGRAPHIC CAMERA OBJECTIVE DISTORTION ON SPECTRAL LINE CURVATURE

I. V. Peisakhson (pp. 125-127)

Received 9 December 1960

The dispersing element of spectrum instruments ism or diffraction grating) causes a warping of spec- lines—each monochromatic image of an infinitely row straight slit presents its own curved arc, nearly abolic.[1] In prism instruments the vertex of these ves is turned toward the long wavelength part of the ctrum, and the curvature increases with increasing active index of the prism material, i.e., with de- asing wavelength. In instruments with reflection dif- tion gratings the curved spectral line is turned with vertex to the short wavelength part of the spectrum, its curvature decreases with decreasing wavelength.

Any objective possessing distortion also images a ment of parallel vertical lines as arcs of different vature. Consequently, the curvature of a line in a ctrogram is determined by the parameters not only of dispersing element, but also of the spectrographic nera objective. Here the radius of curvature R of the is found from the relation

$$\frac{1}{R}=\frac{1}{r}+\frac{1}{r_1}, \qquad (1)$$

ere r and r_1 are radii of curvature of the image of slit, dependent respectively on the dispersing ele- nt and the distortion of the objective.

The curvature of spectral lines causes inconvenience hotometric investigations, particularly in autocolli- ted spectrographs where slit and spectrum are located coincidence so that the center of the slit and its mono- omatic images are situated outside the plane of the ncipal section of the prism or grating. In this case re occurs an inclination of the spectral lines, differ- in the several parts of the spectrogram. If the cen- of the slit image is located at a distance z from the ne of the principal section, then the tangent to the ved spectral line at this point forms with the direc- n of the slit the angle $\beta = z/R$. In instruments with toelectric recording of the spectrum, the warping of image of the entrance slit in the presence of a straight t slit widens the transmission band of the instrument, l by the same token decreases its resolving power.

If the optical system of the spectrograph is designed that at the ends of the spectrogram the line curvature practically the same, then it is possible to compen- e it by curving the jaws of the entrance slit.

For an instrument employing a prism made of a gle material of refractive index n

$$\frac{1}{r}=\frac{n^2-1}{nf}\frac{d\vartheta}{dn}, \qquad (2)$$

ere f is the focal length of the camera objective and s the angular deviation produced by the prism.

The curvature of the line dependent on the camera jective distortion is equal to

$$\frac{1}{r_1}=\frac{w}{f}S_v, \qquad (3)$$

ere w is the angle formed by the dispersed rays with the axis of the objective, and S_v is the third order distortion coefficient (also known as the fifth Seidel sum), fixed by the construction of the objective and the location of its entrance pupil. The magnitude of S_v can be computed by the method explained in ref. 2.

When $S_v > 0$ the distortion is pincushion, when $S_v < 0$, barrel. In mirror objectives (and with satisfactory accuracy also in lenses) S_v does not depend on the wavelength of the light.

In a prism spectrograph the angle w may be considered as a function of n. Then $dw/dn = d\vartheta/dn$. The condition of constant R in formula (1) for all n is

$$\frac{d}{dn}\left(\frac{1}{r}+\frac{1}{r_1}\right)\equiv 0. \qquad (4)$$

Strictly speaking, Eq. (4) can be an identity only when S_v is some slowly changing function of n. We restrict ourselves to the case of small changes of n near $n = n_0$.

Differentiating (2) and (3) and assuming $S_v = \text{const.}$, we obtain

$$\frac{n^2-1}{n}\frac{d^2\vartheta}{dn^2}+\left(1+\frac{1}{n^2}\right)\frac{d\vartheta}{dn}+S_v\frac{dv}{dn}=0. \qquad (5)$$

For a prism close to minimum deviation

$$\frac{d\vartheta}{dn}=\frac{2\sin\frac{\alpha}{2}}{\cos i}, \quad \frac{d^2\vartheta}{dn^2}=\left(\frac{d\vartheta}{dn}\right)^2\tan i.$$

Here α is the angle of refraction, and i is the angle of incidence on the first face of the prism in its principal section.

Let the prism be set at minimum deviation for $n = n_0$, that is, $\sin i = n_0 \sin(\alpha/2)$, and let the image of the slit in light of index $n = n_0$ be located in the middle of the spectrogram. Then from (5) the approximate condition of line curvature constancy in the spectrogram is found in the form

$$S_v=-\left(1+\frac{1}{n_0^2}+\frac{2(n_0^2-1)\sin^2\frac{\alpha}{2}}{1-n_0^2\sin^2\frac{\alpha}{2}}\right). \qquad (6)$$

The condition (6) remains in force both for multiple pass instruments and for instruments with several prisms. The sign of the right-hand side of (6) is always negative, and its absolute value exceeds unity by far, increasing with increasing angle α. For example, for $\alpha = 60°$ and $n_0 = 1.6$, it is necessary to have $S_v \approx -3.6$.

For instruments with a reflection diffraction grating

$$\frac{1}{r}=\frac{\lambda}{f}\frac{d\psi}{d\lambda}, \qquad (7)$$

where λ is the wavelength of light, and ψ is the diffraction angle in the plane perpendicular to the rulings of the grating. The angle w in formula (3) is a function of the wavelength, and $dw/d\lambda = d\psi/d\lambda$. The curvature of the lines in a spectrogram will not depend on λ if

$$\frac{d}{d\lambda}\left(\frac{1}{r}+\frac{1}{r_1}\right)\equiv 0. \quad (8)$$

Assuming S_v = const., we have from (3), (7), and (8)

$$\lambda\frac{d^2\psi}{d\lambda^2}+\frac{d\psi}{d\lambda}(1+S_v)=0. \quad (9)$$

But $\sin\psi = k\lambda N - \sin\varphi$, from which

$$\frac{d\psi}{d\lambda}=\frac{kN}{\cos\psi}, \quad \frac{d^2\psi}{d\lambda^2}=\left(\frac{d\psi}{d\lambda}\right)^2\tan\psi.$$

Here k is the order of the spectrum, N is the number of rulings per unit length in the grating, and φ is the angle of incidence on the grating.

For small changes in angle ψ we obtain from (9) the approximate condition for constant line curvature in a diffraction spectrograph:

$$S_v=-\frac{1+\sin\varphi\sin\psi_0}{\cos^2\psi_0}, \quad (10)$$

where ψ_0 is the diffraction angle of the rays forming the image of the slit in the center of the spectrogram. The sign of the right-hand side of (10) is always negative. Its absolute value is less than unity only in the case that $|\psi_0| < |\varphi|$ and the signs of the angles φ and ψ_0 are different, that is, the incident and diffracted rays pass on different sides of the normal to the grating. For the autocollimated spectrograph where $\psi_0 = \varphi$, formula (10) gives

$$S_v=-(1+2\tan^2\psi_0).$$

Thus in both prism and diffraction spectrographs the curvature of spectral lines may be made practically constant if the camera objective possesses substantial negative (barrel) distortion.

The required values of S_v in a lens objective usuall can be obtained for a particular position of its entrance pupil, that is, prism or grating. If now a concave spheri cal mirror be used as a camera objective, then it can be shown that

$$S_v=-\frac{d^3}{4}+\frac{3d^2}{2}-2d, \quad (11$$

where d is the distance from the dispersing element to the mirror vertex expressed in focal lengths. The value of S_v in (11) reduces to zero for d = 0 and d = 2. Its minimum value equals −0.77 (for d = 0.85). Consequent the curvature of spectral lines in instruments with mirror camera objectives can be compensated by the distortion of the objective and curvature of the slit jaws on when a diffraction grating is used, and far from always, even then.

REFERENCES

1. I. V. Peisakhson, Opt. i Spektr. 4, 481 (1958).
2. G. G. Slyusarev, "Methods of Computation of Optical Systems." Ob'ed. Nauch.-Tekh. Izd. (United Scientifi Technical Publishers), Moscow, 1937.

ZnS:Ag PHOSPHOR WITH BORON AS A COACTIVATOR

A. V. Lavrov (p. 128)

Received 14 January 1961

Most of the coactivators of zinc sulfide phosphors are found among elements in the third column of the periodic table.[1] The present communication increases the number of known ZnS coactivators by adding boron, the lightest element in the third column.

The activation of ZnS by silver in the presence of boron was observed under the following conditions: Silver (in the form of $AgNO_3$) at a concentration of 10^{-4} gm/gm and boron (in the form of the black powdered elemental boron) at a concentration of 5.4×10^{-4} gm/gm were added to phosphor-grade zinc sulfide previously treated with hydrogen sulfide at 500°C. The batch was carefully pulverized and dried. Baking was carried out at 1100°C in a hydrogen sulfide atmosphere. Samples containing either silver or boron alone did not luminesce. Silver activation occurs when silver and boron are introduced simultaneously. The Figure shows the emission spectrum of the ZnS:Ag:B phosphor excited by ultraviolet light (365 mμ) at room temperature. The phosphor has a blue luminescence band with λ_{max} = 434 mμ, which corresponds to the emission of ZnS:Ag with a würtzite lattice.

We measured the particle size of ZnS:Ag and ZnS:Ag:B samples by visual counting under a microscope. The samples were obtained under identical conditions (H_2S, 1100°C, 1/2 hr). Measurements have shown that the introduction of boron does not accelerate crystal growth. Hence under the existing conditions we may not speak of the mineralizing action of boron. In this batch,

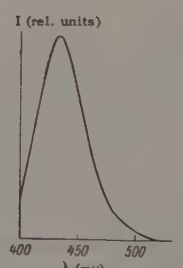

Luminescence spectrum of the ZnS:Ag(10^{-4}):B phosphor (baked in H_2S at 1100°C).

the Ag:B gram-atom concentration ratio was 1:50. Larg boron losses are to be expected in the course of baking, however, due to the considerable volatility of its sulfide.

The ZnS:Ag:B phosphor can be obtained if silver (10^{-4} gm/gm) is introduced at 450°C into zinc sulfide previously baked at 1100°C in hydrogen sulfide, and boro is added in the amount of 5.4×10^{-4} gm of boron for 1 gr of ZnS. If ZnS is subjected to the same preliminary baking in hydrogen sulfide but boron is not added, then low temperature silver activation results in the appearance of blue luminescence four times as faint as in the preceding case. This indicates that in the course of baking an interaction occurs between zinc sulfide and boron (or more precisely between ZnS and B_2S_3). This

raction increases the number of lattice defects which r the intrusion of silver sulfide. These defects apntly are cation vacancies.

I wish to express my appreciation to V. I. Anosov is measurement of the emission spectrum.

REFERENCES

1. F. A. Kröger and S. Dikhoff, Physica 16, 297 (1950).
2. "Handbuch der Präparativen Anorganischen Chemie." Stuttgart, 1954.

DIPOLE MOMENT OF CH_3GeH_3 MOLECULE

A. I. Barchukov and Yu. N. Petrov (p. 129)

Received 14 February 1961

Previous investigations[1,2] of the dipole moment of CH_3GeH_3 molecule have resulted in the divergent valof $\mu = 0.67 \pm 0.02$ and $\mu = 0.635 \pm 0.006$ D, respecy. In the present study we have measured the dipole ent of this molecule described with the help of the resonator proposed by A. M. Prokhorov,[3] which zes a microwave spectrometer as the absorption . The investigation of such a resonator, described ef. 4, showed that it could be utilized for the measent of the dipole moments of molecules by deterng the magnitude of their Stark effects without preary calibration of the magnitude of the modulating .

The dipole moment of the $CH_3Ge^{74}H_3$ molecule was ulated by means of the measured Stark effect for the order transition $J = 1 \rightarrow 2$ ($\nu_0 = 34598$ Mc/s). Taking consideration the selection rule $M = \pm 1$, and exclud- $M = 0$, since this takes place in the ordinary wave rption cell, we obtained for the dipole moment of the ecule the value

$$\mu = 0.644 \pm 0.005 \text{ D}.$$

Within the limits of experimental error this result agreement with that obtained in ref. 2. One can ase that in ref. 1 there occurred systematic errors in determination of the effective value of the modulating . The photograph shows a general view (without the um chamber) of the absorption cell in the form of a resonator, the type used in this investigation.

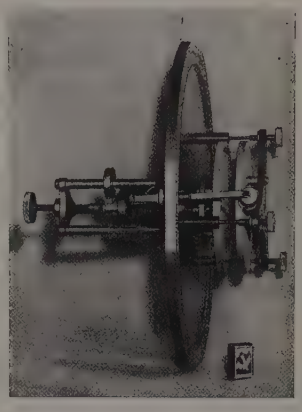

REFERENCES

1. A. I. Barchukov and A. M. Prokhorov, Opt. i Spektr. 5, 530 (1958).
2. V. W. Laurie, J. Chem. Phys. 30, 1210 (1959).
3. A. M. Prokhorov, Zhur. Eksptl. i Teoret. Fiz. 34, 1658 (1958), Soviet Phys.-JETP 7, 1140 (1958).
4. A. I. Barchukov and A. M. Prokhorov, Radiotekh. i Elektron. 4, 2094 (1959).

THE TEMPERATURE DEPENDENCE OF INFRARED ABSORPTION LINES

L. N. Ovander (pp. 129-131)

Received 20 February 1961

In a number of experimental works (see, for example, ref. 1), it has been shown that the integrated intensity of infrared absorption lines for the liquid phase falls off with increasing temperature according to a linear law. Intermolecular interaction manifests a definite influence on the temperature dependence of infrared absorption lines. It has been shown in one of the previous works by the present author[2] that intermolecular interaction, despite its smallness, may have a substantial influence on the temperature dependence of spectra on account of the interaction between intramolecular and intermolecular vibrations. In ref. 2, this connection was examined in the adiabatic approximation for the so-called two-molecule model.

In the present note, an attempt is undertaken to construct a theory of the temperature dependence of infrared absorption lines for a condensed medium, and it is shown that the integrated intensity falls off with increasing temperature according to a linear law, in accordance with the data.[1] The interaction between intramolecular and intermolecular vibrations is brought about through anharmonicity; to avoid misunderstandings, we note that this is not the anharmonicity which exists in the isolated molecule—the latter is not considered at all in the present work. Let us write down the Hamiltonian of the system as follows[3]:

$$H_{\text{кр.}} = \sum_k \hbar\omega_k a_k^+ a_k + \sum_q \hbar\Omega_q b_q^+ b_q + N^{-1/2} \sum_{k,q} B(k, q)\, a_{k+q}^+ a_q (b_q + b_{-q}^+), \quad (1)$$

where a_k^+ and a_k are the operators for the origination and annihilation of phonons corresponding to intramolecular vibrations, $\omega_k = \omega_0 + (\gamma/2)(\cos kd - 1)$ are the frequencies of these phonons, b_q^+ and b_q are the operators for the origination and annihilation of phonons corresponding to intermolecular vibrations, $\Omega_q = \Omega_0 \sin(qd/2)$ are the frequencies of the translational vibrations, $\Omega_q = \Omega_0 + (\Delta\Omega/2)\cdot(\cos qd - 1)$ are the frequencies of the orientational vibrations, and

$$B(k, q) = g_1 \sin\frac{qd}{2} \sin\frac{2k+q}{2} d$$

for translational vibrations and

$$B(k, q) = g_2 \cos\frac{qd}{2} \cos\frac{2k+q}{2} d$$

for orientational vibrations.

The absorption spectrum is found according to the procedure of ref. 4, which is strictly applicable, it appears, only for transitions with small oscillator strengths. Furthermore, a certain lack of strictness appears in the substitution of a crystal for a liquid (the Hamiltonian (1) represents the crystal Hamiltonian[3]).

In this way, for the fundamental vibrational $0 \to 1$ transition, in the case of so-called "weak interaction" between high-frequency and low-frequency phonons (see formula (4.11) of ref. 4), we obtain for the absorption intensity

$$I(\omega) = (1+\eta)\frac{\frac{\Gamma}{2} + A[\omega - (\omega_0 + \Delta)]}{[\omega - (\omega_0 + \Delta)]^2 + \frac{\Gamma^2}{4}}, \quad (2)$$

where

$$A = \frac{\pi}{2} f'(0), \qquad \hbar\Delta = -P\int \frac{f(E)}{E} dE,$$

$$\eta = -P\int \frac{f'(E)}{E} dE, \qquad \Gamma = \frac{2\pi}{\hbar} f(0),$$

$$f(E) = \sum_q B(q, -q)\, B(0, q)\, [(n_q + 1) \times \delta(\hbar\Omega_q - E) + n_q \delta(\hbar\Omega_q + E)],$$

$$n_q = \frac{1}{e^{\frac{\hbar\Omega_q}{kT}} - 1}.$$

In obtaining (2), we neglect the spatial dispersion of the optical branch; i.e., we consider that $\Gamma \ll \Delta\Omega$.

From (2), we obtain without difficulty, for the integrated intensity

$$I = \int I(\omega)\, d\omega = \pi(1 + \gamma).$$

If $kT > \hbar\Omega_q$, then $n_q \approx kT/\hbar\Omega_q$ and $\eta = DT$. By means of a simple evaluation, one can show that D is negative both for translational and for orientational vibrations.

Thus we arrive at the conclusion that anharmonic interaction between intramolecular and intermolecular vibrations leads to a fall in the integrated intensity with increasing temperature, in accordance with the data.[1]

In conclusion, the author thanks S. I. Pekar, K. B. Tolpygo, and M. P. Lisitsa for discussion of the results.

REFERENCES

1. M. P. Lisitsa and Yu. P. Tsyashchenko, Opt. i Spektr. 9, 188, 438 (1960), Optics and Spectroscopy 9, 99, 229 (1960).
2. L. N. Ovander, Vestnik Kiev. Univ., Ser. Fiz. i Khim. No. 3, issue 1, 87 (1960).
3. A. S. Davydov and A. F. Lubchenko, Zhur. Eksptl. i Teoret. Fiz. 35, 1499 (1958), Soviet Phys.-JETP 8, 1048 (1959).
4. Y. Toyozawa, Progr. Theoret. Phys. (Kyoto) 20, 53 (1958).

THE RAMAN SPECTRUM OF BARIUM TITANATE

Ya. S. Bobovich and E. V. Bursian (pp. 131-132)

Received 1 February 1961

The vibrational spectrum method has been applied series of studies to clarify the spontaneous polariza- phenomenon of Seignetto electrics. In particular, um titanate has been repeatedly investigated using ared absorption and reflection spectra, and the most plete data on this question are contained in ref. 1. uthor obtained infrared absorption spectra of a pow- pressed with KBr and of thin $BaTiO_3$ single crystals. tra of single crystals heated above 120° C (cubic ification) are characterized by two broad bands with ima at 495 and approximately 340 cm^{-1}. The influ- e of temperature on the 495 cm^{-1} band was success- followed. As the crystal was cooled from +130 to 0° C in the course of its transition from cubic and agonal, orthorhombic, and rhombohedral modifica- s there is observed a general shift of this band to- is higher frequencies and a more distinct splitting of to two components. An investigation of other titanates the perovskite structure ($PbTiO_3$, $SrTiO_3$, $CaTiO_3$) ied out in ref. 1 revealed the slight influence of the on the nature of the infrared spectrum. From it follows that the spectrum is determined basically he vibrations of the TiO_6 octahedral aggregates.

In the work of Yatsenko,[2] besides the two bands men- ed above* the first overtones were also discovered,

ere is no accurate agreement of the frequencies with values given in ref. 1. The first of the bands has a lder at a frequency about 675 cm^{-1}.

he author has stated. From a comparison of these the other frequency values the calculated mechanical armonicity of the vibrations appears to be unusually e.

We have succeeded in recording the Raman spectrum $BaTiO_3$ crystals. The crystals had a dimension of 2 to m, were grown by the method of Blattner, and were olorized in alcohol vapors at a temperature of 600 to °C. The absorption spectrum of such crystals in the ble region is given in ref. 3. The Curie temperature ermined visually from the moment of disappearance he domain structure was equal to 119 ± 2° C. The stals possessed clearly expressed Seignetto electric perties and gave a hysteresis curve close to rectangle. lattice parameters determined by the x-ray method e a = 3.996 ± 0.002 A and c = 4.028 ± 0.002 A. The ins of the crystals investigated were not submitted to echanical stress.*

many spectroscopic investigations, and in particular ef. 2, such information is absent, introducing some efiniteness into the results.

A method completely analogous to one described lier[4] was applied to excite the Raman spectrum of TiO_3. Its specific characteristic is that the depth of etration of the exciting radiation (the mercury line 4358 A), determined by the absorption coefficient of crystals, has a magnitude not less than several dredths of a millimeter. Therefore, one can assume that the spectrum observed by us arises not from the surface but from the volume.

A photoelectric record of the spectrum obtained is given in the Figure. As is seen the spectrum consists of three bands at 500, 550, and 695 cm^{-1}, of which the latter is much more intense than the others. Their half-width in any case does not exceed 50 cm^{-1}, i.e., nearly three times less than the similar quantity for the infrared absorption bands. It is difficult to reconcile this fact with mechanical anharmonicity as the reason for the breadth of the bands.[2] It is interesting to note that the infrared spectrum of the titanium-containing mineral titanite (sphene) known in the literature[5] in no ways disagrees from the spectra of the other crystals. In its general character the Raman spectrum of barium titanate is very reminiscent of the spectra of rutile[6] and of sphene.[4] This indicates that the vibrations of the TiO_6 octahedral aggregates are principally responsible for the observed bands in the spectra of all of these crystals, and that the spectra do not strongly depend on the nature of the other components.

The isolated octahedral molecule can carry out six different forms of vibrations of which three are active for Raman scattering [according to the Kohlrausch designation[7] $\omega_1(A_{1g}$, nondegenerate), $\omega_2(E_g$, twofold degenerate), $\omega_3(F_{2g}$, threefold degenerate)] and two are active in the infrared spectrum [by the same designations, $\omega_5(F_{1u}$, threefold degenerate) and $\omega_6(F_{1u}$, threefold degenerate)]. One threefold degenerate vibration is observed in neither of the spectra but it makes its contribution in the heat capacity. The surroundings of the molecules can substantially change the vibrational forms. Thus the degeneracy is partially or completely removed depending on the crystal habit. This evidently occurs particularly for the $BaTiO_3$ crystals at room temperature for which the Raman spectra were obtained (the tetragonal modification). On the basis of the above discussion, and also by analogy with the interpreted spectrum of rutile which belongs to the very same modification,[8,9] one can plausibly assume that in the $BaTiO_3$ spectrum observed by us the 695 cm^{-1} band belongs to the A_{1g} type (possibly ω_1) and the 500 and 550 cm^{-1} bands represent resolved components of a twofold degenerate vibration of type $E_g(\omega_2)$.

A more detailed analysis of the vibrational spectrum of crystalline $BaTiO_3$ will be given later.

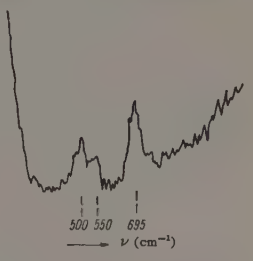

Raman spectrum of barium titanate.

REFERENCES

1. J. T. Last, Phys. Rev. 105, 1740 (1957).
2. A. F. Yatsenko, Izvest. Akad. Nauk SSSR, Ser. Fiz. 22, 1456 (1958).
3. M. S. Kosman and E. V. Bursian, Doklady Akad. Nauk SSSR 115, 483 (1957), Soviet Phys.-Doklady 2, 354 (1958).
4. Ya. S. Bobovich, Opt. i Spektr. 10, 418 (1961), Optics and Spectroscopy 10, 212 (1961).
5. C. Schäfer, F. Matossi, and K. Wirtz, Z. Physik 89, 210 (1934).
6. P. S. Narayanan, Proc. Indian Acad. Sci. 32A, 279 (1950).
7. K. Kohlrausch, "Ramanspektren." Izd. Inostrannaya Lit. Moscow, 1952. Edwards, Ann Arbor, Michigan.
8. B. Dayal, Proc. Indian Acad. Sci. 32A, 304 (1950).
9. P. S. Narayanon, Proc. Indian Acad. Sci. 37A, 411 (1953).

LETTERS TO THE EDITOR

ON THE ARTICLE BY M. V. AKHMANOVA AND G. E. KURILCHIKOVA. INFRARED ABSORPTION SPECTRA OF HYDROXYFLUOROBORIC COMPLEXES OF POTASSIUM AND SODIUM

L. G. Ryss (p. 133)

Received 16 February 1961

In the article,[1] dealing with the study of the infrared spectra of a series of hydroxyfluoroborates, there are several errors and inaccuracies. The data contained in this article may lead to the incorrect interpretation of the properties of this group of compounds.

The authors[1] found that the infrared spectra of $K_3B_3O_3F_6$ and $K_2B_3O_3F_4OH$ are identical. It is apparent, however, that actually one and the same compound $K_2B_3O_3F_4OH$ was investigated.[1] It is hard to obtain a sufficiently pure compound by the synthetic method for $K_3B_3O_3F_6$ which was used by the authors.[1] A more reliable method for the synthesis of this compound was described by Bogdanova and me.[2] In the same article we showed that $K_3B_3O_3F_6$ is easily decomposed by water to $K_2B_3O_3F_4OH$. The authors[1] also failed to perform the analysis of the substances which they had used.

The known equilibrium constants of the hydrolysis of BF_4^- and BF_3OH^-[3] do not leave any doubt that the replacement of F^- by OH^- in the fluoroboric complexes dissolved in water is favored thermodynamically. These complexes are stable in water solutions only at low pH; their stability is increased with the increase in the concentration of F^-. Only BF_4^- and $BF_3CF_3^-$ which are characterized by extremely slow hydrolysis may exist for a long time in the basic solutions. All the remaining known fluoroborates are labile and decompose rapidly in solutions in which they are thermodynamically unstable.

The dissolved $K_2B_3O_3F_4OH$, $K_3B_3O_3F_6$, and $Na_3B_3O_3F_6$ decompose inevitably upon the addition of bases, and only the products of their decomposition—fluorides, boric acid and borates—can be isolated from the basic solutions. The authors[1] point to the extreme similarity of the infrared spectra of the compounds which they isolated from the basic solutions of the compounds and borates (it is possible that they considered these compounds to be identical but did not point to this fact with sufficient clarity). The titles of Tables 2 and 6 and the caption for Fig. 4 contain the names of the isolated compounds without any mention that the spectra were taken not of these compounds but of the products of their decomposition. Evidently the composition of these products might have been most easily elucidated by chemical analysis.

The authors[1] take D_{3h} for the point group symmetry of the $B_3O_3F_6^{3-}$ ion. This symmetry was assumed by several authors for several compounds containing the cyclic B_3O_3 group with three-covalent boron atoms. For this cyclic group to be planar the distortion of the normal valence angles must be so considerable that the existence of this form of the cyclic group becomes questionable. Considerably less distortion of the valence angles would be required in the spatially bent form of this cyclic group, resembling the C-form of cyclohexane. If two boron atoms represent coordination centers (i.e., if they are four-covalent), then the planar form of this cyclic group would require even a greater distortion in the valence angles. Therefore, a more probable form seems to be the one in which the oxygen atom linked to the two four-covalent boron atoms is not contained in the plane formed by the remaining atoms of the cyclic group. For the cyclic group with three four-covalent boron atoms (e.g., $B_3O_3F_6^{3-}$) the most probable structure is the Z-form of cyclohexane.

In table 3 of the same article[1] there are many misprints.

REFERENCES

1. M. V. Akhmanova and G. E. Kurilchikova, Opt. i Spektr. 8, 498 (1960), Optics and Spectroscopy 8, 264 (1960).
2. I. G. Ryss and L. P. Bogdanova, Zhur. Neorg. Khim. 4, 1839 (1959).
3. I. G. Ryss and D. B. Donskaya, Zhur. Fiz. Khim. 33, 107 (1959);
   I. G. Ryss, Doklady Akad. Nauk SSSR 52, 421 (1946);
   I. G. Ryss and P. B. Ust'yanova, Ukrain. Khim. Zhur. 21, 6 (1955).

CORRECTION TO THE ARTICLE BY P. N. NURMUKHAMETOV, E. G. POPOVA, AND S. DOKUNIKHIN. LUMINESCENCE OF CHRYSENE SOLUTIONS AND POWDERS AT 77°K

(pp. 134-135)

Received 16 February 1961

In ref. 1 we have described the luminescence spec- of octane solutions and the green fluorescence and long wavelength absorption spectra of crystalline tiered chrysene at 77°K. It was shown in ref. 2 that "green fluorescence" and the absorption in the visi- region of the crystalline chrysene are caused by the ixtures of naphtacene impurity which is present in rsene in low concentrations and which it is difficult move. The comparison of the spectra of the crystal ples obtained by us with the spectra of naphtacene in talene[3] leads to the conclusion that these spectra be- to the impurities in naphtacene.

The dependence of the type of spectra on the struc- of the crystalline samples and the interpretation of dependence, which was confirmed by x-ray diffrac- studies, must be described in the following way.

The structure of the fluorescence spectra of the im- ties is very sensitive to the size of the microcrystals ne base substance. This is due to the mechanico- sical inhomogeneities and the surface stresses, which ease with the decrease of the size of the little crys- this results in a scatter of the positions of the elec- levels. The scatter depends, among other things, on concentration of impurities which was different in rent samples of chrysene.

The emission spectrum of chrysene is located in the r ultraviolet region.[4,5] The fluorescence spectra of ious crystalline samples obtained by us with a quartz trograph coincided in position with the spectra given ne papers mentioned.

Both the spectrum of the "green fluorescence" of the htacene impurity and that of the base substance—ysene—show the same dependence on sample struc- . In the figure, the spectra of the long wavelength orption and of the fluorescence of a chrysene sample 7°K are given. Comparison of these spectra makes it sible to identify the pure electronic transition bands ~ 26.970 cm^{-1}).

In refs. 4 and 5 only a few vibrational differences in spectra are pointed out; therefore in Tables 1 and 2 give a more complete tentative vibrational analysis he spectra of the crystalline chrysene. In the fluores- ce spectrum, the vibrational differences appear to be

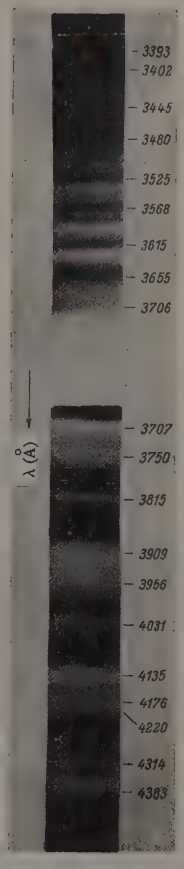

Spectra of fluorescence and of the long wavelength absorption of a sample of crystalline chrysene at 77°K under excitation of light of λ = 365 mμ.

the frequencies 305, 765, and 1395 cm^{-1}. More lines appear in the absorption spectrum; the main differences in this case are 375, 675, 760, and 1380 cm^{-1}.

able 1. Fluorescence Spectrum of Chrysene Powder at 77°K

ν (cm⁻¹)	J	Δν (cm⁻¹)	Interpretation	λ (Å)	ν (cm⁻¹)	J	Δν (cm⁻¹)	Interpretation
26968	v. i.	1	—	4071	24557	v. w.	2411	1015+1395
26867	v. i.	101	100	4135	24177	v. i.	2791	2×1395
26659	v. i.	309	305	4176	23940	w.	3028	—
26413	w.	555	555	4220	23684	i.	3284	305+2×1395
26205	i.	763	765	4267	23429	m.	3539	765+2×1395
25980	m.	988	990	4303	23233	m.	3735	—
25953	m.	1015	1015	4314	23177	m.	3791	—
25846	w.	1122	100+1015	4328	23099	m.	3869	305+765+2×1395
25575	v. i.	1393	1395	4360	22929	i.	4039	—
25271	v. i.	1697	305+1395	4386	22793	i.	4175	3×1395
25024	m.	1944	555+1395	4445	22490	v. w.	4478	305+3×1395
24801	i.	2167	765+1395					

Qualitative estimation of the band intensity: v. i. — very intense; i. — intense; medium; w. — weak; v. w. — very weak.

Table 2. Absorption Spectrum of Chrysene Powder at 77°K

λ (Å)	ν (cm⁻¹)	J	Δν (cm⁻¹)	Interpretation	λ (Å)	ν (cm⁻¹)	J	Δν (cm⁻¹)	Interpretation
3706	26976	i.	0	0—0	3520	28401	w.	1425	—
3692	27078	i.	102	100	3506	28514	m.	1538	—
3669	27248	m.	272	275	3497	28588	m.	1612	—
3655	27352	v. i.	376	375	3480	28727	v. i.	1751	375+1380
3646	27419	i.	443	445	3473	28785	i.	1809	—
3615	27655	v. i.	679	675	3460	28893	i.	1917	—
3604	27739	m.	763	760	3445	29019	i.	2043	675+1380
3587	27870	w.	894	895	3435	29104	w.	2128	760+1380
3581	27917	w.	941	940	3427	29172	m.	2196	—
3568	28019	i.	1043	1045	3417	29257	m.	2281	895+1380
3549	28169	w.	1193	1190	3402	29386	w.	2410	1045+1380
3542	28225	w.	1249	1250	3393	29464	v. w.	2488	—
3525	28361	i.	1385	1380					

For qualitative estimation of intensities see Table 1.

Thus, it appears that Table 3 of ref. 1 gives the common vibrational frequencies which appear in the luminescence spectra of chrysene solutions in octane, and in the spectra of naphtacene which is present in chrysene as an impurity.

It follows from the comparison that the basic normal vibration frequencies which are active in the emission spectra of chrysene and naphtacene are very similar, and that both spectra are determined mainly by the frequencies 300 and 1400 cm^{-1}.

In the emission spectra of the solutions of chrysene the fluorescence bands of the naphtacene impurity did no appear, because the solution concentration was very low (10^{-9} to 10^{-7} mol/liter) and also because the fluorescenc spectrum of chrysene in the visible region was observe by means of a Becquerel fluoroscope.

R. N. Nurmukhametov, E. G. Popova, an N. S. Dokunikhi

RE FERENCES

1. R. N. Nurmukhametov, E. G. Popova, and N. S. Dokunikhin, Opt. i Spektr. 9, 593 (1960), Optics and Spectroscopy 9, 313 (1960).
2. K. S. Krishnan and P. K. Seshan, Acta Phys. Polon. 9, 289 (1936).
3. J. W. Sidman, J. Chem. Phys. 25, 122 (1956).
4. J. Tsujikawa and E. Kanda, Sci. Repts. Research Insts., Tohoku Univ. 4a, 4716 (1952).
5. J. B. Birks and A. J. W. Cameron, Proc. Roy. Soc. A249, 297 (1959).

NOTICE

A NEW JOURNAL IN THE FIELD OF OPTICS

The Optical Society of America plans to issue a new journal, APPLIED OPTICS, which will publish papers on applied optics and related scientific and technical topics (physics, electronics, ionic, ultraviolet and space optics, computation of optical systems, plasma and solid state physics, crystal physics, etc.). Bimonthly publication is planned, each issue being built around one main topic* and containing a review article (about 10,000 words) and some 10 original papers (3000-5000 words each). In addition, publication of scientific and technical notes, book reviews, and news of the scientific community is planned.

*Translation editor's note: The Editors of APPLIED OPTICS would like us to make it clear that only part of each issue will be devoted to the feature subject. The rest of the issue will be devoted to the usual run of contributed paper in any area of applied optics.

The first issues will be devoted to the following topics:

1962	January	Optical Pumping and Masers
	March	Space Optics
	May	Foreign Optics
	July	Optical Engineering
	September	Infrared
	November	Information Theory
1963	January	Astronomy
	March	Instrumentation
	May	Interferometry

In the notice about the appearance of the new journal it was announced that papers may be submitted in Russian.

PRINTER'S CORRECTIONS TO VOL. 10

Contents Vol. 10, No. 1 should include (also to be added to Contents List for Volume 10, page 434)

"Study of Equilibria in Non-Aqueous Solutions of Electrolytes using Absorption Spectra" by N. A. Izmailov and E. I. Gurevich. (19) 9

Volume 10, No. 6, page 432—Author List (Alphabetical)

2nd Col. Reads	Should Read
Gurevich, E. I. (767) 405	Gurevich, E. I. (19) 9, (767) 405
Izmailov, N. A. (767) 405	Izmailov, N. A. (19) 9, (767) 405

O P T I K A I S P E K T R O S K O P I Y A

Volumes I through V

of the papers in the 1956 through 1958 volumes of "Optika i Spektroskopiya" have been trans-
d. These are listed below, and information as to their availability may be obtained from the
ces of translations given hereafter. The capital letters in parenthesis at the end of each
slation identify its source.

LL
miralty Centre for
ientific Information
d Liaison
een Anne's Mansions
ndon, S.W.1, England

sociated Electrical
dustries, Ltd.
search Laboratory
dermaston, Berks.
gland

sociated Technical
rvices, Inc.
.O. Box 271
st Orange, N.J.

RO
ommonwealth Scientific and
ndustrial Research Organ-
zation, 314 Albert Street
ast Melbourne, Australia

USTRIAL GROUP HQ
Isley, Warrington
ancs., England

notoduplication Service
ublication Board Project
ibrary of Congress
ashington 25, D.C.

ffice of Technical Services
25 D Street, S.E.
ashington, D.C.

NTREE
obert F. Rowntree
0 East Norwich Avenue
olumbus 1, Ohio

AEA
Industrial Group HQ
Risley, Lancs.
England

AERE
United Kingdom Atomic Energy
Research Establishment
Harwell, Nr. Didcot
Berks., England

CEA
Commissariat a l'Energie
Atomique
Bellevue
Seine et Oise, France

COURTAULDS LTD.
Foleshill Road
Coventry
England

INFOSEARCH
242 Willesden Lane
London, N.W.2, England

LLU
Department of Scientific and
Industrial Research Lending
Library Unit, 20 Chester Tce.
Regents Park, London, N.W.1
England.

PILKINGTON BROTHERS, LTD.
Research Department
St. Helens, Lancs.
England

SL
Science Library, The Keeper
Science Museum Library
South Kensington
London, S.W.7, England

AEC
Atomic Energy Commission
Technical Information Service
P.O. Box 62
Oak Ridge, Tennessee

ASLIB
8 Palace Gate
London, W.8, England

CNRS
Centre National des Re-
searches Scientifiques
Bellevue
Seine et Oise, France

DSIR HQ
Department of Scientific and
Industrial Research Head-
quarters Library, Chester
House, 5-11 Regent Street
London, S.W.1, England

INSDOC
Hillside Road
New Delhi, 12, India

NRC
National Research Council of
Canada, The Library
Sussex Drive
Ottawa, Canada

PROGIL
10 Quai du Commerce
Lyon 5, France

SLA
Special Libraries Association
Translation Center, John
Crerar Library, 86 East
Randolph Street
Chicago, Illinois

FILLER MATERIAL - NOT IN RUSSIAN ORIGINAL

Translations Sources

TF
Taylor and Francis, Ltd.
Red Lion Court, Fleet St.
London, E.C.4, England

VOLUME I (1956)

AGRANOVICH, V.M.
Theory of the Intrinsic Optical Activity of Molecular Crystals. I. Classical Theory. (LC or SLA)

AGRANOVICH, V.M. and FAIDYSH, A.N.
Migration and Transmission of Electron Excitation Energy from the Base Material to the Impurity in Molecular Crystals in the Presence of two types of Excitons. (LC or SLA)

AGRANOVICH, V.M. and FAIDYSH, A.N.
Influence of Reabsorption on the Quantum Yield of the Luminescence of Solid Solutions of Organic Compounds. (DSIR HQ and ACSIL)

ARKHANGEL'SKAYA, V.A. et al
A simple method for the Determination of the Transmission of Certain Optical Materials in the Schumann Spectrum Range. (INFOSEARCH)

BASOV, N.G. et al
Theory of the Superfine Structure of Rotational Spectra of Molecules Caused by the Electric 2^4-Polar Moment of the Nucleus. (CSIRO)

BATARCHUKOVA, N.R. and DUBROVSKII, G.B.
Effect of Variating Argon Pressure in Electrolodeless discharge on the Reduction of the Wavelength of the Red Line of Cd^{114}. (LLU; SL and NRC)

BROUDE
Spectres d'Absorption des Homologues du Benzene. (PROGIL)

FAIDYSH, A.N., KUCHEROV, I.Ya. and TERSKII, A.A. Disturbances in the Transfer of Excitation Energy in Solid Solution of Naphthacene in Anthracene. (LC or SLA)

FEDOROV, F.I.
Optics of Magnetic Crystals. I. Equations of the Normals. (SLA)

FILIMONOV, V.N.
Title not available. Pp 490-499 (ATS)

FIORINSKAYA, D.A. et al
Infrared Spectra of Sodium Silicate Glasses and their Relationship with the Structure. (INFOSEARCH)

GALANIN, N.L. and CHIZHIKOVA, Z.A.
Transfer of Excitation Energy in Anthracene Crystals Containing Naphthacene as Impurity (ACSIL)

GRUDINKINA, N.P.
Absorption of Ultra-violet Radiation by Water (INFOSEARCH)

IVANOV, A.P. et al
Spectrophotometric study of Mixtures of Powder ed Objects. (INFOSEARCH)

KALITEEVSKII, N.I. and CHAIKA, M.P.
The Ratio of the Magnetic Spin and Quadrupole Moments of the Nuclei U^{233} and U^{235}. (AEC)

KALITEEVSKII and TAIVA
Magnetic Spin. (AERE)

KISELEV, B.A.
Double Monochrometer with Diffraction Gratings (INFOSEARCH)

KITAEVA, V.F. and SOBOLEV, N.N.
Shape and Width of Lines in D.C. Arc Spectra. (AERE)

KOLOMITSOV, Yu.V. et al
Contactless Interference Method for the Contro of Spherical Lens Surfaces. (INFOSEARCH, LLU

KOLYADIN, A.I.
Anomalous Scatter of Light in Glass. (INFOSEARCH)

KORONKEVICH, V.P.
Dispersion of Air in the Visible Region of the Spectrum. (NRC and LLU)

LANDSBERG, G.S., SHATENSHTEYN, A.I. et al
Vibration Spectra of Diphenyl and Decadeutero-Diphenyl. (OTS)

LOTKOVA, E.N. et al
Infrared and Raman Spectra of Boric Anhydride. I. (INFOSEARCH)

NIKITINA, O.N.
Consideration of the Overlapping of the line-band Spectrum in the Analysis of Silica. (INFOSEARCH)

NOSKOV, M.M. et al
Measurement of Optical Constants of Metals in the Infrared Spectrum Region using Multiple Reflections. I. Theoretical Foundations of the Procedure. (INFOSEARCH)

OGANOV, M.N., STRIGANOV, A.R. and SOBOLEV, Yu.P.
Atomic Spectrum of Americium. (AERE and AEC)

FILLER MATERIAL - NOT IN RUSSIAN ORIGINAL

UME I - Cont'd

ITSYNA, I.A.
odification of SF-4 Spectrophotometer for he High-speed Automatic Recording of pectra. (INFOSEARCH)
KIN, Sh.Sh.
n the Raman Spectra of Complex Compounds f Antimony Trichloride with Benzene and ome of its Derivatives. (LC or SLA)
TIAN, S.G.
llumination of a Spectrograph by a Three-imensional Light Source. (INFOSEARCH)
REMET'EV, G.D.
ptical Properties of Uranium Hexafluoride. .. Absorption Spectra in the Visible and eighboring Ultraviolet Region. (AEC)
PANOV, B.I.
egative Luminescence and Negative Photo-ffect. (INFOSEARCH)
IGANOV, A.R. and KOROSTYLEVA, L.A.
tomic Spectra of Plutonium (AERE and AEC)
NBERG, G.V., ZAIDEL, A.N. and PETROV, A.A.
pectral Analysis of Isotopic Compositions f Hydrogen-Deuterium Mixtures. (INDUSTRIAL)
OSLAVSKII, N.G., ZHELUDOV, B.A. and NEVICH, A.E. A Recording Spectrometer or the Long Wave Infrared Region (ROWNTREE)
HAROVA, V.M. and KAGAN, Yu.M.
nvestigation of the Discharge Parameters nd the Character of the Excitation of Ion ines at High Current Densities. (ACSIL)

UME II (1957)

ANOVICH, V.M.
heory of the Intrinsic Optical Activity of olecular Crystals. II. Quantum Theory. LC or SLA)
MOV, A.I.
. Nomogram for use in Spectrum Analysis of are Earth Elements by the Addition Method. SLA)
REYESHCHEV, E.A. and ROZMAN, I.M.
uminescence Spectra of Plastic Scintill-tors with Triphenylpyrazoline. (LC or SLA)
HSHIYEV, N.G.
new Principle of Spectrometry. (LC or SLA)
NDI, V.L.
itle not available. pp 323-329 (SLA)
UDE
pectres d'Absorption des Homologues du enzene. III. Absorption de la umiere par les Benzene Dialcoyles (PROGIL)

BULANIN, M.O.
The Structure of Absorption Bands of Liquid H_2O, D_2O and HDO Determined by the Structure of the Molecules. (NRC)

DEIGEN, M.F.
Contribution to the Theory of Impurity Centres in Isotropic Homopolar Crystals. (PILKINGTON)

FEDOROV, F.I.
Optics of Magnetic Crystals. II. Binormals and Biradials. Optical Surfaces. III. Uni-axial and Unirefractive magnetic Crystals. (LC or SLA)

GROMOV, V.A.
New Method of Exciting Spectra in an atomic beam. (LC or SLA)

IVANOV, A.P.
Some Problems of Spectrophotometry of Light-scattering Media. (CSIRO)

KAGAN, Y.M. and PEREL, U.I.
On the Motion of Ions and the Shape of their Lines in the Positive Column of a Discharge. I. (AERE and AEI)

KARD, P.G.
The Analytical Theory of Optical Properties of Multi-layer Dielectric Coatings. (LC or SLA)

KIZEL, V.A. and STEPANOV, A.F.
Reflection of Light from a Liquid Surface and its connection with the Process of Crystalliz-ation. (LC or SLA)

LEONTOVICH, A.M.
Absorption Spectra of Crystals of Plutonium Salts. (LC or SLA)

LUSHCHIK, Ch.B.
New Methods of Investigation of Relaxation Processes and Trapping Centers in Crystal Phosphors. (LC or SLA)

LISITSA, M.P. and TSVELYKH, N.G.
Optique des coughes fines--phasage dans la re-flexion de la lumiere par les couches minces d'argent, de germanium, de tellure et de selenium. (CEA)

MARKOVA, Z.A.
Application of Infrared Spectroscopy to the Study of some Olefine Absorption on Alumino-Silicate Catalyst. (SLA)

MAZING, M.A. and MANDEL'SHTAM, F.L.
On the Spectral Line Broadening and Shifting a gas Discharge Plasma. (AEI and SL)

RASHBA, E.I.
Theory of Strong Interactions of Electron Ex-citations with Lattice Vibrations in Molecular Crystals. (LC or SLA)

FILLER MATERIAL - NOT IN RUSSIAN ORIGINAL

VOLUME II - Cont'd

ROZMAN, I.M.
Dependence of the Luminescence Yield of Plastic Scintillators with Triphenylpyrazoline on Temperature. (LC or SLA)

SHAMOVSKY, L.M. et al
Structure of Alkali-Halide Phosphors and Mechanism of Luminescence Process (INSDOC)

SIDOROV, T.A. et al
Infrared Spectrum and Molecular Structure of Phosphorus Oxide. I. (DSIR)

SINEINIKOV, K.D. et al
Double Refraction of Fluoride Films (INSDOC)

SHKLAREVSKI, I.N. and RYAZANOV, A.N.
Dispersion se le Saute de Phase des Pellicules Minces d'Aluminium. (CNRS)

VASIL'KOVSKII, A.A.
Calculation of a Thin Multilayer Plate as a one-layer Plate with an Effective Refractive Index. (LC or SLA)

VOLUME III (1957)

CHAIKA, M.P.
Luminosite d'un Spectrometre a Interferometre Fabry-Perot. (LC or SLA)

DEIGEN, M.F. and SHUL'MAN, L.A.
On the Theory of Electron Spin Resonance in f-Centers in Ionic Crystals (Continuum Model of f-Center -- "Smoothed Function") (OTS)

DMITRIEVSKII, O.D., NEPORENT, B.S. and NIKITIN, V.A.
High-speed Infrared Spectrometer for the 0.8 - 3.0 μ Bank. (SLA)

GAL'PERIN, D.Yu.
Application of the Theory of Aberrations of High Orders to the Calculation of Optical Systems. (SLA)

KOTOV, E.I.
Title not available. Pp 115-122 (ATS)

LEVSHIN, V.L.
The Contribution of Soviet Science to Luminescence Research. (ACSIL)

LOBANOVA, N.V. and RAUTIAN, G.N.
New Tables for Calculating Chromaticity Co-ordinates. (SLA)

MARKOV, M.N.
On Comparison of Low-Inertia Receivers of Infrared Radiation. (ACSIL)

OSIPOV, B.
Hyperfine Structure of the Rotational Transition 1=3:4 of the CH_3I^{127} Molecule. (CSIRO)

OSTROVSKII, Yu.I. and PENKIN, N.P.
Relative f-Values of the Spectral Lines of Scandium. (LC or SLA)

PENKIN, N.P. and FRISH, S.E.
The Emission and Absorption Spectra of Uranium. (AERE)

SHATALOV, A.A.
Photochemical Conversion of Color Centers in Heated Alkali-Halide Crystals. (LC or SLA)

SIDOROV, T.A. and SOBOLEV, N.M.
Infrared and Raman Spectra of Boron Oxide. II. Infrared Spectra and Molecular Structure. (PILKINGTON)

SMIRNOV, L.V.
Study of Molecular Dichroism by Means of an Artificial Orientation of the Molecules. (AEC)

VAINSHTEIN, L.A.
The Calculation of Atomic Wave Functions and Oscillator Strengths with an Electronic Computer. (AERE)

ZEMSKOV, E. and VESELAGO, V.
Stark Effect in Rotational Spectra of Molecules of the Asymmetrical Top Type in the Presence of Quadrupole Interaction (the case re=eQq). (CSIRO)

VOLUME IV (1958)

AGRANOVICH, V.M.
On the Capture of "Free" Excitons by Impurities in Molecular Crystals. (OTS)

BARCHUKOV, A.I. and BASOV, N.G.
Measurement of Frequencies and Intensities of Hyperfine Structure Lines of CH_3I (J=0→1 Transition). (LC or SLA)

BARCHUKOV, A.I., MURINA, T.M. and PROKHOROV, A.M.
Microwave Spectrum and Rotational Constants of the C_2H_5Cl Molecule. (LC or SLA)

BARCHUKOV, A.I. and PROKHOROV, A.M.
Microwave Spectrum of the CH_3GeH_3 Molecule. (LC or SLA)

BASOV, N.G. and OSIPOV, B.D.
Lines of Emission for the F=5/2-3/2, J=1, K=1 Transition of the Rotational Spectrum of the CH_3I^{127} Molecule. (LC or SLA)

BATARCHUKOVA, N.R.
Comparative Investigations of the Metrological Qualities of the Spectral Lines of ^{206}Pb and ^{114}Cd. (LC or SLA)

FILLER MATERIAL - NOT IN RUSSIAN ORIGINAL

ME IV - Cont'd

LNAYA, F.A.
vestigation of the Instantaneous Brightness
a Flash Discharge. (AEC)
YSH, A.N.
perimental Proof of the Theory of the Transer of Excitons by Diffusion. (LC or SLA)
H, S.E. and YAKHONTOVA, V.E.
w Data Regarding the Excitation Functions of elium Lines. (DSIR)
ANIN, M.D. and CHIZHIKOVA, Z.A.
n the Quenching of Luminescence of Organic bstances upon Excitation by α-particles. C or SLA)
ANIN, M.D.
n the Causes for the Dependence of the Luminescence Yield of Organic Substances on the nergy of the Ionizing Particles. (LC or SLA)
ASIMOV, F.M., TEL'TEVSKII, I.A., et al
ffraction Gratings from the State Optical nstitute. (LC or SLA)
VICH, I.M.
ayonnement d'un Tube d'Impulsion Puissant Moment de l'Explosion. (LC or SLA)
OVA, N.A.
diospectroscopic Investigation of CH_3GeCl_3 LC or SLA)
NOV, A.P.
heoretical Investigations of the Behavior of uminescent Radiation of Dispersed Luminescent articles. (LC or SLA)
NKOV, R.G.
nfrared Spectra of Cellulose Fibres. COURTAULDS)
AN, Yu.M. and PEREL, V.I.
n the Motion of the Ions and the Profile of he Spark Lines in the Positive Column of a ischarge. II. Radical Motion of the Ions n a low pressure Discharge. (AEC)
AN, Yu.M. and PEREL, V.I.
n the Motion of Ions and the Shape of their ines in the Positive Column of a Discharge. II. The directed motion of Ions in a Discharge at Arbitrary Pressure. (AERE)
S, M. and SEMENOV, B.Z.
he Absorption and Luminescence Spectra of ickel-Activated Alkali-Halide Crystals. LC or SLA)
LOVA, T.N.
ultilayer Dielectric Coatings with a High oefficient of Reflectance on Glass Surfaces. LC or SLA)
CHENKO, A.F. and RASHBA, E.I.
n the Excitonic States of a Molecular Crystal containing Different Molecules. (OTS)

LYZINA, L.A.
Method of Precipitation of Solid Dye Layers from Solutions; Corrections due to the Reflectance made in Absorption Measurements of these layers. (LC or SLA)

NIKITIN, V.A.
Relationship between the Scanning Speed and the Resolving Power of a Spectral Instrument. (LC or SLA)

PARFIANOVICH, I.A.
Interaction between Electrons and the Activator in NaCl-Ni and NaCl-Cu Phosphors. (LC or SLA)

PEDOS, F.Z. and SVENTITSKII, N.S.
A Low-voltage Vacuum pulsed Discharge for Exciting Spectra. (DSIR)

PROTAS, I.R.
Plates for Vacuum Ultraviolet Photography. (LC or SLA)

ROZMAN, I.M.
On the Theory of Quenching of Fluorescence of Solutions. (NRC)

ROYEV, L.M., FILIMONOV, V.N. and TERENIN, A.N.
Changes in the Infrared Spectra of Molecules Interacting with the Adsorption Centers of a Silica-Alumina Catalyst. (ATS)

SEVCHENKO, N.A. and FLORINSKAYA, V.A.
Infrared Spectral Transmittance of Porous and Quartzoid Glasses. (LC or SLA)

SEVCHENKO, N.A. and FLORINSKAYA, V.A.
Reflection Spectra of Quartz Crystal Plates cut at Different Angles to the Optical Axis within the 7-24$_\mu$ Wavelength Range.(LC or SLA)

SHIROKSHINA, Z.V. and SUIKOVSKAYA, N.V.
Preparation of Infrared Transmitting Films. (LC or SLA)

SIDOROV, T.A.
Infrared Spectra at Low Temperatures and the Structure of Quartz and Crystobarlite. (PILKINGTON)

SLYUSAREV, G.G. and KULIKOVSKAYA, N.I.
Distribution of Light Energy Changed in the Diffraction Pattern by Variable Transmittance Filters. (LC or SLA)

STEPANOV, B.I. and PRIMA, A.M.
Vibrational Spectra of Silicates. I. (PILKINGTON)

TAGIROV, R.B.
A Method of Measuring the Reflection Coefficient of Mirrors. (LC or SLA)

TARASOVA, L.I. and FEOFILOV, P.P.
Polarization of Luminescence and the Nature of Luminescent Centers in NaCl-Ag and KCl-Tl Crystals. (LC or SLA)

TOLSTOI, N.A.
Possibility of Using Pulse Lamps for Studying the Relaxations of Luminescence of Photoconductivity. (LC or SLA)

FILLER MATERIAL - NOT IN RUSSIAN ORIGINAL

VOLUME IV - Cont'd.

TOPORETS, A.S.
Absorption and Scattering of Light in Pigments (LC or SLA)
YEREMENKO, V.A.
Luminescence of Cadmium Sulfide Crystals. (LC or SLA)
ZAIDEL, A.N.
Determination de la composition Isotopique d'apres les Spectres d'Absorption. (CEA)

VOLUME V (1958)

BARCHUKOV, A.I. and PROKHOROV, A.M.
Quadrupole Coupling, Dipole Moment and Barrier of Internal Rotation of the CH_3GeH_3 Molecule as Determined from its Rotational Spectrum. (LC or SLA)
BELYANIN, V.B.
Multiplet Splitting of the Ground Term of the Holmium Atom. (OTS)
BOCHKOVA, C.P., RAZUMOVSKAYA, L.P. and FRISH, S.E. A simplified method of Spectral Analysis of Inert Gases for purity. (AERE)
DISTLER, G.I.
Infrared Polarization Filters. (LC or SLA)
KOSTISHIN, M.T.
Optical Constants of Germanium in Region 2-25μ (PILKINGTON)
KOVARSKII, V.A.
Theory of Non-Radiation Transitions in an F-Center. (ATS)
MOROZ, L.P.
Imaging of Separate Objects by an Aberration less Optical System in a Field which is more or less luminant than the Objects Themselves. (LC or SLA)
PEDOS, F.Z. and SVENTITSKII, N.S.
Excitation des spectres dans la Region du Vide par une Decharge pulsee a basse tension. (CEA)
SINEL'NIKOV, K.D. and RYAZANOV, A.N.
Resolving Power of Optical Systems Increased (LC or SLA)
TITUSHINA, V.P. and FABRIKANT, V.A.
Etude de la Divergence du Flux de Rayonnement de la Raie 2537A d'une Decharge dans le Mercure. (LC or SLA)
VOYEVODSKII, V.V., MOLIN, Yu.N. and CHIBRIKIN, B.M. Spectra of Electron Paramagnetic Resonance of Cr-Aromatic Compounds with Various Substitutes. (OTS)
YAROSLAVSKII, N.G. and STANEVICH, A.E.
The Rotational Spectrum of H_2O in the long Wavelength Region of the Infrared 50-1500μ (200-7 cm^{-1}) (ROWNTREE)

THIS LIST WILL BE BROUGHT UP TO DATE FROM TIME TO TIME

February 20, 1961

FILLER MATERIAL - NOT IN RUSSIAN ORIGINAL

Dipole Moment of CH_3GeH_3 Molecule . . . . . A. I. Barchukov and Yu. N. Petrov 67 (129)
The Temperature Dependence of Infrared Absorption Lines . . . . . L. N. Ovander 68 (129)
The Raman Spectrum of Barium Titanate . . . . . Ya. S. Bobovich and E. V. Bursian 69 (131)

LETTERS TO THE EDITOR

On the Article by M. V. Akhamnova and G. E. Kurilchikova: Infrared Absorption Spectra of Hydroxyfluoroboric Complexes of Potassium and Sodium . . . . . L. G. Ryss 72 (133)
Correction to the Article by P. N. Nurmukhametov, E. G. Popova, and N. S. Dokunikhin: Luminescence of Chrysene Solutions and Powders at 77°K 71 (134)

NOTICE

A New Journal in the Field of Optics 72
Printer's Corrections to Vol. 10 72

EDITOR'S NOTE

Comments on the scientific content of the translated Russian articles published in OPTICS AND SPECTROSCOPY are invited. They should be addressed as a Letter to the Editor of the Journal of the Optical Society of America and forwarded to the Editor of that journal, Dr. D. B. Judd, National Bureau of Standards, Washington 25, D. C.

UNIVERSITY OF ILLINOIS 3
LIBRARY
UNDERGRADUATE DIV
NAVY PIER GRAND AVE
CHICAGO 11 ILL

VOL. XI, NO. 1 OPTICS AND SPECTROSCOPY JULY 1961

CONTENTS

(Numbers in parentheses are original Russian page numbers.
These Russian page numbers are also quoted at the head of each paper.)

The Measurement of the Absolute Values of Oscillator Strengths in Atomic Spectra. I. Sodium . . . . . Yu. I. Ostrovskii and N. P. Penkin 1 (3)

The Effect of Vibration on Hyperfine Structure Constants . . . . . A. G. Makhanek 6 (12)

Quantum Effects in a Double Potential Well and Spectroscopy of the Hydrogen Bond . . . . . E. A. Pshenichnov and N. D. Sokolov 8 (16)

The Theory of Line Intensities in the Spectrum of Scattered Light. I. The Quantum Model (Condon Approximation) . . . . . L. L. Krushinskii and P. P. Shorygin 12 (24)

Calculation of the Electro-Optical Parameters and Integrated Infrared Band Intensities of the Acetylene and Hydrocyanic Acid Molecules and Their Deuterium Substitution Products . L. M. Sverdlov 18 (35)

The Infrared Spectrum of Lithium Vapor . . . . . K. P. Vasilevskii and V. I. Baikov 21 (41)

Molecular Vibrations of Sulfur Compounds: SF_5Cl . . . . . K. Venkatesvarlu and K. Sathianandan 24 (46)

Molecular Vibrations of Sulfur Compounds: SF_4 . . . . . K. Venkatesvarlu and K. Pillai 26 (51)

Infrared Absorption Spectrum and Symmetry of the Hexaethyldisiloxane Molecule . . . . . G. G. Kirei and M. P. Lisitsa 28 (55)

Transmission of Organic Solvents in the Far Infrared Region of the Spectrum . . . . . A. E. Stanevich and N. G. Yaroslavskii 31 (61)

Study of the Equilibria in Nonaqueous Solutions of Electrolytes by Means of Absorption Spectra III. Picric Acid and Sodium Picrate in Dioxane-Water and Benzene-Alcohol Mixtures . . . . . N. A. Izmailov and E. L. Gurevich 34 (67)

Spectral Investigation of the Aggregation of Dyes in Solvents of Low Polarity. . . . . Kh. L. Arvan and N. E. Zaitseva 38 (74)

Study of Electronic Phototransfer Reactions in the Solid Phase by EPR . . . . . N. N. Bubnov, V. V. Voevodskii, N. V. Fock, and B. N. Shelimov 40 (78)

Effect of Mechanical Treatment on the Absorption Spectrum of Cadmium Sulphide Crystals at Low Temperature . . . . . E. F. Gross, M. Bancie-Grillot, E. Grillot, and B. S. Rasbirin 43 (84)

Microscopic Studies of Electroluminescence in ZnS-Cu,Al Single Crystals . . . . . A. M. Bonch-Bruevich, Ya. E. Kariss, and V. A. Molchanov 45 (87)

The Phase of Electroluminescence Light Pulses as a Function of Excitation Voltage Parameters . . . . . A. N. Georgobiani and M. V. Fock 48 (93)

The Relation Between the Blue and Green Bands in the Electroluminescence of ZnS:Cu Phosphors . . . . . M. V. Fok 50 (98)

On the Luminescence of Charged Polycrystalline ZnS Layers Under the Action of DC Electric Fields . . . . . V. M. Fridkin 54 (105)

Photoelectric Method of Recording an Achromatic Interference Fringe . . . . . V. P. Koronkevich, G. A. Lenkova, N. S. Babenko, and A. I. Lokhmatov 58 (112)

Duration of the Flash of Tubular Flash Lamps . . . . . V. I. Vasiliev, M. S. Levchuk, and I. S. Marchak 61 (118)

SHORT COMMUNICATIONS

On Nuclear Magnetic Resonance in Solids . . . . . B. N. Provotorov 63 (123)

Effect of Spectrographic Camera Objective Distortion on Spectral Line Curvature . . . . . I. V. Peisakhson 65 (125)

ZnS:Ag Phosphor With Boron as a Coactivator . . . . . A. V. Lavrov 66 (128)

(Contents continued on inside back cover)